THEORY & VALIDATION

DROPLET SIZE

DATE: December 2023

This report describes the ATEX modelling of initial droplet size following expansion to atmospheric pressure. It also includes results of validation of initial droplet size and subsequent rainout modelling by the UDM model. This work was carried out as part of work for a JIP on non-flashing and flashing liquid jets and two-phase (droplet) dispersion. The current report is derived from results in the JIP Phase III report C4 and the JIP Phase IV report B.

No.	Date	Reason for Issue	Prepared by	Verified by	Approved by
1	Jan 2006	SAFETI 6.5 (Phase II JIP)	Witlox and Harper	Harper	
2	Oct 2009	Phast (Risk) 6.6 (Phase III JIP)	Witlox, Oke and Harper	Harper and Witlox	
3	May 2011	Phast (Risk) 6.7 (Phase IV JIP)	Witlox	Harper and Stene	
4	May 2021	Apply new template	D. Vatier		

Date: December 2023

Prepared by: Digital Solutions at DNV

ABSTRACT

This report describes the modelling of initial droplet size [Sauter Mean Diameter (SMD) and droplet size distribution] and droplet rainout carried out as part of JIP Phase IV work on non-flashing and flashing liquid jets and two-phase (droplet) dispersion. It represents an update and follow-up of work previously reported as part of JIP Phase II and III work.

The aim of this JIP sponsored work programme was to systematically improve modelling of two-phase aspects of accidental releases of superheated or flashing jets. Phase I work governed a review on flashing liquid jets and two-phase dispersion. The Phase II work is the application of Phase I recommendations for additional scaled water experiments and model improvement. The Phase III work involved added scaled experiments for water, gasoline, cyclohexane, butane and propane (carried out by Cardiff University), large-scale butane experiments (carried out by INERIS), and the development, implementation and validation of improved droplet size correlations. The Phase IV work included sub-cooled water and xylene experiments (carried out by HSL), and further refinement and validation of initial droplet size and (distributed) rainout.

New options of droplet size calculations have been added to the ATmospheric EXpansion model ATEX, which calculates the expansion from orifice to ambient conditions. The original ATEX included a Weber-number correlation for mechanical break-up, and a flashing correlation from the CCPS book (based on CCPS experiments). Additional criteria added are according to the TNO Yellow Book (Weber, Reynolds number correlation), a correlation developed by George Melhem (modified Weber correlation generalised to include flashing), new correlations developed as part of JIP Phase II and JIP Phase III, and a modified CCPS correlation. For the new Phase III JIP correlation, the option of meta-stable liquid (liquid to liquid expansion between stagnation and orifice conditions; non-equilibrium) is applied for the discharge (DISC) calculations.

The model validation includes a wide range of experiments for both SMD and total rainout. The experiments include the Phase IV JIP HSL rainout experiments, the CCPS rainout experiments, as well as all 2-phase elevated releases from the existing UDM validation dataset (EEC propane, Desert Tortoise and FLADIS ammonia, Goldfish HF). Adopted rainout methods comprised both UDM methods including explicit modelling of the droplets (range of CCPS and Phase III JIP correlations), as well as more simple methods based on rainout correlations without droplet modelling (e.g. correlations by DeVaull and King).

From this validation it is concluded that the modified CCPS droplet size correlation provided the best overall prediction of rainout, while the Phase III JIP droplet size correlation provided the best overall prediction of the initial droplet size. Therefore the modified CCPS droplet size correlation has been selected as the default droplet size correlation.

With some exceptions the above new versions of ATEX and UDM are available in Phast 6.7. The Phase II and Yellow Book correlations are unavailable, as is the droplet 'parcels' extension to the UDM.

The current report first details the above improvements of the ATEX and UDM models. Subsequently it reports results of the model validation.

Table of contents

List of tables

List of figures

1 INTRODUCTION

This report describes the modelling of initial droplet size [Sauter Mean Diameter (SMD) and droplet size distribution] and droplet rainout carried out as part of JIP Phase IV work on non-flashing and flashing liquid jets and two-phase (droplet) dispersion. It represents an update and follow-up of work previously reported as part of Phase II and III work on non-flashing and flashing liquid jets and two-phase droplet dispersion. It contains additional updates, i.e.

- Addition of modified CCPS droplet size correlation, and inclusion of this correlations in validation
- Added validation for Phase IV HSL water and xylene rainout experiments

Frequently accidents occur which involve liquid or two-phase releases of hazardous chemicals into the atmosphere. Rainout of these chemicals may result in reduced concentrations in the remaining cloud, but it can also lead to extended cloud duration because of re-evaporation of the rained-out liquid, and additional hazards such as pool fires. Thus for accurate hazard predictions, it is important to accurately predict both the amount of rainout and re-evaporation of the cloud. See
Figure 1 below for a schematic sketch of the problem.

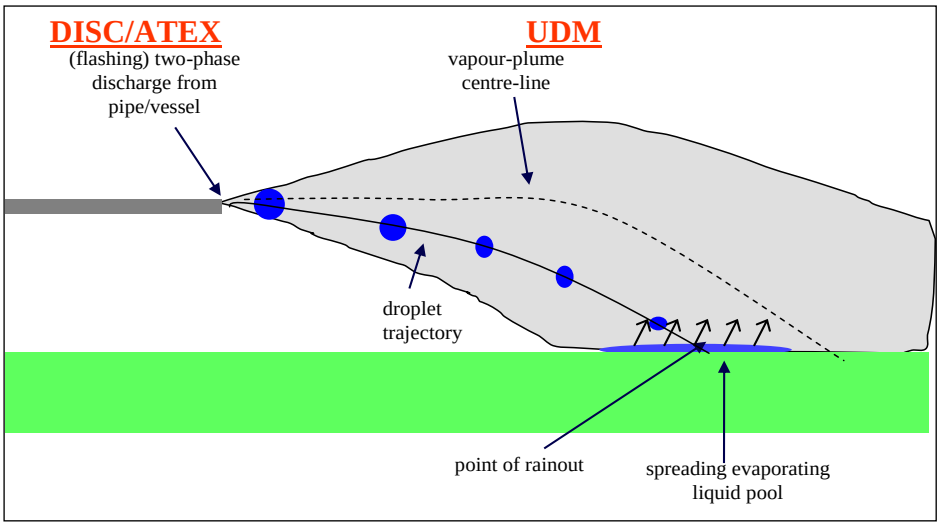

Figure 1. Droplet evaporation and rainout

After elevated two-phase discharge, evaporating droplets move away from the plume centre-line. If droplets reach the substrate, rainout occurs leading to the formation of a spreading liquid pool which provides a secondary source of vapour

As shown in Figure 1, the Phast discharge model DISC calculates the expansion from stagnation to orifice conditions, and the subsequent expansion from orifice to ambient conditions. The latter expansion is calculated by the Phast sub-model ATEX. For liquid releases from a vessel, the meta-stable liquid assumption (non-equilibrium) is assumed at the orifice (100% liquid, orifice = ambient pressure). During the ATEX expansion the liquid is assumed to break up into droplets and ATEX calculates the initial droplet size (Sauter Mean Diameter, SMD), following expansion to ambient conditions. The latter droplet size is input to the Phast dispersion model UDM for subsequent dispersion calculations. This includes droplet equations (conservation of mass, momentum and energy) and modelling of rainout and subsequent pool evaporation.

Phases of Droplet modelling JIP

The Joint Industry Project on Two-Phase Releases and Atmospheric Dispersion was instigated to examine, experimentally and with modelling, the phenomena of droplet formation, transport and evaporation, and rainout.

Following a literature review in Phase I[1], Phase II[2,3,4] focused on experimental work with water to measure post-expansion droplet size and derivation of ATEX post-expansion droplet correlations (initial droplet size following expansion to ambient conditions). Phase III[5,6] included the further refinement and validation of initial droplet size correlations using a wider range of chemicals and large-scale releases, and the development of a new UDM methodology to predict distributed rainout (rather than rainout at a single point). Phase II and III also included significant improvements to the solution of droplet equations within the UDM to correct long-standing numerical problems.

Contrary to expectations, the greatest difficulties and uncertainties in both Phase II and III involved the measurements of droplet size for non-flashing sub-cooled releases, in particular the inability to measure the large irregular droplets which constitute a significant proportion of the mass. Phase IV[7] therefore focused on sub-cooled water and xylene experiments

(carried out by HSL). This was also envisaged to avoid added complexities relating to flashing releases such as significant droplet evaporation prior to rainout and inaccuracies of rainout measurements caused by significant pool evaporation. Thus the key objectives of the Phase IV project were to validate (and possibly further refine) the Phase III correlation for droplet size distribution, and to validate rainout predictions and the new methodology for distributed rainout.

Structure of report

Chapter 2 provides an overview of the DISC/ATEX modelling of the initial droplet size including a description of a range of correlations for SMD and droplet size distribution. It also outlines the overall method for discharge (DISC/ATEX) and dispersion (UDM) simulations.

Chapter 3 reports results of the validation of the models for SMD and droplet size against a range of experiments, i.e. the CCPS[8] (flashing jets of water, CFC-11, chlorine, cyclohexane, monomethylamine), STEP[9,10] (flashing propane jets), HSL experiments by Allen[11, 12, 13] (flashing propane jets), VKI[27] (flashing R134-A jets) and the Cardiff Phase II water experiments[3]. It also reports validation against butane and water experiments carried out by Ecole des Mines and INERIS as reported in the paper by Touil et. al.[14]. Finally it includes validation against the added Phase III Cardiff and INERIS experiments.

Chapter 4 includes results of validation against the Phase IV HSL water and xylene experiments using two different correlations for the initial droplet size, i.e. the CCPS SMD correlation and the Phase III JIP SMD correlation. The validation includes flow rates, droplet size and distributed rainout. For the xylene experiments, it also includes temperature drop and concentrations.

Chapter **5** includes validation results for a range of correlations predicting the initial droplet size (SMD) against all known experiments for which SMD droplet size measurements are available.

Chapter **6** includes validation for predicting total amount of rainout for a wider range of methods and a wider set of experiments. The methods include both UDM methods including explicit modelling of the droplets (range of CCPS and Phase III JIP correlations), as well as more simple methods based on rainout correlations without droplet modelling. The experiments include the Phase IV JIP HSL rainout experiments, the CCPS rainout experiments, as well as all 2-phase elevated releases from the UDM validation dataset (Desert Tortoise, EEC, FLADIS, Goldfish).

Chapter **7** includes a discussion of the overall validation results, lists the key conclusions and provides recommendations for future work.

2 MODELLING OF INITIAL DROPLET SIZE (DISC/ATEX) AND DROPLET DISPERSION (UDM)

2.1 Introduction

Once the Phast (Risk) atmospheric expansion model ATEX has obtained the conditions at the end of the expansion to atmospheric pressure, it calculates the representative droplet size under these conditions for liquid and two-phase releases. The droplet size is required in the UDM dispersion modelling for the calculation of drop thermodynamics and trajectory.

This chapter provides an overview of the DISC/ATEX modelling of the initial droplet size including a description of a range of correlations for SMD and droplet size distribution. It also outlines the overall method for discharge (DISC/ATEX) and dispersion (UDM) simulations.

The plan of this chapter is as follows:

- Section 2.2 introduces the nomenclature and general concepts of droplet size distribution, mass distribution for droplet mass, Sauter Mean Diameter, and critical droplet size below which rainout does not occur
- Section 2.3 describes the SMD correlations currently applied in ATEX
- Section 2.4 describes the droplet size distributions currently applied in the UDM
- Section 2.5 summarises how the DISC/ATEX discharge simulations and the UDM dispersion simulations are carried out for both non-flashing and flashing jets.

2.2 General theory for droplet size distribution

The description included below partly corresponds to the description for droplet size distribution included in Section 10.2 in the CCPS release book[18].

Droplet size distribution

At every downwind distance, there will be a range of existing droplet sizes. The droplet size distribution can be expressed by means of the cumulative probability distribution function $F(D_p)$, where $F(D_p)$ is the fraction of droplets with droplet size less than the droplet diameter D_p. It is given by

$$F(D_p) = \int_0^{D_p} f(d_p)\,d(d_p) = \int_0^{D_p/d_d} p(t)\frac{dt}{t}, \qquad with\ F(0)=0,\ F(\infty)=1 \tag{1}$$

where

d_p is the droplet diameter ($0<d_p<\infty$)
d_d is the Sauter Mean drop diameter as defined below (m)
t is the normalised droplet diameter, $t = d_p/d_d$
$f(d_p)$ is the probability distribution function for d_p
$p(t)$ is the probability distribution function for the normalised diameter $t = d_p/d_d$; note that $p(d_p/d_d) = d_d\ f(d_p)$

Sauter Mean Diameter

The UDM requires as input the initial Sauter mean droplet diameter d_d, which is defined by:

$$d_d = d_{32}, \; with \; d_{mn} = \frac{\int_0^\infty d_p{}^m f(d_p) d(d_p)}{\int_0^\infty d_p{}^n f(d_p) d(d_p)} = d_d{}^{m-n} \frac{\int_0^\infty \tau^{m-1} p(\tau) d\tau}{\int_0^\infty \tau^{n-1} p(\tau) d\tau} \quad (2)$$

Mass distribution function for droplet mass

A mass distribution function $F_m(D_p)$ for the droplet mass $m_d(d_p) = \pi \rho_L d_p^3/6$, can be introduced,

$$F_m(D_p) = \frac{\pi}{6} \rho_L \int_0^{D_p} d_p{}^3 f(d_p) d(d_p) = \frac{\pi}{6} \rho_L d_d{}^3 \int_0^{D_p/d_d} t^2 p(t) dt \quad (3)$$

Let N_d be the total number of droplets (total number of droplets for instantaneous, total droplets released per second for continuous), then $N_d F_m(D_p)$ is the total mass of the droplets with droplet size less than the droplet diameter D_p.

Thus the mass fraction $\upsilon_{drop}(D_p)$ of droplets with droplet diameter less than D_p is given by

$$\nu_{drop}(D_p) = \frac{F_m(D_p)}{F_m(\infty)} \quad (4)$$

Mass fraction of droplets which rain out

Let m_{cld} be the total cloud mass (kg for instantaneous, kg/s for continuous), m_{cL} the total liquid component mass, and η_{cL} the liquid mass fraction, then

$$m_{cL} = \eta_{cL} m_{cld} = N_d F_m(\infty) \quad (5)$$

Let d_p^{cr} be the critical droplet diameter below which no rainout occurs and let z_d be the vertical height of the droplets (as calculated for the SMD adopted by the UDM droplet equations), then the mass fraction m_{cL}^{ro} of liquid that rains out is given by

$$m_{cL}{}^{ro} = \left[\nu_{drop}(d_p{}^{cr}) \; m_{cL} \right]_{at \; z_d = 0} \quad (6)$$

2.3 SMD droplet size correlations (ATEX)

This section includes the correlations for the Sauter Mean Droplet Diameter dd which are implemented into the new ATEX atmospheric expansion model:

- Section 2.3.1 describes the droplet size correlation based on the Weber mechanical break-up criterion, and the CCPS flashing correlation according to the RELEASE book. This includes both the original Phast 6.6 correlation (based on the minimum of mechanical and flashing droplet sizes) and a modified CCPS correlation (using mechanical droplet size for sub-cooled and flashing for superheated releases). The modified CCPS correlation is the new Phast default droplet size correlation.
- Section 2.3.2 describes the droplet size correlation recommended by the TNO Yellow Book.
- Section 0 describes the droplet size correlation recommended by Melhem and adopted in the program SuperChems.
- Section 2.3.4 describes the now out-of-date correlation developed as part of JIP Phase II.

- Section 2.3.5 describes the droplet size correlation developed as part of Phase III of DNV's droplet joint-industry project, i.e. based on a new Weber/Reynolds mechanical break-up criterion, and a new flashing criterion (partly based on Kitumura transition criterion).

It is noted that ATEX applies the following cut-off values for d_d:

$$[d_d]_{ATEX} = \max\left\{ d_{d\min} \ , \ \min(d_d, d_{d\max}) \right\} \quad (7)$$

where:

$d_{d\min}$ is the minimum allowable drop size, set in the Discharge Parameters for Phast, and with a default value of 0.01 μm.

$d_{d\max}$ is the maximum allowable drop size , set in the Discharge Parameters for Phast , and with a default value of 10,000 μm.

2.3.1 Original CCPS (default 6.6) and modified CCPS (default from 6.7) correlation (Weber/CCPS)

Mechanisms for Droplet Formation

The discharge drop size model assumes there are two possible mechanisms for droplet formation: "mechanical or aerodynamic" break up; and "flashing" break-up. The aerodynamic break up mechanism gives the droplet diameter, d_{da}, as a function of the critical Weber number. The flashing break-up gives the droplet diameter, d_{df}, as a function of the partial expansion energy.

In line with the CCPS recommendation in the RELEASE book, the original default Phast 6.6 correlation calculates the droplet diameter for both mechanisms, and then sets the value d_d as follows:

$$d_d = \min\left\{ d_{da} \ , \ d_{df} \right\} \text{ , original CCPS} \quad (8)$$

The above criterion has however the problem that it may pick-up erroneously the mechanical break-up criterion in the flashing regime leading to too low droplet sizes and therefore under-prediction of droplet sizes.

Therefore the recommended new default from Phast 6.7 is a modified CCPS correlation, which selects the mechanical droplet size for subcooled releases and the flashing droplet size for flashing releases[i]:

$$d_d = \begin{cases} d_{da} \text{ , if subcooled} \\ d_{df} \text{ , if superheated} \end{cases} \text{ , modified CCPS} \quad (9)$$

The details of the calculations for each mechanism are described below. See Chapter 3 of the verification manual for the UDM Thermodynamic model for further details and a literature review.

Mechanical break-up criterion

For the mechanical or aerodynamic break-up mechanism, the droplet diameter d_{da} (m) [Sauter Mean Diameter] is calculated as a function of the critical Weber number, as follows[ii]:

$$d_{da} = \frac{\sigma_L \, We_{crit}}{u_f^{\,2} \, \rho_a} \quad (10)$$

where:

u_f is the final velocity, calculated at the end of expansion to atmospheric pressure (m/s)

ρ_a is the atmospheric density (kg/m^3) [at atmospheric pressure and temperature]

[i] The flashing droplet break-up criterion is applied for superheat >0.01C (to avoid rounding errors near the boiling point.), and the mechanical break-up criterion otherwise.

[ii] JUSTIFY. Mechanical break-up is not used for instantaneous releases, not sure why.

σ_L is the surface tension of the liquid (N/m) [at post-expansion temperature]
We_{crit} is the value of the critical gas Weber number, set in the Discharge Parameters for Phast, and with a default value of 12.5 following recommendation by the TNO yellow book [see also Brown and York (1962)[15], Heinze (1955)[16])].

Flashing break-up criterion

For the flashing break-up mechanism, the droplet diameter d_{df} (m) is calculated as a function of the partial expansion energy E_p (J/kg).

The correlation in ATEX is based on a formulation by Woodward and Papadourakis[17]; see also the book by Johnson and Woodward[18] on the RELEASE model for predicting aerosol rainout in accidental releases. Using the original UDM model, Woodward calculated droplet diameters such as to best match observed rainout data for the CCPS rainout experiments. These "experimental" drop sizes were correlated against a number of differing parameters, and it was found that E_p was the most effective correlator for droplet size.

The droplet diameter d_{df} is calculated as follows:

$$d_{df} = 0.833*10^{-3} - 0.0734*10^{-3} \ln(E_p) \qquad (11)$$

Here the partial expansion energy is given by[iii,iv]

$$\begin{aligned} E_p &= -\Delta h - (P_{st} - P_a)v_{st} && P_v^c(T_{st}) \geq P_{st} \\ &= -\Delta h - \left[P_v^c(T_{st}) - P_a\right]v_{st} + \left[P_{st} - P_v^c(T_{st})\right]v_{st} && P_a < P_v^c(T_{st}) < P_{st} \\ &= (P_{st} - P_a)v_{st} && P_v^c(T_{st}) < P_{st}, P_v^c(T_{st}) \leq P_a \end{aligned} \qquad (12)$$

$$\Delta h = \left\{\eta_{Lf} h_L(P_a, T_f) + (1-\eta_{Lf}) h_v(P_a, T_f)\right\} - h(P_o, T_o) \qquad (13)$$

where:

P_{st} is the stagnation[v] pressure (N/m^2)
T_{st} is the stagnation temperature (K)
Δh is the change in material enthalpy from stagnation to post-flash conditions (J/kg)
P_a is the ambient pressure (N/m^2)
v_{st} is the specific volume at storage pressure and temperature
η_{Lf} is the final liquid fraction, at the end of the expansion to atmospheric pressure
T_f is the final temperature, at the end of the expansion to atmospheric pressure
$h_v(P,T)$ is the vapour enthalpy at pressure P (Pa) and temperature T (K)
$h_L(P,T)$ is the liquid enthalpy at pressure P (Pa) and temperature T (K)

The three cases in the above equation for partial expansion energy correspond to two-phase to two-phase expansion, superheated liquid (liquid to two-phase expansion) and sub-cooled liquid (liquid to liquid expansion), respectively[vi]. The superheated liquid case comprises two separate pressure related terms: the second is for the initial depressurisation to saturated vapour temperature P_{st} to P_v^c , the first the migration along the saturated temperature curve from P_v^c to P_a . Note that as the saturated vapour pressure approaches the ambient pressure the partial expansion energy term for superheated liquids approaches that for sub-cooled liquids.

The RELEASE report contains full details on the CCPS experiments and the derivation of the above droplet correlation from the CCPS experiments. See the UDM thermodynamics verification manual for further details.

The flashing droplet correlation is derived from experiments involving releases from leaks only. Therefore its applicability to releases from pipes and for instantaneous releases is questionable.

[iii] CODE CORRECTED. For the case of conservation of energy assumption, the term Δh instead of -Δh was used erroneously in the equation prior to Phast 6.4.2

[iv] CHECK. Currently the enthalpy change Δh is calculated from the orifice exit conditions to the atmosphere instead from the stagnation conditions to the atmosphere, which appear to be more appropriate and is also in line with the RELEASE book.

[v] For releases from long pipes, the stagnation data are chosen to correspond with the pipe exit data (inconsistent assumption with line rupture). The implication on the above corrections needs to be further checked for pipes.

[vi] IMPROVE. In the sub-cooled liquid case, the Δh term in the liquid expansion is absent since it is negligible. However, for simplicity and consistency it would be better to include.

In the case of the release from a vessel (without attached pipe) and 'frozen liquid' assumption between the stagnation and the orifice conditions (i.e. no flashing within the orifice), the above droplet size formula should always be associated with an isentropic atmospheric expansion. For the latter case conservation of energy should not be applied.

2.3.2 Appleton/Wheatley correlation recommended by TNO Yellow-book

For finite-duration spray releases, the TNO Yellow Book[19] recommends the initial droplet-size calculation method based on the work by Appleton[20] and presented by Wheatley[21]. It is defined as follows[vii]:

$$d_d = 1.89\, d_f \sqrt{1+3\frac{We_{Lf}^{0.5}}{\mathrm{Re}_{Lf}}} \quad , \quad if \quad \left\{We_{Lf} < 10^6\, \mathrm{Re}_{Lf}^{-0.45} \;\; and \;\; T_o < 1.11 T_{boil}^c\right\}$$
$$= \frac{\sigma_L\, We_{crit}}{u_f^{\,2}\, \rho_a} \quad , \quad else \qquad (14)$$

Here the liquid Weber number and the liquid Reynolds correspond to the post-expansion state,

$$\mathrm{Re}_{Lf} = \frac{\rho_L\, u_f\, d_f}{\mu_L} \quad , \quad We_{Lf} = \frac{\rho_L\, u_f^{\,2}\, d_f}{\sigma_L} \qquad (15)$$

where u_f is the post-expansion velocity, d_f the post-expansion diameter, and with all material properties evaluated at the post-expansion temperature T_f.

Note that the above equation actually represents two types of 'mechanical-breakup' criteria. The second part of this criterion is identical to the Weber criterion (10) currently applied for mechanical break-up in Phast, however with We_{crit} = 15 applied instead of We_{crit}=12.5.

Furthermore note that T_o is the exit (orifice) temperature (prior to the expansion); T_{boil}^c is the normal boiling temperature of the released component, i.e. the saturated temperature at ambient pressure, $T_{boil}^c = T_v(P_a)$.

[vii] CHECK. The TNO yellow book recommended the conservation of energy assumption in conjunction with this formula for post-expansion calculations. This seems to imply that the frozen liquid assumption is not applied for stagnation to orifice expansion.

2.3.3 Melhem correlation (modified Weber generalised for flashing)

Mechanical break-up correlation

The original Weber number correlation adopts a constant critical Weber number We_{crit} excluding droplet viscosity effects. Melhem et al.[22] modified this correlation to include droplet viscosity effects referring to a correlation of Brodkey[23] for the viscosity number N_{vi}. This correlation is given by Equations (1), (4) in his paper. In our notation, this modified correlation becomes:

$$d_{da} = \frac{\sigma_L}{(u_o - u_a)^2 \rho_a} \left\{ We_{crit} + 14 N_{vi}^{1.6} \right\} \quad with \quad N_{vi} = \frac{\mu_L}{\sqrt{\rho_L \sigma_L d_{da}}} \qquad (16)$$

Here We_{crit} is quoted to be between 10 and 20, with a typical value of 12[viii]. For ATEX implementation the default value of 12.5 is adopted consistent with the original 6.4 ATEX Weber number correlation.

It is noted that for small liquid viscosities the above equation reverts to the original PHAST6.4 droplet-size correlation, with the exception that PHAST6.4 uses the post-expansion velocity u_f instead of the excess orifice velocity u_o-u_a . It is seen that for larger values of droplet viscosity the droplet size using the above equation is larger than the original size. Also for this case the above equation may need to be solved iteratively for d_{da}.

Generalisation for superheated liquids

The above correlation is further generalised for superheated liquids by Melhem as follows,

$$d_{df} = \frac{\sigma_L}{2A_E \rho_a} \left\{ We_{crit} + 14 N_{vi}^{1.6} \right\} \quad with \quad N_{vi} = \frac{\mu_L}{\sqrt{\rho_L \sigma_L d_{df}}} \qquad (17)$$

Here We_{crit} = 12.5 again assumed; the surface tension σ_L of the liquid (N/m), the liquid density and the liquid viscosity are all evaluated at the final post-expansion temperature. Furthermore A_E is quoted to represent the difference in internal energies between the initial stagnation state and the final post-expansion state minus the work done by expansion from the release pressure to the ambient pressure. This represents the total amount of energy available for heat transfer, turbulence etc. Following further private communication with Melhem, the following expression is adopted:

$$A_E = E_{\exp} = \left\{ h(P_{st}, T_{st}) - h(P_a, T_f) \right\} - \left\{ P_{st} v(P_{st}, T_{st}) - P_a v(P_a, T_f) \right\} \qquad (18)$$

Note that the droplet size reduces with increasing A_E.

Overall criterion

The overall adopted correlation is as follows:

$$d_d = \begin{cases} d_{da} , & for \ \Delta T_{sh} \le \Delta T_B \\ d_{df} , & \Delta T_{sh} > \Delta T_B . \end{cases} \qquad (19)$$

That means that the mechanical break-up correlation is used for subcooled jets, and for superheat larger than ΔT_B=0.01K the superheated correlation is used. The superheat ΔT_{sh} is defined in Equation (36).

[viii] Melhem (private communication) indicates that the precise value of C depends on the fluid/mixture, with value mostly around 12.0.

2.3.4 JIP Phase II correlation (out of date)

The Phase II JIP correlation was derived from a series of scaled water experiments as presented by Cleary, Bowen and Witlox[3]. This correlation has now been superseded by the Phase III correlation and therefore is no longer recommended.

Mechanical break-up criterion

This criterion was derived from experimental data for sub-cooled water jets. The droplet Sauter Mean Diameter SMD = d_{da} (m), using the mechanical (aerodynamic) break-up criterion, is calculated as a function of the ratio L/d_o, the orifice liquid Reynolds number Re_{Lo} and the orifice liquid Weber number We_{Lo}, as follows:

$$\begin{aligned} \frac{d_{da}}{d_o} &= F(We_{Lo}, \mathrm{Re}_{Lo}, \frac{L}{d_o}), \quad 2 < \frac{L}{d_o} < 50 \\ &= F(We_{Lo}, \mathrm{Re}_{Lo}, 2), \quad \frac{L}{d_o} < 2 \\ &= F(We_{Lo}, \mathrm{Re}_{Lo}, 50), \quad \frac{L}{d_o} > 50 \end{aligned} \qquad (20)$$

Here the function F is given by

$$F(We_{Lo}, \mathrm{Re}_{Lo}, \frac{L}{d_o}) = 64.73\, We_{Lo}^{-0.533}\, \mathrm{Re}_{Lo}^{-0.014} \left(\frac{L}{d_o}\right)^{0.114} \qquad (21)$$

and

$$\mathrm{Re}_{Lo} = \frac{\rho_L u_0 d_0}{\mu_L}, \quad We_{Lo} = \frac{\rho_L u_0^{\,2} d_0}{\sigma_L} \qquad (22)$$

with

d_o	orifice diameter (m)
L	thickness of vessel wall (case of release from hole in vessel); or pipe length (for release from pipe) (m)
σ_L	surface tension of the liquid (N/m) [at orifice temperature T_o]
u_0	orifice velocity, valid prior to expansion to atmospheric pressure (m/s)
ρ_L	the liquid density [at T_o] (kg/m^3)
μ_L	the liquid dynamic viscosity (Pa s) [at T_o; note that $v_L = \mu_L/\rho_L$ is the kinematic viscosity]

Transition criterion to flashing

This transition criterion was derived from experimental data for flashing jets. As illustrated in Figure 2, the SMD d_d is herewith expressed as a tri-linear curve as function of the superheat ΔT_{sh}

$$\Delta T_{sh} = T_o^{\,u} - T_v^c(P_a) \qquad (23)$$

Here T_o^u is the temperature immediately upstream of the orifice, and $T_v^c(P_a)$ the saturated temperature at the ambient pressure P_a.

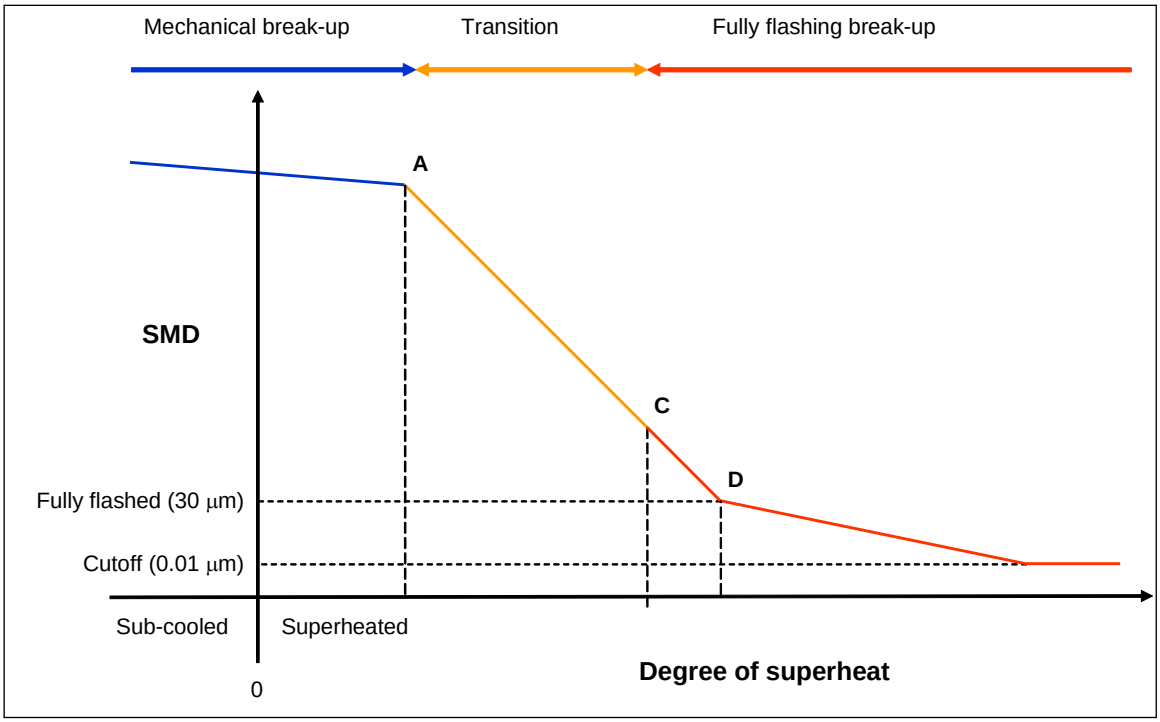

Figure 2. **Tri-linear curve for Sauter Mean Diameter as function of superheat**
The figure plots the Sauter Mean Diameter d_d (m) as function of superheat ΔT_{sh}. Prior to point A mechanical break-up applies. Between points A and C transition to flashing occurs. After point D the SMD reduces with 0.1μm /K.

The following criteria define the start point A and end point C of transition to flashing,

$$Ja\ \ \phi = 55\ We_v^{-\frac{1}{7}}\ \ ,\ \ with\ \ \phi = 1 - e^{-2300\left(\frac{\rho_v}{\rho_L}\right)} \qquad (24)$$

$$Ja\ \ \phi = 150\ We_v^{-\frac{1}{7}} \qquad (25)$$

where ρ_v and ρ_L are the vapour and liquid density evaluated at T_o. In accordance with the paper by Kitumura, the vapour Weber number We_v and the Jacob number Ja are evaluated as

$$We_v = \frac{\rho_v u_o^{\ 2} d_o}{\sigma_L} \quad , \quad Ja = \frac{C_{pL}\Delta T_{sh}}{h_{fg}} \frac{\rho_L}{\rho_v} \qquad (26)$$

Where C_{pL} is the specific heat of the liquid (J/kg/K), and h_{fg} the latent heat of evaporation (J/kg), both evaluated at the orifice temperature.

By use of Equation (26) into Equations (24) and (25), it can be shown that the start point A and end point C of flashing transition are satisfied for $\Delta T_{sh} = \Delta T_{sh}^{A}$ and $\Delta T_{sh} = \Delta T_{sh}^{C}$, respectively with[ix]

[ix] In the evaluation of ΔT_{sh}^{A}, ΔT_{sh}^{C}, d_d^{A}, d_d^{C}, the properties in Equations (27) and (28) are currently set at the superheat $\Delta T_{sh} = T_o - T_v^{c}(P_a)$ instead of the appropriate superheat of ΔT_{sh}^{A} or ΔT_{sh}^{C}. This avoids an iterative solution for ΔT_{sh}^{A}, ΔT_{sh}^{C} in superheat and is less CPU-intensive. Moreover it is shown in Chapter 4 of the JIP Phase III report C4 for a specific example (water) that the predictions are very close.

$$\Delta T_{sh}{}^{A} = \frac{h_{fg}}{C_{pL}} \frac{\rho_v}{\rho_L} \frac{55\, We_v^{-\frac{1}{7}}}{\phi} \quad , \quad \Delta T_{sh}{}^{C} = \frac{h_{fg}}{C_{pL}} \frac{\rho_v}{\rho_L} \frac{150\, We_v^{-\frac{1}{7}}}{\phi} \qquad (27)$$

Note that for the end point C the SMD droplet diameter is assumed to have been reduced with a factor of 2.4 with respect to the mechanical break-up value, thus

$$d_d{}^{C} = \frac{d_d{}^{A}}{2.4} \qquad (28)$$

Prior to point C the assumption of meta-stable liquid is assumed (liquid-to-liquid expansion from stagnation to orifice conditions; non-equilibrium). After point C fully flashing is assumed, with liquid to two-phase expansion from stagnation to orifice conditions (equilibrium).[x]

Overall SMD correlation

Thus the following criterion is applied (tri-linear curve for SMD):

(1) Before the start of transition (point A), the mechanical breakup SMD = d_{da} is applied
(2) Subsequently d_d reduces linearly (with slope defined such that it passes through point C) until it reaches point D, defined by $d_d{}^{D} = 30\text{x}10^{-6}$m. Thus along this part:

$$d_d = G_{lin}(\Delta T_{sh}) = d_d{}^{A} - \frac{\Delta T_{sh} - \Delta T_{sh}{}^{A}}{\Delta T_{sh}{}^{C} - \Delta T_{sh}{}^{A}} \left[d_d{}^{A} - d_d{}^{C} \right] \qquad (29)$$

with as inverse function,

$$\Delta T_{sh} = G_{lin}{}^{-1}(d_d) = \Delta T_{sh}{}^{A} + \frac{d_d{}^{A} - d_d}{d_d{}^{A} - d_d{}^{C}} \left[\Delta T_{sh}{}^{C} - \Delta T_{sh}{}^{A} \right] \qquad (30)$$

Note that the superheat $\Delta T_{sh}{}^{D}$ at point D is defined by,

$$\begin{aligned} \Delta T_{sh}{}^{D} &= \Delta T_{sh}{}^{A}, \quad if \quad d_d{}^{A} \le d_d{}^{D} \\ &= G_{lin}{}^{-1}\left(d_d{}^{D}\right), \quad if \quad d_d{}^{A} > d_d{}^{D} \end{aligned} \qquad (31)$$

(3) Afterwards it decays with 1µm every 10 degrees of superheat.

Thus the following criterion is applied for the evaluation of the Sauter mean droplet diameter d_d

$$\begin{aligned} d_d &= d_{da}, && if \ \Delta T_{sh} \le \Delta T_{sh}{}^{A} \\ &= G_{lin}(\Delta T_{sh}), && if \ \Delta T_{sh}{}^{A} < \Delta T_{sh} \le \Delta T_{sh}{}^{D} \\ &= \max\left\{ d_{d\min}, \min(d_d{}^{A}, d_d{}^{D}) - 10^{-7} (\Delta T_{sh} - \Delta T_{sh}{}^{D}) \right\}, && if \ \Delta T_{sh} > \Delta T_{sh}{}^{D} \end{aligned} \qquad (32)$$

[x] The superheat upstream the orifice, $T_o{}^{u}$, approximately equals the superheat immediately downstream of the orifice, T_o, in case of the meta-stable liquid. Therefore DISC/ATEX always applies the orifice temperature T_o in evaluating the superheat for purpose of the evaluation of the droplet SMD.

2.3.5 JIP Phase III correlation

The Phase III JIP correlation was derived by Cardiff University as part of Stage A of Phase III of the JIP from a new series of scaled water and cyclohexane experiments. This new correlation supersedes the preceding Phase II correlation which is no longer recommended. The Phase III correlation has the same form as the Phase II correlation.

Mechanical break-up criterion

The correlation for mechanical break-up was derived from experimental data for sub-cooled jets. The droplet Sauter Mean Diameter SMD = d_{da} (m), using the mechanical (aerodynamic) break-up criterion, is calculated as a function of the ratio L/d_o, the orifice liquid Reynolds number Re_{Lo} and the orifice liquid Weber number We_{Lo} as follows:

$$\begin{aligned}\frac{d_{da}}{d_o} &= F\left[(We_{Lo}, \mathrm{Re}_{Lo}, \frac{L}{d_o}, \frac{\mu_{Lo}}{\mu_{water,stp}}, \frac{\sigma_{Lo}}{\sigma_{water,stp}}, \frac{\rho_{Lo}}{\rho_{water,stp}}\right], \quad 0.1 < \frac{L}{d_o} < 50 \\ &= F\left[We_{Lo}, \mathrm{Re}_{Lo}, 0.1, \frac{\mu_{Lo}}{\mu_{water,stp}}, \frac{\sigma_{Lo}}{\sigma_{water,stp}}, \frac{\rho_{Lo}}{\rho_{water,stp}}\right], \qquad \frac{L}{d_o} < 0.1 \\ &= F\left[We_{Lo}, \mathrm{Re}_{Lo}, 50, \frac{\mu_{Lo}}{\mu_{water,stp}}, \frac{\sigma_{Lo}}{\sigma_{water,stp}}, \frac{\rho_{Lo}}{\rho_{water,stp}}\right], \qquad \frac{L}{d_o} > 50\end{aligned} \quad \textbf{(33)}$$

Here the function F is given by[xi]

$$F\left[(We_{Lo}, \mathrm{Re}_{Lo}, \frac{L}{d_o}, \frac{\mu_{Lo}}{\mu_{water,stp}}, \frac{\sigma_{Lo}}{\sigma_{water,stp}}, \frac{\rho_{Lo}}{\rho_{water,stp}}\right] = 74 We_{Lo}^{-0.854} \mathrm{Re}_{Lo}^{0.441} \left(\frac{L}{d_o}\right)^{0.114} \left(\frac{\mu_{Lo}}{\mu_{water,stp}}\right)^{0.971} \left(\frac{\sigma_{Lo}}{\sigma_{water,stp}}\right)^{-0.368} \left(\frac{\rho_{Lo}}{\rho_{water,stp}}\right)^{-0.107} \quad \textbf{(34)}$$

and

$$\mathrm{Re}_{Lo} = \frac{\rho_L u_{vc} d_0}{\mu_L}, \quad We_{Lo} = \frac{\rho_L u_{vc}^2 d_0}{\sigma_L} \quad \textbf{(35)}$$

with

d_o	orifice diameter (m)
L	thickness of vessel wall (case of release from hole in vessel); or pipe length (for release from pipe) (m)
σ_L	surface tension of the liquid (N/m) [at orifice temperature T_o]
u_{vc}	vena contracta velocity, valid prior to expansion to atmospheric pressure (m/s); the vena contracta velocity is related to the orifice velocity u_o by $u_o = C_d u_{vc}$. Here the discharge coefficient C_d = 1 in case of a release from a pipe
ρ_L	the liquid density [at T_o] (kg/m^3)
μ_L	the liquid dynamic viscosity (Pa s) [at T_o; note that $v_L = \mu_L/\rho_L$ is the kinematic viscosity]

Furthermore the subscript "water,stp" indicates properties of water taken at standard temperature and pressure (1 atmosphere and 0 °C)[xii].

[xi] The coefficients here are slightly different to those in the Phase III report. The fitted coefficients were rounded in that report to 2 decimal points from the values actually used in the model. Verification has shown this can give SMDs up to 5% too high. Extending precision to 3 decimal points gives results correct to within 1 µm.

[xii] The ATEX model currently assumes atmospheric pressure P_a instead of 1 atm. Typically this will make little or no difference.

Transition criterion to flashing

This transition criterion was derived from experimental data for flashing jets. As illustrated in Figure 3 the SMD d_d is herewith expressed as a tri-linear curve as function of the superheat ΔT_{sh}

$$\Delta T_{sh} = T_o^{\,u} - T_v^c(P_a) \qquad (36)$$

Here T_o^u is the temperature immediately upstream of the orifice, and $T_v^c(P_a)$ the saturated temperature at the ambient pressure P_a. Unlike the Phase II correlation, it is now presumed that it is valid to model the release as a meta-stable liquid (with a solid liquid core at the exit of the orifice) for the entire range of superheats.

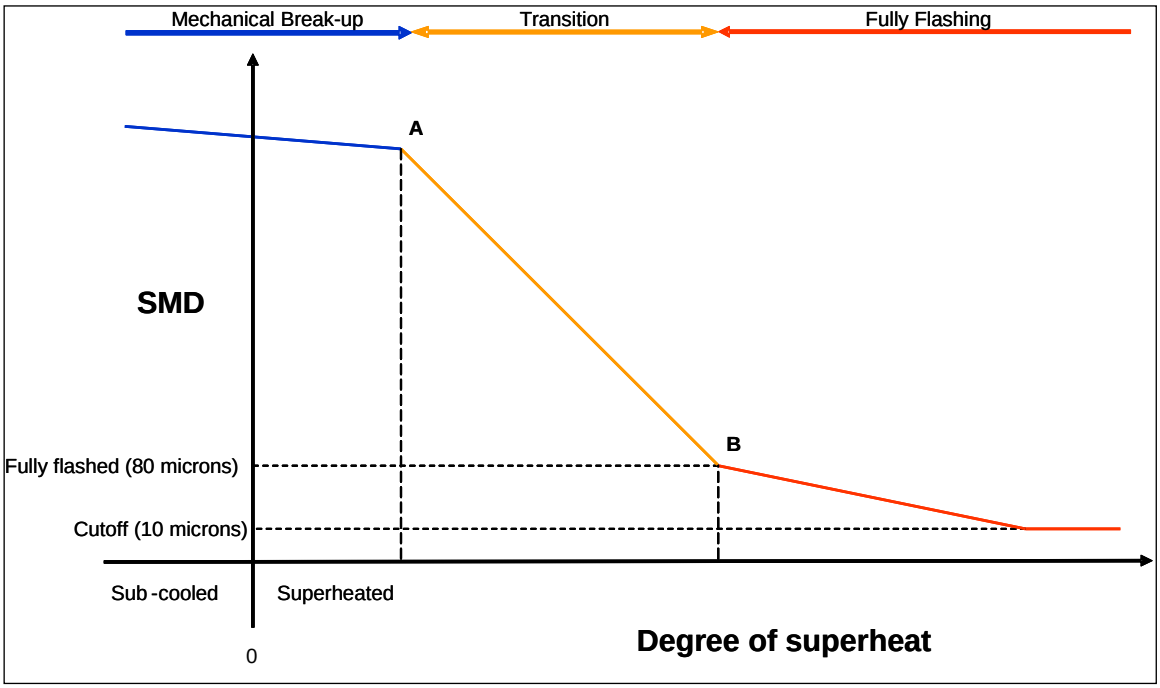

Figure 3. **Tri-linear curve for Sauter Mean Diameter as function of superheat**
The figure plots the Sauter Mean Diameter d_d (m) as function of superheat ΔT_{sh}. Prior to point A mechanical break-up applies. Between points A and B transition to flashing occurs. After point B the SMD reduces with 0.1µm /K.

The model incorporates the definition of criteria for transition between regimes based on the thermodynamic properties of the liquid (Jakob number Ja) and the ratio of inertia forces to surface tension forces in the spray (vapour Weber number We_v). In order to permit similarity scaling for use of the transition criteria with other liquids the Jakob number is modified by a correction factor (ϕ) as defined by Kitamura *et al*[24], based on the liquid to vapour density ratio. The transition points A and B are defined by the following equations,

Point A: $$Ja\ \phi = 48\ We_v^{-\frac{1}{7}}\ ,\ with\ \phi = 1 - e^{-2300\left(\frac{\rho_v}{\rho_L}\right)} \qquad (37)$$

Point B: $$Ja\ \phi = 108\ We_v^{-\frac{1}{7}} \qquad (38)$$

where ρ_v and ρ_L are the vapour and liquid density evaluated at T_o. In accordance with the paper by Kitumura, the vapour Weber number We_v and the Jacob number Ja are evaluated as

$$We_v = \frac{\rho_v u_o^{\,2} d_o}{\sigma_L} \quad , \quad Ja = \frac{C_{pL}\Delta T_{sh}}{h_{fg}} \frac{\rho_L}{\rho_v} \qquad (39)$$

Here C_{pL} is the specific heat of the liquid (J/kg/K), and h_{fg} the latent heat of evaporation (J/kg), both evaluated at the orifice temperature.

When $\Delta T_{sh} = \Delta T_{sh}^{B}$ then the fully flashing SMD is assumed to be a constant, in this case 80μm. Thereafter the SMD is assumed to decrease at a constant rate of 1 μm per 10 degrees of superheat (same as Phase II correlation) until the SMD reaches a final constant value chosen equal to 10 μm.

By use of Equation (39) into Equations (37) and (38), it can be shown that the start point A and end point B of flashing transition are satisfied for $\Delta T_{sh} = \Delta T_{sh}^{A}$ and $\Delta T_{sh} = \Delta T_{sh}^{B}$, respectively with[xiii]

$$\Delta T_{sh}{}^{A} = \frac{h_{fg}}{C_{pL}} \frac{\rho_v}{\rho_L} \frac{48\, We_v^{-\frac{1}{7}}}{\phi} \quad , \quad \Delta T_{sh}{}^{B} = \frac{h_{fg}}{C_{pL}} \frac{\rho_v}{\rho_L} \frac{108\, We_v^{-\frac{1}{7}}}{\phi} \qquad (40)$$

Overall SMD correlation

Thus the following criterion is applied (tri-linear curve for SMD):

1. Before the start of transition (point A), the mechanical breakup SMD = d_{da} is applied
2. Subsequently d_d reduces linearly with slope defined such that it passes through point B, with point B defined by $d_d^{B} = 80\text{x}10^{-6}$m and ΔT_{sh}^{B} . Thus along this part:

$$d_d = G_{lin}(\Delta T_{sh}) = d_d{}^{A} - \frac{\Delta T_{sh} - \Delta T_{sh}{}^{A}}{\Delta T_{sh}{}^{B} - \Delta T_{sh}{}^{A}} \left[d_d{}^{A} - d_d{}^{B} \right] \qquad (41)$$

3. Afterwards it decays with 1μm every 10 degrees of superheat.

Thus the following criterion is applied for the evaluation of the Sauter mean droplet diameter d_d

$$\begin{aligned} d_d &= d_{da} , && if\ \Delta T_{sh} \le \Delta T_{sh}{}^{A} \\ &= G_{lin}(\Delta T_{sh}) , && if\ \Delta T_{sh}{}^{A} < \Delta T_{sh} \le \Delta T_{sh}{}^{B} \\ &= \max\left\{ d_{d\min} , \min(d_d{}^{A}, d_d{}^{B}) - 10^{-7} (\Delta T_{sh} - \Delta T_{sh}{}^{B}) \right\}, && if\ \Delta T_{sh} > \Delta T_{sh}{}^{B} \end{aligned} \qquad (42)$$

2.4 Droplet size distribution and partial rainout (UDM)

2.4.1 No droplet size distribution (original Phast formulation)

The current Phast 6.7 model does not explicitly model a probability droplet distribution, and it calculates a single deterministic value of the SMD droplet diameter only. Complete rainout is assumed as soon as the droplets hit the ground.

2.4.2 Lognormal distribution (from RELEASE book)

In the RELEASE CCPS book the distribution p(t) of the normalised droplet t = d_p/d_{pm} is assumed to follow a log-normal distribution:

$$f(d_p) = \frac{p(t = d_p / d_{pm})}{d_p} , \quad with \quad p(t) = \frac{1}{(2\pi)^{1/2} \ln(\sigma_G)} \exp\left[-\frac{1}{2} \left(\frac{\ln t}{\ln(\sigma_G)} \right) \right]^2 \qquad (43)$$

[xiii] In the evaluation of ΔT_{sh}^{A} , ΔT_{sh}^{B}, d_d^{A} the properties in Equation (39) are currently set at the superheat $\Delta T_{sh} = T_o - T_v^{c}(P_a)$ instead of the appropriate superheat of ΔT_{sh}^{A} or ΔT_{sh}^{B}. This avoids an iterative solution for ΔT_{sh}^{A}, ΔT_{sh}^{B} in superheat and is less CPU-intensive. Moreover it is shown in Chapter 4 in the JIP Phase III report C4 report for a specific example (water) that the predictions are very close.

where:

d_p is the droplet diameter ($0<d_p<\infty$)

d_{pm} is the average drop diameter (m)

$f(d_p)$ is the probability distribution function for d_p

σ_G is the geometric spread of the normalised droplet diameter distribution; in the RELEASE book a value of 1.8 to 1.9 is adopted

Thus a Gaussian probability distribution is assumed for $\ln(d_p/d_{pm})$ with spread $\ln(\sigma_G)$.

The above formulation is not currently implemented in the UDM.

2.4.3 Rosin-Rammler distribution (Elkobt and recommended by Phase III JIP)

Different forms of distribution functions may be obtained from standard atomisation references[25]. The one advocated by Eltkobt[26] applies the Rosin-Rammler size distribution, which is commonly assumed for droplet size distributions. It can be presented in terms of the mass fraction $\upsilon_{drop}(D_p)$ of droplets with droplet diameter less than D_p,

$$\nu_{drop}(D_p) = 1 - e^{-a_{RR}\left(\frac{D_p}{d_d}\right)^{b_{RR}}} \quad (44)$$

The values (adopted by Elkobth and the values derived as part of the experimental work of Phases III of the droplet modelling JIP) are summarised in the table below

Correlation	a_{RR}	b_{RR}
Elkobt	0.422	5.32
Phase III of JIP	0.4 (mechanical) linear transition 0.79 (fully flashing)	2.00 (mechanical) linear transition 0.97 (fully flashing)

Note that the above equation is conveniently presented in terms of the SMD d_d, which allows easy evaluation by the UDM. A precise mathematical formula for b_{RR} is given below,

The Figure below shows the volume undersize distribution $\upsilon_{drop}(D_p)$ corresponding to an example taken from the experimental work of the Phase III JIP in the case of a fully flashing water jet (case of a 1 mm nozzle at 180C and 250 mm downstream). The figure includes the lognormal distribution[xiv], the original Elkobth Rosin-Rammler distribution, the new proposed Rosin-Rammler distribution, as well as the recorded data. It is seen that the new proposed correlation produces the most accurate results.

[xiv] The lognormal distribution has been applied with a geometric spread of σ_G = 21.738 microns corresponding to the recorded droplet size distribution.

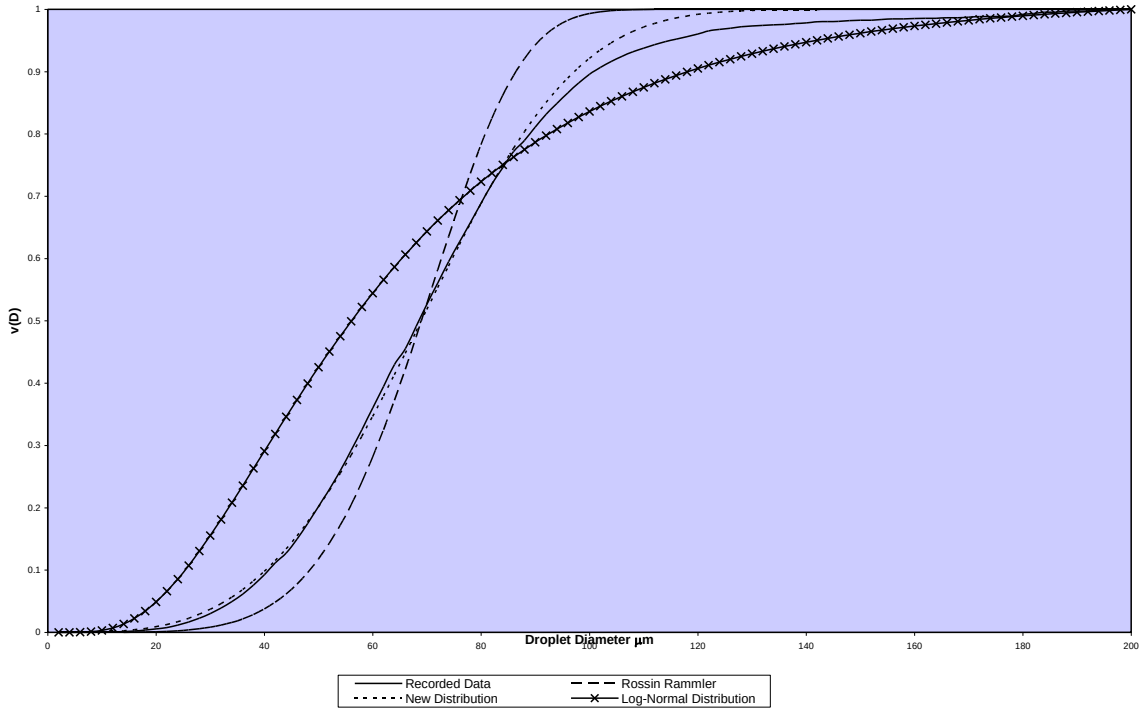

Figure 4. **Example of volume droplet undersize functions**
Case of flashing water jet with 1mm nozzle at 180°C 250mm downstream

Phase III droplet-size distribution correlation

A precise mathematical formula for a_{RR} and b_{RR} is given below,

$$\begin{aligned} a_{RR} &= a_{RR}{}^{A}, && if\ \Delta T_{sh} \le \Delta T_{sh}{}^{A} \\ &= a_{RR}{}^{A} + \frac{\Delta T_{sh} - \Delta T_{sh}{}^{A}}{\Delta T_{sh}{}^{B} - \Delta T_{sh}{}^{A}} \left[a_{RR}{}^{B} - a_{RR}{}^{A} \right], && if\ \Delta T_{sh}{}^{A} < \Delta T_{sh} \le \Delta T_{sh}{}^{B} \\ &= a_{RR}{}^{B}, && if\ \Delta T_{sh} > \Delta T_{sh}{}^{B} \end{aligned} \qquad (45)$$

$$\begin{aligned} b_{RR} &= b_{RR}{}^{A}, && if\ \Delta T_{sh} \le \Delta T_{sh}{}^{A} \\ &= b_{RR}{}^{A} + \frac{\Delta T_{sh} - \Delta T_{sh}{}^{A}}{\Delta T_{sh}{}^{B} - \Delta T_{sh}{}^{A}} \left[b_{RR}{}^{B} - b_{RR}{}^{A} \right], && if\ \Delta T_{sh}{}^{A} < \Delta T_{sh} \le \Delta T_{sh}{}^{B} \\ &= b_{RR}{}^{B}, && if\ \Delta T_{sh} > \Delta T_{sh}{}^{B} \end{aligned} \qquad (46)$$

Here $a_{RR}{}^{A}$ = 0.4 and $b_{RR}{}^{A}$ = 2.00 are values for mechanical break-up, and $a_{RR}{}^{B}$ = 0.79 and $b_{RR}{}^{B}$ = 0.97 are values for flashing break-up. See Part A of the Phase III report for full details of the derivation of the above droplet size distribution correlation from a best fit against a range of water and cyclohexane experiments (accounting for 'clipping' of experimental data).

Critical droplet size

The choice of the critical droplet size was discussed in Section 6.5 of the Phase I report[1], and is briefly summarised below.

Everyday experience with a variety of aerosols leads to the conclusion that droplets of the order of 30 μm[xv] or less for most realistic release scenarios will not rainout, but either evaporate before settling, or are carried along with the jet. For example, this is consistent with experience of providing seeding for laser diagnostic studies, where particle sizes less than 30μm are sought to ensure particles generally follow and hence represent the gas-phase flow.

Note that also discussions are included in the CCPS RELEASE book regarding the critical droplet size d_p^{cr} below which rainout does not occur. A formula for d_p^{cr} is derived [see Equation (10.20) in RELEASE book]. Here a critical vertical velocity is utilised to allow the critical droplet size to pass out of the global jet boundary, along with a drag coefficient correlation and force balance on droplet buoyancy and drag forces. Likewise, using the UDM approach, droplets trajectories are explicitly modelled and a criterion can be developed when these droplets pass out of the global jet boundary (an appropriate cloud width needs to be selected for this).

Currently the critical droplet size below which rainout occurs may be specified by the UDM user. The default value of d_p^{cr} = 30 micrometer.[xvi] is currently recommended. For future implementation an improved formulation may be considered (e.g. possibly in line with the formulation suggest above, allowing rainout only for those droplets outside the jet boundary).

2.5 Method for discharge (DISC/ATEX) and dispersion (UDM) simulations

The following assumptions are applied currently in the discharge simulations:

- Only the initial rate is assumed (i.e. the steady-state model in DISC is applied)
- The conservation of energy assumption is applied in the ATEX expansion calculations in line with the recommendations from the PHASE I review[1]. However in case of the frozen liquid assumption and release from vessel without pipe, isentropic assumption should always be applied in conjunction with the old and modified CCPS correlation[xvii]. See Appendix B in report C4 for a detailed discussion.
- Only the leak scenario (also known as orifice scenario or vessel scenario) has been applied so far[xviii].

The assumption of meta-stable liquid is always applied (non-equilibrium; liquid-to-liquid expansion from stagnation to orifice conditions, with orifice pressure = ambient pressure) in the DISC/ATEX simulations.

The precise method for carrying out the discharge (DISC/ATEX) and the dispersion (UDM) calculations is described below:

1. Evaluation of post-expansion droplet size characteristics (using DISC/ATEX)

   Droplet data are set from DISC/ATEX calculations assuming a meta-stable liquid (non-equilibrium; liquid-to-liquid expansion from stagnation to orifice conditions, with orifice pressure = ambient pressure; see also Table 1).

   (a) Case of old and modified Weber/CCPS correlations and TNO correlation.
   The post-expansion SMD diameter d_d is evaluated in terms of post-expansion data (velocity u_f, liquid fraction f_{Lf}, temperature T_f); see Section 2.3.1 and Section 2.3.2 for details.

   (b) Case of Melhem correlation.
   The post-expansion SMD diameter d_d is evaluated in terms of the excess orifice velocity (u_o-u_a) and post-expansion fluid properties (liquid viscosity μ_L, surface tension σ_L, liquid fraction f_{Lf}, temperature T_f); see Section 0 for details.

   (c) Case of Phase III JIP correlation.
   The post-expansion SMD diameter d_d and droplet-size distribution parameter b_{RR} are evaluated in terms of orifice data (velocity u_o, temperature T_o); see Section 2.3.5 for details.

2. Evaluation of orifice data and other post-expansion data (using DISC/ATEX)

   Subsequently the flow rate is set as well as the orifice and post-expansion velocity, pressure, temperature, liquid fraction. The above assumption of meta-stable liquid is always applied, which means that the values of the orifice

[xv] In the Phase I report a value of 20μm was mentioned, but recent experience suggests a more accurate value would be 30μm. This is the opinion of Phil Bowen based on intuition and practical experience.

[xvi] IMPROVE. In the Phase III UDM version one input parameter defines both the cut-off size for partial rainout, d_{pr} and the droplet size until which the droplet equations are solved (i.e. non-equilibrium model is adopted), d_{eq}; thus $d_{pr}=d_{eq}$. If the droplet size of a droplet parcel drops below d_{eq}, all liquid for that parcel is assumed to evaporate resulting in a discontinuity in liquid fraction. As a result the cut-off is currently chosen to be small by default, $d_{eq}= d_{pr}$ =10μm. For Phase IV two separate values for d_{eq} and d_{pr} are considered, with $d_{pr} >> d_{eq}$, e.g. d_{eq}=10μm and d_{pr}=30 μm.

[xvii] JUSTIFY. The current PHAST default is the minimum "thermodynamic change" which can result in either isentropic or conservation of energy.

[xviii] IMPROVE. To develop and add description of method for line ruptures (DISC), time-varying releases (TVDI) and 2-phase release from long pipelines (PBRK)

velocity u_o, the orifice liquid fraction $\eta_{Lo}=1$, the orifice temperature T_o, the orifice pressure $P_o=P_a$ and the superheat ΔT_{sh} correspond to the meta-stable liquid assumption. The meta-stable assumption is strictly speaking applied to the vena-contracta[xix] state and not the orifice state, i.e, using u_{vc}, $\eta_{vc}=1$, $P_{vc}= P_a$, and superheat ΔT_{sh} . These vena contracta data are input to ATEX, and the post-expansion data are calculated by ATEX from these data.

3. Evaluation of dispersion data

The above post-expansion data (flow rate, liquid fraction, velocity, temperature, SMD diameter d_d, and in case of new JIP correlation b_{RR}) are subsequently used as input to the dispersion model UDM to carry out the dispersion calculations (including droplet modelling and rainout).

Data	Meta-stable		Fully flashing	
	stagnation	vena contracta	stagnation	vena contracta
Liquid fraction	$\eta_{st}=1$	$\eta_{vc}=1$	$\eta_{st}=1$	$\eta_{vc}<1$
Pressure	$P_{st} > P_a$	$P_{vc} = P_a$	$P_{st} >> P_a$	$P_{vc} \geq P_a$
Temperature	T_{st}	$T_{vc} \approx T_{st}$	T_{st}	$T_{vc} < T_{st}$
Velocity	$u_{st} = 0$	u_{vc}	$u_{st} = 0$	u_{vc}

Table 1. **Values of DISC discharge data at stagnation point and orifice**
The table gives data at the stagnation point (upstream of the orifice) and at the orifice (immediately downstream of the orifice at the vena contracta, prior to atmospheric expansion)

3 MODEL VALIDATION - JIP PHASE II&III: DROPLET SIZE AND FLOW RATE

3.1 DISC/ATEX validation for droplet size (STEP,HSL,VKI, Phase II Cardiff)

This section describes the validation for the new droplet size calculations against experimental data for a range of experiments (STEP, HSL, VKI, Cardiff). Details of the experiments are described in Appendix E.

[xix] The orifice velocity u_o is the actual/observed orifice velocity. It corresponds to the product of the vena contractor velocity u_{vc} (as calculated by the discharge models) and the discharge coefficient (C_d). Likewise the vena contract area A_{vc} is the product of the orifice area A_o and C_d.

3.1.1 Assumptions for DISC/ATEX simulations

1. For the experiments considered in this section it was found that orifice data (data immediately prior to the atmospheric expansion) were not available, but only stagnation data (vessel storage data) were given.

2. The runs are carried out in a maximum of two stages

    a. First DISC/ATEX calculations are carried out assuming a meta-stable liquid (non-equilibrium; liquid-to-liquid expansion from stagnation to orifice conditions, with orifice pressure = ambient pressure). From this the values of the SMD post-expansion diameter and b_{RR} are derived.

    b. In case of the Phase II correlation with fully flashing (beyond point C, i.e. superheat $\Delta T_{sh} > \Delta T_{sh}^{C}$), DISC calculations are redone, but now with fully-flashing liquid. From these the other post-expansion data are derived.

3. The conservation of momentum assumption is applied in the ATEX expansion calculations in line with the recommendations from the Phase I review report[1] in case equilibrium is assumed for the orifice state. However in case of the frozen liquid assumption and release from vessel without pipe, isentropic assumption should always be applied in conjunction with the old CCPS correlation. See Appendix C for a detailed discussion. For all other cases the assumption of conservation of energy is currently recommended.

4. The DISC vessel scenario based on the “Bernoulli model” was always applied for both L/d>0 and L/d=0.[xx]

5. Although possible, the discharge coefficient C_d in each DISC run has not been varied to match the observed release rates. [xxi]

[xx] IMPROVE. In future to try to attempt to use DISC line rupture scenario for similar experimental set-up. Given lack of data, suggest to apply the pipe roughness value of 4.57×10^{-5} m for L/d>0 ratios.

[xxi] JUSTIFY. It is observed that simulated results (i.e. SMDs) using the default value of C_d in DISC for sharp-edged orifices (i.e. $C_d = 0.6$) generally compare better with measured data than results using recommended C_ds from experimental data.

3.1.2 Overview of experimental conditions

Table 2 and Table 3 summarise the experimental conditions for the various experiments as well as the experimental SMD measurements.

Experiment	STEP	HSL	VKI[27]	Phase II Cardiff 1	Phase II Cardiff 2
Material	Propane	Propane	R134-A	Water	water
storage pressure (bara)	10.75	Saturated (7.5)	8.25	11.0	11.5
storage temperature (C)	Saturated (29.8)	16	23	155	155
orifice diameter (mm)	5	4	1	1	0.75
L/D	0?	10	0	3.4	4.53
ambient pressure (bar)	0.9 bar	1atm	1atm	1atm	1atm
ambient temperature (C)	30	10?	20?	20?	20?
Experimental measurements					
Flow-rate (kg/s) [for ATEX]	0.2	0.09	?	?	?
Orifice velocity (assume meta-stable liquid) (m/s) [for ATEX]	20.87 (from flow rate)	14.17 (from flow rate)	26.0 (from C_d)	32.75 (from C_d)	35.96 (from C_d)
downstream location (mm)	95	500	187	250	250
Post-expansion SMD	27.0*1.2=32.4	50	80-100	63	60

Table 2. Experimental data – STEP, HSL, VKI, Phase II Cardiff

Experiment	BU-OR	BU-PI	WA-OR1	WA-OR2	WA-PI1	WA-PI2	WA-PI3
Material	Butane	Butane	Water	Water	water	Water	Water
storage pressure (bara)[xxii]	3	3	9.2	11.4	9.4	9.2	11.4
storage temperature (C)	23.85	23.85	164	167	136	164	167
Orifice diameter (mm)	5	1.65	2	2	2	2	2
L/D	0	60.61	0	0	50	50	50
ambient pressure (atm)	1?	1?	1?	1?	1?	1?	1?
ambient temperature (C)	23.85?	23.85?	*10*	*9*	*13*	*12*	*8*
Experimental measurements							
Flow-rate (kg/s) [for ATEX]	?	?	*0.08*	*0.09*	*0.08*	*0.06*	*0.07*
Orifice velocity (assume meta-stable liquid) (m/s) [for ATEX]	19.72 (from C_d)	19.72 (from C_d)	28.13 (from flow rate)	31.75 (from flow rate)	27.38 (from flow rate)	21.10 (from flow rate)	24.70 (from flow rate)
downstream location (mm)	200[xxiii]	200	200	200	200	200	200
Post-expansion SMD[xxiv]	80	80	79, 67/350	61 ,76/228	83,76/229	73, 70/212	61, 79/246

Table 3. Experimental data - Touil et al.

Notes on STEP experiments

1. The released material consists of 99.5% propane and 0.5% butane, and was modelled in ATEX/DISC as 100% propane.

2. The release considered was that of a 'blowdown', i.e. an inherently transient case, However the authors claim that PDA data taken throughout the release is also valid for consideration of the 2-phase 'quasi-steady' region also.

3. The authors needed to use 'protection cylinders' to ensure high quality data. This provides a certain degree of intrusion and obstruction, which can influence measurements. The authors are aware of this, and tentatively claim that shielding the spray is likely to provide a 20% underestimate of droplet size, which is taken into account in the figures quoted within.

[xxii] CHECK. To check that indeed pressures in paper by Touil are gauge pressure and not total pressure.

[xxiii] The paper provides the SMD as a function of distance from the nozzle for the butane experiments. For BU-OR it increases from 80 to 120µm between 0 and 1100mm distance from the nozzle. For BU-PI it varies between 60-120µm between 0 and 700mm distance. The given values correspond to 200mm from the nozzle.

[xxiv] For the water experiments, the first figure is the quoted figures in the paper. The second figure is the SMD for the droplets with D < 150 µm (the ones with a log-normal distribution), while the third figure is for the entire droplet population, including the few large droplets (150 µm < D < 600 µm). The latter two figures are from private communication with Prof. Bigot.

4. Only initial conditions are presented for one of the release conditions, for which most experimental data are presented. This corresponds to the case of 5 mm, 11 bara initial pressure for which the results are summarised in Figure 7[xxv] in the paper by Hervieu and Veneau[9]. From this figure the following follows:

    a. After an initial rapid pressure drop, liquid release occurs between 1 and 6 seconds, with the gauge pressure gradually decreasing from 10 barg to 9.5barg. Therefore the total storage pressure (P1) over this period is taken to be the averaged pressure of 10.75 bara. Saturated conditions are assumed for the storage rate, with the saturated vapour temperature at this pressure being 29.8C[xxvi].
    b. The observed flow rate over this period is approximately 0.2 kg/s. From this the ATEX orifice velocity is determined (assuming 100% liquid).

5. In the paper it is noted that the conditions in the expansion tank are selected such that the 'inside pressure elevation' does not exceed 1 bar. As a result, the 'ambient conditions' correspond to a pressure of less than 1 bar, and the value of 0.9 bar is selected. Moreover an ambient temperature of 20C was presumed.

6. The value of L appears not to be mentioned in the paper. The value of L/D is assumed to be sufficiently small, and therefore L/D=0 is selected.

7. The results for the SMD (d_{32}) are included in Figure 9b and Table 2 in the paper by Hervieau and Veneau. Those measured at 60mm and 90mm are 31.2 and 27μm, respectively, with corresponding mean velocities of 26.02 and 31.84 m/s, respectively.

Notes on HSL experiments

1. The droplet size data is generated using the laser diffraction technique (Malvern Analyser) outside of its usual range of applicability. The author attempts to re-process the data to provide quantitative analysis, but his results should still be regarded with a degree of caution.

2. The data is effectively presented in terms of droplet size distribution, and hence the global SMD has had to be derived assuming a form of the size distribution function proposed during the course of this programme.[xxvii]

3. The flow rate equals 0.09 kg/s. From this the ATEX orifice velocity is determined (assuming 100% liquid).

Notes on Phase II Cardiff experiments

1. The experimental measurements were taken under quasi-steady state conditions. However, given that (and as confirmed by the von Karman data) significant reduction in SMD over small changes in superheat temperature (2° C) during transitional superheat conditions occur, additional PDA data for transitional conditions is required, with improved control of pressure and temperature.

2. Storage temperature of 155C is presumed in DISC runs corresponding to the orifice temperature (immediately upstream of the orifice). The total pressure of 11 bar (Cardiff 1) and 11.5 bar (Cardiff 2) is taken as storage pressure in DISC.

3. The discharge coefficient C_d is characterised as the ratio of the actual discharge through the orifice to the ideal value. The discharge coefficient is chosen $C_d = 0.70$ (Cardiff 1) and 0.75 (Cardiff 2). The velocity is subsequently set as follows:

$$u_o = C_d \sqrt{\frac{2(P_{st} - P_a)}{\rho_{Lo}}} \qquad (47)$$

$$C_d = \frac{4Q}{\pi d_o^{\,2} \sqrt{2\rho_{Lo}(P_{st} - P_a)}} \qquad (48)$$

[xxv] DOC. Ideally this Figure should be scanned into the current document.

[xxvi] The reported averaged temperature measurements over this period in the discharge line are around 30C, but selection of this temperature would lead to vapour! As a result, saturated conditions are selected (29.8C) which are very close. In line with this, the ambient temperature is selected 30C.

[xxvii] DOC. Choice of data needs extra.

Notes ad VKI experiments

1. Externally pressurised nitrogen is used to control pressure within the vessel. Whilst this is considered a reasonable experimental approach at this stage, an ideal system would eliminate totally the potential of dissolved gases influencing the process.

2. The released material is R134-A, which corresponds to 1,1,1,2-tetrafluoroethane[28] and has CAS ID 811972.

3. The global SMD values quoted have been estimated from the spatially distributed SMD values quoted in the paper. The data from Figure 7 in the paper by Yildiz et al.[27] have been selected. These correspond to a 1mm nozzle experiment with a gauge backpressure of 7.0-7.5 bars and a superheat of 49 C[xxviii] (with SMD measurements at 187mm).

4. The value of L appears not to be mentioned in the paper. The value of L/D is assumed to be sufficiently small, and therefore L/D=0 is selected.

5. The ATEX orifice velocity is determined using a discharge coefficient $C_d = 0.75$ and Equation (47).

Notes on experiments by Touil et al.

1. The experiments with butane were made at INERIS and all information from this are directly provided from the paper by Touill. For the water experiments additional information was obtained from Professor Pierre Bigot (Private Communication) regarding the value of the ambient temperature and the SMD values. He also provided an experimental value of the (steady-state) flow rate (kg/s of released water). The orifice velocity (pre-expansion velocity just inside the nozzle) was not measured.

2. It was indicated that the water is sub-cooled in the tank. Orifice or pipe is directly linked to the tank (no pipe between tank and test section). Thus the liquid fraction equals 100% at both pipe and orifice entrance.

3. In the paper the SMD was indicated as function of distance from the nozzle. The figures below (from Bigot, Private Communication) indicate the droplet velocity as function of downstream distance from the orifice (L/D=0) or the pipe (L/D=50).

4. For the butane experiments, the ATEX orifice velocity is determined using a discharge coefficient $C_d = 0.75$ and Equation (47). It is not needed for the water experiments since the flow rate is known for these experiments.

[xxviii] CHECK. A superheat of 49C corresponds to a temperature of 23C, since the boiling temperature of R134-A equals -26C. This has been applied as the storage temperature in DISC, but the temperature mentioned in the VKI experiment may refer to the orifice temperature. To further check.

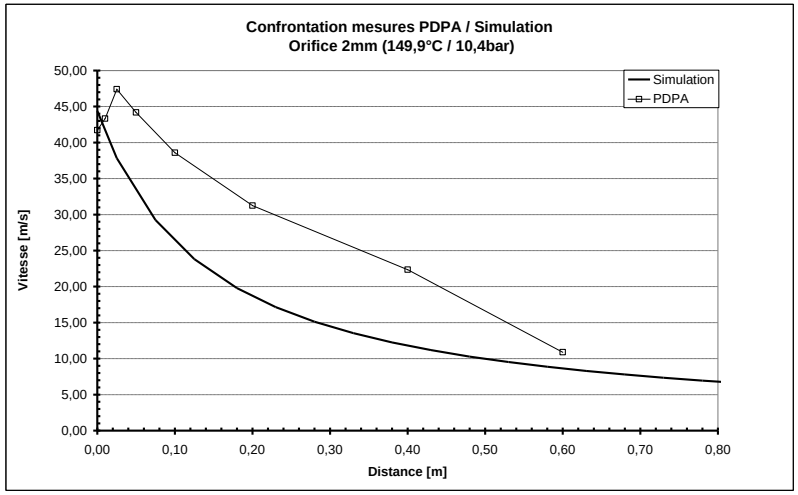

(a) not modelled in this report

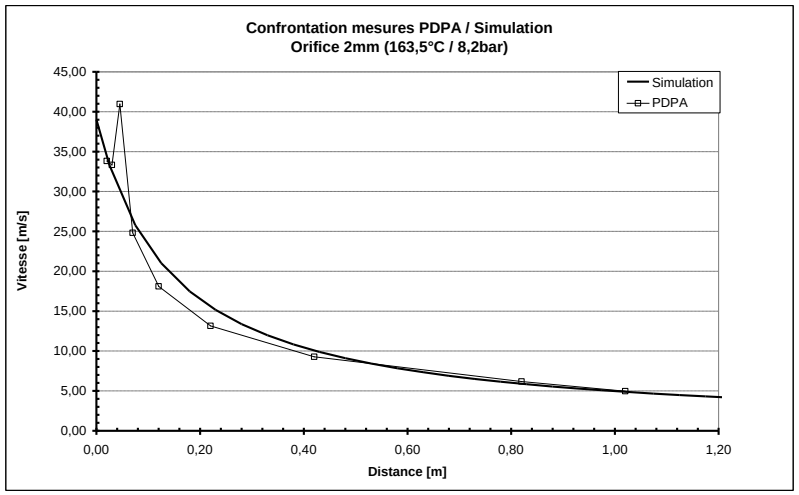

(b) WA-OR1

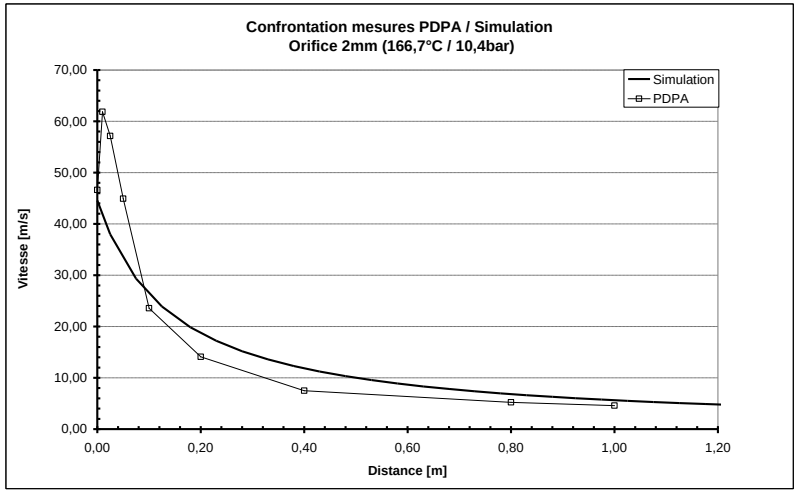

(c) WA-OR2

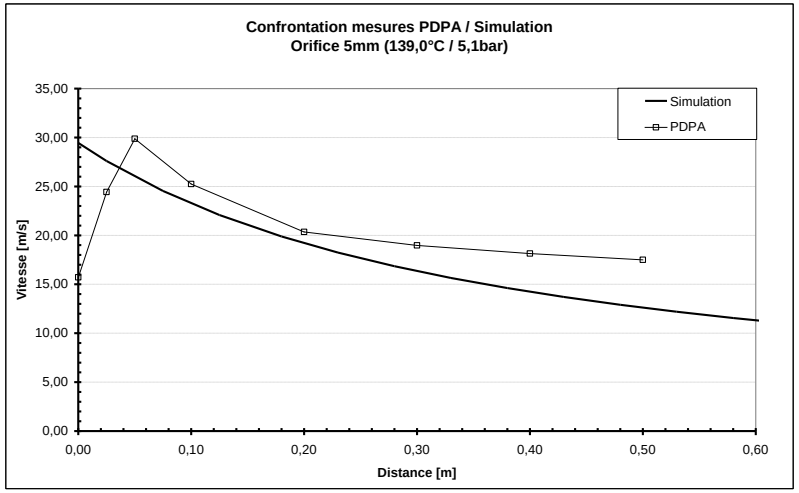

(d) not modelled in this report

Fig 3.2.5 : development of the axial velocity downstream of the orifice; modelled by Bigot (simulation) versus experimental (PDFA)

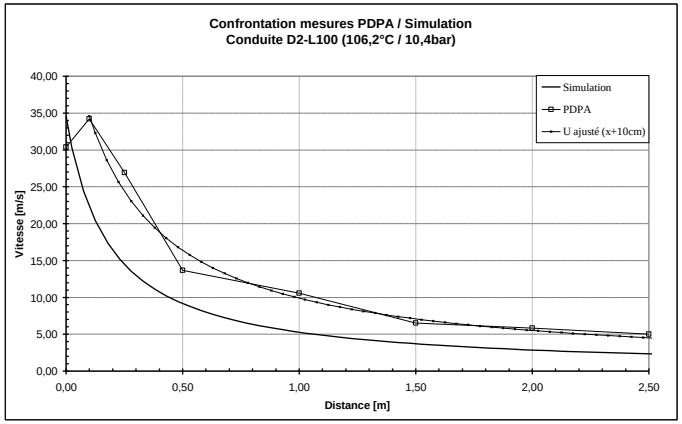

(a) not modelled in this report?

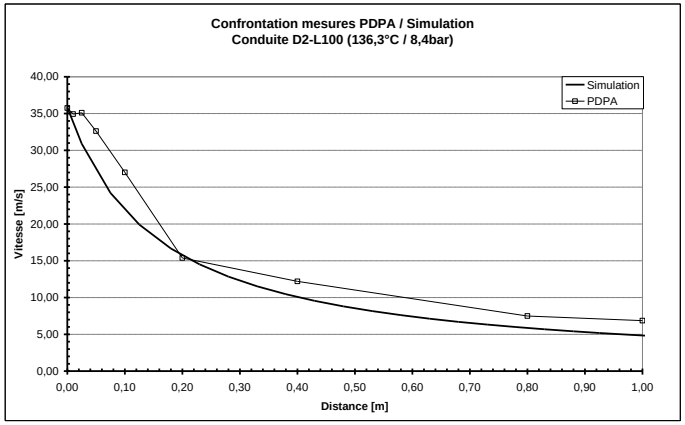

(b) WA-PI1

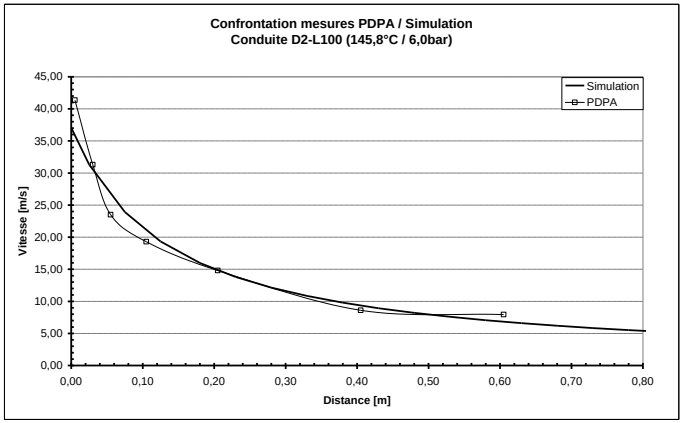

(c) not modelled in this report?

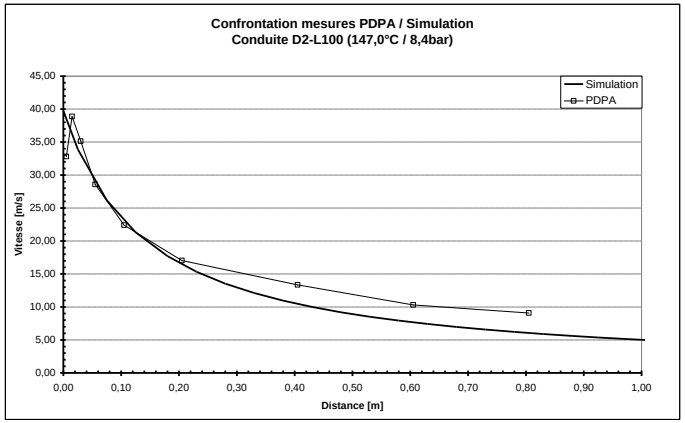

(d) not modelled in this report?

Fig 3.2.6 : development of the axial velocity downstream of the pipe; modelled by Bigot (simulation) versus experimental (PDFA)

3.1.3 Observed versus predicted SMD's; other DISC predictions

Table 4 includes the experimental SMD measurements as well as results from ATEX and DISC simulations.

Note that the experimental SMD measurements have all been considered as the post-expansion SMD predicted by ATEX/DISC. The justification for this is further explained below.

SMD correlations for flashing jets have been derived at a reasonable downstream distance after jet break-up phenomena have been completed, and also far enough downstream so that measurements are not limited optically by spray density issues. As flashing jets break-up considerably earlier than those undergoing mechanical break-up, well-established sprays may be presumed considerably closer to the exit orifice in the former case. By comparison with other published data on droplet size for flashing jets, the only data-set which is quoted significantly upstream from the 250mm location is the STEP data, which itself is then limited by flow field obstructions to mitigate the dense-spray issue. The VKI dataset is obtained within a similar downstream region (187mm), and so is comparable with the Cardiff dataset. The HSL data is double the downstream distance of the VKI and Cardiff datasets, probably again due to optical limitations using the laser diffraction technology. Hence, the downstream distances utilised in obtaining the Cardiff and VKI datasets are considered a good compromise given the current experimental limitations, and are justified at this stage as best estimates for source term SMD droplet size. These may be overcome in future using the new generation of optical diagnostic techniques, specifically designed for dense spray measurements.

Table 4. Observed versus predicted SMD's; other DISC predictions

Experiment	STEP	HSL	VKI	Phase I Cardiff 1	Phase II Cardiff 2
Experimental measurements					
Downstream location (mm)	95	500	187	250	250
Post-expansion SMD	27.0*1.2=32.4	50	80-100	63	60
ATEX SMD predictions (µm)					
Yellow Book (cons. momentum)	531	926	286	680	564
Yellow Book (isentropic)	4.6	5.8	15.1	21.2	21.0
CCPS flashing (isentropic)	97.2	129	197	119	119
CCPS mechanical (isentropic)	3.8	4.8	12.6	17.6	17.5
JIP–II	26.3	29.2	28.7	30.0	29.9
Proposed JIP–III	75	77	77	77	77
Melhem	8.4	12.4	30.9	31.9	31.9
DISC predictions					
Metastable orifice velocity	63.9	50.8	34.5	46.8	45.6
Orifice liquid mass fraction[29]	0.9445	0.957	1	1	1
Flow rate	0.131	0.0693	0.0156	0.0179	0.00978

[29] Although DISC was run with 'flashing enabled' for JIP-II results, the predicted amount of flashing between stagnation and the orifice is still relatively small.

Table 5. Observed versus predicted SMD's; other DISC predictions (Experiments - Touil et al.)

Experiment	BU-OR	BU-PI	WA-OR1	WA-OR2	WA-PI1	WA-PI2	WA-PI3
Experimental measurements							
Flow-rate (kg/s)	?	?	*0.08*	*0.09*	*0.08*	*0.06*	*0.07*
Downstream location (mm)	200[30]	200	200	200	200	200	200
Post-expansion SMD	80	80	79, 67/350	61 ,76/228	83,76/229	73, 70/212	61, 79/246
ATEX SMD predictions (µm)							
Yellow Book (cons. moment.)	487	487	888	694	948	1590	1140
Yellow Book (isentropic)	36.0	36.0	15.2	13.8	48.7	15.4	13.8
CCPS flashing (isentropic)	264	264	97.9	90.6	180	97.9	90.6
CCPS mechanical (isentropic)	30.0	30.0	12.7	11.5	40.5	12.8	11.5
JIP–II	522	502	28.8	28.2	382	29.3	28.7
Proposed JIP–III	370	593	76	76	79	77	76
Melhem	29.6	29.6	26.2	25.0	47.8	26.4	24.9

Figure 5, Figure 6, Figure 7 and Figure 8 include SMD graphs as function of superheat corresponding to the Phase II Cardiff 1 (water), Phase II Cardiff 2 (water), STEP (propane) and VKI (R-134A) experiments, respectively.
Figure 9 and Figure 10 include results for the INERIS butane experiments; Figure 11, Figure 12, Figure 13, Figure 14 and Figure 15 include results for the Ecole de Mines water experiments.

The figures include the experimental data point, and the following SMD correlations:

- the proposed new JIP-III correlation
- the JIP-II correlation
- the CCPS mechanical break-up and flashing correlation; note that the CCPS advises to use as the droplet size the minimum of these two. Note that in line with the CCPS book the isentropic assumption has been applied for this. The latter would ensure that the CCPS flashing criterion will match the CCPS rainout data (see later on in this report).
- the TNO Yellow Book correlation either based on conservation of momentum (as stated in the Yellow Book) or conservation of entropy (alternative assumption aligned with the CCPS book).
- the combined Melhem mechanical and flashing correlations with droplet sizes selected based on the CCPS minimum droplet size criterion.

The following can be concluded:

1) TNO Yellow Book droplet size correlation

   a) In conjunction with the conservation of momentum assumptions (as proposed in the new Yellow Book) it results overall in significant over-prediction of the droplet size.
   b) The TNO Yellow Book correlation in conjunction with the isentropic assumption results overall in significant under-prediction of the droplet size.
   c) In case the frozen (meta-stable) liquid assumption would not be applied (and DISC would need to be applied instead of ATEX) different conclusions could be obtained.

2) CCPS droplet size correlation

   a) In case the CCPS correlation is applied in conjunction with the frozen-liquid assumption and conservation of momentum assumption is was seen that the droplet size was in general largely over-predicted. As a result, in line with what was done in the UDM runs for the RELEASE book, the CCPS correlation should be applied with the frozen-liquid assumption in conjunction with the isentropic assumption.
   b) The CCPS book erroneously advises to take the minimum of the mechanical break-up and the flashing break-up correlation. This assumption results in incorrect prediction of CCPS rainout (see later on). For the current validation also it results in incorrect behaviour for increasing superheat. As can be seen from the figures, in the sub-cooled region it may pick up the mechanical break-up criterion while in the superheated region it may pick the flashing correlation. Moreover for several cases at low superheat the flashing droplet size results in a larger value than the mechanical droplet size. The above demonstrates the need for an appropriate transition criterion as is applied in the newly proposed JIP correlation.

[30] The paper provides the SMD as a function of distance from the nozzle for the butane experiments. For BU-OR it increases from 80 to 120µm between 0 and 1100mm distance from the nozzle. For BU-PI it varies between 60-120µm between 0 and 700mm distance. The given values correspond to 200mm from the nozzle.

c) The CCPS correlation overall results in too large predictions of the droplet size except for Bigot's water experiments for which close agreement was obtained with the experimental data.

3) JIP-II correlation

a) For the Cardiff experiments naturally close agreement is obtained with the JIP-II correlation, since the correlation was fitted to these experiments. For the STEP experiment also close agreement is obtained.
b) For VKI and Bigot's water orifice experiments the JIP-II correlation under-predicts. The accuracy of the new correlation could be further improved by modifying the slope during transition.
c) For the Ecole de Mine water pipe experiments, the current runs are carried out using the vessel leak assumption, which may not be considered to be appropriate given the large L/D ratio. As a result it could be recommended to carry out instead DISC runs using the line rupture scenario.

4) New JIP-III correlation

a) The predicted droplet sizes based on the new JIP-III correlation give overall best agreement with measured data from all experiments considered when compared with predictions from other droplet size models.
b) For the STEP, Ecole de Mine low-pressure butane releases[31] and Cardiff (Phase II) experiments, the new JIP-III correlation over-predicts, albeit marginally, for the STEP and Cardiff experiments.
c) The predicted droplet sizes based on the new JIP-III correlation show excellent agreement with the VKI R134-A and Ecole de Mine water experiments, all of which are predicted to lie in the fully-flashing droplet break-up regime.

5) Melhem correlation

a) Generally under-predicts experimental data with an average deviation of 61% and maximum deviation of 75%.[32]
b) When compared with the CCPS mechanical correlation:
   i) Predicts very close results in the sub-cooled regime
   ii) Predicts similar profiles for droplet size as a function of superheat in the superheat region
   iii) Predicts larger droplet sizes for the STEP and VKI propane releases
c) When compared with the new JIP-III correlation:
   i) Generally predicts smaller droplet sizes for all regimes.
   ii) Predicts worse or similar droplet sizes when compared with experimental data. This is with exception of the Ecole de Mine low-pressure butane releases.
d) For the Ecole de Mine butane experiments:
   i) Predicts generally smaller droplet sizes when compared to other correlations between $0 < \Delta T_{sh} < 20K$
   ii) Simulated droplet sizes approach the CCPS mechanical and TNO (isentropic) correlations for $\Delta T_{sh} > 20K$
e) For the Ecole de Mine and Cardiff water experiments:
   i) Predicts generally smaller droplet sizes when compared to other correlations between $0 < \Delta T_{sh} < 30K$
   ii) Simulated droplet sizes approach the proposed JIP-III correlation for $\Delta T_{sh} > 30K$

6) Comparison of accuracy of JIP-III and CCPS (flashing) correlations

a) The JIP-III correlation provides the most accurate results for the Cardiff, VKI, Ecole de Mine and STEP experiments, for which the CCPS flashing correlation over-predicts.
b) The JIP-III correlation more severely over-predicts the butane experiments than the CCPS flashing correlation.
c) It seems to be the case that for low stagnation pressures (low velocities) the JIP-III correlation over-predicts. The CCPS flashing correlation has a general trend for over-prediction.

7) Other observations:

a) For Bigot's water experiments at the lower superheats the introduction of flashing in the Yellow-Book and CCPS mechanical break-up criteria (using isentropic assumption) results in the reduction of the post-expansion velocity and therefore an increase of the droplet size. This can be explained using the conservation and energy equations (64), (66):

$$\frac{1}{2}\left(u_f^{\,2} - u_0^{\,2}\right) = h_0 - h_f = h_L(P_o,T_o) - \left\{\eta_{Lf} h_L(P_a,T_f) + \left(1-\eta_{Lf}\right) h_v(P_a,T_f)\right\} \qquad (49)$$
$$= \left[h_L(P_o,T_o) - h_L(P_a,T_f)\right] - \left(1-\eta_{Lf}\right)\left[h_v(P_a,T_f) - h_L(P_a,T_f)\right]$$

[31] The JIP-III correlation is seen to agree very well with more recent INERIS and Cardiff (Phase III) SMD data for butane. It is likely that the Ecole de Mine measurements were unable to capture larger droplets due to resolution limitations of available droplet size measuring technology at the time.

[32] Slightly smaller droplet sizes are simulated where this correlation is applied in conjunction with the frozen fluid and isentropic assumptions as against the frozen fluid and conservation of momentum assumptions. Results of the former have not been presented, while the latter is chosen as the default setting for simulations employing the Melhem correlation.

Because of the frozen liquid assumption, the orifice pressure equals the ambient pressure: $P_o=P_a$. For sub-cooled jets no flashing occurs and the final post-expansion temperature equals the orifice temperature: $\eta_{Lf}=1$, $T_o=T_f$, and therefore both terms between brackets [ ] are zero in the above equation; therefore $u_f=u_{0.}$ For superheated jets both terms between brackets are positive and increasing. For Bigot's water experiments at the lower superheats, the flashing appears to be sufficiently large (using the isentropic assumption) that the second term is dominant. Thus $u_f < u_o$ and this results in an increase of the droplet size.

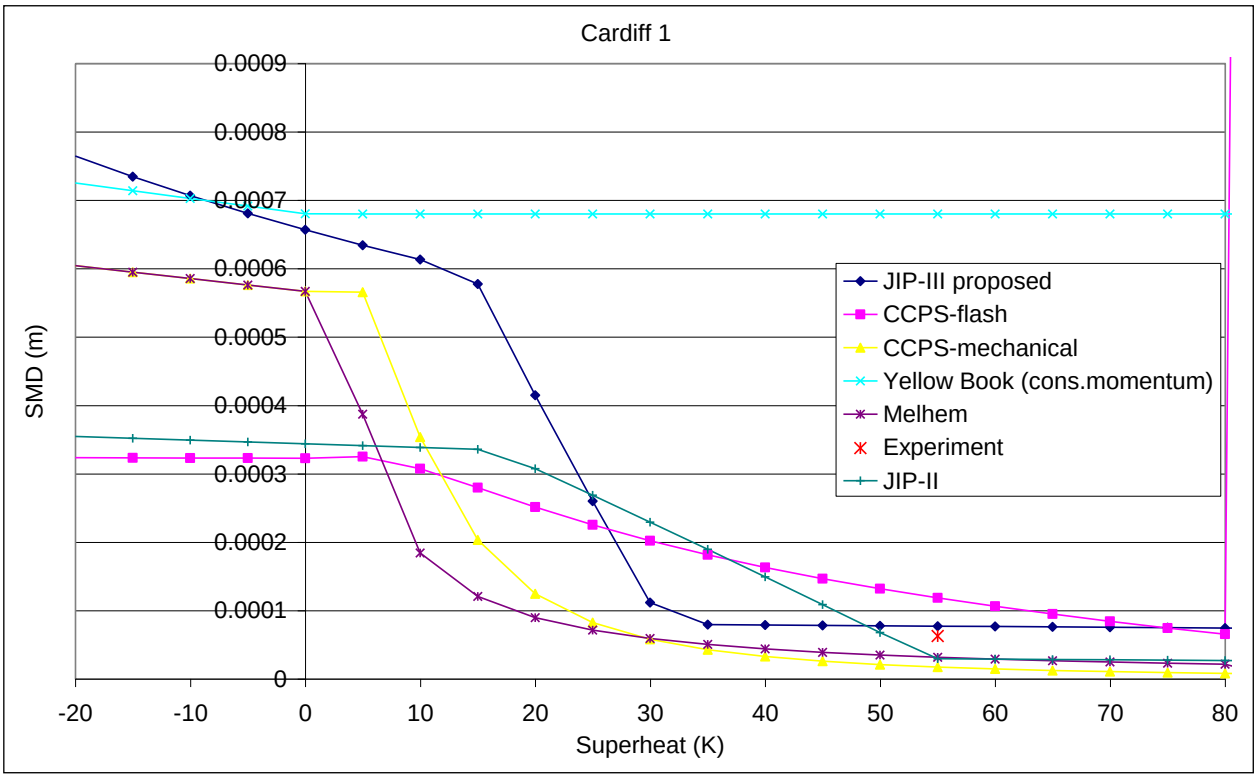

Figure 5. **Validation of ATEX SMD correlations against Phase II Cardiff 1 experiment**

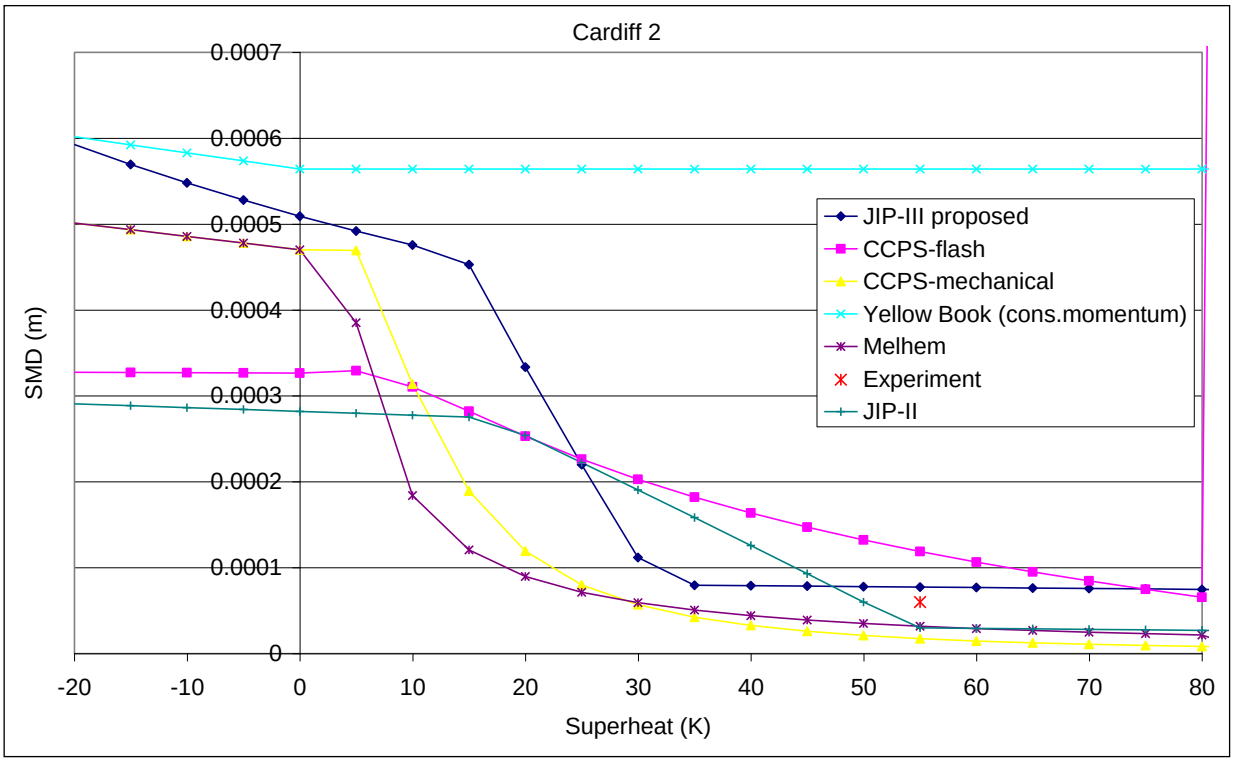

Figure 6. **Validation of ATEX SMD correlations against Phase II Cardiff 2 experiment**

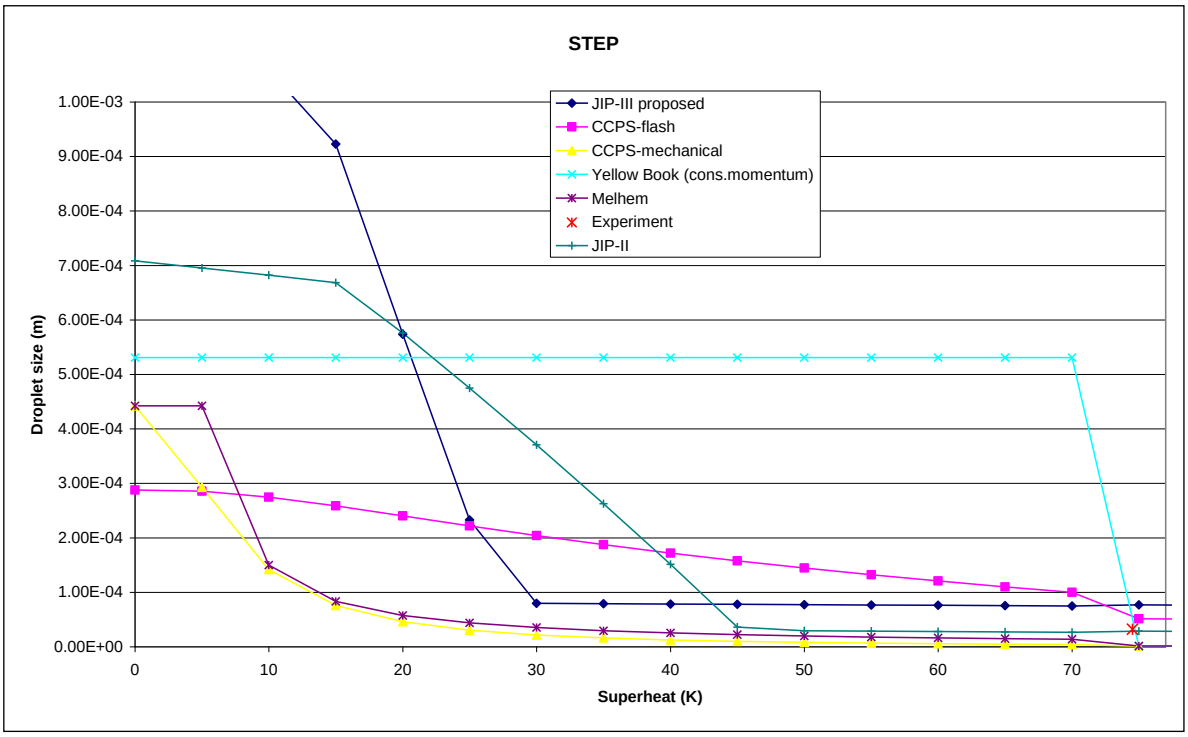

Figure 7. **Validation of ATEX SMD correlations against STEP experiment**

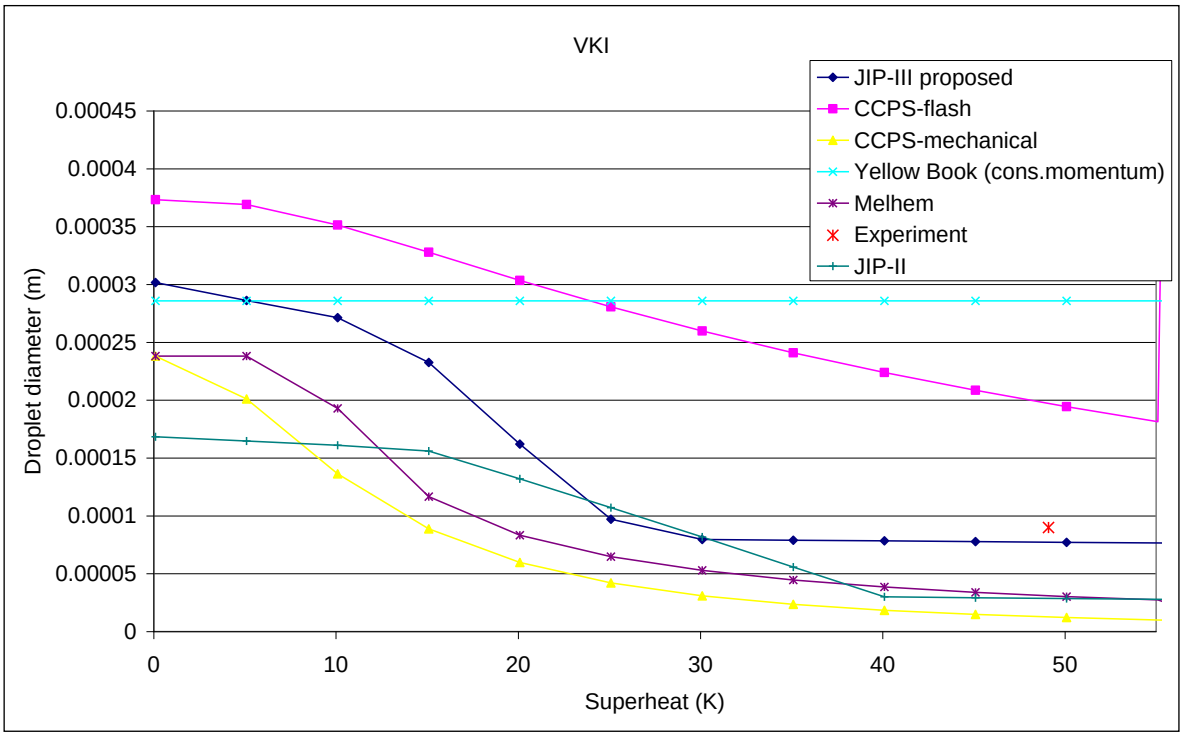

Figure 8. **Validation of ATEX SMD correlations against VKI experiment**

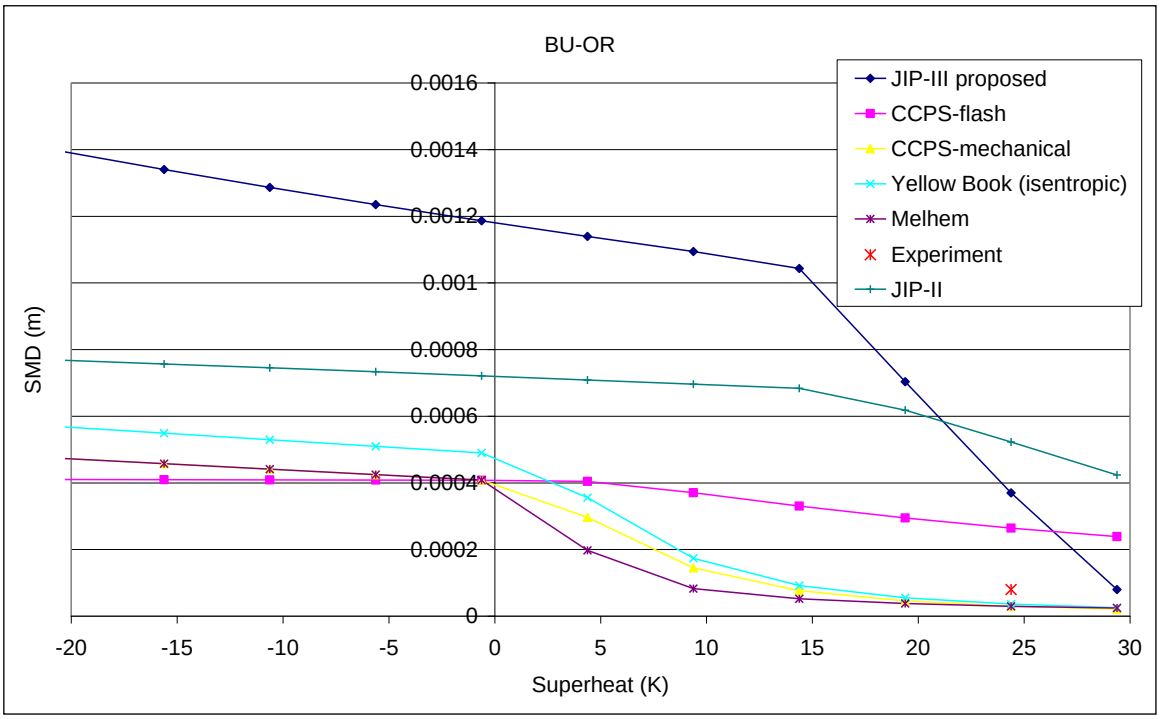

Figure 9. **Validation of ATEX SMD correlations against BU-OR experiment**

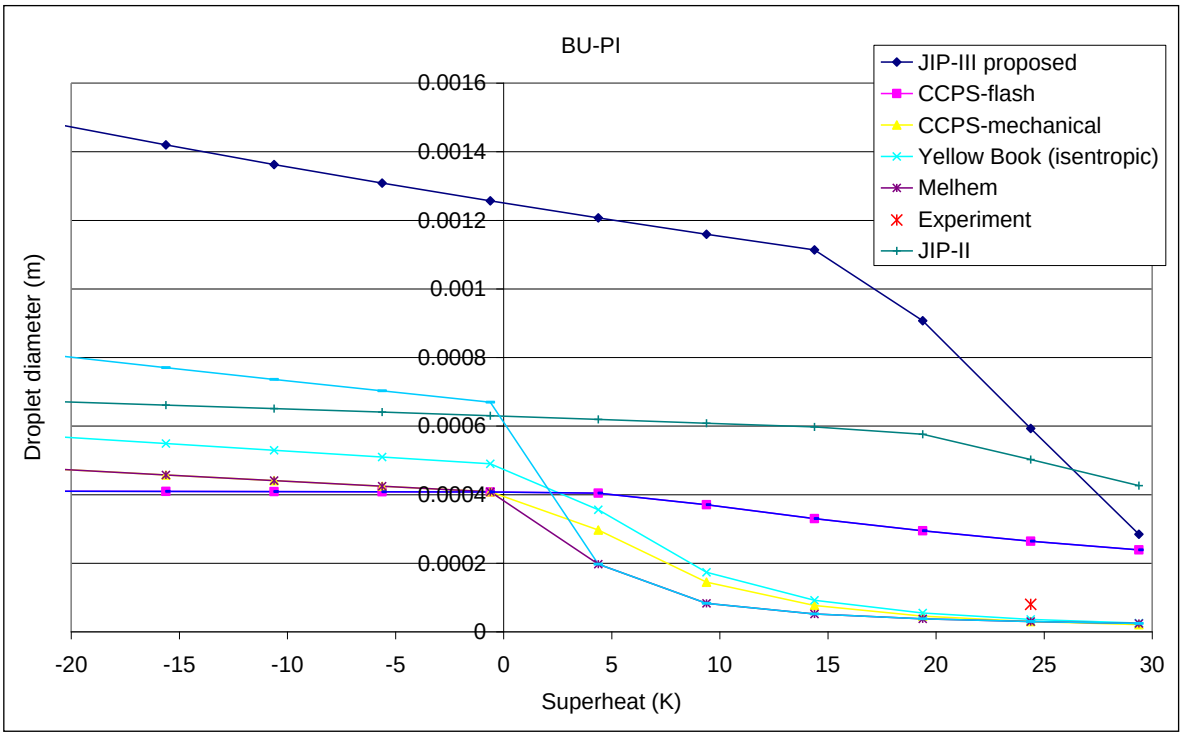

Figure 10. **Validation of ATEX SMD correlations against BU-PI experiment**

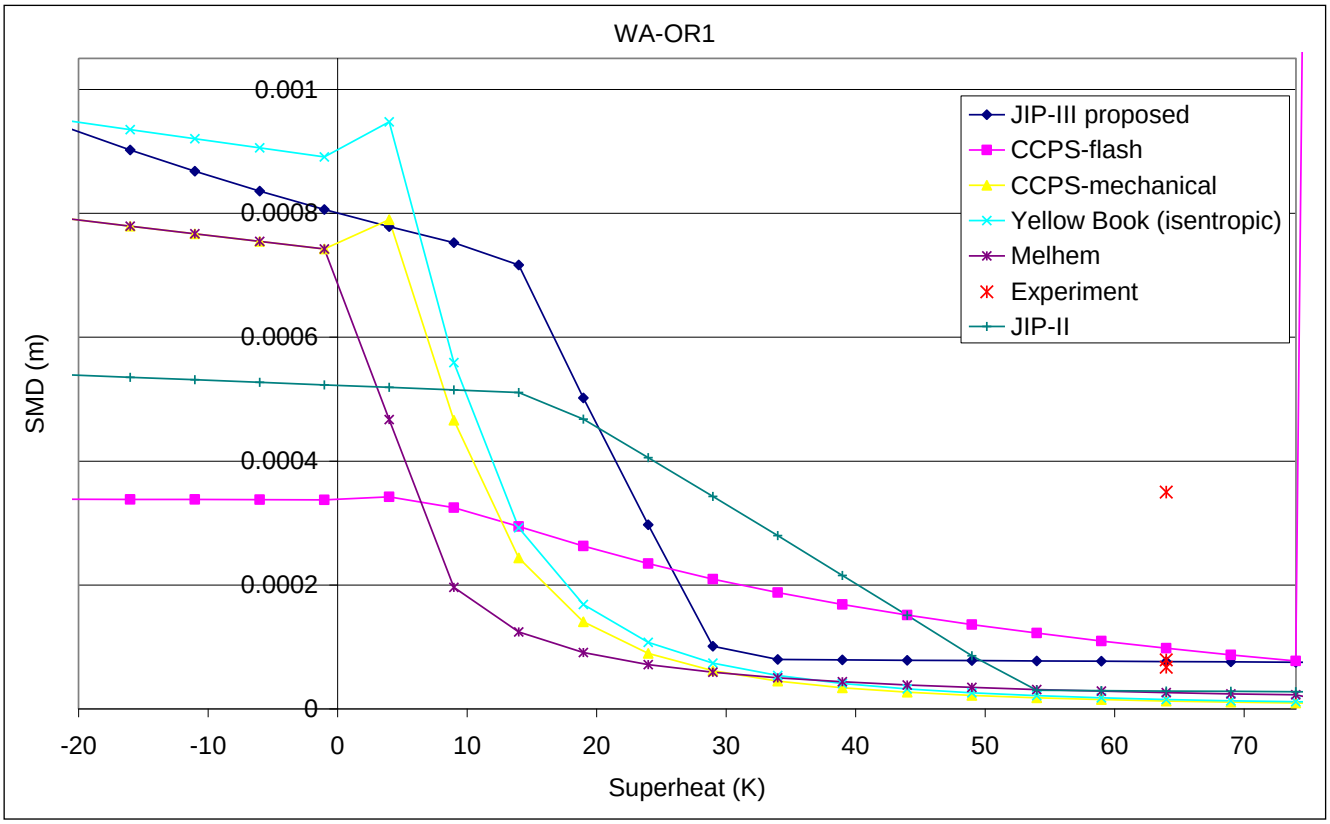

Figure 11. Validation of ATEX SMD correlations against WA-OR1 experiment

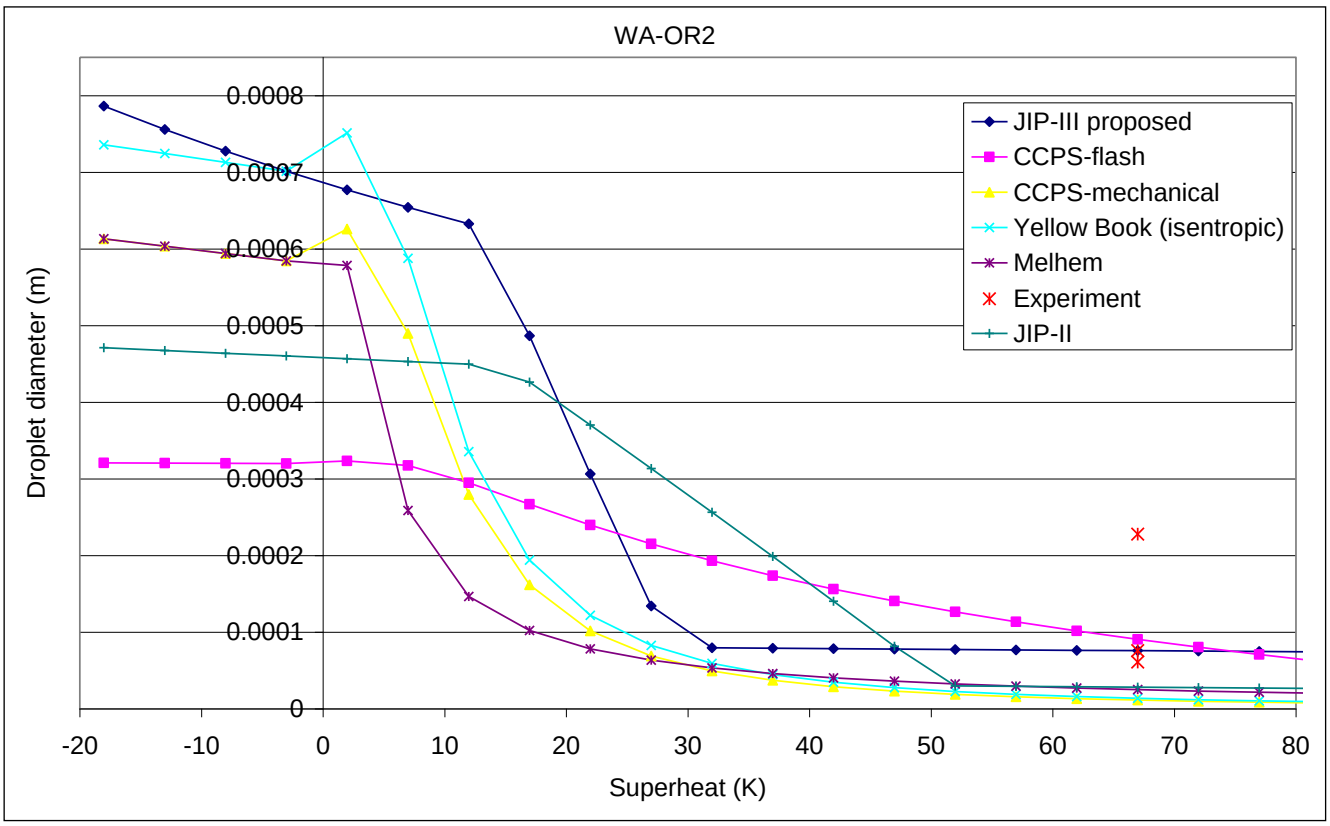

Figure 12. Validation of ATEX SMD correlations against WA-OR2 experiment

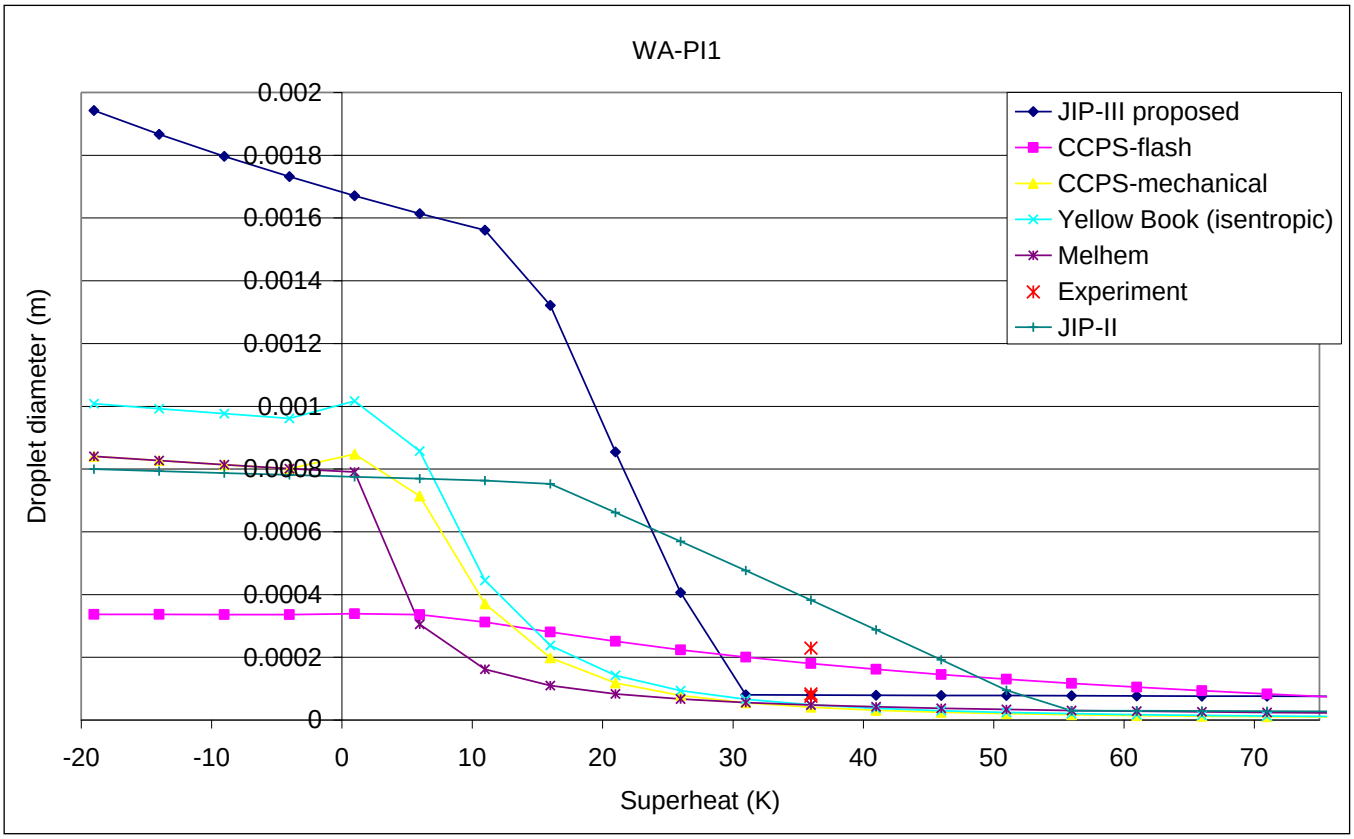

Figure 13. Validation of ATEX SMD correlations against WA-PI1 experiment

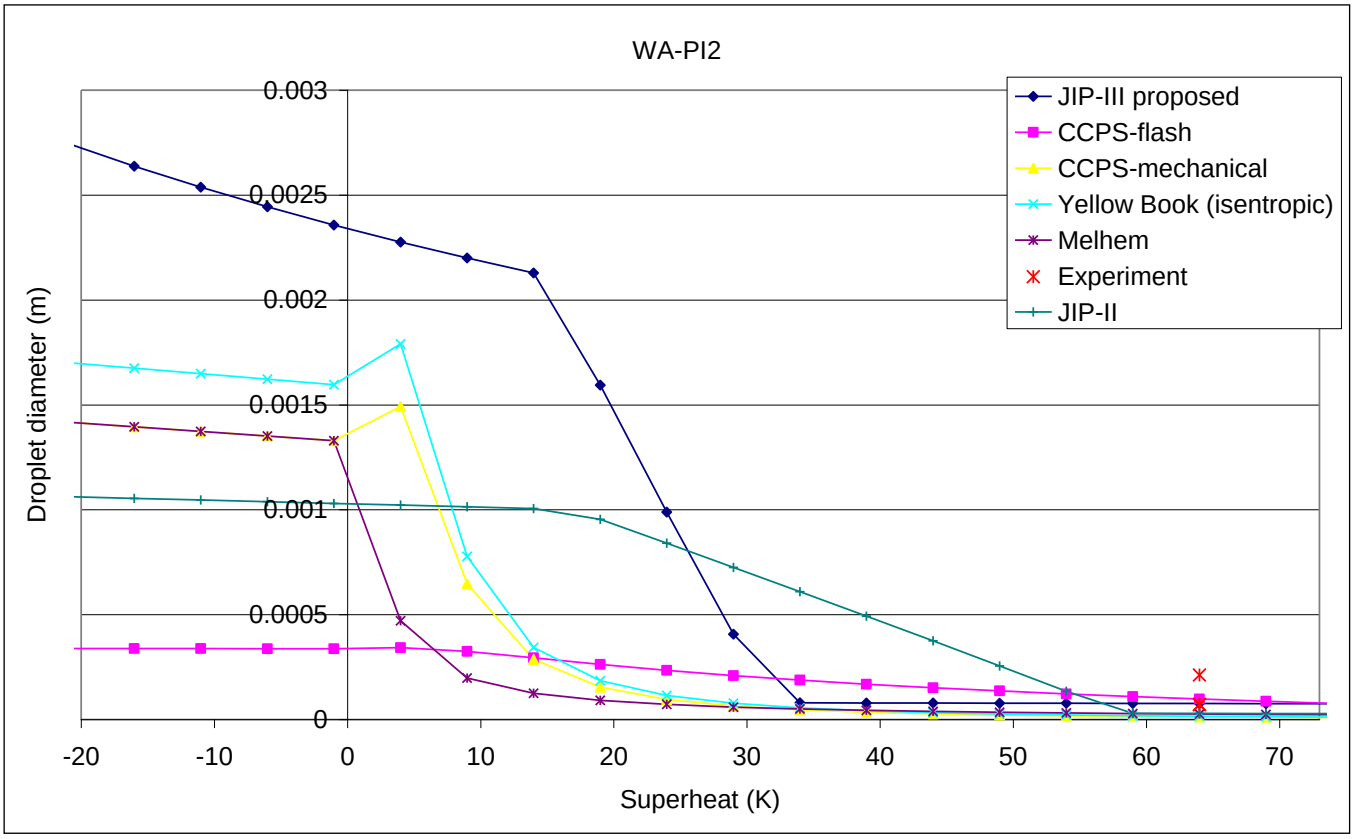

Figure 14. Validation of ATEX SMD correlations against WA-PI2 experiment

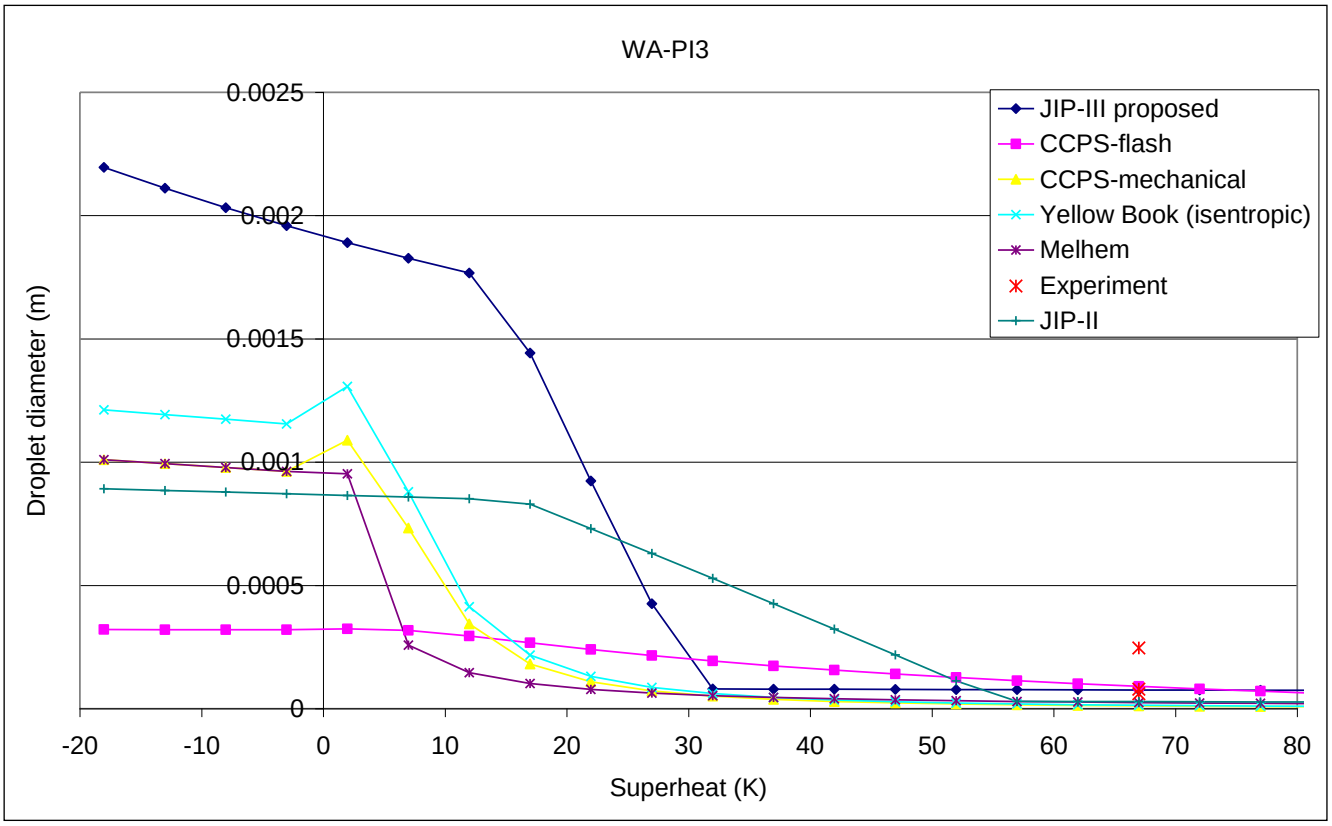

Figure 15. Validation of ATEX SMD correlations against WA-PI3 experiment

3.2 DISC validation for droplet size and flow rate (Phase III Cardiff experiments)

As part of the Phase III project, scaled experiments for water, gasoline, cyclo-hexane, propane and butane were carried out at Cardiff University. This involved both flow rate and droplet size measurements across a wide range of superheats covering the mechanical to the fully-flashing break-up regimes. The work involved the following:

- Experiments for water including variation of superheat. These were required to further validate and possibly improve the SMD correlation as a function of superheat. Two experiments (involving different orifice sizes, 0.75 mm and 1 mm) were carried out where droplet size measurements were taken across the full relevant range of superheats. These measurements were taken using new advanced PDA technology for dense sprays recently acquired by Cardiff University.

- Additional experiments for other chemicals than water, i.e. cyclo-hexane, propane and butane (orifice sizes up to 2 mm). This included measurement of flow rate, accurate characterisation of discharge and added near-field downstream measurements (droplet distribution). In addition to these cyclo-hexane, propane and butane experiments, also a limited number of gasoline experiments were carried out to provide preliminary indications of how useful the methodology is for multi-component fluids.

Table 6 presents a summary of experimental conditions for the Cardiff water, gasoline, cyclo-hexane, propane and n-butane experiments.

The following presents the results of the validation of the DISC droplet size and flow rate predictions against measured data from the Phase III Cardiff water, cyclo-hexane, butane, propane and gasoline experiments. Predicted droplet sizes based on the Phase II and Phase III (proposed) are compared against experimental data. Simulated flow rates are based on the default PHAST 6.53 method (i.e. “PHAST 6.53 (old method-No Flashing)”: meta-stable liquid assumption). Further details on the experimental set-up and description of the adopted discharge model can be found in Part A and Part C1 of the Phase III report.

Table 7 to Table 13 detail experimental conditions, measured plus DISC simulated flow rate and droplet size data for the Cardiff water, cyclo-hexane, gasoline, n-butane and propane experiments respectively. Predicted droplet sizes based on the Phase II and Phase III (proposed) are also compared against experimental data.

From Table 7 to Table 13, it can be seen that:

- The Phase II droplet size correlation generally under-predicts droplet sizes when compared with measured data (and the Phase III correlation). The JIP-II droplet size correlation is generally observed to under-predict measured data by about 50% on average. This is with exception to simulated droplet sizes for n-butane experiments where the Phase II correlation is seen to over-predict by about 60% on average.
- The Phase III (JIP-III) correlation is seen to generally agree better with measured data when compared with the JIP-II correlation.

Figure 16 to Figure 19 show the performance of the JIP-III, JIP-II and CCPS (Phast 6.53.1 default) droplet size correlations against the Cardiff Phase III SMD measurements for the water, cyclo-hexane, butane, propane and gasoline experiments. It can be seen that the Phase III correlation:

- gives overall best agreement with measured data when compared with the Phase II and CCPS (Phast 6.53.1) correlations. The CCPS and JIP-II correlations generally under-predict measured data with the CCPS correlation performing worst of the 3 correlations.
- generally under-predicts SMD data for multi-component mixtures (i.e. Gasoline)
- tends to marginally over-predict SMD data below 500 µm
- tends to marginally under-predict SMD data above 500 µm
- Simulated data based on the JIP-III correlation is seen to generally lie within ± 30% of measured data.

The results presented in Table 7 to Table 13 are further illustrated in
Figure 20 to Figure 29. These compare DISC simulated droplet size data based on the JIP-III correlations against measured SMD data for the Phase III Cardiff water, cyclo-hexane, and n-butane and propane experiments.

Figure 20 to Figure 22 also compare predicted SMDs based on the Phase-II and Phase-III correlations against the Cardiff Phase III experiments for water (0.75 mm and 1 mm) and cylco-hexane (1 mm) respectively, where:

- The Phase III SMD model is seen to agree better with measured SMD data particularly in the transition and fully-flashing break-up regimes.
- The seemingly poor agreement of the Phase II and Phase III correlations in the mechanical break-up regime is due to the location of the PDA measuring device at distances optimised for transition and fully-flashing as

against mechanical break-up SMD measurements (i.e. PDA distances too close to the orifice for accurate mechanical break-up SMD measurements).

Table 6. Phase III Cardiff experiments: experimental conditions

Fuel	Break-up	Diameter (mm)	L/D	Pressure (barg)
Water	Sub-cooled	1	1.01	6, 10, 14
Water	Sub-cooled	2	0.5	6, 10, 14
Water	Flashing	0.75	3.4	10
Water	Flashing	1	4.5	10
Cyclo-hexane	Sub-cooled	0.75	1.4	6,8,10,12,14
Cyclo-hexane	Sub-cooled	1	1.01	6,8,10,12,14
Cyclo-hexane	Sub-cooled	2	0.5	6,8,10,12,14
Cyclo-hexane	Flashing	1	1.01	7.5, 10
Cyclo-hexane	Flashing	2	0.5	10
Gasoline	Sub-cooled	0.75	4.53	6,8,10,12,14
Gasoline	Sub-cooled	1	3.4	6,8,10,12,14
Gasoline	Flashing	1	1.01	10
n-Butane	Flashing	0.75	1.4	10
n-Butane	Flashing	1	1.01	8
n-Butane	Flashing	2	0.5	7
Propane	Flashing	1	1.01	6
Propane	Flashing	2	0.5	7

Table 7. Cardiff water (1,2 mm): experimental data and flow-rate/SMD predictions

	1 mm Tests (L/d = 1.01)			2 mm Tests (L/d = 0.5)		
Test number	**1**	**2**	**3**	**1**	**2**	**3**
Ambient temperature (C)	17	17	17	17	17	17
Ambient pressure (mbar)	1000	1000	1000	1000	1000	1000
Relative humidity (%)	70	70	70	70	70	70
Stagnation temperature (C)	17	17	17	17	17	17
Stagnation pressure (bara)	7.71	10.58	14.75	7.16	11.1	14.77
Mean Measured flow rate (kg/s)	0.0209	0.0254	0.0269	0.0723	0.0896	0.1060
Predicted flow rate (kg/s)	0.0198	0.0236	0.0283	0.0757	0.0970	0.1132
Mean Deviation flow rate (%)	-5.5%	-7.1%	5.1%	4.7%	8.2%	6.8%
Measured Global SMD (µm)	1203	1060	800	1250	1106	967
Predicted SMD (JIP – III) (µm)	949	757	603	1390	1017	835
Predicted SMD (JIP – II) (µm)	488	402	331	699	535	453
Mean Dev. SMD (JIP-III)(%)	-21.1%	-28.6%	-24.7%	11.2%	-8.1%	-13.6%
Mean Dev. SMD (JIP-II)(%)	-59.4%	-62.0%	-58.6%	-44.1%	-51.6%	-53.2%

Table 8. Cardiff cyclohexane (0.75mm): experimental data and flow-rate/SMD predictions

Test set	**Cardiff JIP Phase III: 0.75 mm Cyclo-Hexane tests**				
Test number	**1**	**2**	**3**	**4**	**5**
Ambient temperature (C)	17	17	17	17	17
Ambient pressure (mbar)	1000	1000	1000	1000	1000
Relative humidity (%)	70	70	70	70	70
Stagnation temperature (C)	16	16	16	16	16
Stagnation pressure (barg)	6	8	10	12	14
Mean Measured flow rate (kg/s)	0.0084	0.0098	-	-	0.0111
Predicted flow rate (kg/s)	0.0084	0.0097	0.0109	0.0119	0.0128
Mean Deviation flow rate (%)	0.1%	-0.9%	-	-	15.7%
Measured Global SMD (µm)	442	343	262	331	233
Predicted SMD (JIP – III) (µm)	613	511	444	396	359
Predicted SMD (JIP – II) (µm)	293	251	222	201	185
Mean Dev. SMD (JIP-III)(%)	38.6%	49.0%	69.6%	19.7%	54.4%
Mean Dev. SMD (JIP-II)(%)	-33.8%	-27.0%	-15.1%	-39.1%	-20.3%

Table 9. Cardiff cyclohexane (1mm): experimental data and flow-rate/SMD predictions

Test set	**Cardiff JIP Phase III: 1 mm Cyclo-Hexane tests**				
Test number	**1**	**2**	**3**	**4**	**5**
Ambient temperature (C)	17	17	17	17	17
Ambient pressure (mbar)	1000	1000	1000	1000	1000
Relative humidity (%)	70	70	70	70	70
Stagnation temperature (C)	16.5	16	16	16	16
Stagnation pressure (barg)	5.8	7.73	9.74	11.58	12.66
Mean Measured flow rate (kg/s)	0.0191	0.0227	0.0241	0.0223	0.0241
Predicted flow rate (kg/s)	0.0147	0.0170	0.0190	0.0208	0.0217
Mean Deviation flow rate (%)	-23.1%	-25.3%	-21.0%	-6.9%	-9.9%
Measured Global SMD (µm)	832	676	537	518	486
Predicted SMD (JIP – III) (µm)	678	566	490	439	415
Predicted SMD (JIP – II) (µm)	325	278	246	224	214
Mean Dev. SMD (JIP-III)(%)	-18.6%	-16.3%	-8.9%	-15.1%	-14.4%
Mean Dev. SMD (JIP-II)(%)	-61.0%	-58.8%	-54.3%	-56.7%	-56.0%

Table 10. Cardiff cyclohexane (2mm): experimental data and flow-rate/SMD predictions

Test set	Cardiff JIP Phase III: 2 mm Cyclo-Hexane tests				
Test number	**1**	**2**	**3**	**4**	**5**
Ambient temperature (C)	17	17	17	17	17
Ambient pressure (mbar)	1000	1000	1000	1000	1000
Relative humidity (%)	70	70	70	70	70
Stagnation temperature (C)	17	17	17	17	17
Stagnation pressure (barg)	5.92	8.61	10.69	12.61	15.06
Mean Measured flow rate (kg/s)	0.0533	0.0549	0.0780	0.0838	0.0864
Predicted flow rate (kg/s)	0.0543	0.0675	0.0762	0.0834	0.0918
Mean Deviation flow rate (%)	1.8%	23.0%	-2.3%	-0.5%	6.2%
Measured Global SMD (µm)	966	956	825	717	510
Predicted SMD (JIP – III) (µm)	1099	834	716	639	567
Predicted SMD (JIP – II) (µm)	508	401	352	319	288
Mean Dev. SMD (JIP-III)(%)	13.8%	-12.8%	-13.2%	-10.8%	11.2%
Mean Dev. SMD (JIP-II)(%)	-47.5%	-58.1%	-57.3%	-55.4%	-43.5%

Table 11. Cardiff gasoline (0.75mm): experimental data and flow-rate/SMD predictions

Test set	Cardiff JIP Phase III: 0.75 mm Gasoline tests				
Test number	**1**	**2**	**3**	**4**	**5**
Ambient temperature (C)	17	17	17	17	17
Ambient pressure (mbar)	1000	1000	1000	1000	1000
Relative humidity (%)	70	70	70	70	70
Stagnation temperature (C)	17	17	17	17	17
Stagnation pressure (barg)	6.83	9.44	11.25	12.72	14.53
Mean Measured flow rate (kg/s)	0.0101	0.0115	0.0124	0.0130	0.0135
Predicted flow rate (kg/s)	0.0078	0.0094	0.0104	0.0111	0.0121
Mean Deviation flow rate (%)	-22.5%	-18.1%	-16.3%	-14.7%	-10.2%
Measured Global SMD (µm)	885	796	715	612	608
Predicted SMD (JIP – III) (µm)	297	235	208	191	171
Predicted SMD (JIP – II) (µm)	258	211	190	177	161
Mean Dev. SMD (JIP-III)(%)	-66.4%	-70.5%	-70.9%	-68.8%	-71.9%
Mean Dev. SMD (JIP-II)(%)	-70.8%	-73.4%	-73.4%	-71.1%	-73.6%

Table 12. Cardiff gasoline (1mm): experimental data and flow-rate/SMD predictions

Test set	Cardiff JIP Phase III: 1 mm Gasoline tests				
Test number	1	2	3	4	5
Ambient temperature (C)	17	17	17	17	17
Ambient pressure (mbar)	1000	1000	1000	1000	1000
Relative humidity (%)	70	70	70	70	70
Stagnation temperature (C)	17	17	17	17	17
Stagnation pressure (barg)	6.45	8.99	12.81	12.9	15.04
Mean Measured flow rate (kg/s)	0.0141	0.0229	-	0.0245	0.0253
Predicted flow rate (kg/s)	0.0134	0.0163	0.0198	0.0199	0.0216
Mean Deviation flow rate (%)	-5.1%	-28.9%	-	-18.9%	-14.8%
Measured Global SMD (µm)	472	403	375	382	355
Predicted SMD (JIP – III) (µm)	358	279	218	217	196
Predicted SMD (JIP – II) (µm)	297	240	194	194	177
Mean Dev. SMD (JIP-III)(%)	-24.3%	-30.8%	-41.9%	-43.2%	-44.8%
Mean Dev. SMD (JIP-II)(%)	-37.1%	-40.4%	-48.2%	-49.3%	-50.0%

Table 13. Cardiff butane and propane: experimental data and flow-rate/SMD predictions

	N-Butane Tests			Propane Tests	
Orifice Size (mm)	0.75	1	2	1	2
L/d ratio (-)	1.4	1.01	0.505	1.01	0.505
Ambient temperature (C)	18	18	18	18	18
Ambient pressure (mbar)	1000	1000	1000	1000	1000
Stagnation temperature (C)	17	16	17	16	17
Stagnation pressure (barg)	9.76	8.10	7.36	6.44	7.40
Mean Measured flow rate (kg/s)	0.0106	0.0169	0.0723	0.0167	0.0723
Predicted flow rate (kg/s)	0.0093	0.0150	0.0573	0.0125	0.0537
Mean Deviation flow rate (%)	-12.2%	-11.1%	-20.8%	-24.8%	-25.8%
Measured Global SMD (µm)	91	108	167	62	76
Predicted SMD (JIP – III) (µm)	103	130	159	76	76
Predicted SMD (JIP – II) (µm)	149	189	260	29	28
Mean Dev. SMD (JIP-III)(%)	13.2%	20.8%	-4.9%	22.8%	0.3%
Mean Dev. SMD (JIP-II)(%)	64.0%	75.7%	55.4%	-54.0%	-63.0%

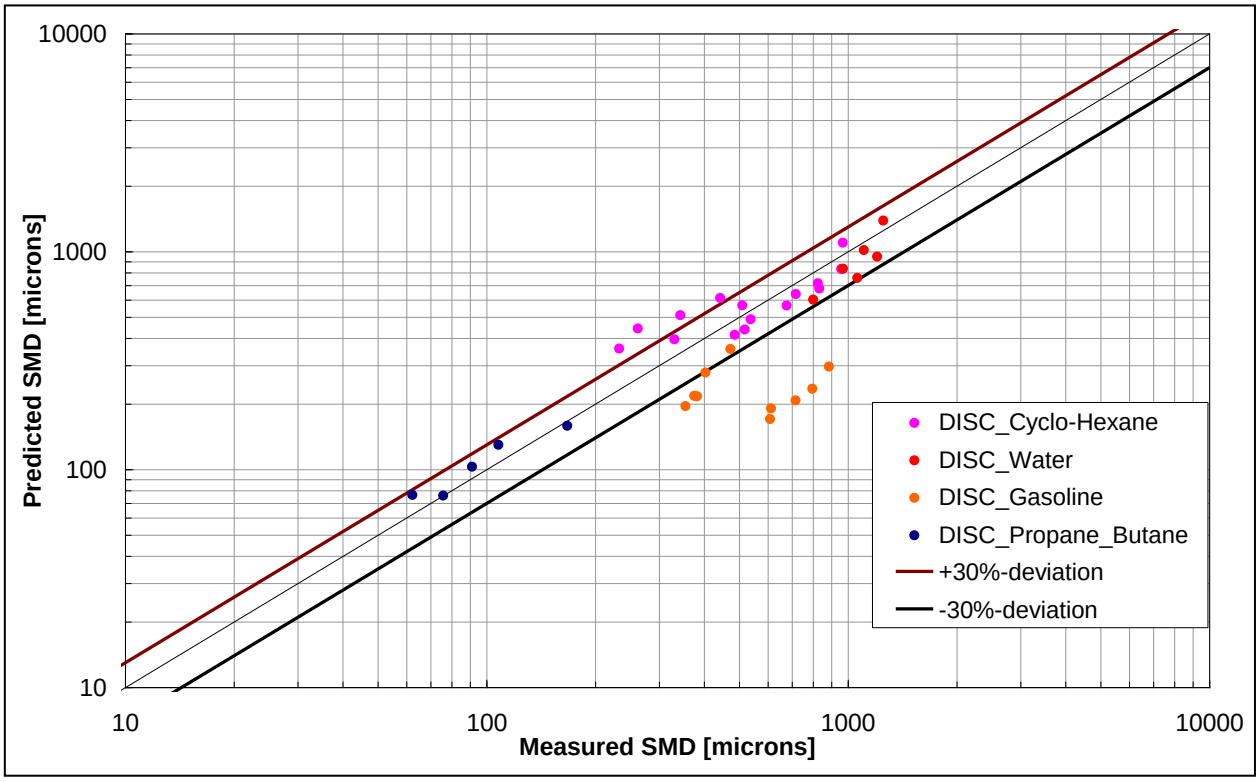

Figure 16. **Performance of JIP-III ATEX SMD correlations against Phase III Cardiff experiments**

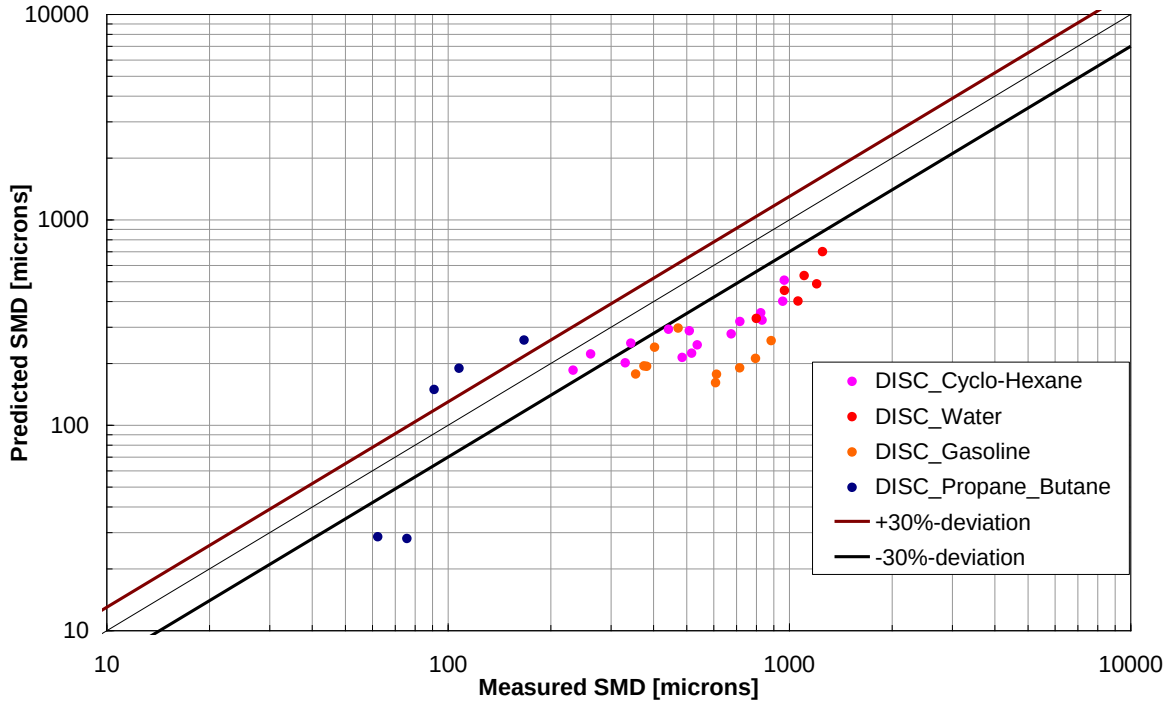

Figure 17. **Performance of JIP-II ATEX SMD correlations against Phase III Cardiff experiments**

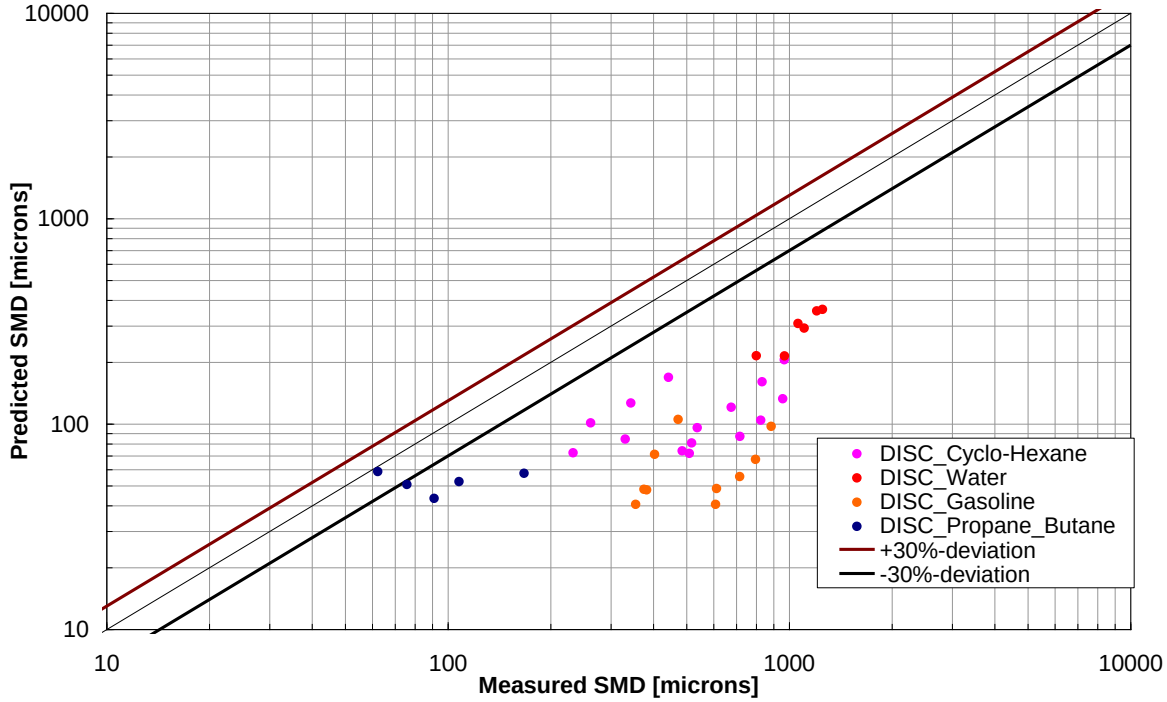

Figure 18. **Performance of the CCPS (Phast 6.53.1) ATEX SMD correlations against Phase III Cardiff experiments**

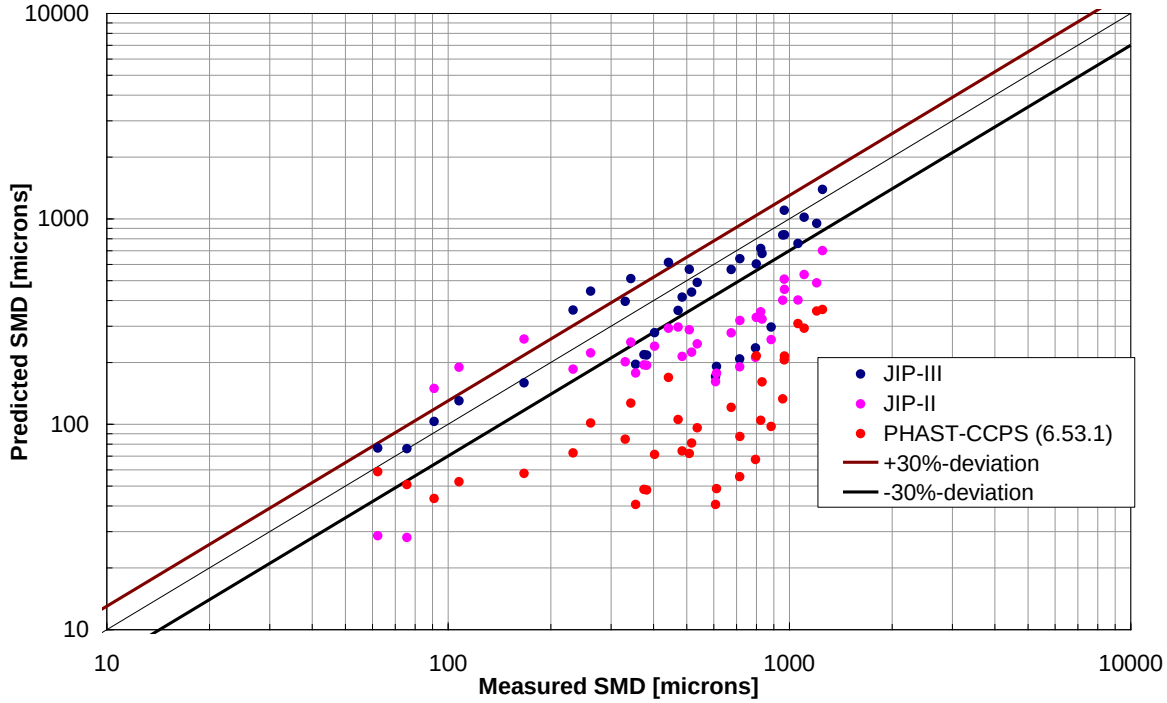

Figure 19. **Overall comparison of the CCPS (Phast 6.53.1), JIP-III and JIP-II ATEX SMD correlations against Phase III Cardiff experiments**

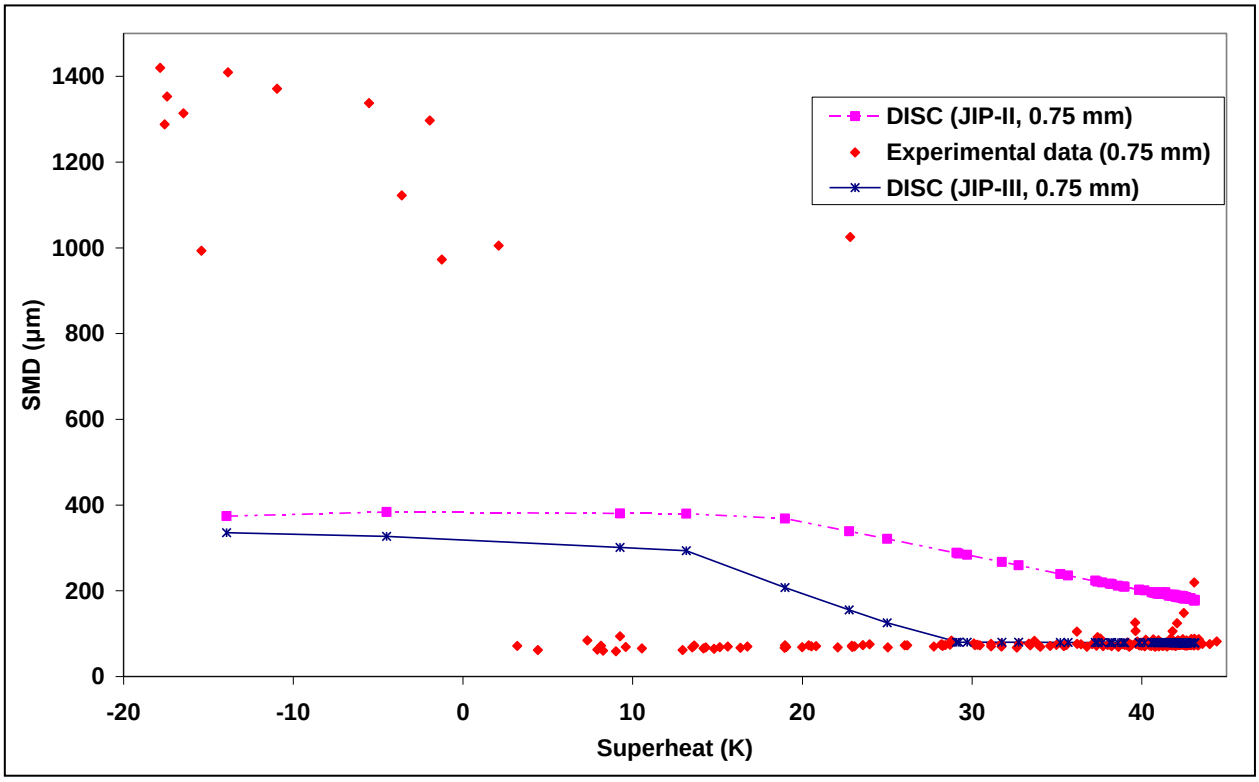

Figure 20. Validation of JIP ATEX SMD correlations against Cardiff water (0.75mm)

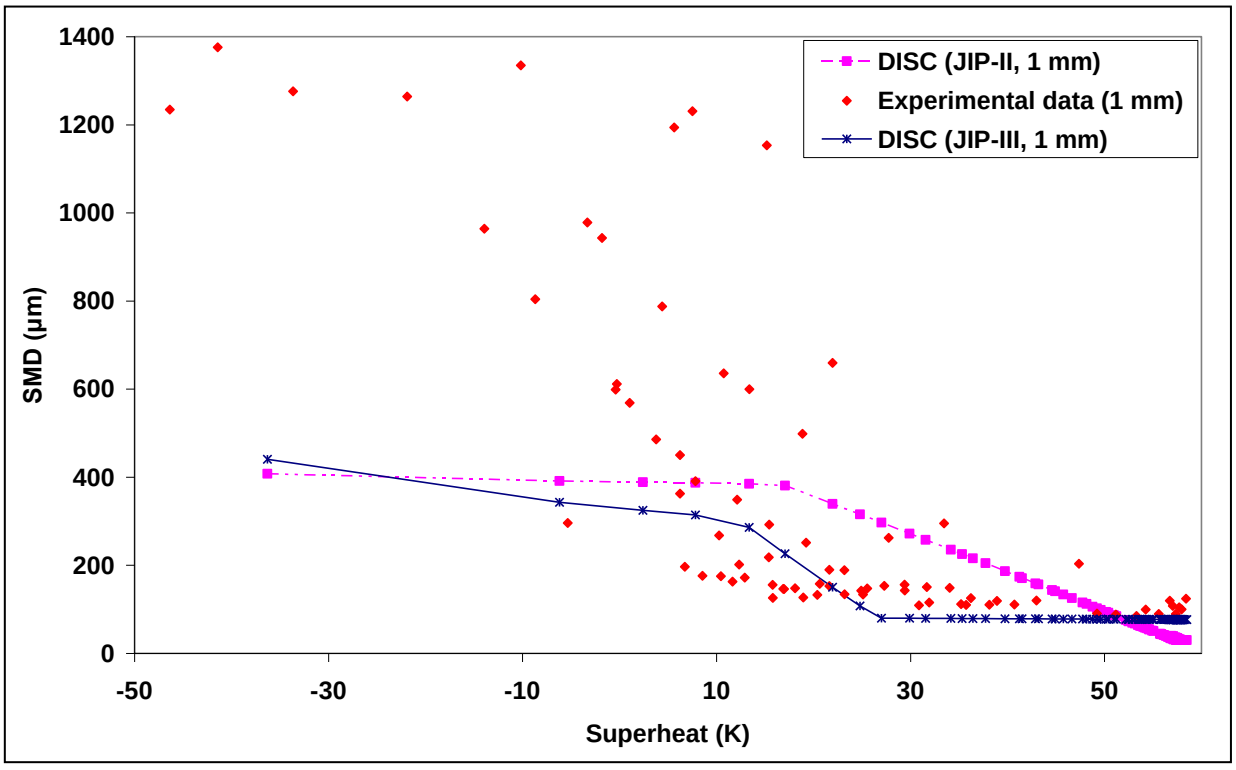

Figure 21. Validation of JIP ATEX SMD correlations against Cardiff water (1mm)

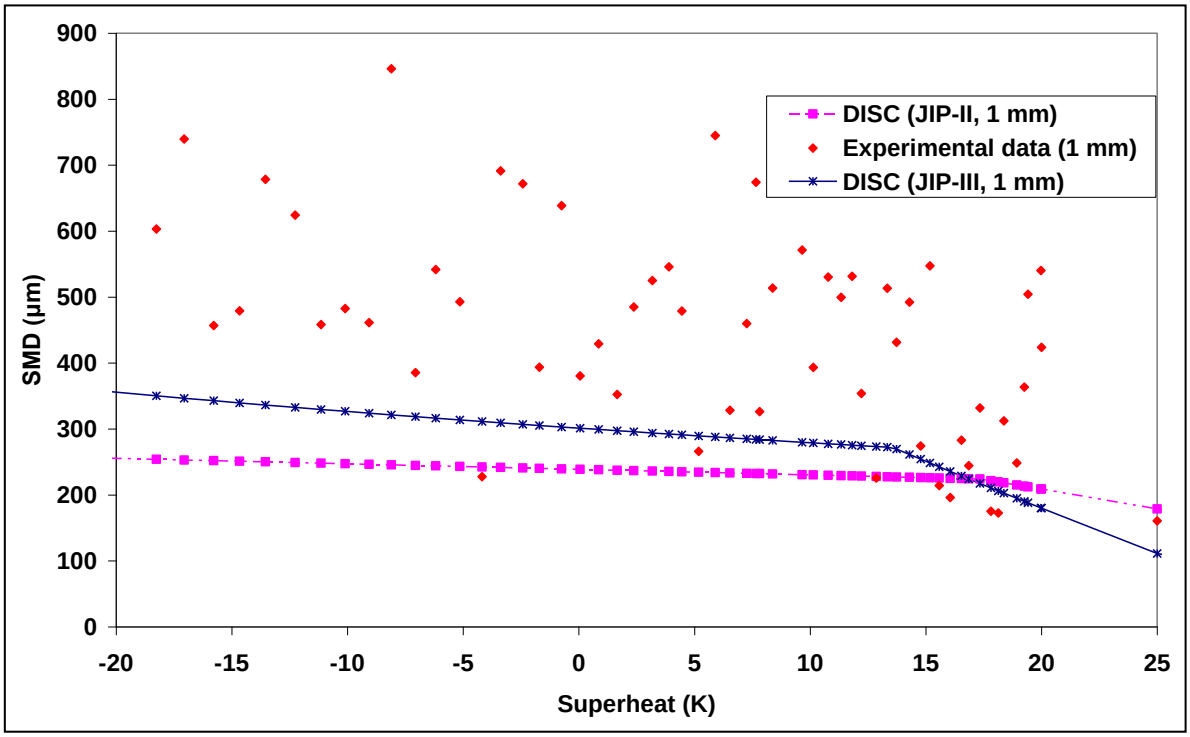

Figure 22. **Validation of JIP ATEX SMD correlations against Cardiff cyclohexane (1mm, 7.5barg)**

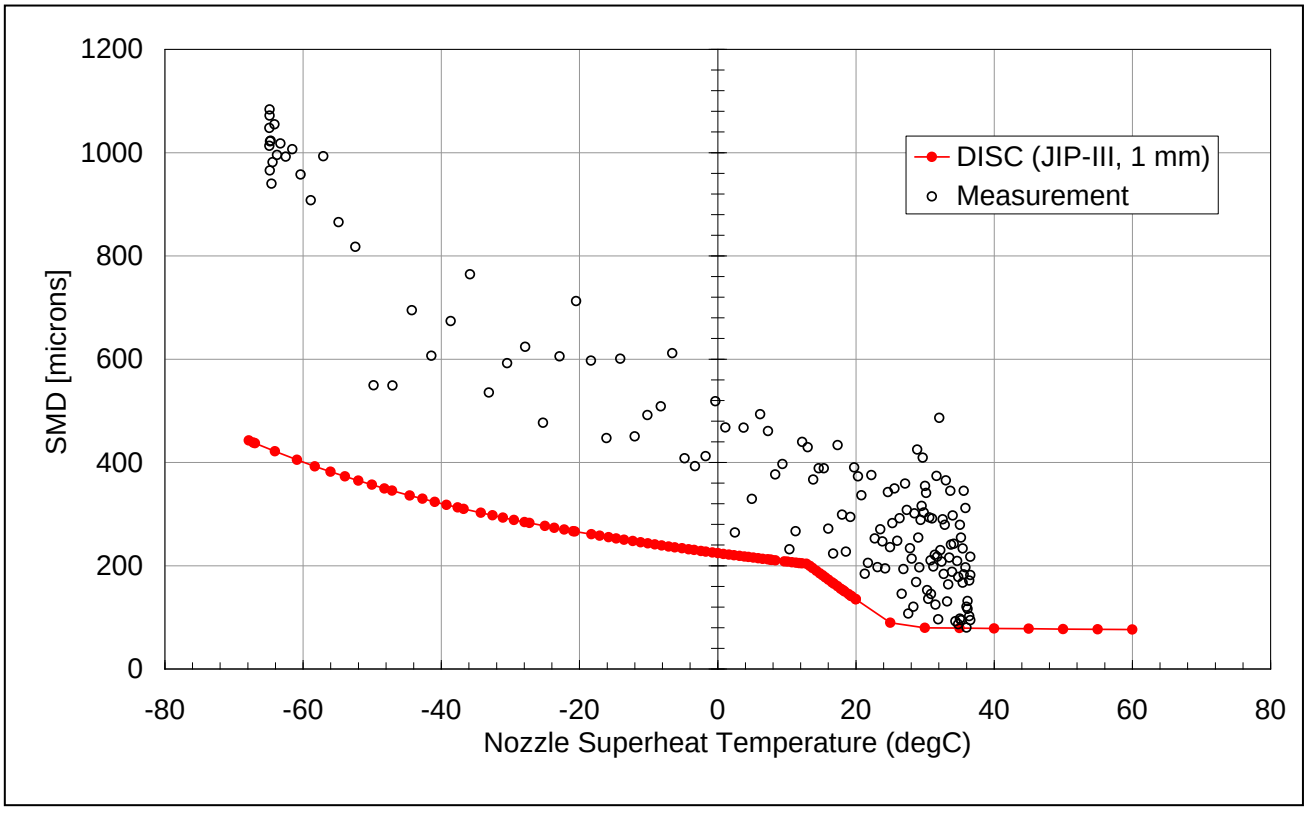

Figure 23. **Validation of JIP-III ATEX SMD correlation against Cardiff cyclohexane (1mm,12barg)**

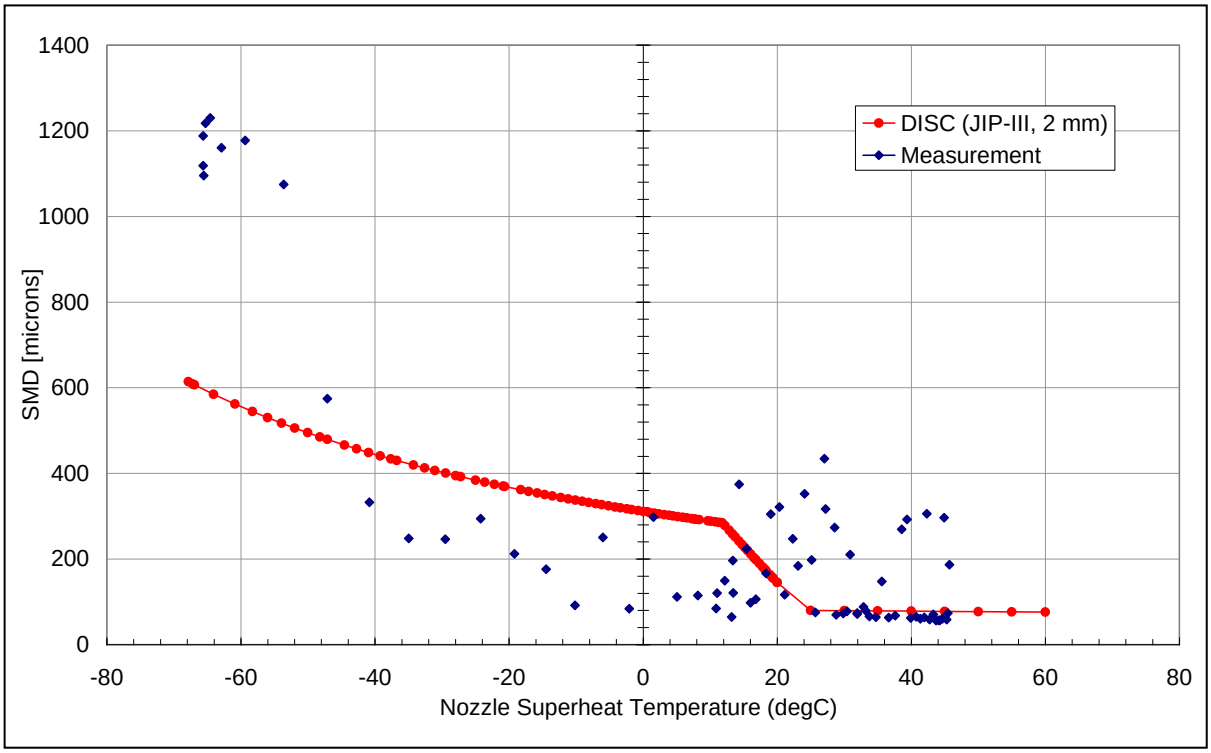

Figure 24. **Validation of JIP-III ATEX SMD correlation against Cardiff cyclo-hexane (2 mm, 12 barg)**

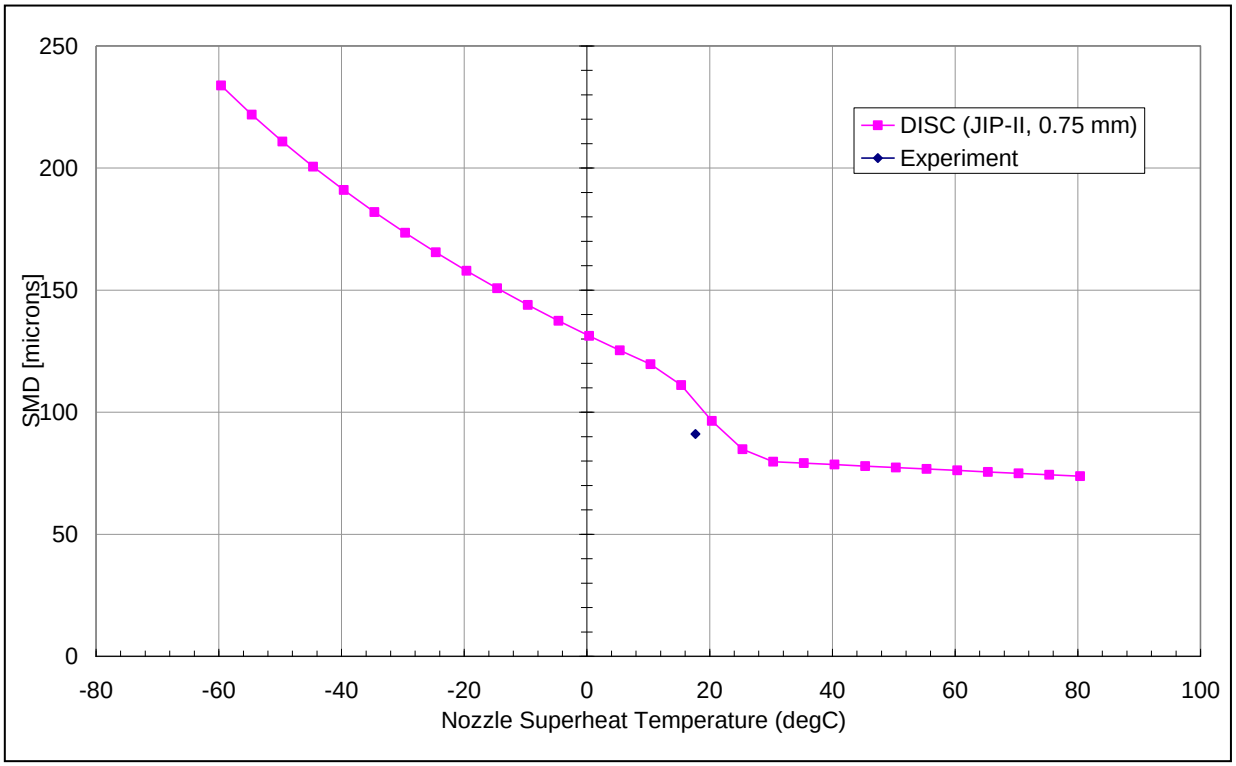

Figure 25. **Validation of JIP-III ATEX SMD correlation against Cardiff butane (0.75mm,10barg)**

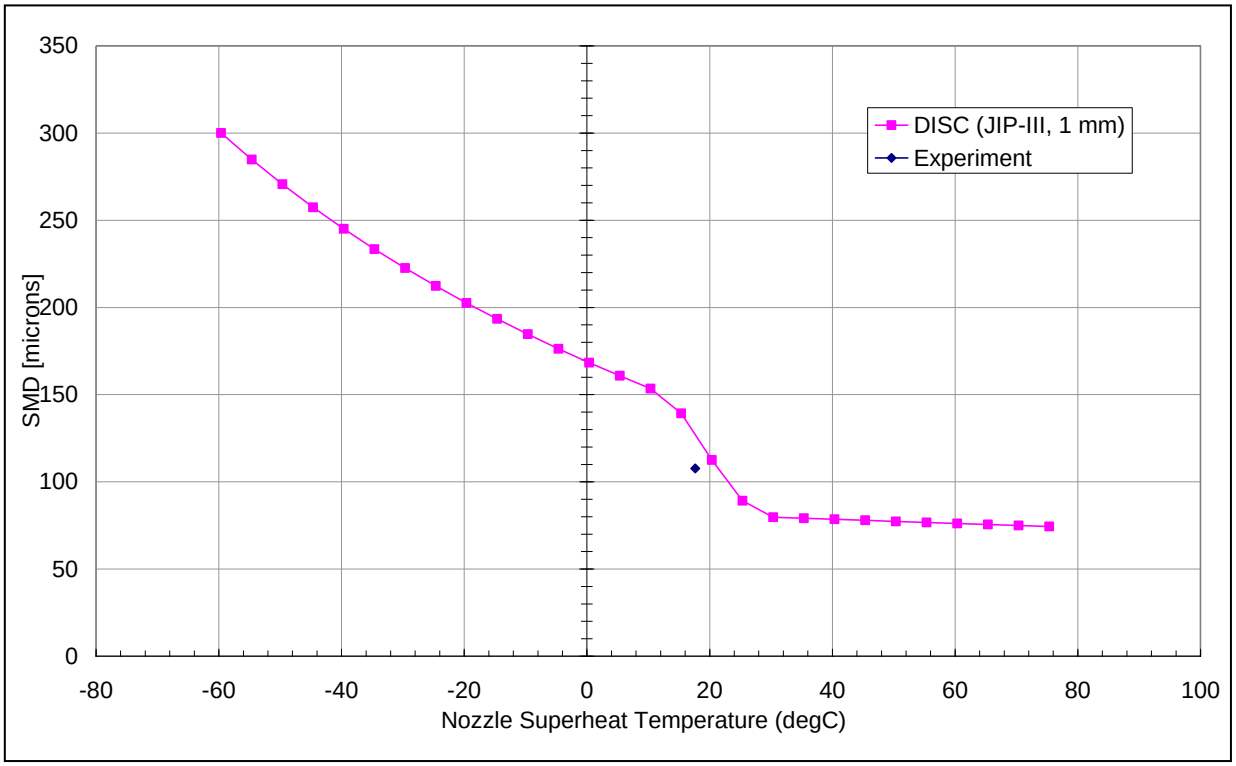

Figure 26. **Validation of JIP-III ATEX SMD correlation against Cardiff butane (1mm, 8barg)**

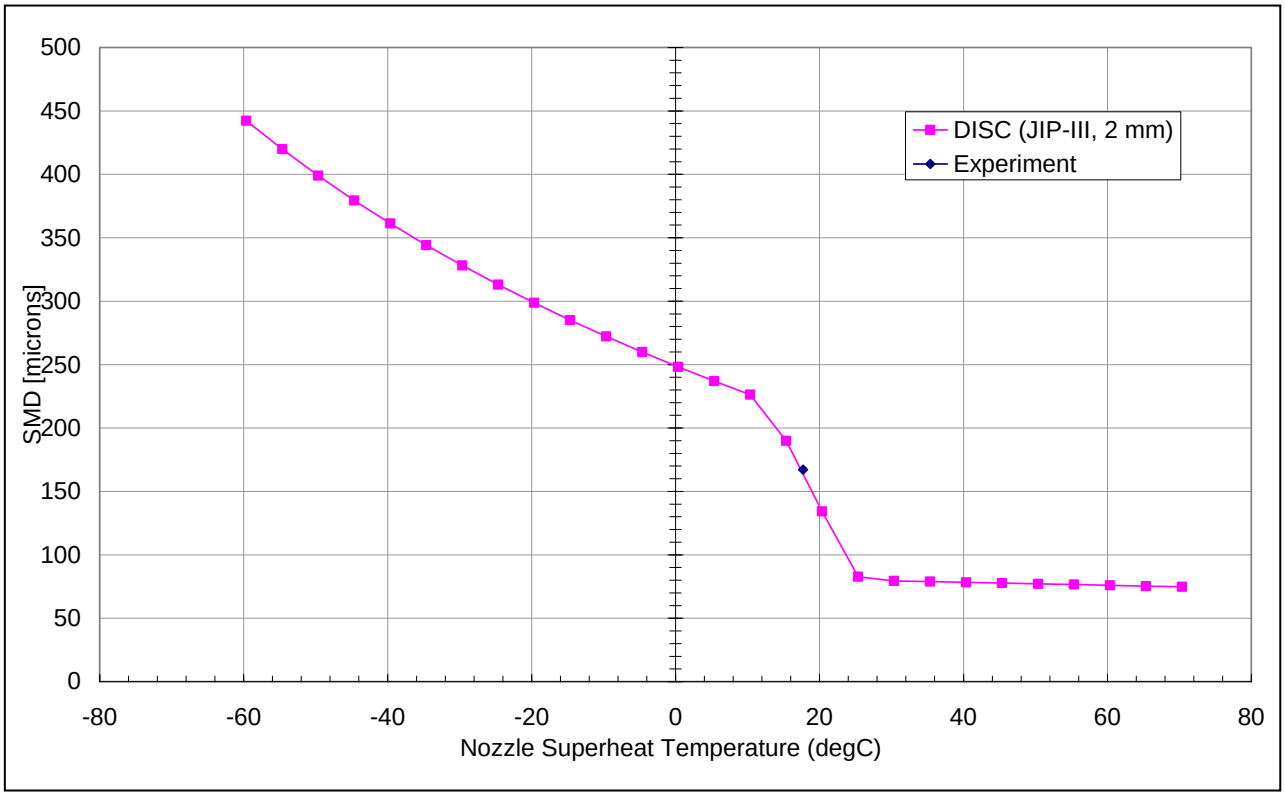

Figure 27. **Validation of JIP-III ATEX SMD correlation against Cardiff butane (2mm,7barg)**

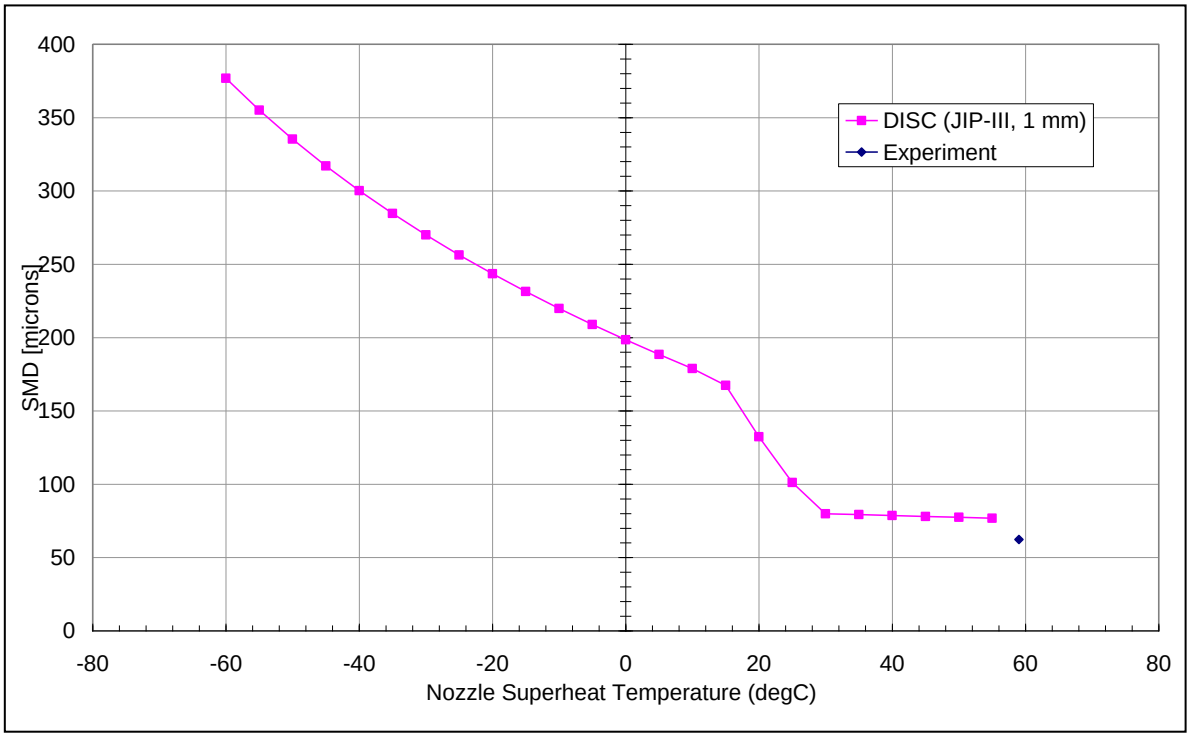

Figure 28. **Validation of JIP-III ATEX SMD correlation against Cardiff propane (1mm,6barg)**

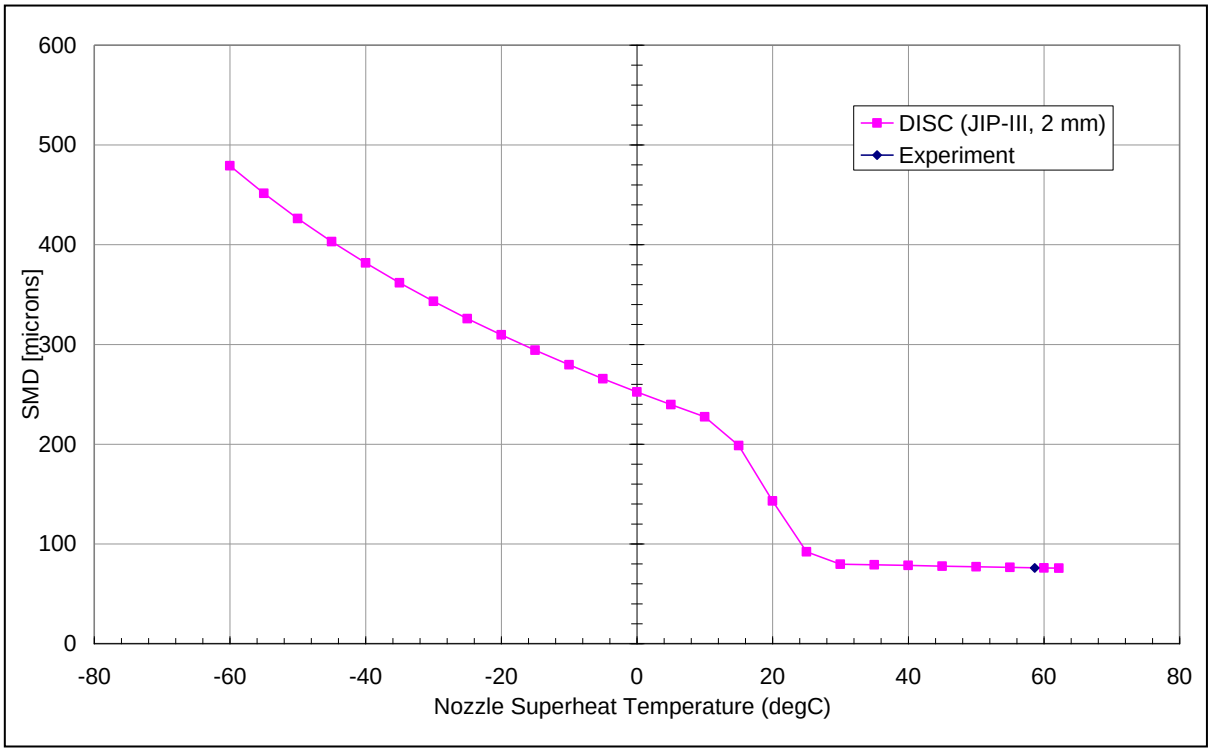

Figure 29. **Validation of JIP-III ATEX SMD correlation against Cardiff propane (2 mm,7barg)**

3.3 DISC validation for droplet size and flow rate (Phase III INERIS experiments)

As part of the Phase III project, large-scale butane experiments were carried out by INERIS in France:

- The release was from a 10 meter long pipe (30mm inner diameter) attached to a horizontal cylindrical tank filled with liquid butane with pressurised nitrogen gas at the top. The grade of the butane was 99.5%, and therefore it was modelled as pure butane in ATEX/DISC. The butane liquid in the tank was pre-heated in order to provide a sufficient superheat. The pressure was kept constant via the pressuring gas.

- Circular sharp-edged orifices of 5, 10 and 15 mm were attached to the end of the pipe, and the orifice pressure and orifice temperature were measured at the end of the pipe. Because of the small orifice size relative to the pipe diameter, the orifice pressure was found to be virtually identical to the tank pressure. The orifice temperature was originally equal to the ambient temperature, and subsequently increased with time (while the pipe was heating up).

- The flow rate was derived from the tank weight. From this the ATEX orifice velocity is determined (assuming 100% liquid).

- An ambient pressure of 1atm was used. Experiments were not carried out under foggy conditions (high humidity), since for these cases no accurate measurements could be taken.

Videos were taken for each experiment on a short-time jet to establish the appropriate downwind distance for accurate droplet-size ("post-expansion") measurements. This should be close enough to correspond to post-expansion conditions (no air entrainment effects), and far enough to avoid inaccuracy because of a liquid core.

Table 14 presents a summary of experimental conditions (stagnation pressures, range of superheat, orifice diameter and PDA equipment settings) for the INERIS experiments.

Table 14. Phase III INERIS butane - experimental conditions

Test Number	Orifice diameter (mm)	Release pressure (barg)	Release temperature (ºC)	PDA axial distances (cm)	PDA* resolution D_{max} (µm)
1	5	6	15-26	60	700
2	10	6	26-27	60,85	800
3	10	10	19-22	60,85	800
4	15	6	17-21	60,85	750
5	10	6	9-10	40,60,85	750
6	10	2	7-9	40,60,85	750

*Note: Sufficient range for the distribution of number of droplets, but larger droplets may be missed resulting in possibly inaccurate droplet volume distribution

The following presents the results of the validation of the DISC droplet size and flow rate predictions against measured data from the Phase III INERIS pure n-butane experiments. Predicted droplet sizes based on the Phase II and Phase III (proposed) correlations are compared against experimental data. Simulated flow rates are based on the default Phast 6.53 method [i.e. "Phast 6.53 (old method-No Flashing)"]. Further details on the experimental set-up and description of the adopted discharge model can be found in Part B and Part C1 of this report.

Table 15 details experimental conditions, measured plus DISC simulated flow rate and droplet size data for the INERIS pure n-butane experiments. Predicted droplet sizes based on the Phase II and Phase III (proposed) correlations are also compared against experimental data.

From Table 15, it can be seen that:

- The Phase III droplet size correlation generally under-predicts droplet sizes when compared with measured data (and the Phase II correlation).
- The Phase II (JIP-II) correlation is seen to generally agree better with measured data when compared with the JIP-III correlation.
- The above is contrary to the results of the comparison of predicted SMDs based on the proposed JIP-III (and JIP-II) correlation against the Ecole de Mine and Cardiff (Phase-III) n-butane data, where the JIP-III model is seen to over-predict in the former, while showing very good agreement with measured data in the latter. The lack of agreement between the INERIS and the predicted JIP-III correlation data is judged to be due to the adopted resolution for the INERIS PDA equipment (only up to 750 or 800 μm). The more recent Cardiff experiments were based on more advanced PDA equipment with wider and more accurate droplet size resolution (up to 2181 μm).

The results presented in Table 15 are further illustrated in Figure 30 to Figure 34. These compare DISC simulated droplet size data based on the JIP-III and JIP-II correlations against measured SMD data for the INERIS pure n-butane experiments. These figures show that the JIP-III correlation tends to under-predict for higher pressures (10 barg; Figure 32), over-predict for lower pressures (2 barg; Figure 34), and predicts very well for 6 barg experiments (Figure 30, Figure 31 and Figure 33).

Figure 35 to Figure 37 show the effect of increase in orifice diameter (5 mm to 10 mm), increase in upstream stagnation pressure (5.8 barg to 9.8 barg) and decrease in upstream stagnation pressure (5.8 barg to 2 barg) on predicted and measured droplet sizes respectively. From these figures it can be seen that:

- The Phase III droplet size correlation predicts droplet sizes to increase with orifice diameter, while the INERIS data suggest otherwise (see Figure 35). The predictions based on the Phase III correlation is in agreement with expected droplet size behaviour with increase in orifice diameter for a fixed stagnation pressure and temperature. As mentioned earlier, the observed discrepancy in the INERIS data is judged to be due to the adopted resolution for the INERIS PDA equipment.[33]
- In agreement with the INERIS data, the Phase III droplet size correlation predicts droplet sizes to decrease with increase in upstream stagnation pressure (see Figure 36). Both the measured and predicted data agree with expected droplet size behaviour following an increase in upstream stagnation pressure.
- The Phase III droplet size correlation predicts droplet sizes to increase with decrease in upstream stagnation pressure, while the INERIS data suggest pressure drop to have negligible impact on SMDs (see Figure 37). The predictions based on the Phase III correlation agrees with expected droplet size behaviour following a decrease in upstream stagnation pressure. As mentioned earlier, the observed discrepancy in the INERIS data is judged to be due to the adopted resolution for the INERIS PDA equipment[34].

[33] INERIS quotes that a lognormal fit of the droplet size distribution profile shows the correct results for their experiments!

[34] INERIS quotes that their experiments show the correct trend, i.e. little effect of pressure!

Table 15. INERIS butane: experimental data and flow-rate/SMD predictions

Experiment	INERIS1	INERIS2	INERIS3	INERIS4	INERIS5	INERIS6
Material	Butane	Butane	Butane	Butane	Butane	Butane
storage pressure (barg)	6.0	6.0	10.0	6.0	6.0	2.0
orifice temperature (C)	15,18,26	26,27	19,21.5	19,21.5	19,21.5	19,21.5
orifice diameter (mm)	5	10	10	15	10	10
L/D	0	0	0	0	0	0
ambient pressure (bar)	1atm	1atm	1atm	1atm	1atm	1atm
ambient temperature (C)	14.6	8.7	13.4	8.4	8.2	4.4
Flow rate (kg/s)						
Measured flow rate (for ATEX)	0.42	1.40	1.77	2.35	1.27	0.75
Predicted flow rate	0.32	1.29	1.66	2.90	1.30	0.82
Deviation (%)	-23.2	-7.9	-6.0	+23.5	+2.4	+9.3
Orifice velocity (assume meta-stable liquid) (m/s) [for ATEX]	47.11	47.58	60.31	47.22	47.22	27.28
Droplet distribution						
downstream location (mm)	600	850	600	850	850	600
Measured SMD	435,413,373	312,247	324,283	267,247	267,247	267,247
DISC post-expansion SMD (JIP-III)[35]	196	79	85	91	130	398
DISC post-expansion SMD (JIP-II)	414	356	366	573	496	978

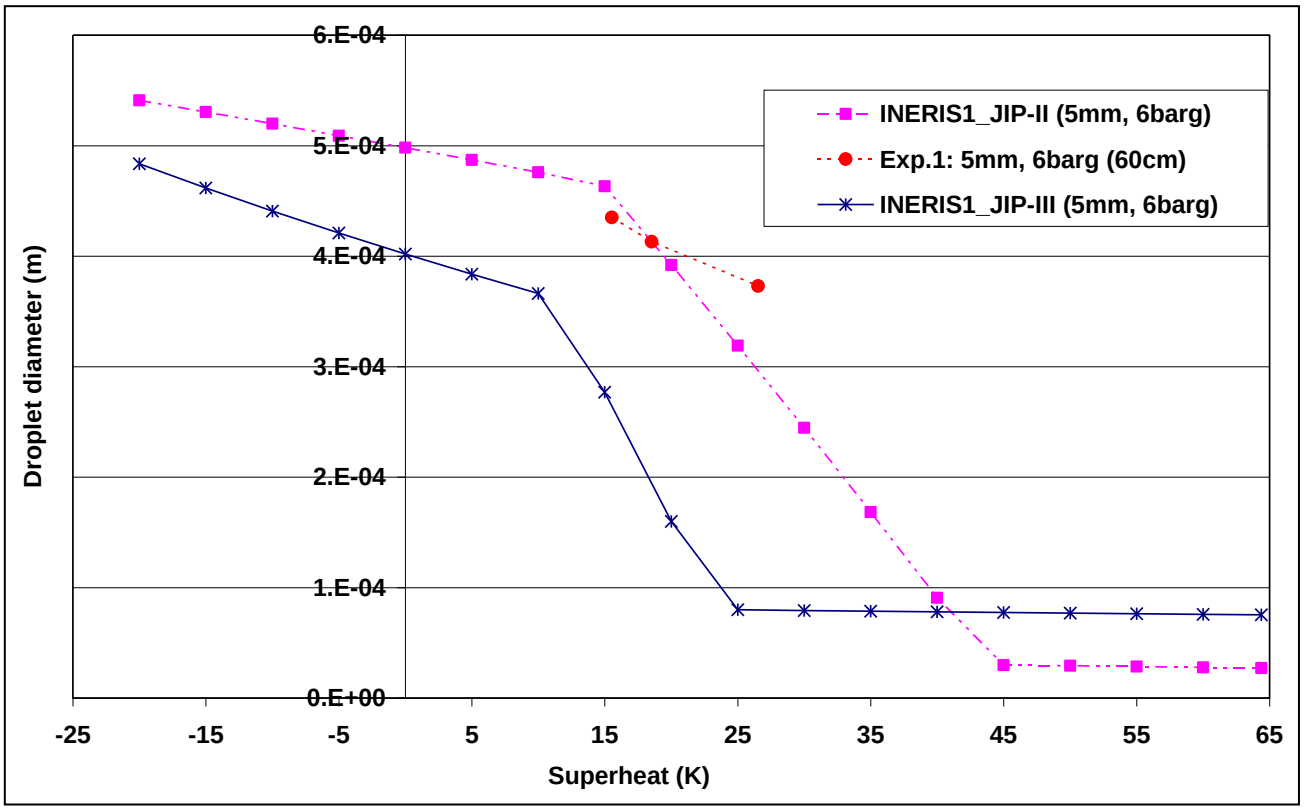

Figure 30. Comparison of JIP ATEX SMD correlations against INERIS1 butane (5mm,6barg)

[35] Note that the simulated release rates and droplet sizes correspond to average values, which have been taken over the range of measured/reported upstream temperatures for each test.

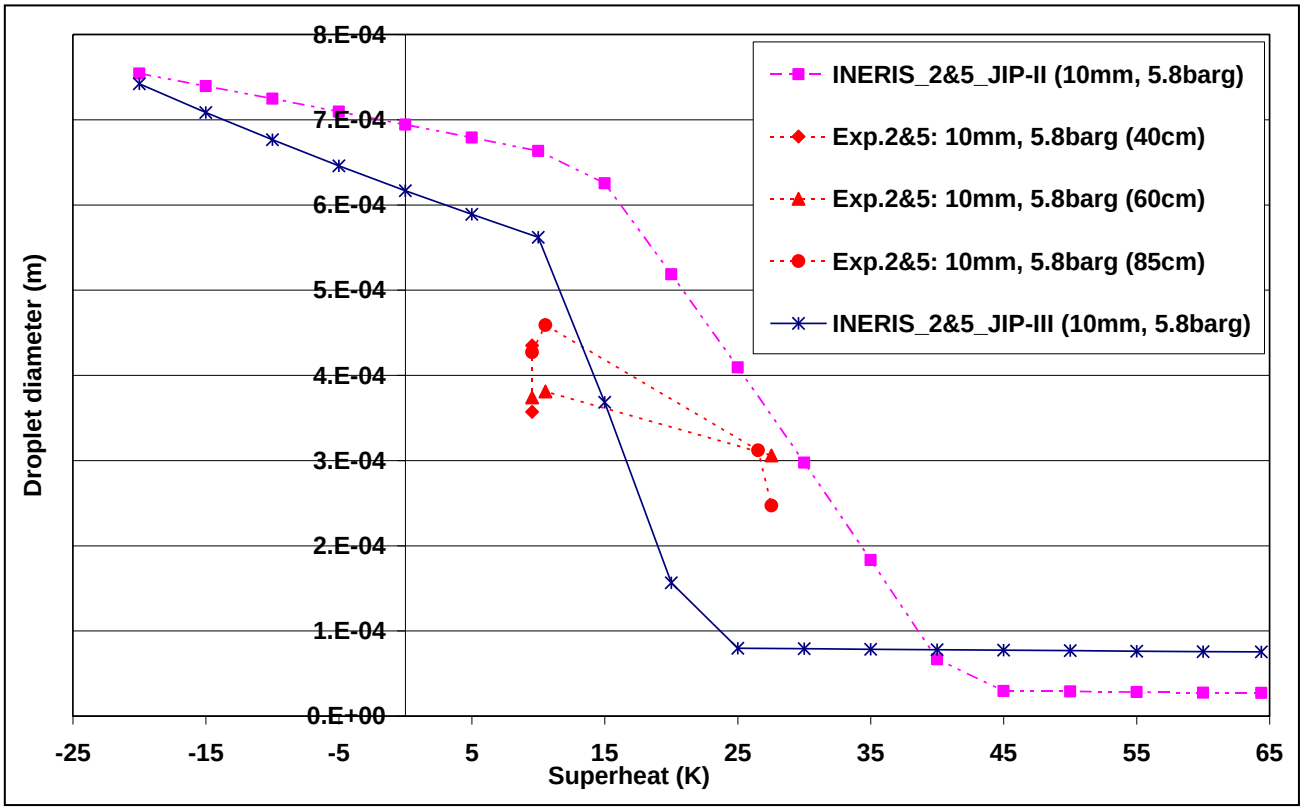

Figure 31. Comparison of JIP ATEX SMD correlations against INERIS2&INERIS5 (10mm,5.8barg)

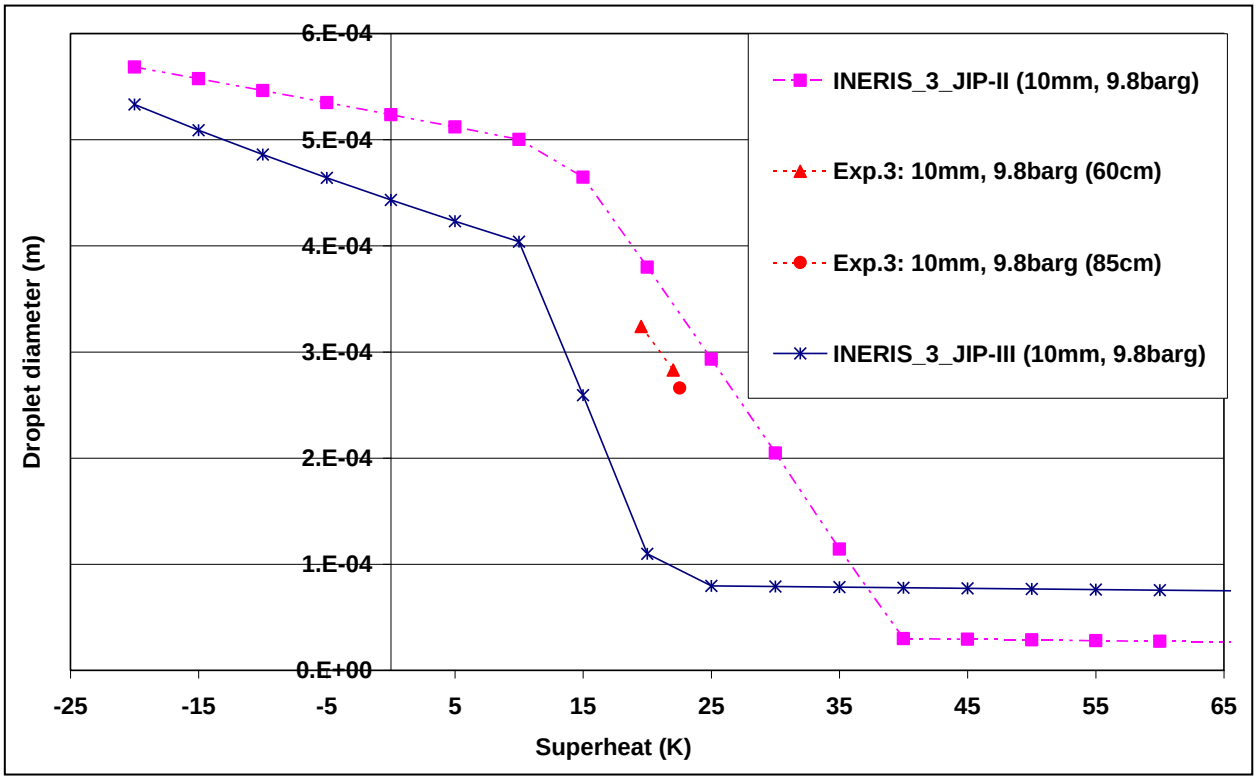

Figure 32. Comparison of JIP ATEX SMD correlations against INERIS3 (10mm, 9.8barg)

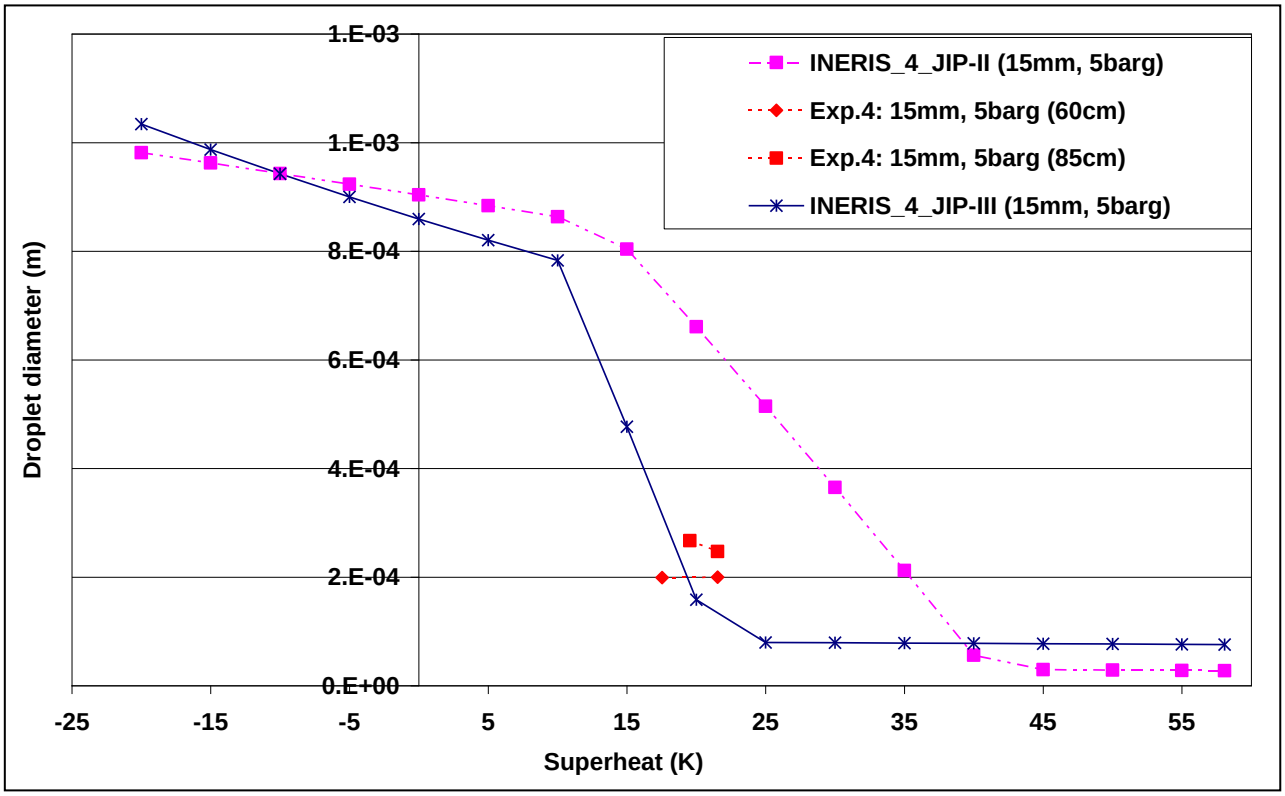

Figure 33. Comparison of JIP ATEX SMD correlations against INERIS4 (15mm, 5barg)

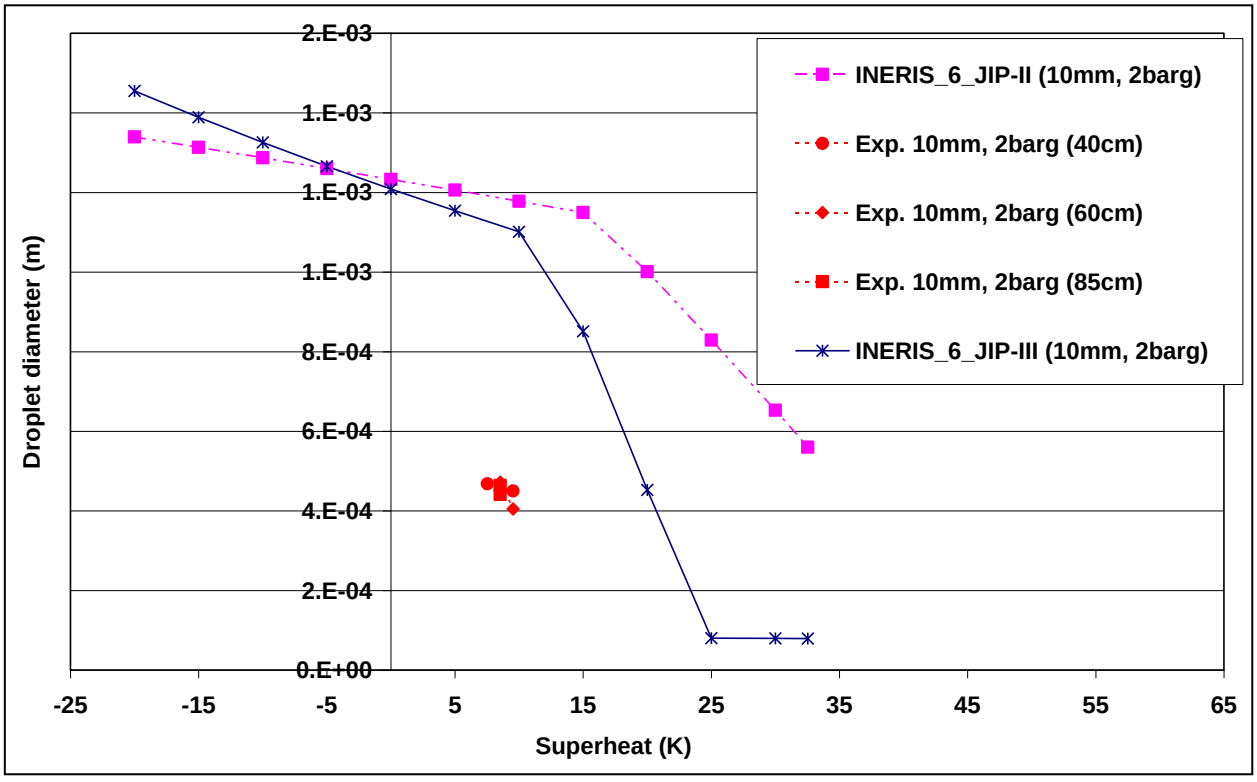

Figure 34. Comparison of JIP ATEX SMD correlations against INERIS6 (10mm,2barg)

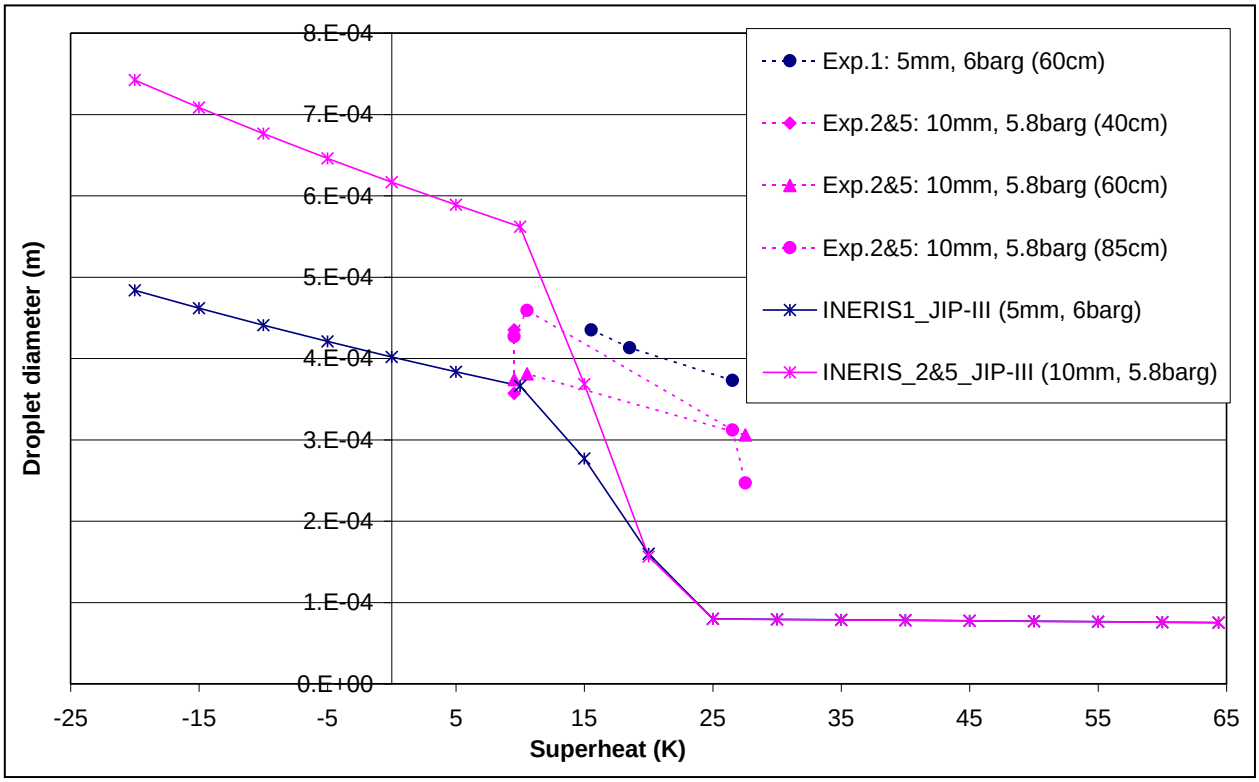

Figure 35. **Comparison of JIP ATEX SMD correlations against INERIS showing effect of orifice diameter (5,10mm)**

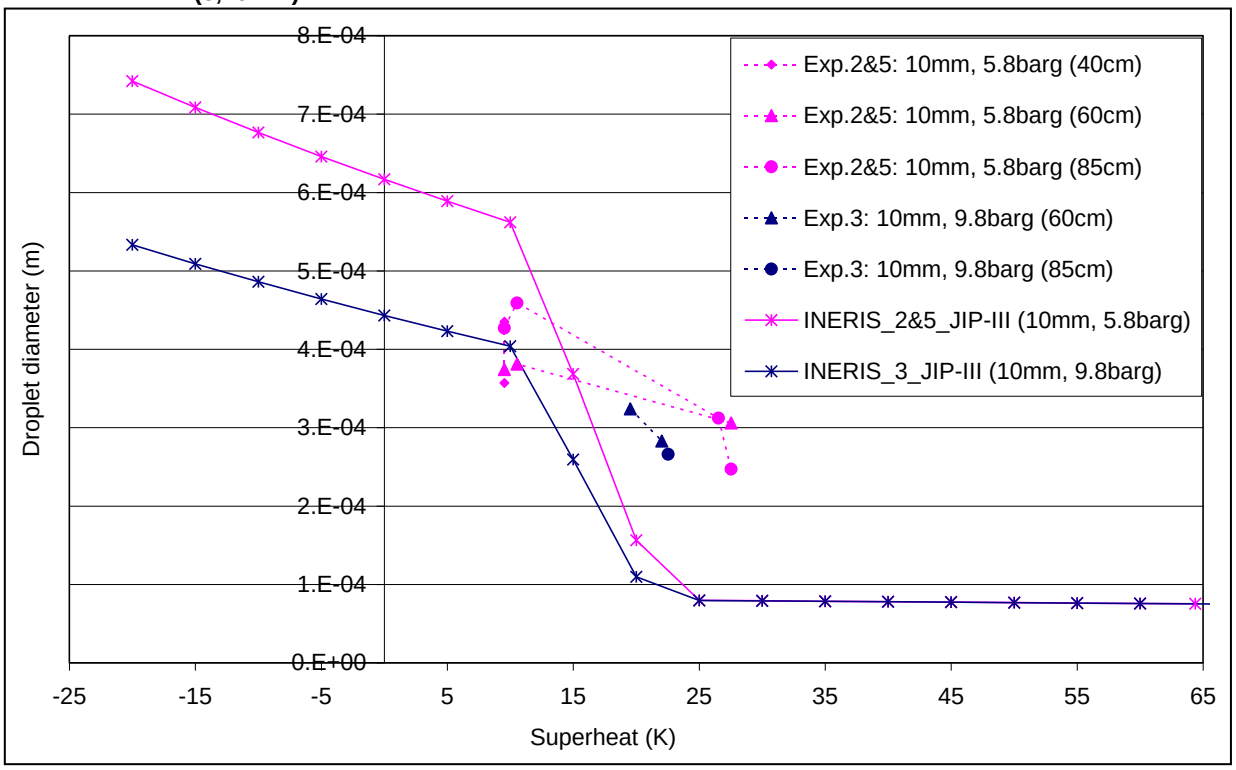

Figure 36. **Comparison of JIP ATEX SMD correlations against INERIS showing effect of stagnation pressure (5.8,9.8barg)**

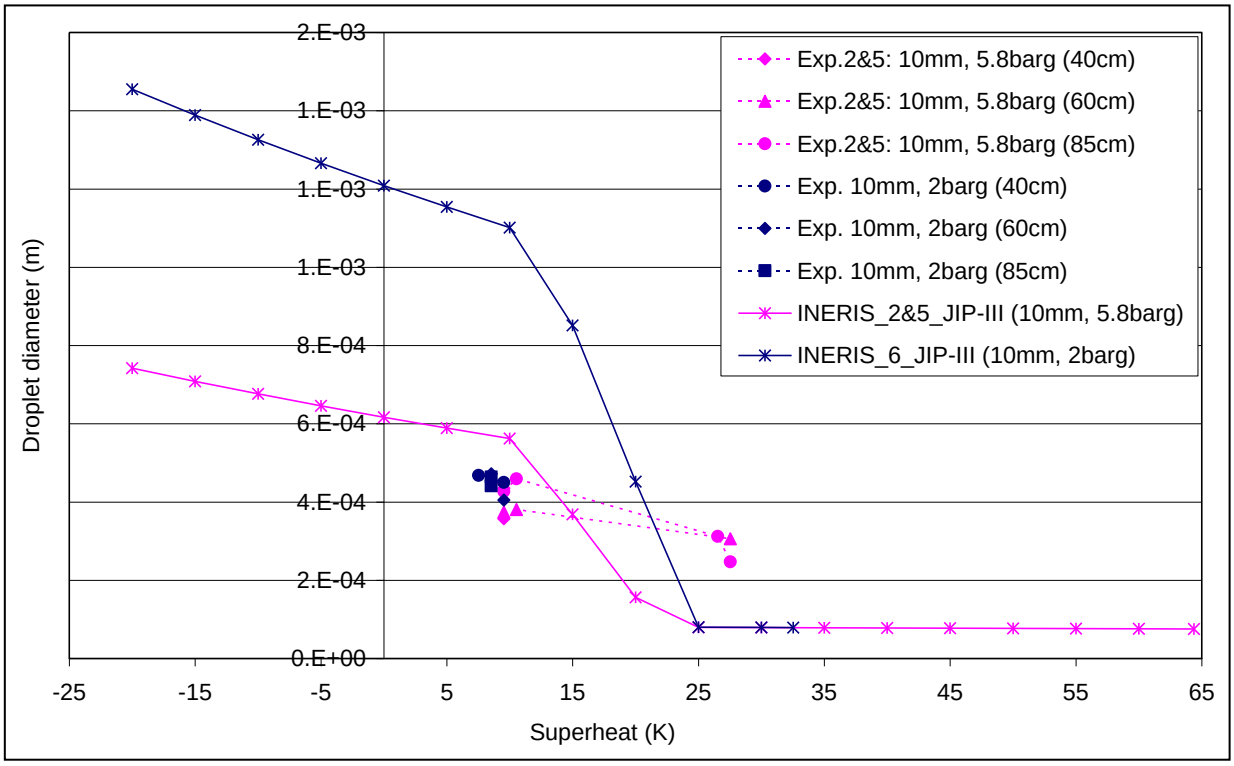

Figure 37. **Comparison of JIP ATEX SMD correlations against INERIS showing effect of stagnation pressure (5.8,2barg)**

4 MODEL VALIDATION - JIP PHASE IV HSL RAINOUT EXPERIMENTS

This chapter includes results of validation against the HSL water and xylene experiments using two different correlations for the initial droplet size, i.e. the CCPS SMD correlation and the Phase III JIP SMD correlation. The validation includes flow rates, droplet size and distributed rainout. For the xylene experiments, it also includes temperature drop and concentrations. Validation against other datasets (including CCPS experiments) and using other methods (i.e. simple rainout correlations) is given in Chapter 6.

4.1 Model input

Part A of the current Phase IV JIP report includes a detailed description of the HSL water and xylene experiments.

Discharge modelling

The HSL experiments included measurements of flow rates and initial droplet size distribution. The validation against these data was carried out using the Phast discharge model DISC.
Table 16 includes the input data for the DISC simulations.

The Bernoulli law was applied to calculate the flow rate.

Two different droplet size correlations were applied:

- The Phase III JIP droplet size correlation was applied to set the post-expansion SMD and droplet-size distribution. The 'conservation of momentum' option was applied for the Phase III JIP droplet size correlation to define the other post-expansion velocity and post-expansion liquid fraction. L/d_o for the nozzles used in the HSL experiments is taken to be 1, as described in the Part A report. This is the same L/d as is applied in Phast 6.6 for the (non-default) Phase III JIP correlation.

- For the CCPS correlation, the isentropic expansion method is adopted since the CCPS correlation is not valid using the conservation of momentum option. Phast 6.6 uses as default the CCPS correlation using as expansion method 'minimum thermodynamic change', which for most cases corresponds to the isentropic assumption. Unlike the modified CCPS correlation, the original CCPS correlation may pickup erroneously the flashing-breakup droplet size in the subcooled regime, in case this would be smaller than the mechanical-breakup droplet size.

Pressure and temperature were varied between the different experiments in line with the experimental measurements. Water simulations were carried out at 280K. Most xylene simulations were at 284.15K, apart from the case of 5mm 8,5 barg which was significantly colder at 274.75K. As reported in Part 'A', no pressure measurements were taken, so we have used an average pressure at the test site (~385m above sea-level) of 96.785 kPa.

	D	E	F	L	M	N	O	P	Q
3	**Input**	**Description**	**Units**	**Limits**		**JIP**	**CCPS**	**CCPS modified**	
4	**Index**			**Lower**	**Upper**				
5		**Material**							
6	N	Stream name	-			XyleneMix2			
8		**Storage state**							
9	2	Specification flag (0 = P&T&LF, 1 = P&T, 2 = Tbub, 3 = Pbub, 4 = Tdew, 5 = Pdew, 6 = P&LF, 7 = T&LF)	-	0	7	1			
10	3	Gauge pressure	Pa	0		4.00E+05			
11	4	Temperature	K	10	1000	284.15			
12	5	Liquid fraction (MOLE basis)	mol/mol	0	1	1			
13		**Vessel data**							
14	6	Total inventory	kg	10		1.00E+02			
15	7	Orifice diameter	m	0.001	50	0.0025			
16	8	Liquid head	m	0		0			
17		**Atmospheric expansion data**							
18	9	Atmospheric pressure	Pa	50000	120000	96,785			
19	10	Atmospheric temperature	K	10		284.15			
20	11	Atmospheric humidity	-	0	1	0.7			
21	12	Wind speed	m/s	0		0			
22		**Scenario data**							
23	13	Scenario flag (4 = leak, 5 = fixed duration)	-	4	5	4			
24	14	Phase to release for 2-phase storage (1 = vapour, 2 = 2-phase, 3 = liquid)	-	1	3	3			
25	15	Fixed duration	s	0	10000	600			
26		**PARAMETERS (values to be changed by expert users only)**							
27	16	Multi-component modelling flag (1 = MC, 0 = PC)	-	0	1	0			
28	17	Flashing allowed to orifice?	-			FALSE			
29	18	Use Bernoulli model for metastable liquid releases?				TRUE			
30	19	Is discharge coefficient specified? TRUE = Specified	-			FALSE			
31	20	Orifice L/D ratio	-	0	1000	1			
32	21	Input discharge coefficient	-	0	1	1			
33	22	ATEX expansion method (0 = min thrm change, 1 = isentropic, 2 = cons moment)	-	0	2	2	1	1	
34	23	Droplet correlation method (0 = PHAST 6.4, 4 = Melhem, 5 = JIP3)	-	0		5	0	0	
35	24	Force mechanical or flashing breakup (0 = No, 1 = force mechanical, 2 = force flashing, 4 = modified CCPS transition)	-	0	4	0	0	4	

Table 16. DISC input data for HSL experiments (case of xylene, 4 barg, 2.5 mm)
Column N gives the parameter settings for the JIP Phase III correlation. Columns O and P give the changes required for the CCPS and modified CCPS correlations, respectively.

Dispersion modelling

The HSL experiments also include measurements further downstream, including measurement of rainout, plume concentrations and plume measurements. The validation against these data was carried out using the Phast dispersion model UDM. Table 17 includes the key input data not already given above for the UDM simulations.

Input	Units	Value
Duration of release	s	100
Stability class		D
Wind speed (constant with height)	m/s	0.1
Surface roughness length	m	0.005
Number of droplet parcels (JIP correlation)		20
Release height	m	1
Temperature of dispersing surface	m	284.15

Table 17. Additional UDM input data for HSL experiments

As modelled flow rates were very close to the experimental ones the former were used in the UDM simulations. The UDM assumes the release duration is long enough that steady-state rainout and concentration predictions are obtained (in line with the experimental data where releases were typically in the range 50-100s). Rainout is normally expressed as percentages of either measured flow rate for experiments, or modelled flow rate for simulations.

Wind speed is not used for the discharge simulations. As the releases were carried out indoors, the minimum value of 0.1 m/s was used in the UDM simulations alongside the assumption of neutral conditions (stability class D). The low value of surface roughness of 0.005 was selected in the UDM simulations corresponding to flat terrain. These are assumptions, but sensitivity tests on the 2.5 mm 8 barg case (windspeed between 0.1 and 5 m/s, and surface roughness between 5mm and 50cm) showed that these parameters had negligible effect on rainout mass, though higher windspeeds did move rainout position downwind (by as much as 2m for the 5 m/s case).

4.2 Model results - water experiments

For the water experiments, the input data in Section 4.1 was used, except as follows:

- Temperature was assumed to be 280K
- 'Minimum thermodynamic change' expansion was selected (though for sub-cooled Bernoulli releases this will not affect results)

A variety of correlations were tested for droplet SMD, as described below.

4.2.1 Flow rate

These results of the Phast discharge predictions against the data observed by HSL are very satisfactory. Results for the incompressible (Bernoulli) model are within 4 percent (see Table and figure below). The compressible (default Phast 6.7) model tends to over-predict by up to 20%.

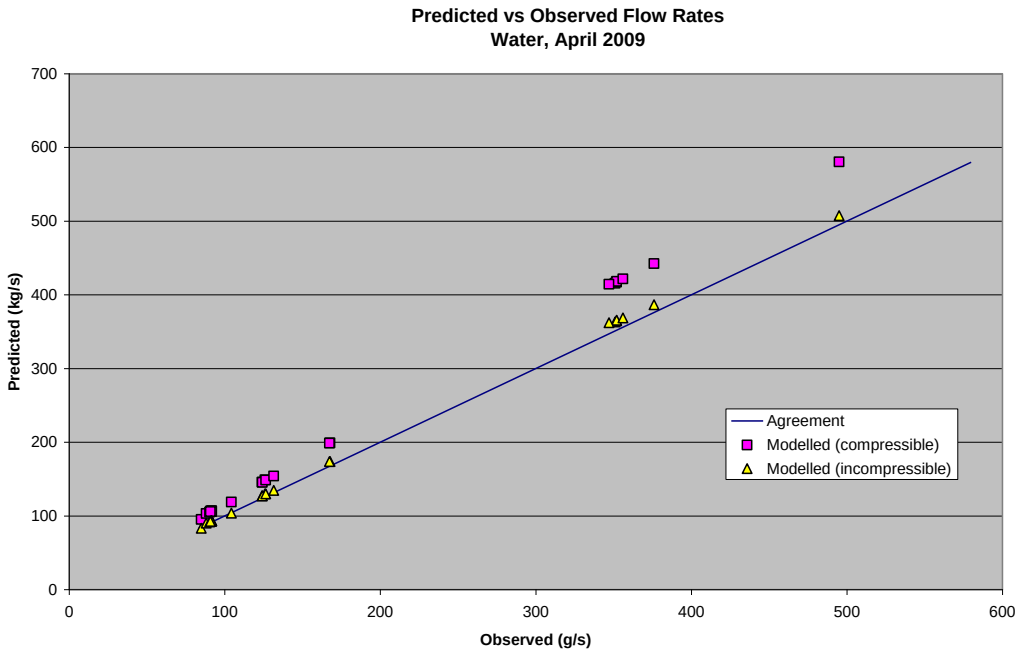

Figure 38. DISC validation of flow rate (HSL water experiments)

Rainout was collected for a subset of these experiments. As described later for xylene, multiple runs at the same nominal pressure (but slightly different actual pressures) were required so trays could be re-positioned. To model this we have used a single simulation with 'averaged' initial conditions. These averaged runs are given in the table below:

Experiment	Stagnation Pressure (kPag)	Nozzle (mm)	Measured flow (g/s)	Incompressible	
				Flow (g/s)	Error (%)
5bar2.5	499	2.5	91	93	2.0
9.5bar2.5	948	2.5	125	128	2.9
4.78bar5	478	5	352	365	3.7

Table 18. DISC validation of flow rate (HSL water experiments)

4.2.2 Droplet size and distribution

The HSL water experiments were intended to reproduce the Cardiff water experiments reported in Phase III of the droplet modelling JIP. The purpose was to compare the results of the photographic droplet size measurements by HSL against the PDA measurements by Cardiff University. This would enable to optimise the photographic technique before subsequent application to xylene. See the Part A report for further details of the HSL droplet size measurements.

In the PDA measurements it was already found that a few large droplets could dominate the droplet volume distribution. Furthermore the PDA technique excludes droplets which are 'too' non-spherical. Furthermore there was the potential issue of 'optical' effects which would lead to possible non-real droplets to be included by the PDA. The HSL photographic experiments showed that non-spherical droplets persist over quite a large time, and that non-spherical droplets contribute to most of the mass. Furthermore secondary break-up was seen to occur resulting in smaller droplets (rather than because of droplet evaporation). The phenomenon of non-spherical droplets and secondary breakup is expected to be less crucial for flashing jets because of smaller droplet sizes. Given the above issues not significant time was spent in further comparing the PDA measurements against the photographic measurements.

The Phast models (DISC, UDM) assume a droplet size distribution with spherical droplets and ignore secondary breakup of the droplets. Thus in case no evaporation takes place the droplet size distribution will be fixed along the downwind direction. Moreover the initial droplet size distribution is applied in the model immediately downstream of the orifice, where at the moment no jet break-up length is accounted for.

As described in detail in the Part A report a method was developed to derive an 'equivalent' spherical droplet size distribution from the photographic droplet size measurements at the centre-line at a given downstream distance (at which the inner liquid core has largely disappeared). Here all droplets with non-spherical droplets are approximated by droplets with equivalent diameter. Hundreds of droplets are found per photographic image, while one needs tens of images to obtain a sufficiently accurate droplet size distribution. It is very difficult to obtain an accuracy distribution profile given that only a few droplets may contribute to a large part of the overall mass. More accurate distributions are expected (with same number of images) in case of smaller SMDs.

Photographic images were taken at 500 (1.25m) and 1000 (2.5m) nozzle diameters downwind of the release point, and the obtained droplet size distributions are plotted in Figure 39, which also plots the JIP III predicted droplet distribution.

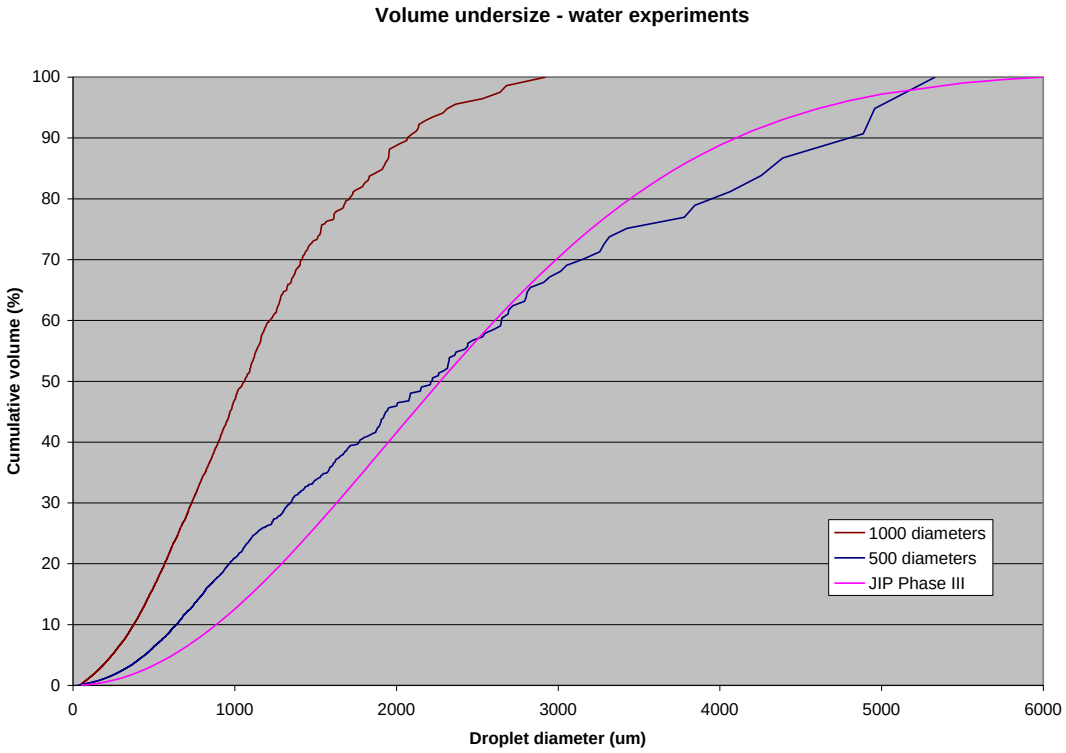

Figure 39. Validation of droplet size distribution (HSL water experiment, 2.5mm, 10 barg)

The downwind distance from nozzle is varied to examine effect of downstream distance on droplet size distribution. It is seen that the Phase III JIP distribution agrees very well with the distribution measured at 500 diameters distance, while

distribution measured at 1000 diameters distances results in significantly smaller droplets. This is most likely because of secondary break-up.

Case	SMD (µm)	Flashing or mechanical?
Experimental		
500 diameters	1245	
1000 diameters	673	
Modelled		
CCPS (Phast 6.6)	326	Flashing
CCPS modified	398	Mechanical
JIP III	1736	Mechanical
Melhem	1107	Mechanical

Table 19. SMD validation (HSL water experiment, 2.5mm, 10barg)

SMD values obtained from these distributions are given in Table 19, along with SMDs predicted using a variety of methods:

- CCPS (Phast 6.6) uses isentropic expansion and the default CCPS droplet size correlations, taking the minimum of flashing and mechanical droplet sizes. It gives the same results as the Phast 6.6 default settings[36].
- CCPS (modified) uses isentropic expansion, but chooses mechanical or flashing correlation based on superheat (i.e. will use the mechanical correlations is $\Delta T_{sh} < 0.01$)
- JIP Phase III uses conservation of momentum and the JIP Phase III droplet correlation. It too will use the mechanical correlation for all sub-cooled releases.

The JIP Phase III and experimental (at 500 diameters) SMDs agree quite well, as one would expect from Figure 39. However the CCPS and modified CCPS methods significantly under-predict the SMD. Moreover the CCPS method actually uses the flashing correlation for releases that are ~90K below their boiling point.

4.2.3 Distributed rainout

See Part A for details on the HSL experimental data for distributed water rainout. These were found by HSL to be very reproducible. The CCPS mechanical break-up Weber criterion (rainout assumed at one single downwind distance) and the Phase III droplet size JIP correlation (with distributed rainout), both predict rainout at a considerable smaller distance than the experimental data; see Figure 40 below. This is expected to be caused not so much by incorrect initial droplet size distribution but more by

(a) ignoring break-up length
(b) ignoring secondary break-up
(c) the simplified assumption that droplet all move with the same velocity (with the overall cloud), while in reality larger droplets will keep their momentum longer and will move faster.

What is noticeable is that the spread of rainout predicted by JIP III + parcels is very small, in contrast to the measured rainout which extends over 5m. This is a consequence of the very large SMDs predicted by the JIP Phase III correlation (2690 and 4150 µm respectively for the 2.5mm and 5mm nozzles). As a consequence drag effects are relatively insignificant and the height of the different parcels do not diverge.

The above will be further discussed in Chapter 4.3.6.

[36] Phast actually will choose conservation of momentum, but this does not appear to affect droplet sizes even for the flashing correlation.

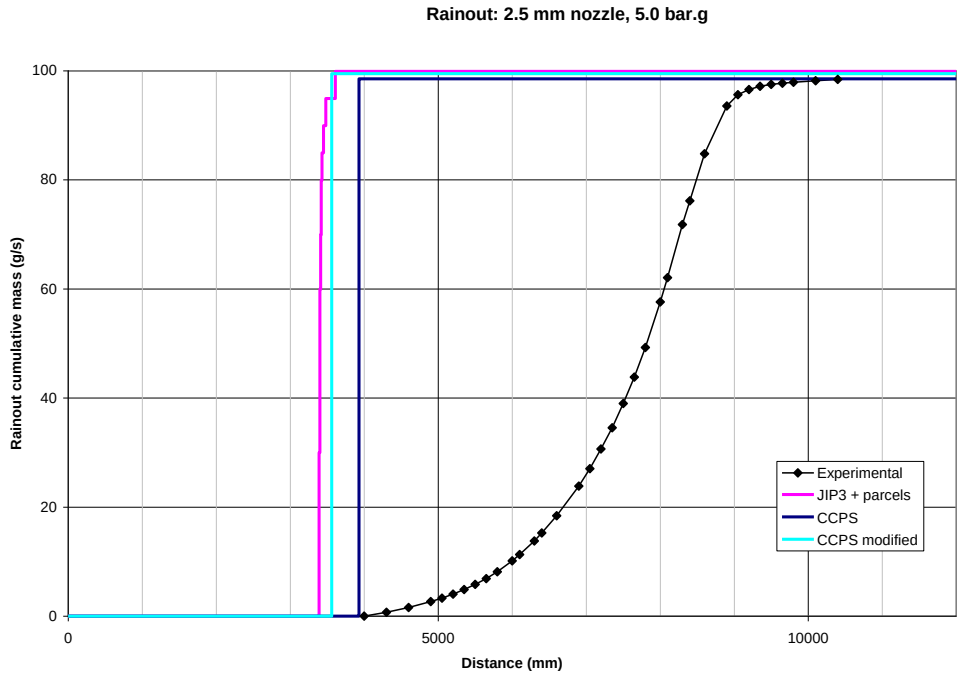

(a) 5 mm nozzle, 4.8 barg

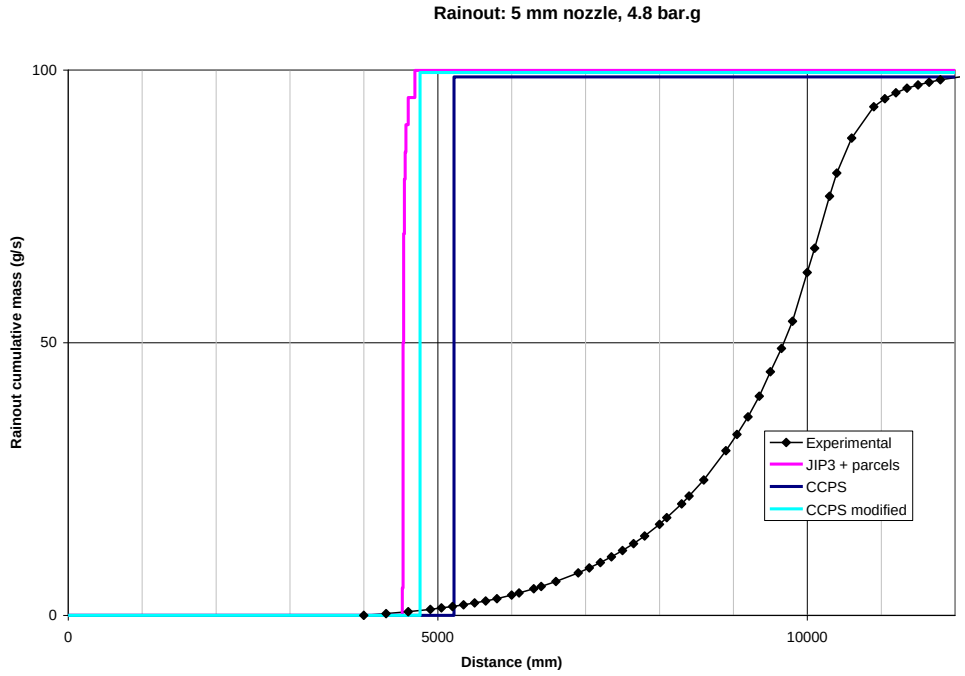

(b) 2.5 mm nozzle, 5 barg

Figure 40. Validation of distributed rainout (HSL water experiments)
UDM predictions are provided for HSL water experiments based on both the JIP Phase III and the current Phast 6.54 (CCPS) droplet size correlations.[37].

[37] Experimental flow rates of 350.2 g/s (5mm nozzle) and 91.4 g/s (2.5mm nozzle) are used instead of modelled values, though these are very close.

4.2.4 Summary

The Bernoulli model predicts discharge rates extremely well. The JIP Phase III correlation predicts well the early (500 diameters downwind) distribution of droplet sizes, but considerably over-predicts further downwind. This secondary break-up is not accounted for in the UDM. The CCPS correlations (especially the Phast 6.6 default, which mistakenly uses the flashing correlation) under-predicts droplet size significantly.

All methods predict nearly 100% rainout and agree with experimental findings. However all correlations also predict rainout too early, and even using parcels does not predict the longitudinal extent of rainout.

4.3 Model results - xylene experiments

Experimental results were obtained for a range of pressures and two different orifice sizes. In general measurements were made independently. Thus separate experiments were carried out to measure droplet size, rainout and concentration. The exception is mass flow rate which is available for all runs where temperature and rainout were measured. Moreover experimental conditions varied between these runs. The experimental conditions are given under each relevant section below.

4.3.1 Flow rate

The experimental programme included experiments for which simultaneously flow rate was measured and rainout collected. The flow rate results for these experiments are discussed in the current section, while the rainout results will be presented in Section 4.3.3. For each nominal pressure, several repeat experiments were done in order that rainout capture trays could be re-positioned so as to cover the entire spread of rainout. Inevitably these repeat experiments are at slightly different conditions. Figure 41 therefore plots:

- the individual repeat experiments (both experimental and modelled);
- the average of the experimental flow rates for each group of repeat experiments;
- modelled flow rates produced using averaged initial conditions

Two things are apparent. Firstly especially at higher values modelled flow rates exceed experimental ones. A possible explanation for divergence at larger flow rates is that some pressure drop is being experienced between the reservoir (where it is measured) and the orifice. Secondly the 'averaged' points represent well the individual clusters of points. Accordingly we use these averaged initial conditions for all rainout simulations[38].

As flow rates do diverge at higher pressures, we use experimental flow rates in the rainout simulations, with other post-expansion droplet size (velocity, droplet SMD) calculated by the discharge model.

The experimental programme also collected flowrate data used in experiments to measure temperature drop (see Section 4.3.4), but these flows are not plotted here. They follow the same pattern.

[38] As a check, rainout simulations were carried out for each run in the 5mm group clustered around 8.5 barg (a case where both temperature and pressure varies between runs), and rainout compared with that predicted using an averaged approach. The results were identical to within 0.1%

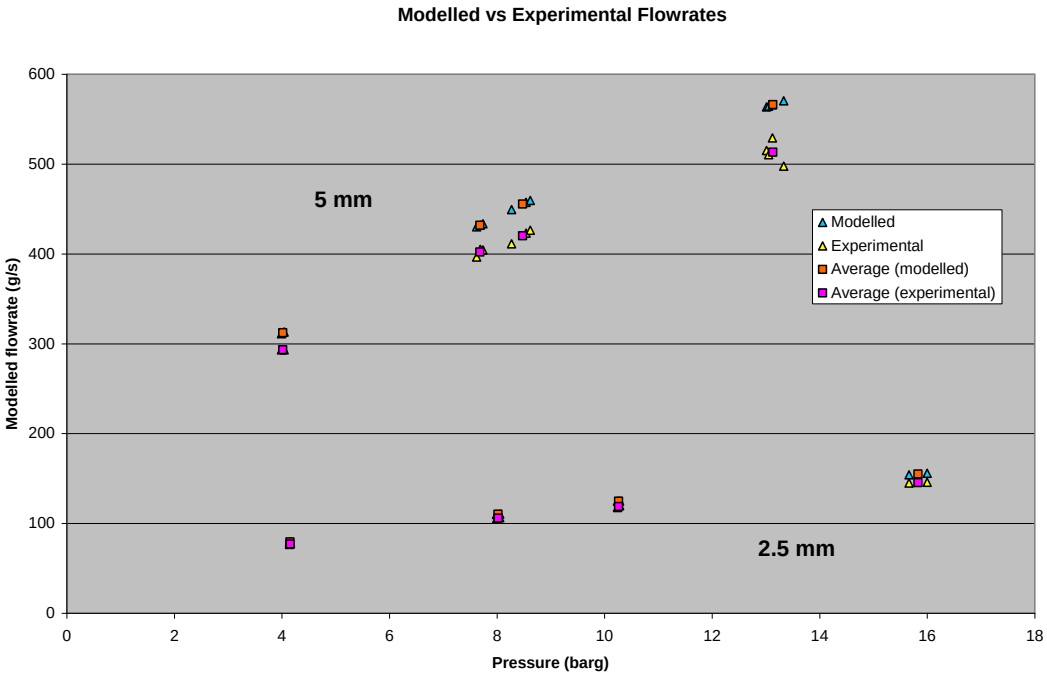

Figure 41. Validation of flow rate (HSL xylene experiments)

The key discharge characteristics (nozzle size and pressure) and outputs (flow rates and droplet sizes) for the averaged experimental data and model runs are summarised in
Table 20 and Table 21.

Nozzle diameter (mm)	Average pressure (barg)	Pressure range (barg)	Average temperature (°C)	Average flow rate		
				Measured (g/s)	Modelled (g/s)	Deviation (%)
2.5	4.2		11.0	77	79	3.1
2.5	8.0		11.0	106	110	4.3
2.5	10.3		11.0	119	125	5.1
2.5	15.8	15.7 - 16.0	11.0	145	155	6.6
5	4.0		11.0	293	312	6.5
5	7.7		11.0	402	432	7.4
5	8.5	8.3 - 8.6	2.3[39]	420	455	8.4
5	13.1	13.0 - 13.3	5.0	513	566	10.3

Table 20. Validation of flow rate (HSL xylene experiments)
For those cases where the pressure range is not specified, all repeat experiments were within 0.1 bar of the average. Furthermore where the fluid temperature is specified as 11.0 °C, it was not measured and expected to be in the range 10-12°C.

[39] Temperature ranged between 1 and 5°C

Nozzle diameter	Pressure	Velocity	Droplet SMD (µm)		
(mm)	(barg)	(m/s)	CCPS	JIP	Melhem
2.5	4.2	30.8	335	1357	930
2.5	8.0	42.8	173	894	481
2.5	10.3	48.4	135	765	376
2.5	15.8	60.2	88	581	244
5	4.0	30.3	346	2081	961
5	7.7	41.9	181	1380	502
5	8.5	43.9	165	1406	459
5	13.1	54.6	106	1039	296

Table 21. Modelled SMD and (vena contracta) velocity

It was found for all xylene simulations, that the SMD values for CCPS were identical to those of modified CCPS. Thus it was always picking up the correct mechanical break-up correlation.

4.3.2 Droplet size

The measurement of droplet size distributions used a set of images from other experimental runs. The experimental conditions and measured and predicted SMDs are shown in Table 22:

Pressure	SMD	SMD (CCPS, Phast 6.6)		SMD (JIP)		SMD (Melhem)	
(barg)	Measured (µm)	Modelled (µm)	Deviation (%)	Modelled (µm)	Deviation (%)	Modelled (µm)	Deviation (%)
4.0	707	349	-51	1455	106	969	37
8.0	744	174	-77	938	26	485	-35
12.0	805	116	-86	725	-10	323	-60
16.0	522	87	-83	605	16	242	-54

Table 22. Validation of SMD (HSL xylene experiments, 2.5 mm nozzle)

Except for the low pressure case of 4 barg, it is seen that the JIP SMD correlation produces overall the most accurate results. Both the Melhem and Phast 6.6 CCPS correlation under-predict the SMD, with Melhem performing better than the Phast 6.6 CCPS correlation.

In these experiments ambient and fluid temperature was assumed to be 6^{o}C following feedback from HSL.

As explained in the Part 'A' report, SMDs are not reported for the 5mm orifice due to problems obtaining meaningful results from the droplet imaging. In all cases droplet size distributions were measured at 800 diameters (2m) downwind.

Measured and predicted droplet size distributions for the 2.5mm orifice are compared in Figure 42 through Figure 45. Also plotted on the distributions are measured and JIP predicted SMDs. The CCPS SMD is not associated with a distribution and is shown as a vertical line.

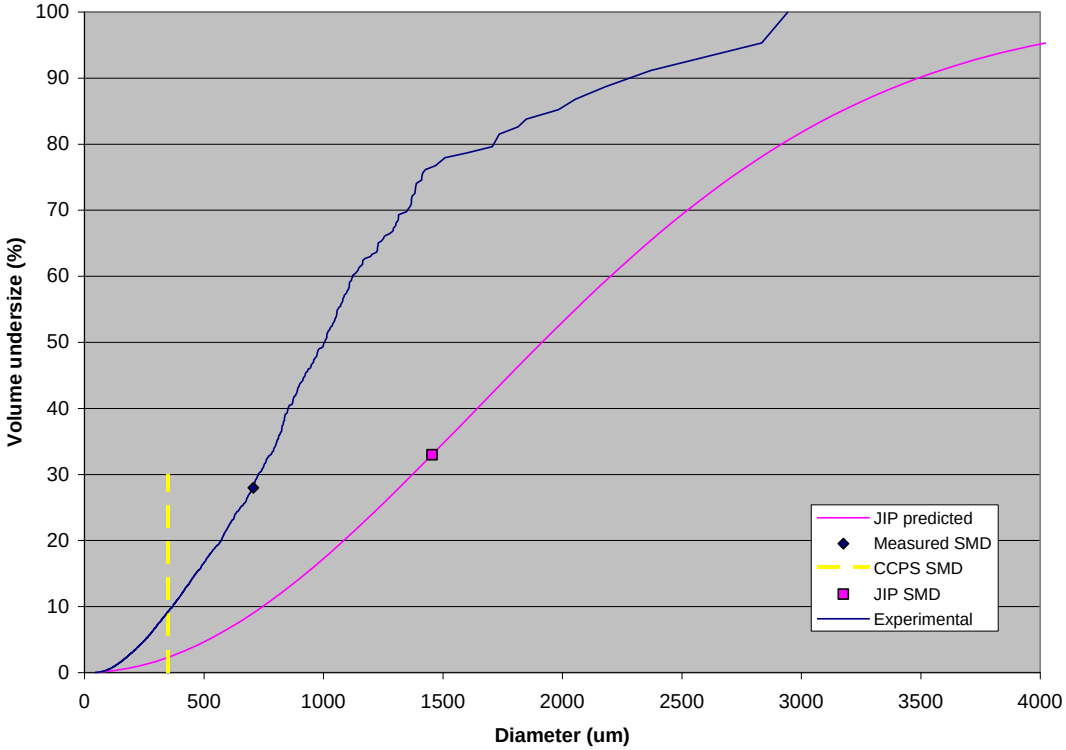

Figure 42. Validation of droplet size distribution (xylene, 2.5 mm, 4 barg)

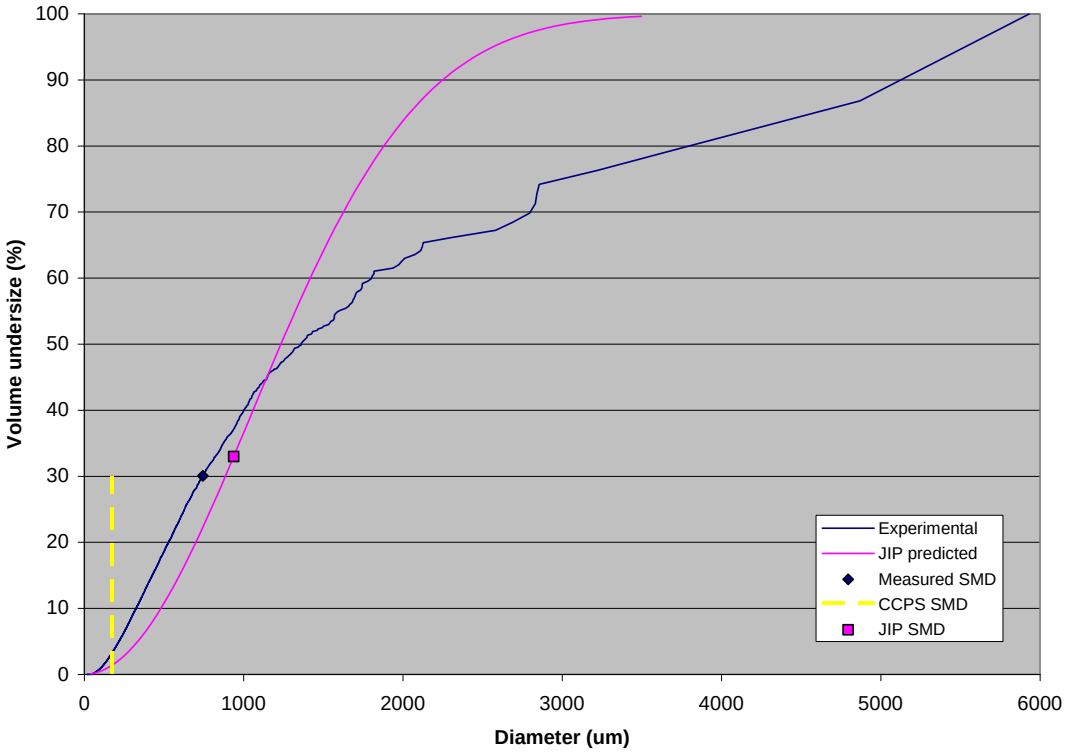

Figure 43. Validation of droplet size distribution (xylene, 2.5 mm, 8 barg)

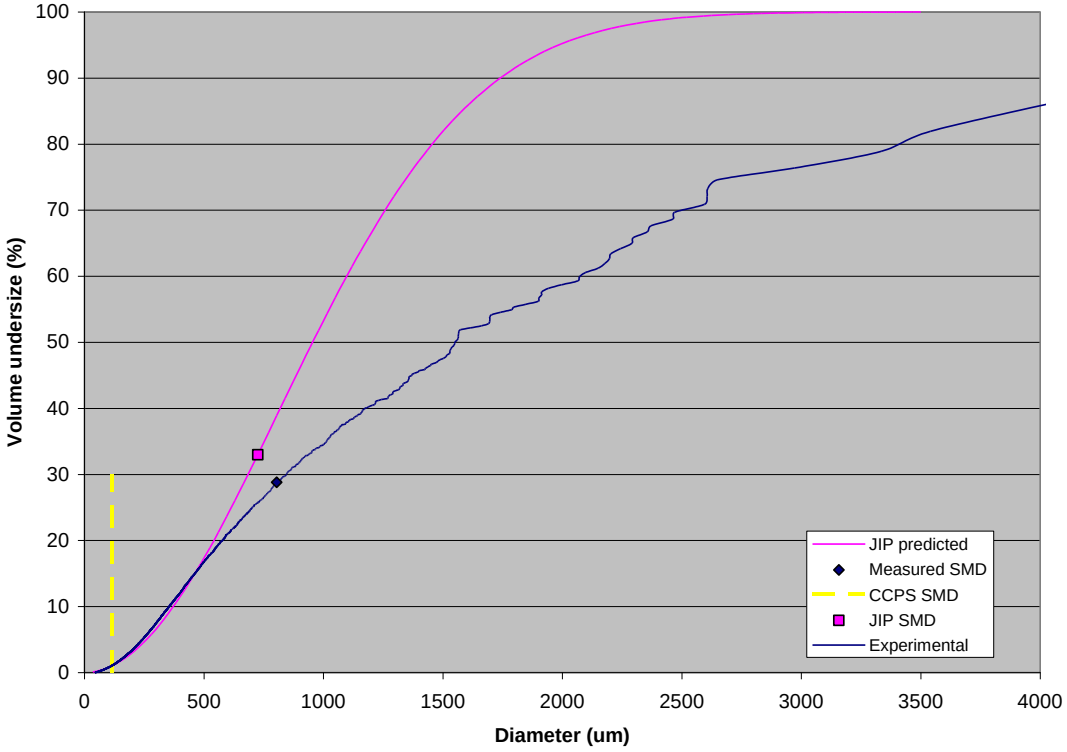

Figure 44. Validation of droplet size distribution (xylene, 2.5 mm, 12 barg)

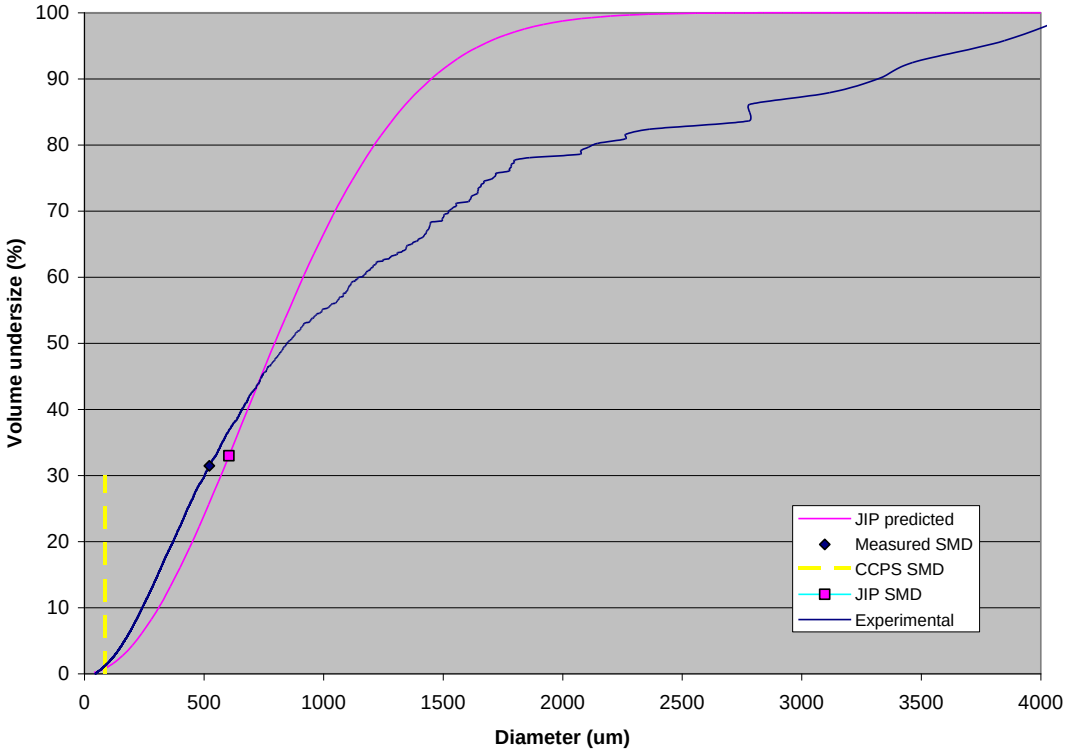

Figure 45. Validation of droplet size distribution (xylene, 2.5 mm, 16 barg)

The JIP Phase III correlation has a tendency to over-predict cumulative volume at high diameters, apart from the 4 barg case where it always under-predicts. As indicated earlier, this may be caused by inaccuracies resulting from missing or clipping of data for larger droplets during correlation development from PDA experiments. The experimental measurements are highly sensitive to small numbers of very large droplets. For example just 3 droplets may account for the final 25% of the mass.

The experimentally measured and predicted distributions for the JIP Phase III correlation are compared in Figure 46. The CCPS correlation predicts droplets 4 – 10 times as large as the JIP Phase III correlation. In terms of the distribution of droplet sizes, only a few percent of the mass in the JIP Phase III distribution has a similar or smaller size to that predicted by the CCPS correlation.

The measured droplet size distribution shown in Figure 46 shows no clear pattern with pressure. It is however shown in the Part A report that in line with the modelled droplet size the measured droplet size does reduce with increasing pressure, in case droplets larger than 1200mm are excluded.

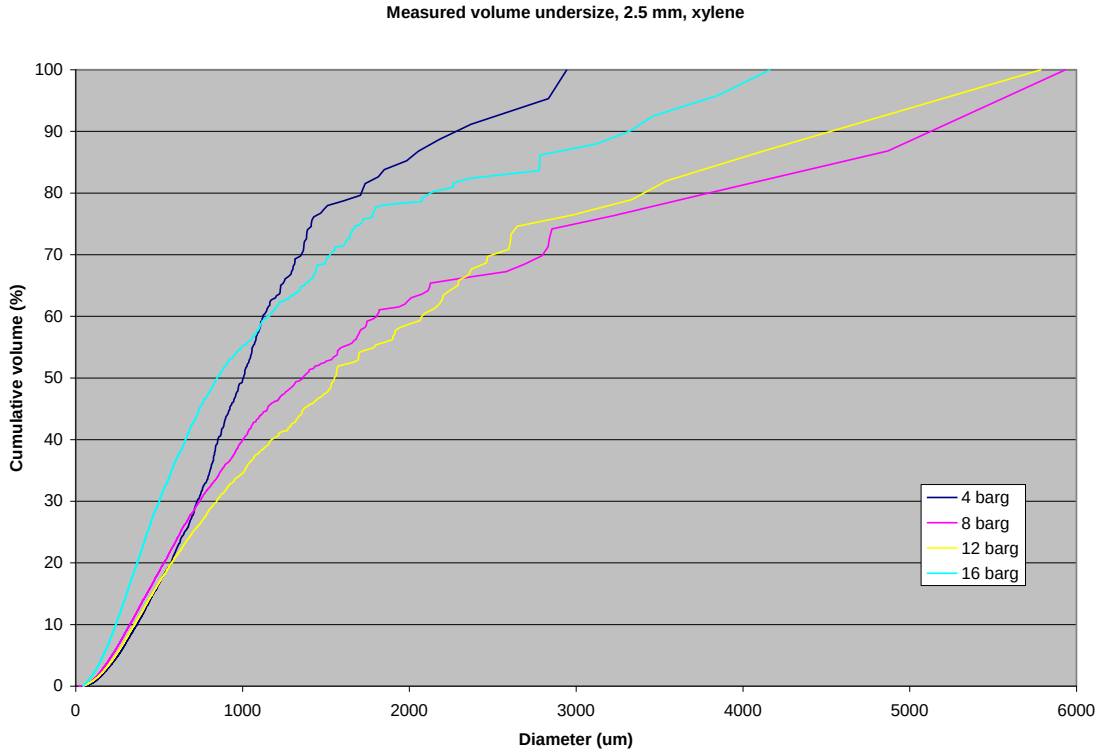

(a)

Measured

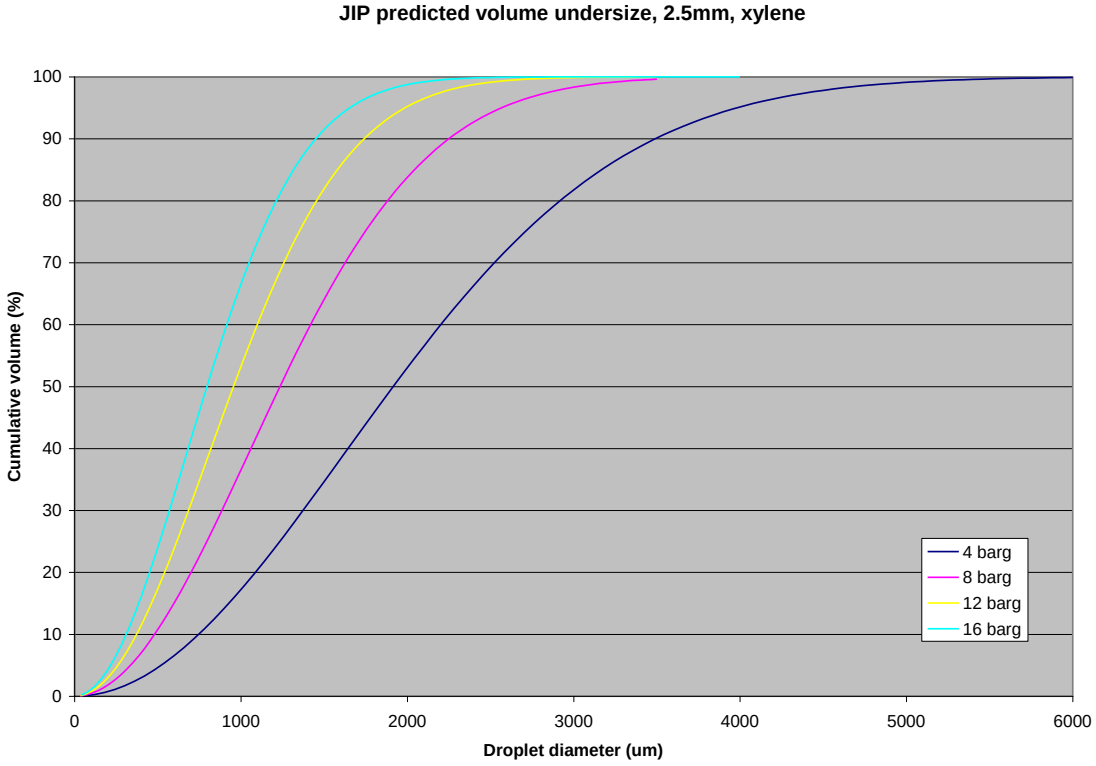

(b) JIP Phase III correlation

Figure 46. Validation of droplet size distribution (xylene, 2.5 mm)

4.3.3 Rainout mass and distribution (including verification of time to rainout)

The UDM rainout simulations used as input the discharge data given in
Table 20 and Table 21. Measured flow rates were used instead of modelled ones, as the two diverge at higher flows. Other UDM inputs (SMD, u_{vc}) are taken from DISC / ATEX calculations[40].

Table 23, includes rainout predictions using both the CCPS and JIP Phase III droplet size correlations. The rainout percentages are expressed as a function of experimentally observed flow rate (Experimental) or modelled flowrate (JIP and CCPS). Rows where significant rainout may have occurred beyond the last tray and was therefore not captured are highlighted in yellow[41]. The same data are plotted in Figure 47:

Nozzle (mm)	Pressure (barg)	Measured (%)	CCPS (%)	JIP (%)	Melhem (%)
2.5	4.2	96.8	96.7	99.5	99.3
2.5	8.0	91.4	90.8	98.9	98.0
2.5	10.3	90.4	86.7	98.6	97.1
2.5	15.8	82.1	75.1	97.7	94.0
5	4.0	94.3	97.2	99.7	99.3
5	7.7	89.9	93.1	99.5	98.3
5	8.5	95.3	95.2	99.7	98.8
5	13.1	85.2	88.8	99.4	97.2

Table 23. Validation of total rainout percentage (HSL xylene experiments)

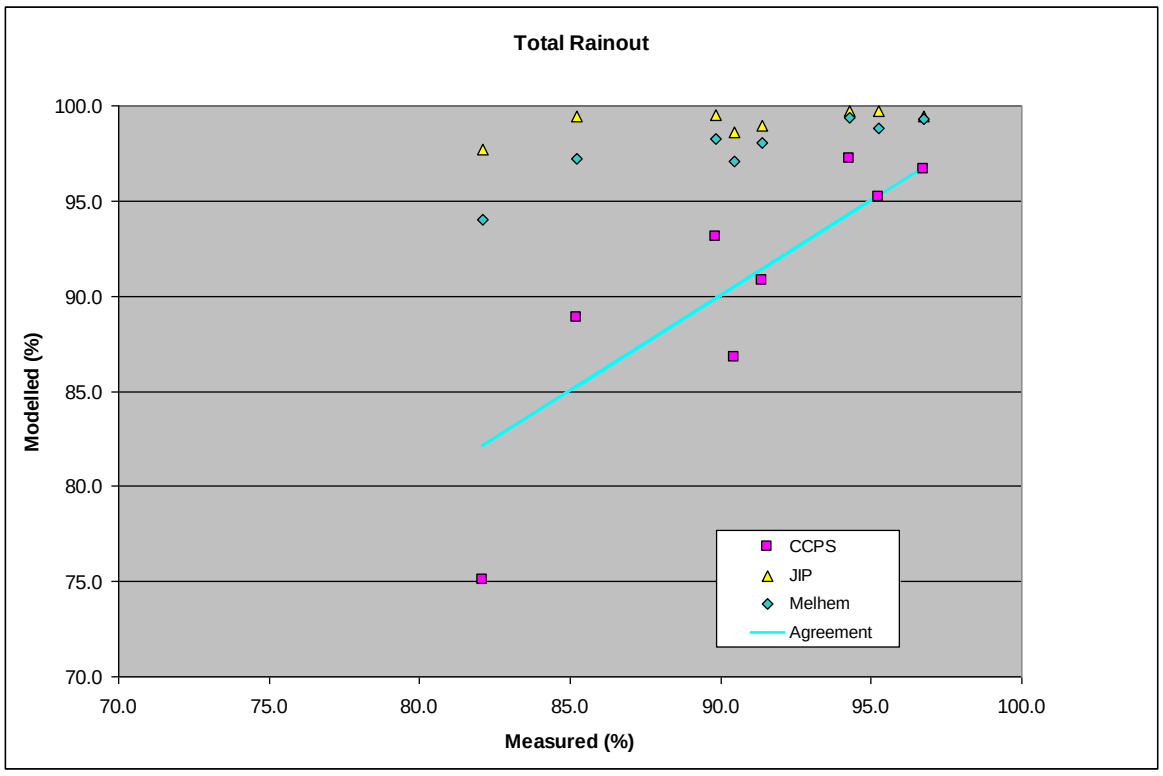

Figure 47. Validation of total rainout percentages (HSL xylene experiments)

The consequence of the much smaller droplets predicted by the CCPS correlation is clear. The CCPS correlation predicts lower rainout, as smaller droplets experience more evaporation. There is in fact good agreement with the experimental data for the total rainout, despite the likely underestimate of rainout for the 5mm 4 barg case. The Phase III JIP correlation over-estimates the total amount of rainout, predicting almost 100% rainout in all cases. It under predicts both average rainout. The Melhem correlation lies between the other two.

[40] The vena contract velocity u_{vc} could be calculated from Q assuming C_d = 0.6, but this assumption may be incorrect for these nozzles.

[41] Judged from Figure 53 and Figure 56 below

Perhaps surprising is the lower than expected rainout. For the 2.5 mm, 10 barg experiment 10% of the xylene does not rain out, and this is not atypical. For the 16 barg case this is 18% (though this may be reduced by a few percent once allowance is made for not all the rainout being captured). Either this mass evaporates, or comprises small droplets that remain in suspension[42].

An idea of how well the rainout distance is predicted by the different approaches can be gleaned from plotting measured against modelled rainout distance. For the Melhem and CCPS correlations (without droplet parcels), there is a unique rainout distance, but for the JIP Phase III parcels logic rainout is distributed longitudinally. We therefore plot instead the median rainout distance (i.e. the distance by which 50% of the total mass that rains out has done so). These results are shown in Figure 48.

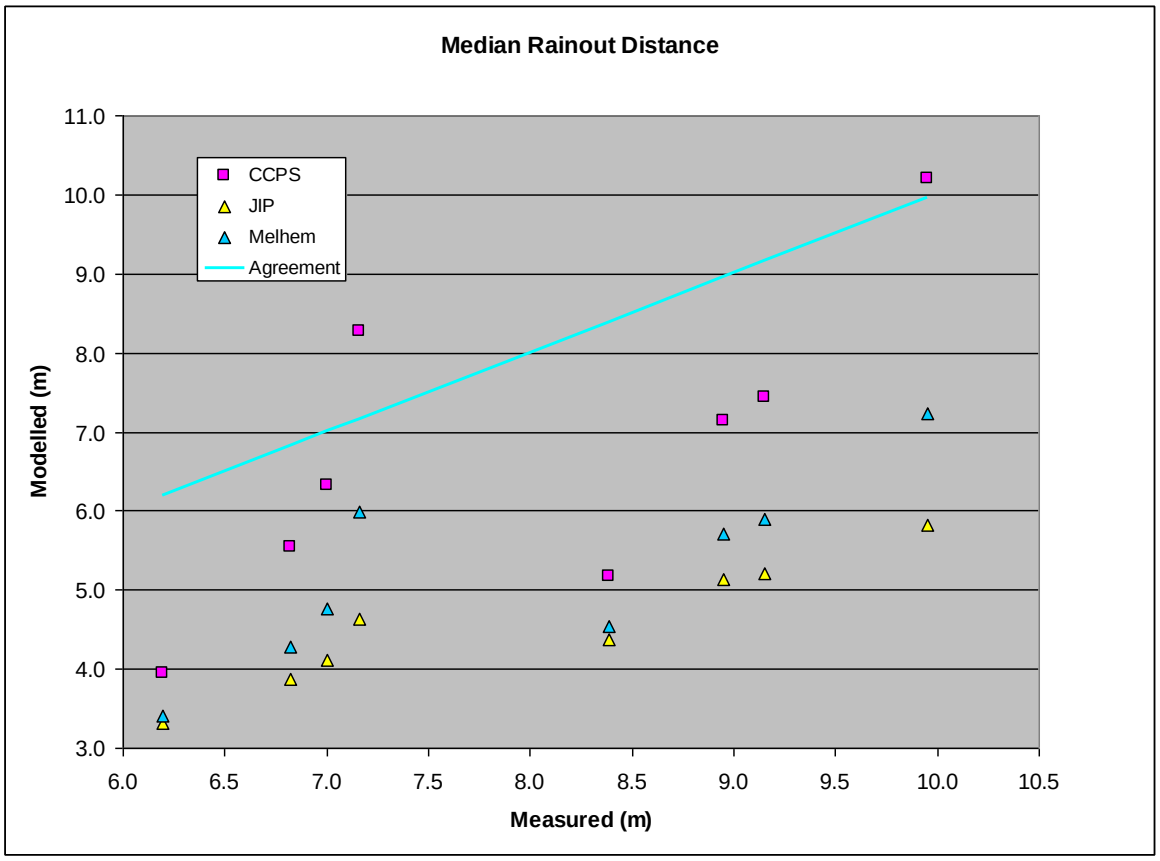

Figure 48. Validation of median rainout distance (HSL xylene experiments)

The measured point at 8.4m downstream distance is the 5 mm 4 barg experiment where significant rainout may not have been captured, and therefore the measured value is likely to be an underestimate. The tendency is for all correlations to underestimate rainout distances, though less so for CCPS.

Plots for individual xylene rainout simulations and experimental data are shown below for all experiments. These show cumulative rainout as a function of distance downstream on the release. The JIP Phase III results show a 'staircase' effect due to the use of multiple droplet parcels that rain out at increasing distances. The CCPS method uses only one parcel and therefore predicts rainout at one location. The rainout distances reflect droplet size: larger droplets will, in the UDM, rain out first due to relatively less drag. So JIP Phase III rains out first, then Melhem, and finally CCPS.

[42] Imaging of the plume after rainout may reveal which

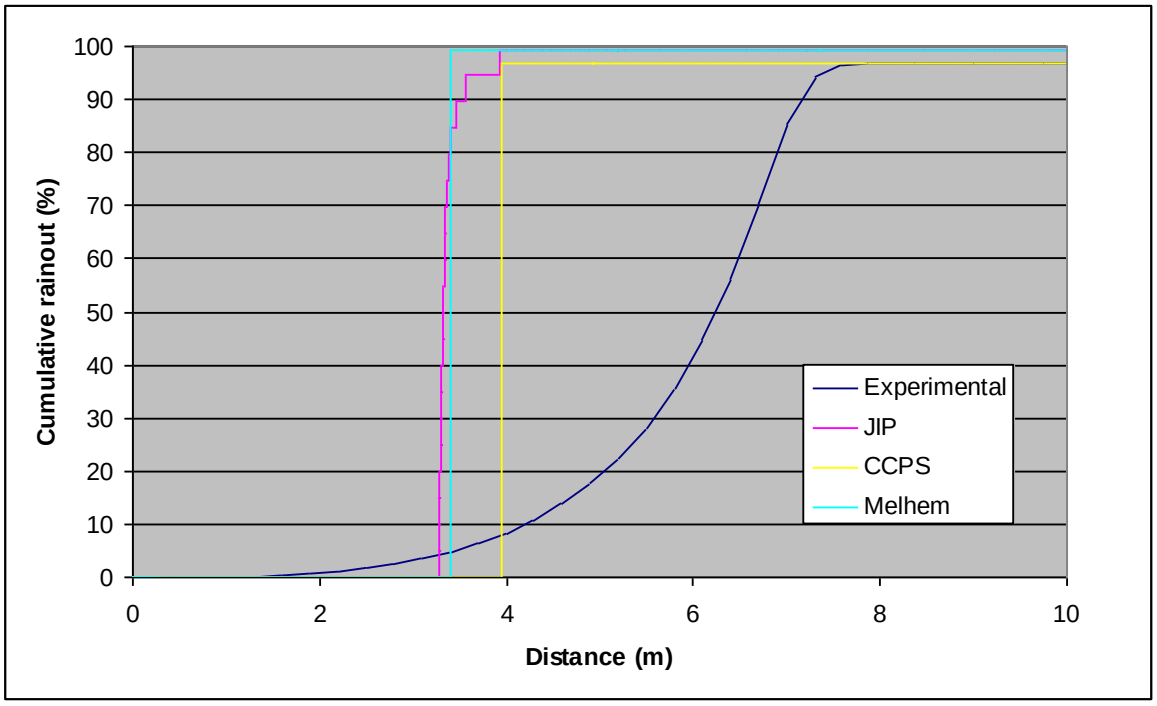

Figure 49. Validation of distributed rainout (xylene, 2.5 mm, 4.2 barg)

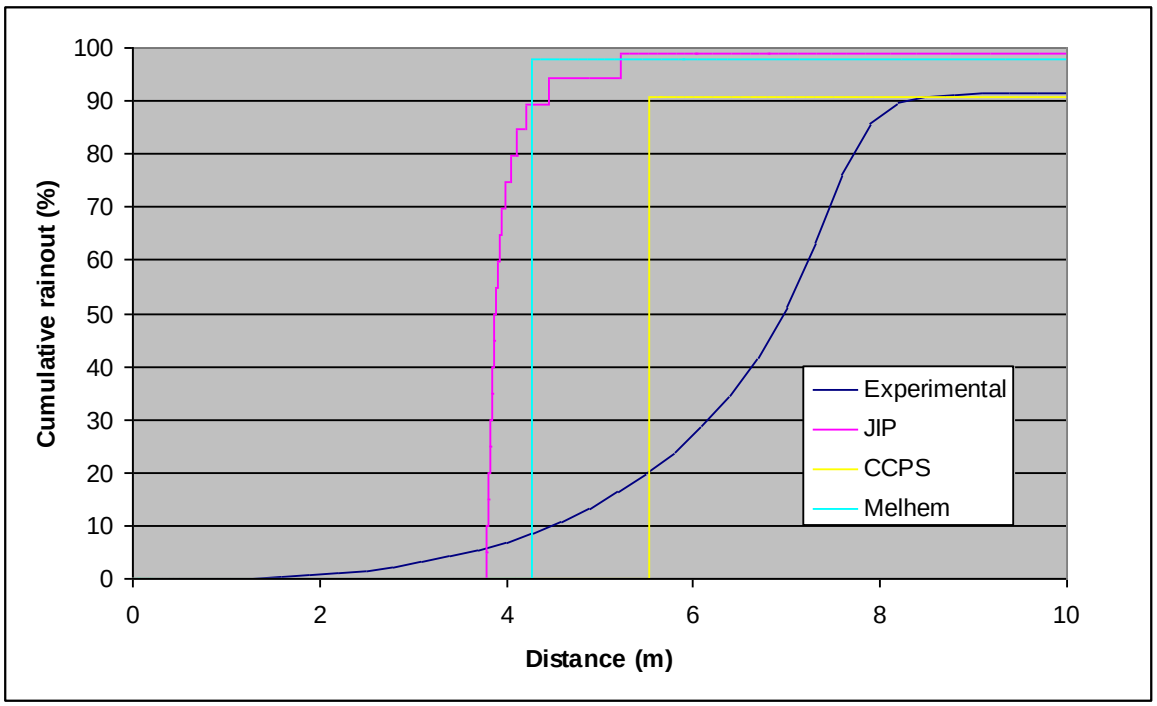

Figure 50. Validation of distributed rainout (xylene, 2.5 mm, 8 barg)

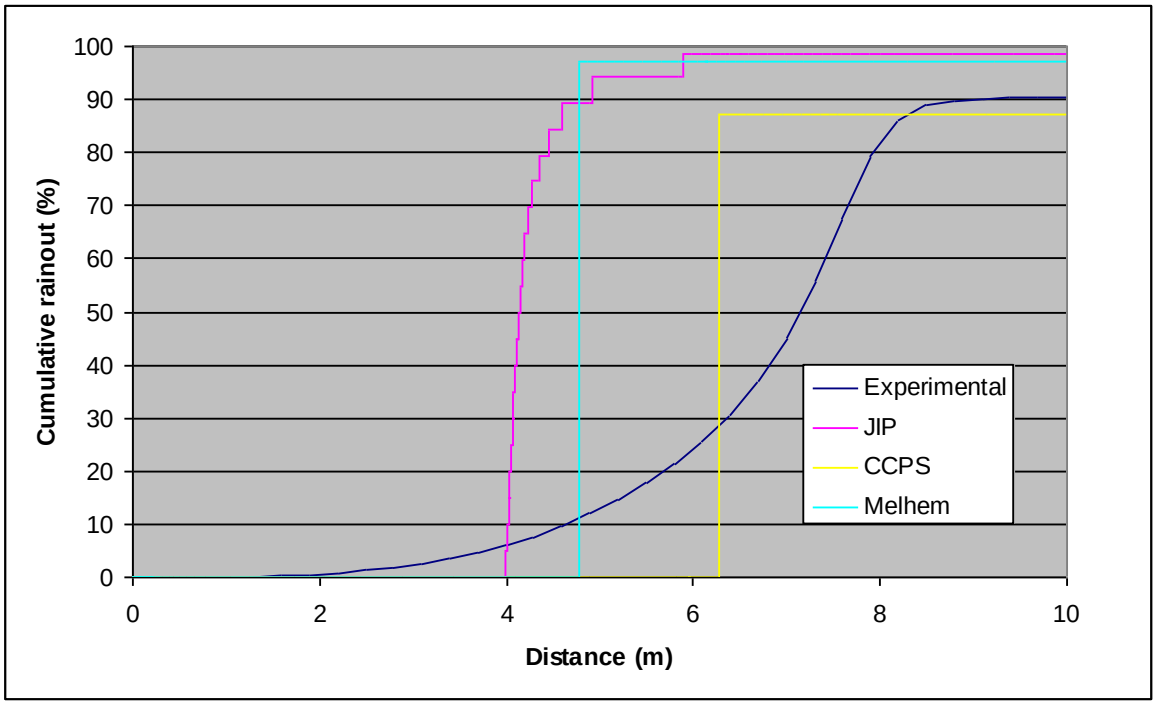

Figure 51. Validation of distributed rainout (xylene, 2.5 mm, 10.3 barg)

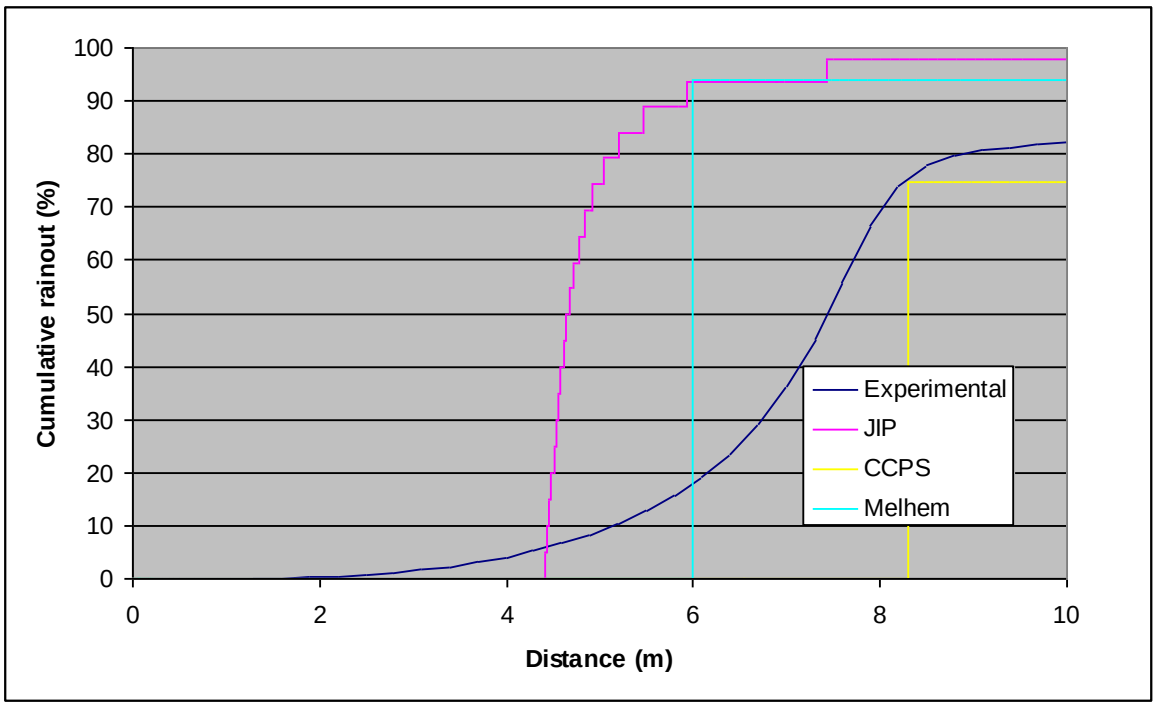

Figure 52. Validation of distributed rainout (xylene, 2.5 mm, 15.8 barg)

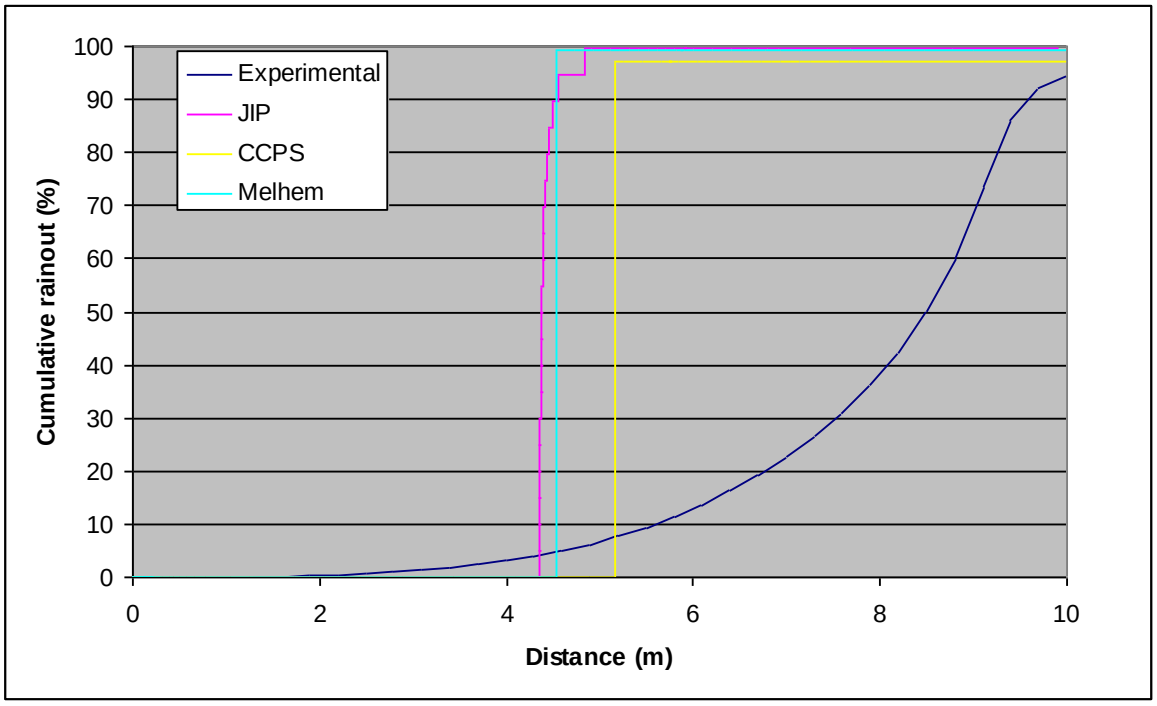

Figure 53. Validation of distributed rainout (xylene, 5 mm, 4 barg)

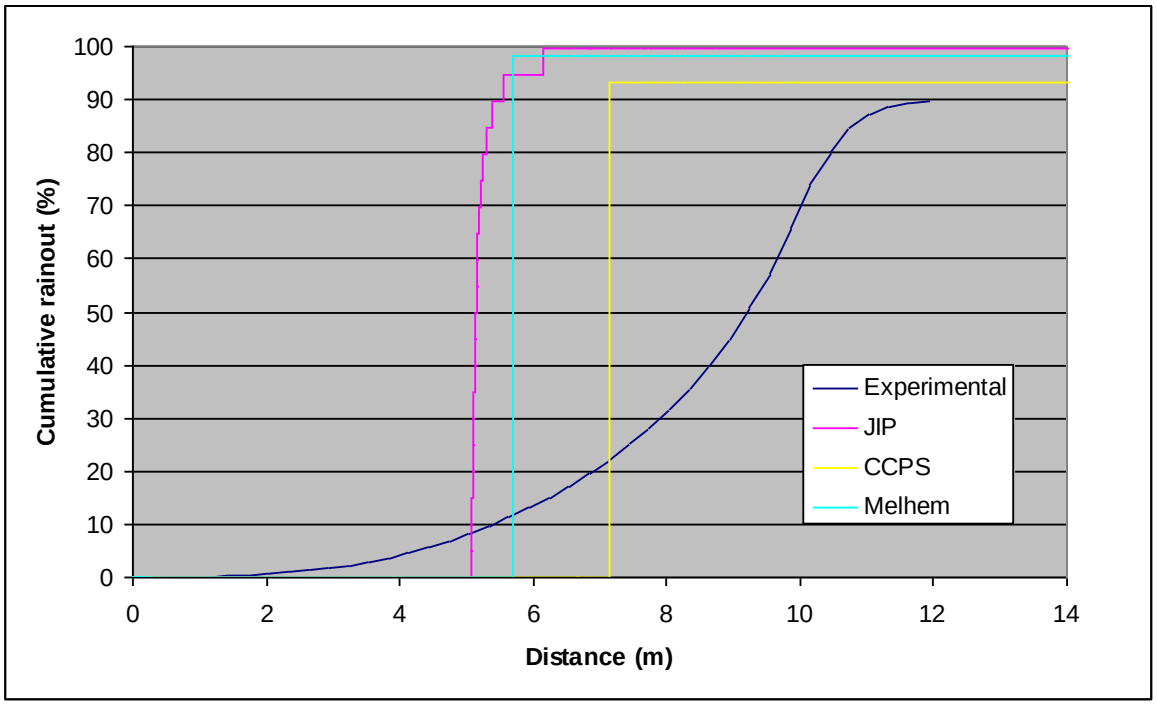

Figure 54. Validation of distributed rainout (xylene, 5 mm, 7.7 barg)

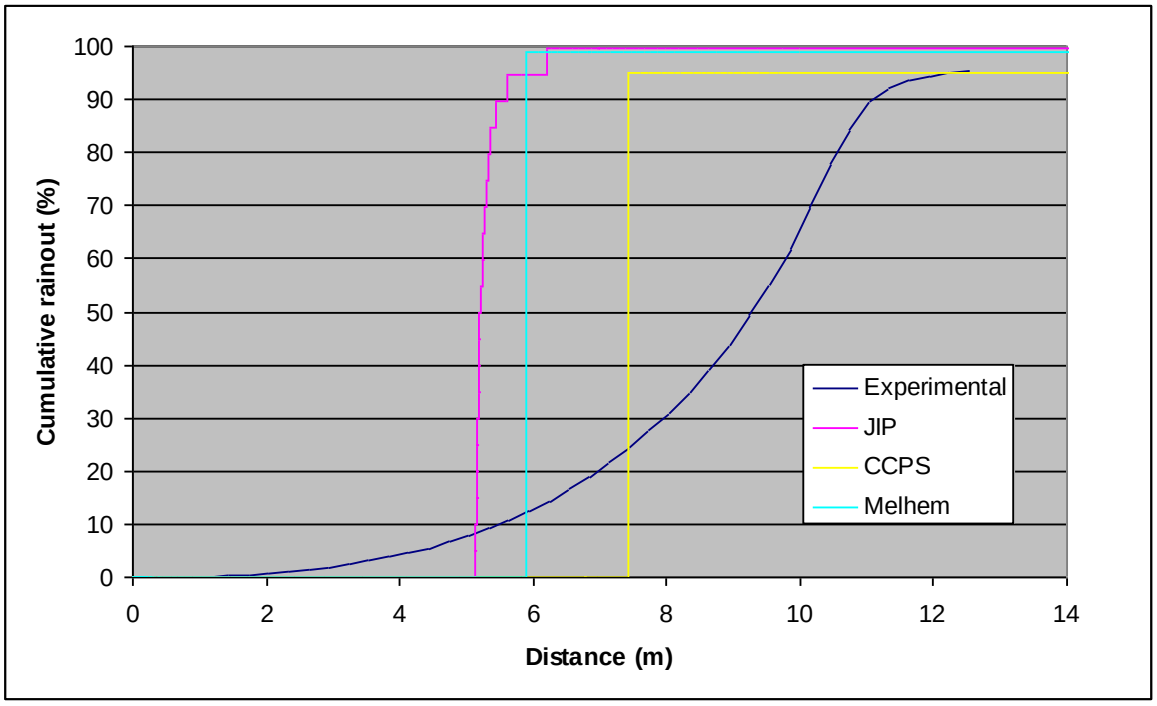

Figure 55. Validation of distributed rainout (xylene, 5 mm, 8.5 barg, cold release)

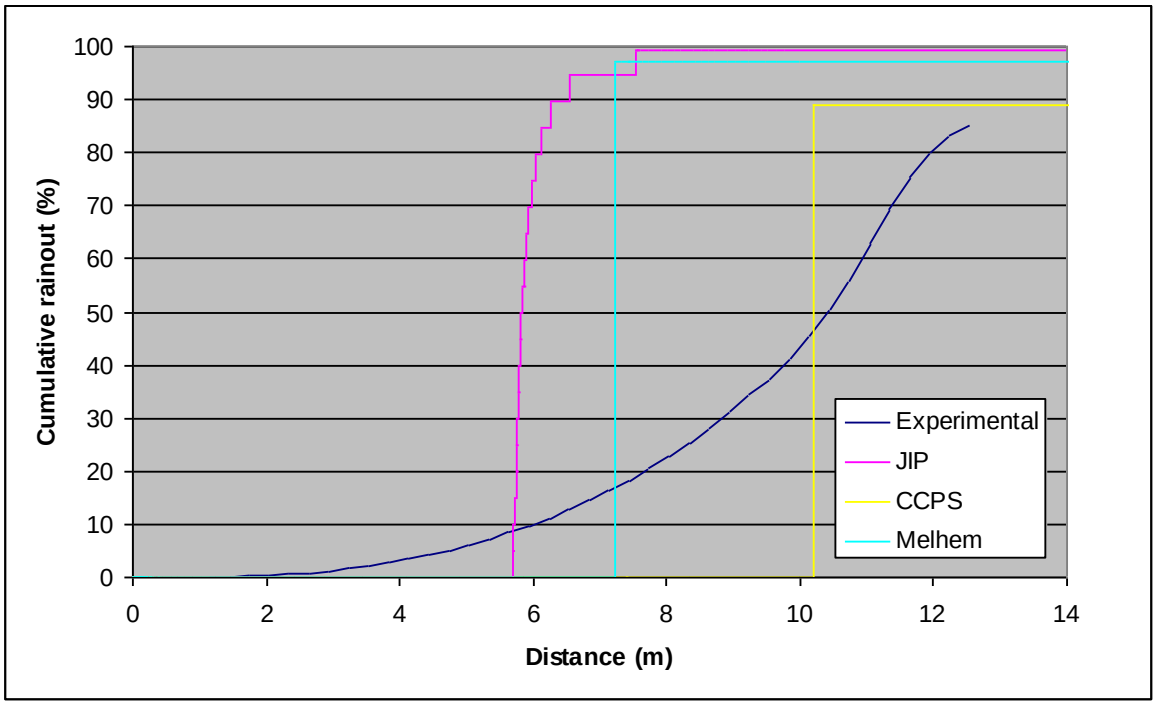

Figure 56. Validation of distributed rainout (xylene, 5 mm, 12.75 barg)

Verification of Time to Rainout

Using an analytical solution of vertical droplet acceleration, and ignoring drag between droplet and the surrounding plume, it is possible to verify the UDM predictions for time to rainout (although no measurements of this have been carried out). For droplets accelerating solely due to gravity:

$$\frac{d^2 z}{dt^2} = -g \qquad (50)$$

For an initial droplet height z_0 = 1m the solution for z = 0 (i.e. rainout) is:

$$t_{ro} = \sqrt{\frac{2z_0}{g}} = 0.4515s \quad \textbf{(51)}$$

The equivalent equation in the UDM is:

$$m_d \frac{d\, u_{dz}}{dt} = -u_{dz} \frac{dm_d}{dt} + F_{body} + F_{drag} \quad \textbf{(52)}$$

By setting F_{drag} = 0 (and setting cloud density ρ_{cld} = 0) this reduces to the same provided $dm_d/dt = 0$. We take the CCPS 4 barg 5mm case (as this has maximum rainout and therefore minimum dm_d/dt). The UDM predicted time to rainout is 0.484s, some 7% longer. The difference here is accounted for by the UDM calculating time in continuous cases using a finite-difference approach rather than using a linked ODE, and by the ~ 3% rainout [43].

[43] In a separate project this work has been done, and using that UDM code the equivalent UDM calculation for large (1mm) droplets is 0.4516s.

4.3.4 Temperature

The measured and modelled temperature drop in the plume for 2.5mm and 5mm releases are given in Table 24 and Table 25 respectively. The temperature drop is the decrease of temperature relative to the ambient temperature which was quoted by HSL to be very close to the stagnation temperature. The adopted stagnation temperature is 6.5C[44]. The measured data are given at a series of heights above the floor (mm), while the model predicts data at the centre-line only. The measurements are taken at 6 meter downstream of the orifice.

PRESSURE (barg)	**4.2**	**7.95**	**8.0**	**11.5**	**15.4**
Height above floor (mm)	***Cooling in °C - Measured at given height above floor***				
1375	-0.35	-0.35	-0.26	-0.10	-0.85
1215	-0.30	-0.58	-0.25	-0.54	-1.39
1060	-0.40	-1.07	-0.78	-1.11	-2.64
920	-0.63	-2.23	-1.69	-1.73	-2.95
760	-1.05	-2.53	-2.00	-2.01	-3.13
615	-2.19	-2.57	-2.17	-2.08	-3.22
445	-2.70	-2.50	-2.21	-2.02	-3.09
290	-2.53	-1.59	-2.38	-1.91	-2.76
Droplet size correlation	***Cooling in °C – Modelled at plume centre-line height***				
CCPS	-0.29	-1.16	-1.17	-1.72	-2.09
JIP Phase III	-0.03	-0.07	-0.07	-0.11	-0.13

Table 24. Validation of temperature drop (xylene, 2.5mm, 6 m downstream)

PRESSURE (barg)	**4.0**	**7.7**	**11.5**
Height above floor (mm)	***Cooling in °C - Measured at given height above floor***		
1375	0.04	0.09	-1.35
1215	0.09	-0.08	-2.68
1060	-0.06	-1.54	-2.90
920	-1.19	-1.89	-3.18
760	-2.50	-1.51	-3.29
615	-2.56	-1.74	-3.25
445	-2.65	-2.06	-2.85
290	-2.48	-1.79	-2.76
Droplet size correlation	***Cooling in °C – Modelled at plume centre-line height***		
CCPS	-0.41	-1.13	-1.53
JIP Phase III	-0.03	-0.06	-0.04

Table 25. Validation of temperature drop (xylene, 5mm, 6 m downstream)

The same data are plotted in Figure 57 through Figure 63. In each case the centreline height and vapour temperature results from both the CCPS and JIP Phase III simulations are also plotted.

[44] The actual temperatures are either 5 or 7 C, which are very close to the adopted value of 6.5C.

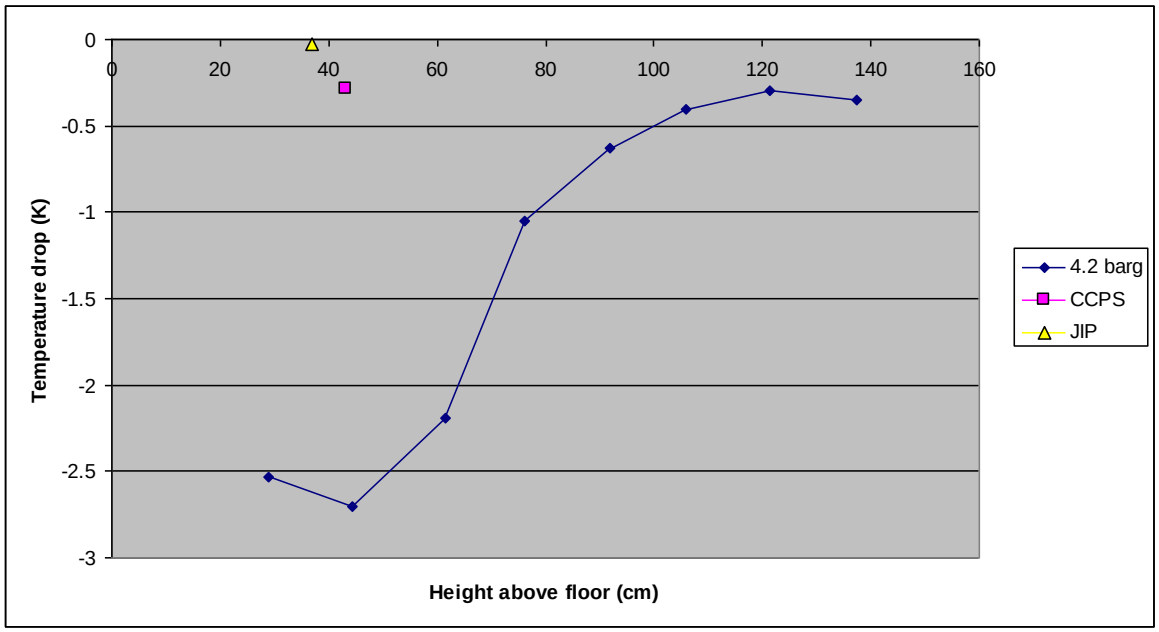

Figure 57. Validation of temperature drop (xylene, 2.5mm, 4.2 barg, 6 m downstream)

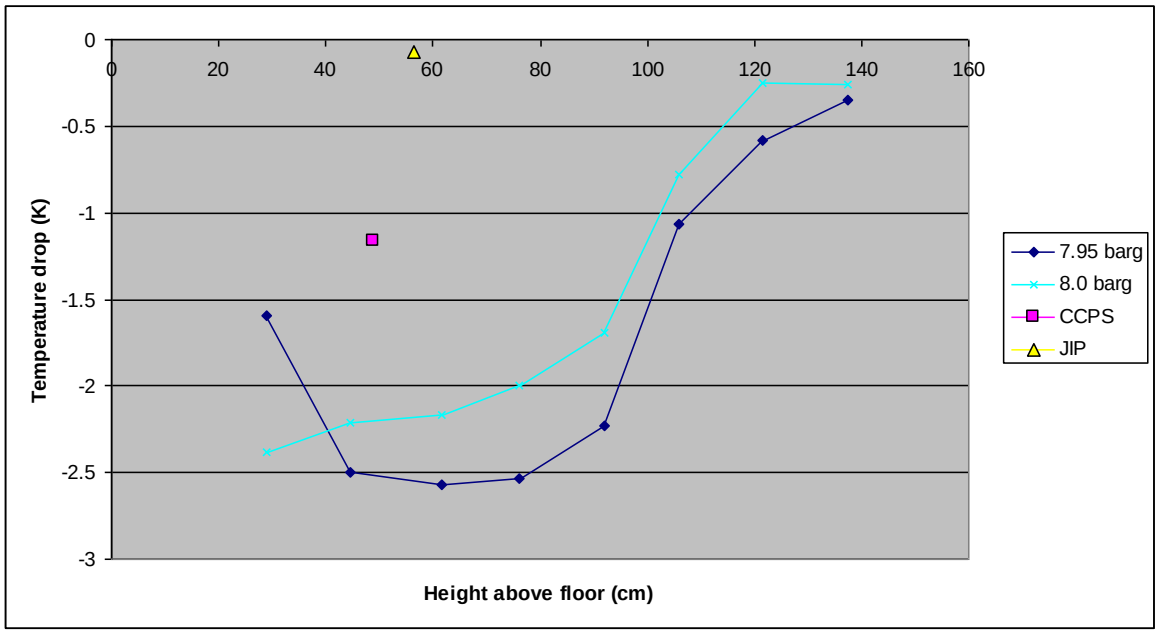

Figure 58. Validation of temperature drop (xylene, 2.5mm, 7.95&8 barg, 6 m downstream)

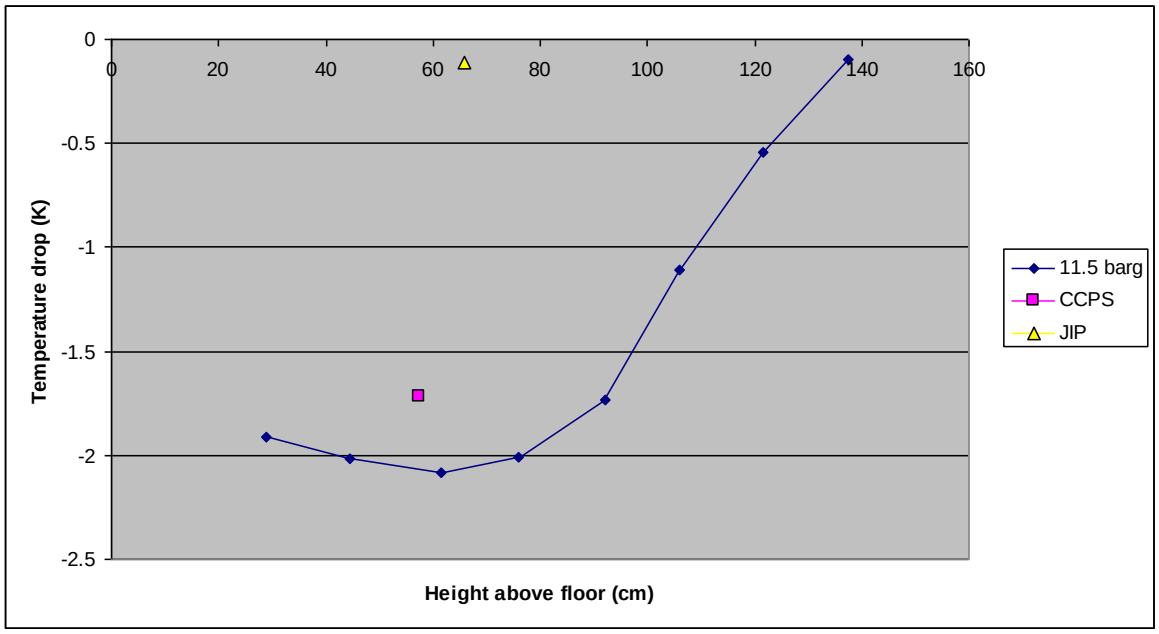

Figure 59. Validation of temperature drop (xylene, 2.5mm, 11.5 barg, 6 m downstream)

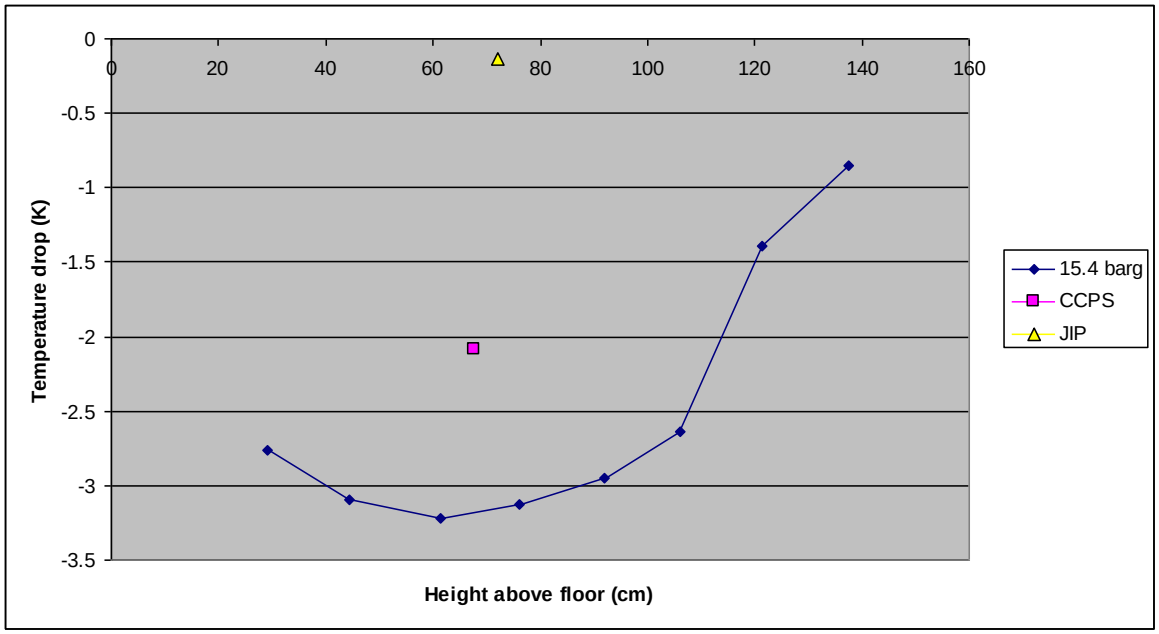

Figure 60. Validation of temperature drop (xylene, 2.5mm, 15.4 barg, 6 m downstream)

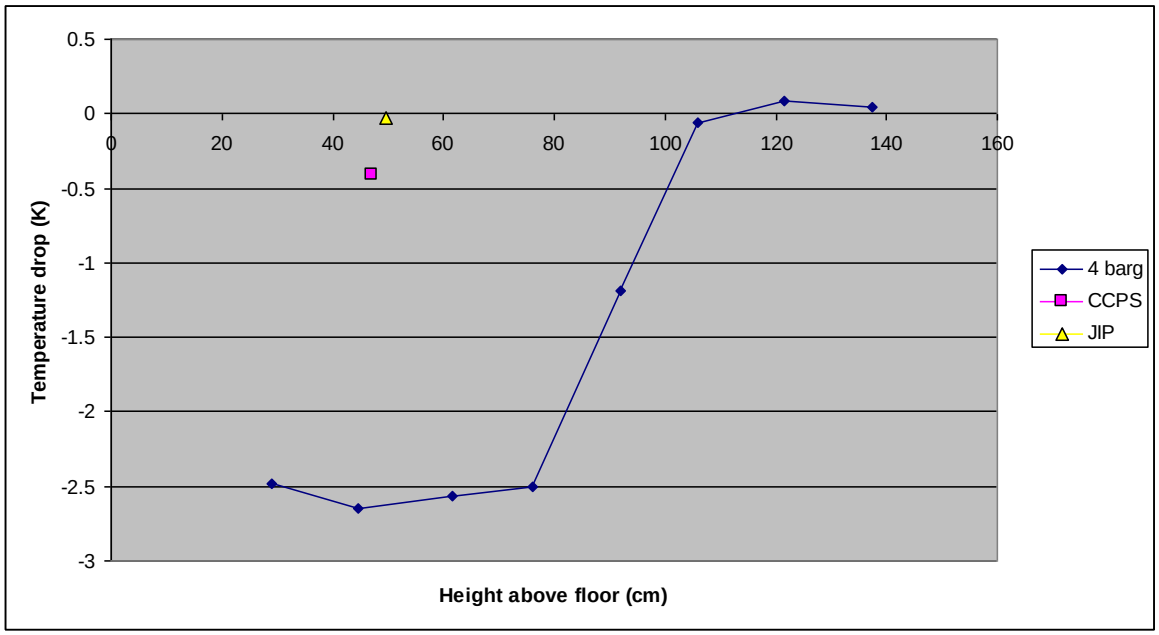

Figure 61. Validation of temperature drop (xylene, 5mm, 4 barg, 6 m downstream)

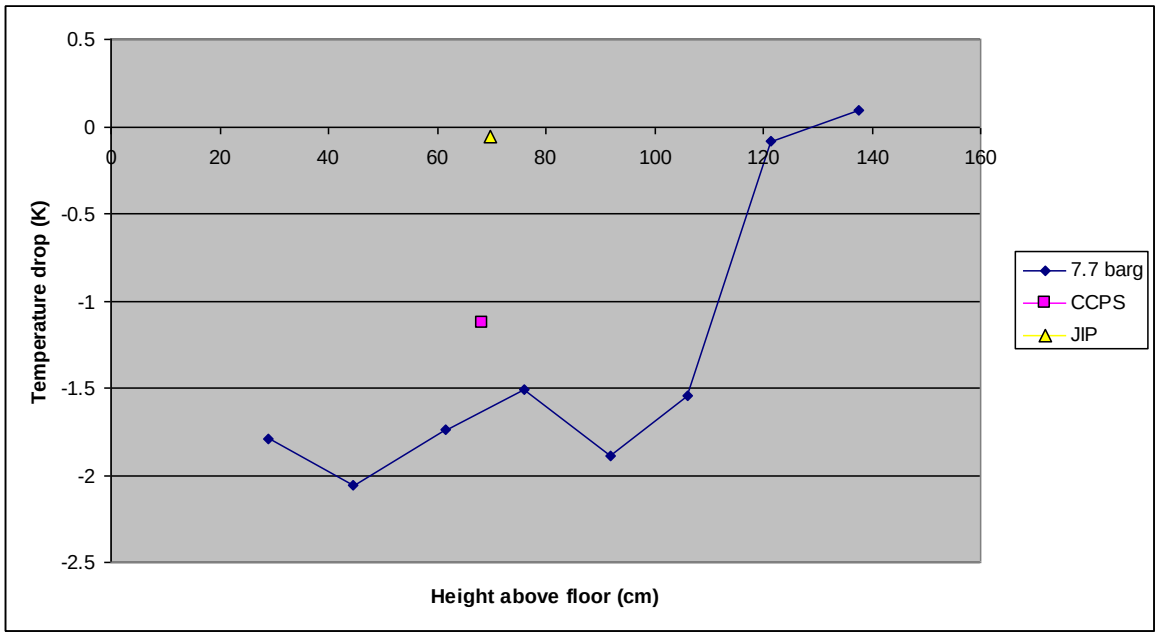

Figure 62. Validation of temperature drop (xylene, 5mm, 7.7 barg, 6 m downstream)

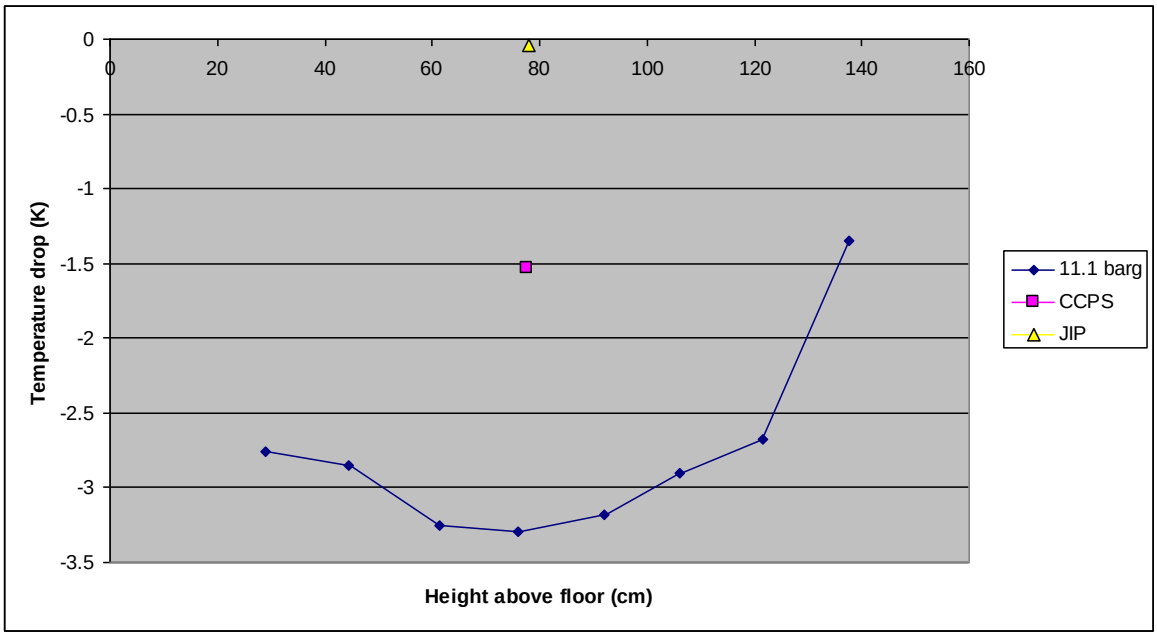

Figure 63. Validation of temperature drop (xylene, 5mm, 11.1 barg, 6 m downstream)

A temperature drop in the vapour indicates evaporation of liquid. Moreover two runs at near identical conditions (2.5 mm nozzle, 7.95 and 8 barg; Figure 58) show there is considerable variability in temperature measurements.

In most cases[45] the measured temperature drop as a function of height indicates unique temperature minimum, suggesting it corresponds to the jet centreline. We have therefore plotted the measured maximum temperature drop against modelled centreline temperature drop in the figures below.

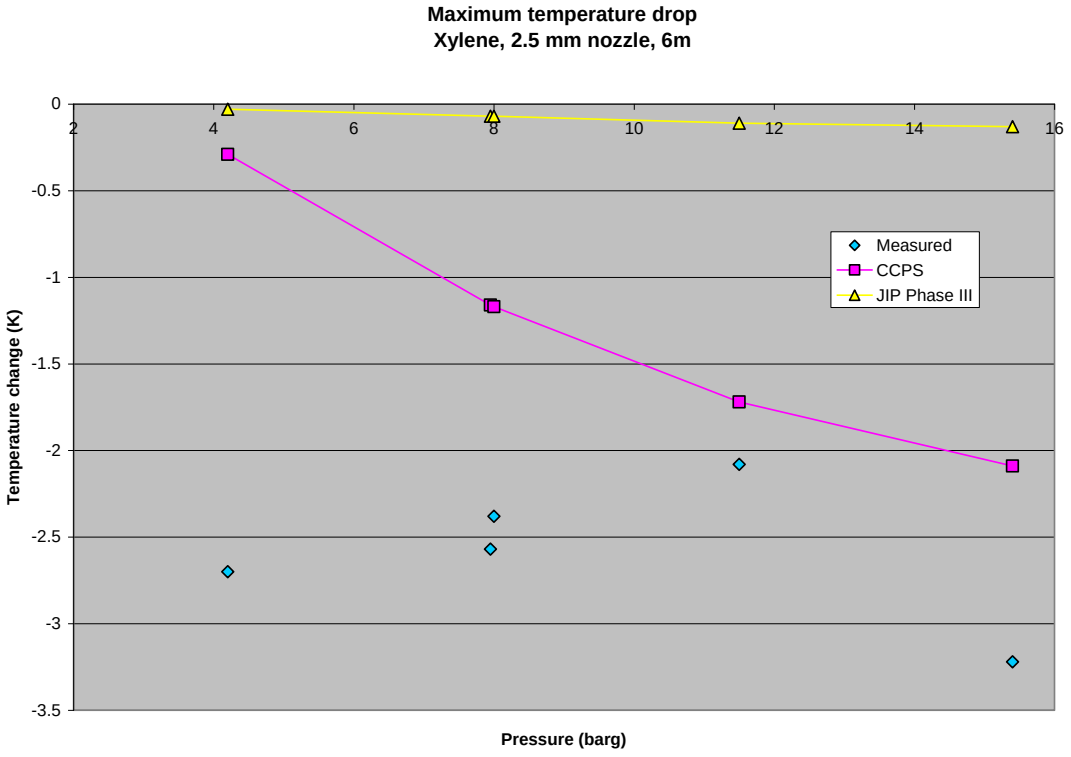

(a) 2.5 mm nozzle

[45] Except the 7.7 barg 5mm case

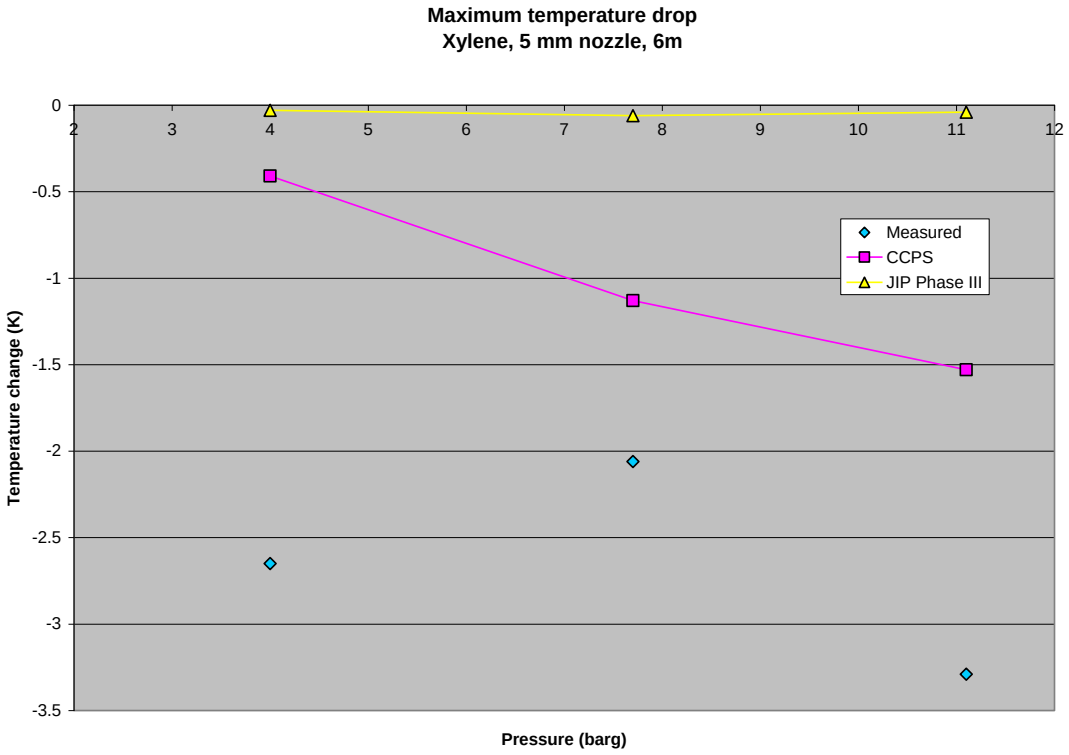

(b) 5 mm nozzle

Figure 64. Maximum temperature drop at 6m downwind

Even if our prediction of total rainout mass is good (as in the CCPS case), the model predicts that all non-rained out liquid has evaporated at a downstream distance of 6m, whereas in fact the actual evaporation by that point is less. This should mean the CCPS results tend to over-predict temperature drop. The fact we see the opposite trend suggests either liquid evaporating and cooling after impingement on the thermocouple, or that fluid temperature was below ambient temperature. As observed temperature differences were in the order of 2 degrees or less, either could easily account for the difference. Figure 63 shows no clear trend of measured temperature drop against pressure, which one would expect as smaller droplets evaporate more rapidly. So perhaps it is impinged liquid that accounts for the drop in temperature.

For the JIP results there is hardly any temperature drop and this is consistent with the very small amounts of evaporation predicted.

These temperature data do point towards the fraction of released material that doesn't rain out evaporating rather than persisting as very small droplets remaining in suspension within the plume.

A further thing to note is that both CCPS and JIP Phase III simulations seemed to give a reasonable approximation of the centreline height, if we assume the latter is indicated by the height of maximum temperature drop.

The 4 barg cases even for CCPS under-predict temperature drop. This may be due to the significantly larger droplets. It is slightly worrying though that the measured temperature drop in these cases is not significantly lower than for the higher pressures.

4.3.5 Concentration

The Part 'A' report describes in detail the concentration measurements for the xylene experiments. The experiments were carried out for a range of pressures with concentrations measured at a number of downstream distances from the source; see
Table 26.

2.5 mm orifice		5 mm orifice	
pressure (barg)	**downstream distance (m)**	**pressure (barg)**	**downstream distance (m)**
4	2, 6, 8	4	6, 10
8	2, 6, 9	8	6, 10
10	6, 9	9.3	6
16	6, 10	12.5	6, 12

Table 26. Matrix of experimental conditions for xylene concentration measurements

All runs were carried out with fluid and ambient temperatures approximately 20 Celsius, relative humidity of 25% and ambient pressure of 1020 mbar. Pool modelling was switched off because evaporation rates were very small compared to the amount of residual vapour in the cloud, and because the current pool modelling makes use of 'cloud over pool' model that performs weakly for high rainout cases.

For each run/distance concentrations were measured at 6 sampler locations, 1 – 6, as shown by Figure 65.

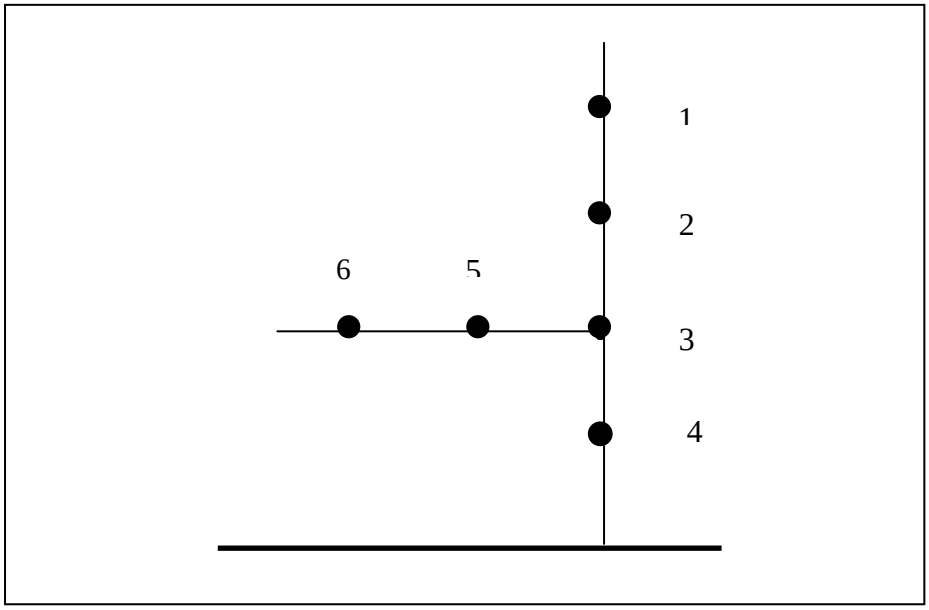

Figure 65. Layout of measurement array looking along the jet direction
The spacing of all points is 0.25 m and the lowest point is 0.25 m above the floor.

The measured concentrations in volume percent are given in the table below. Note that where a value of '>1' is given, the actual concentration is unknown but is ≥ 1 %[46].

[46] We have used at cut-off of 0.99% - values greater than this are assumed to be ≥ 1%

Orifice (mm)	Pressure (barg)	Distance (m)	Sampler						
			1	2	3	4	3	5	6
2.5	4	2	0.18	0.40	0.21	0.17	0.21	0.01	0.00
		6	0.03	0.09	0.49	0.18	0.49	0.10	0.08
		8	0.02	0.03	0.06	0.08	0.06	0.06	0.08
	8	2	≥1	0.78	0.24	0.21	0.24	0.03	0.01
		6	0.09	0.25	0.51	0.35	0.51	0.15	0.27
		9	0.07	0.07	0.09	0.09	0.09	0.08	0.18
	10	6	0.15	0.65	≥1	0.57	≥1	0.22	0.48
		9	0.03	0.07	0.10	0.18	0.10	0.09	0.18
	16	6	0.27	≥1	≥1	0.98	≥1	0.22	0.75
		10	0.09	0.15	0.20	0.34	0.20	0.10	0.64
5	4	6	0.12	≥1	0.96	0.39	0.96	0.14	≥1
		10	0.05	0.10	0.10	0.23	0.10	0.08	0.38
	8	6	0.18	0.98	0.76	0.33	0.76	0.09	0.96
		10	0.07	0.19	0.22	0.99	0.22	0.09	0.78
	9.3	6	0.14	0.95	0.56	0.90	0.56	0.15	0.48
	12.5	6	0.20	≥1	0.82	0.72	0.82	0.18	0.23
		12	0.11	0.55	0.77	0.86	0.77	0.49	0.97

Table 27. **Measured xylene concentrations**
For the 2.5 mm nozzle concentrations are measured at downstream distances 2m (upstream or rainout), 6m (typically centre of rainout) and EORZ (end of rainout zone). For the 5 mm nozzle, no data are measured at 2m (too high saturated conditions to allow accurate concentration measurement).

The figures below plot experimental and modelled concentrations using the CCPS and JIP correlations. For each orifice/pressure/distance combination, 2 plots are given: one for the vertical profile (samplers 1-4) and another for the crosswind profile (samplers 3, 5, 6). Where concentrations are ≥ 1%, they are plotted = 1%.

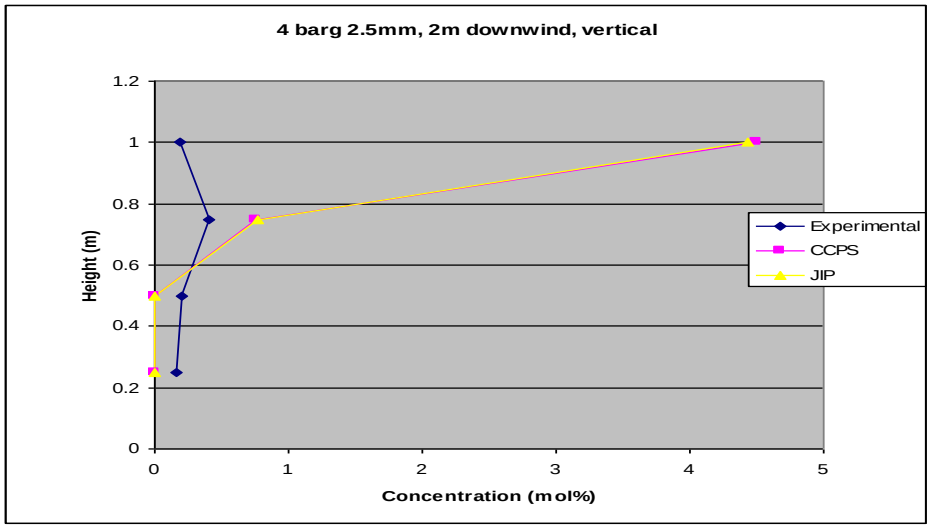

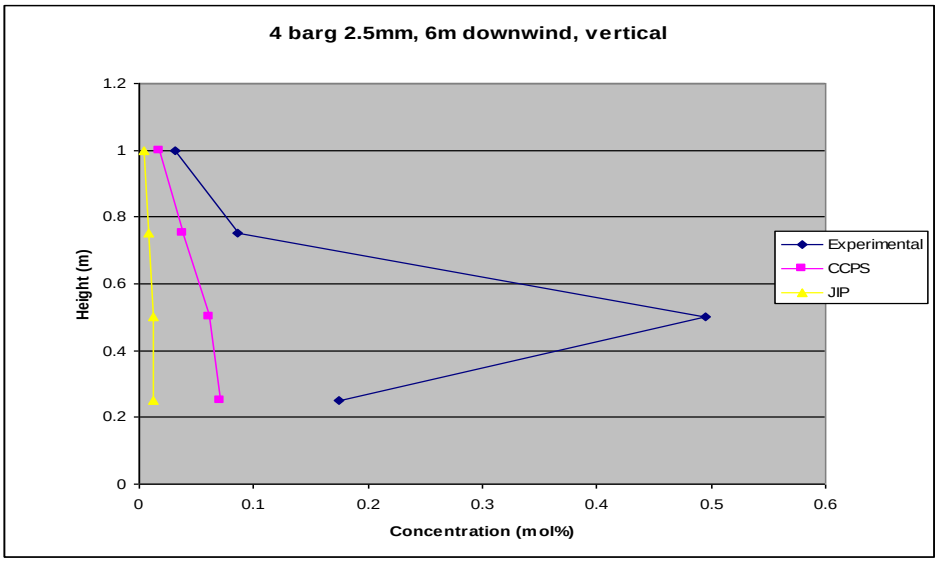

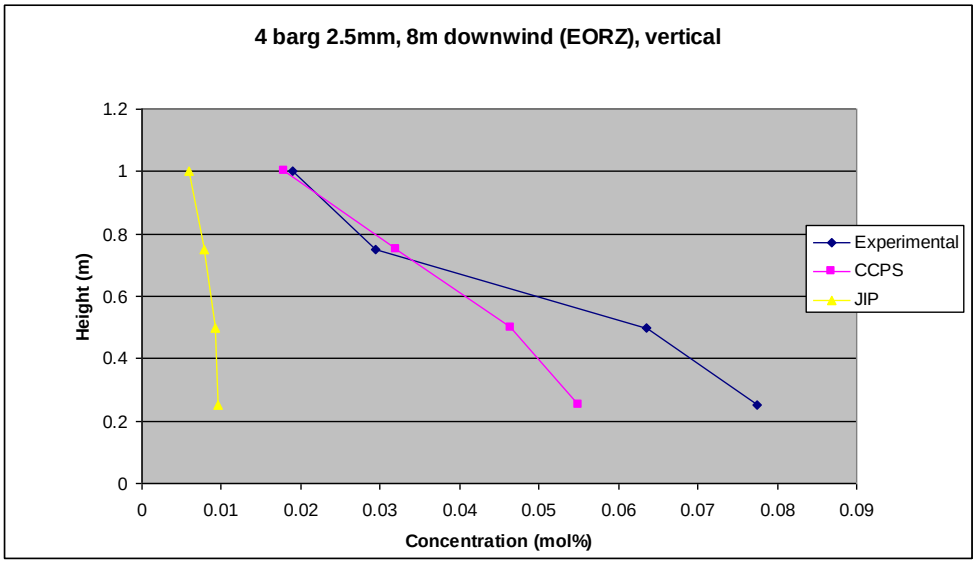

Figure 66. Vertical concentration profiles for 4 bar 2.5 mm case.

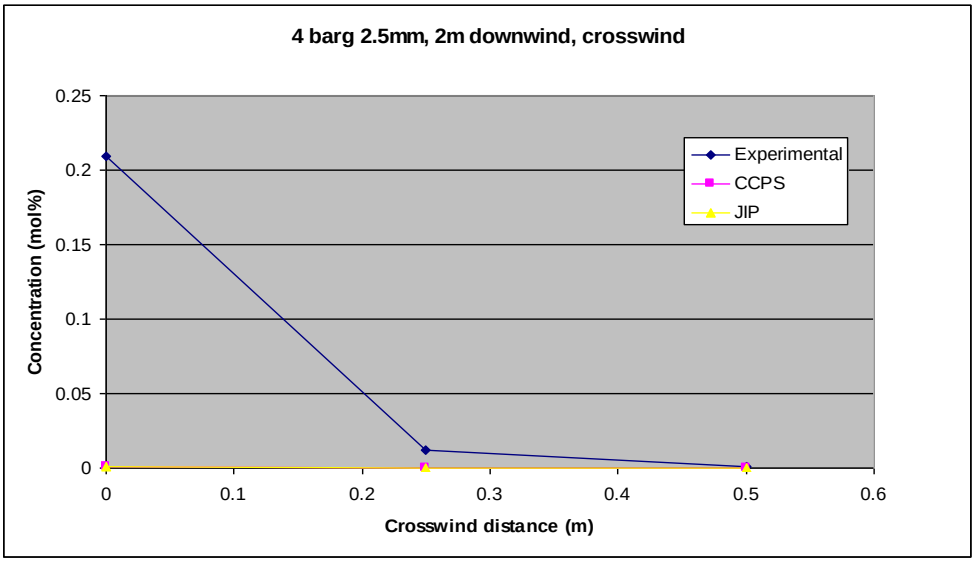

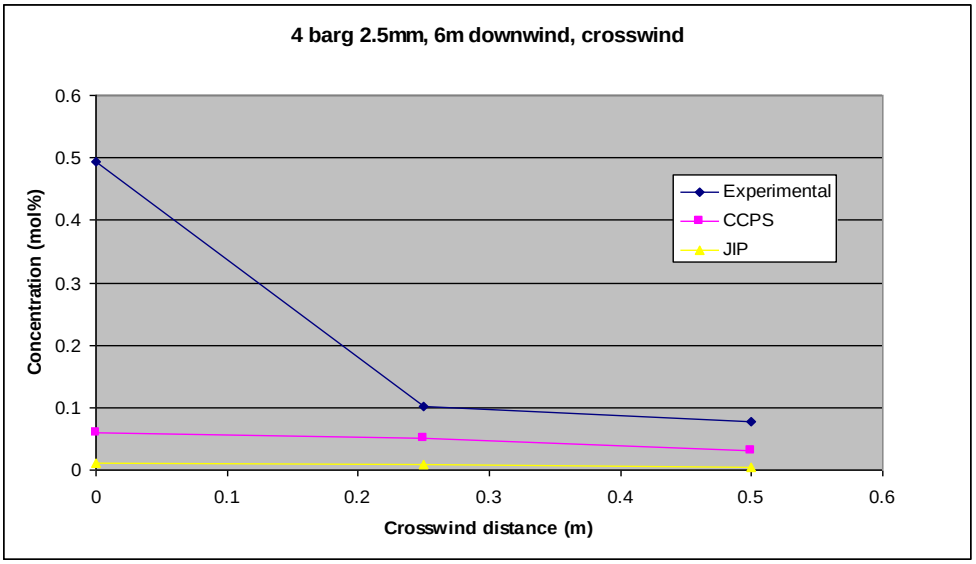

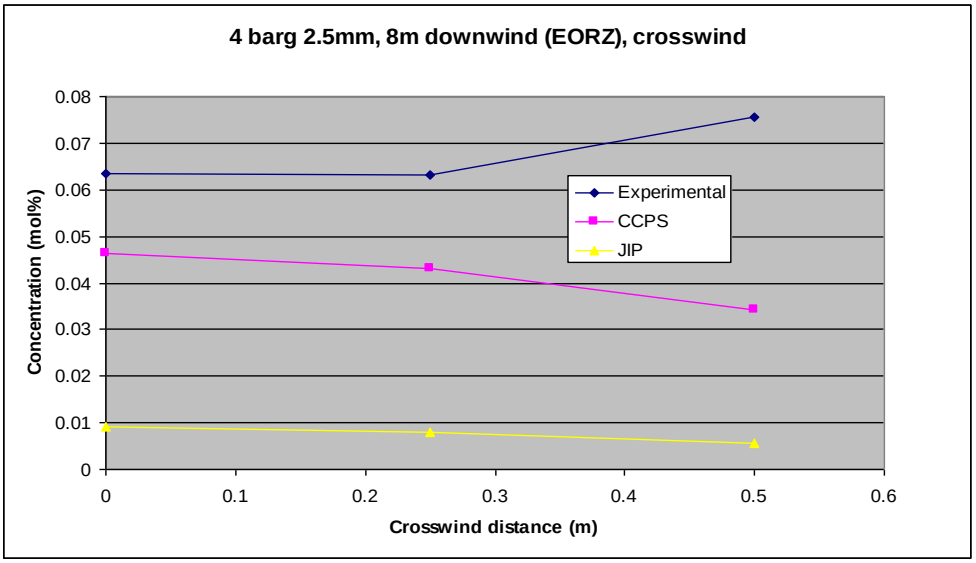

Figure 67. Horizontal concentration profiles for 4 bar 2.5 mm case

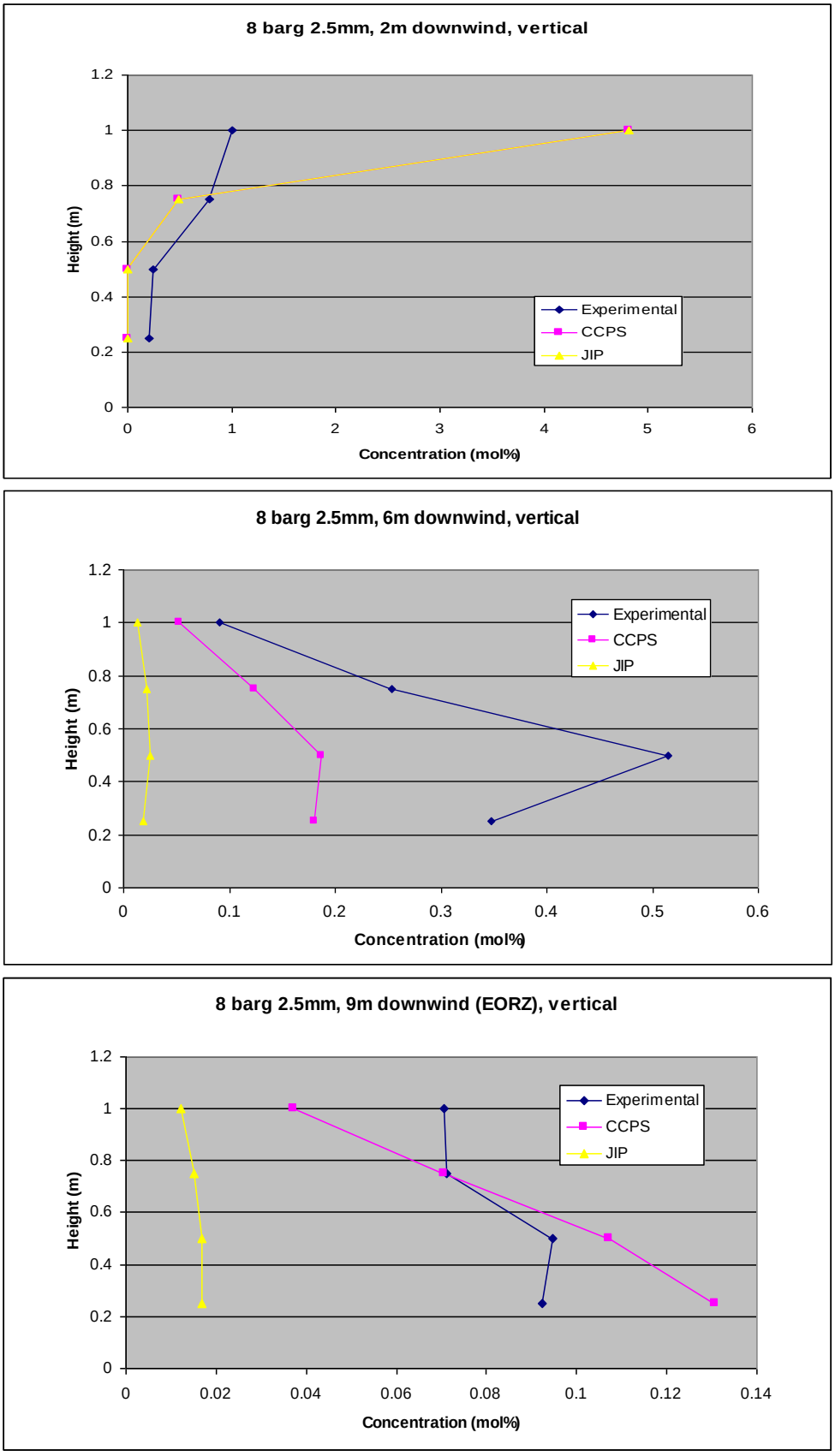

Figure 68 . Vertical concentration profiles for 8 bar 2.5 mm case

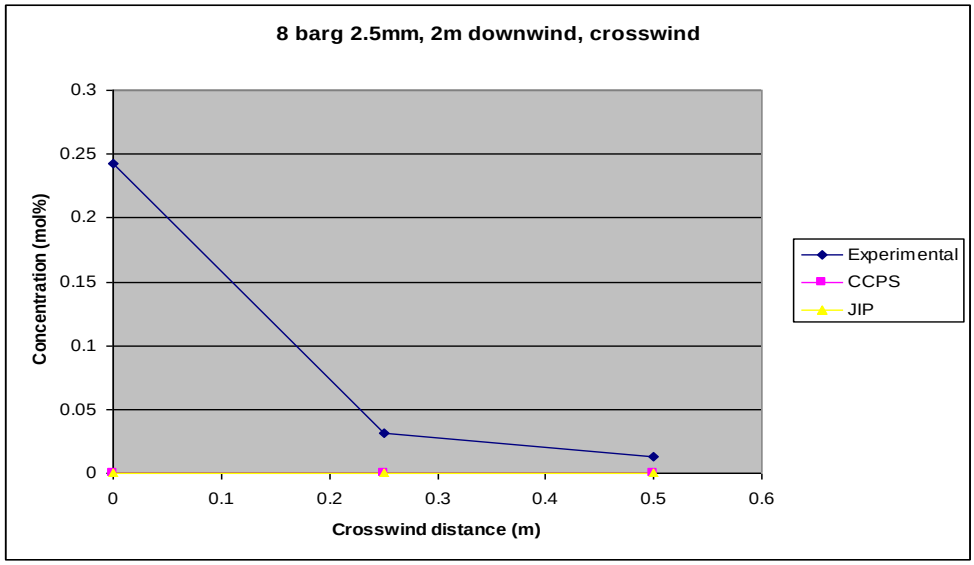

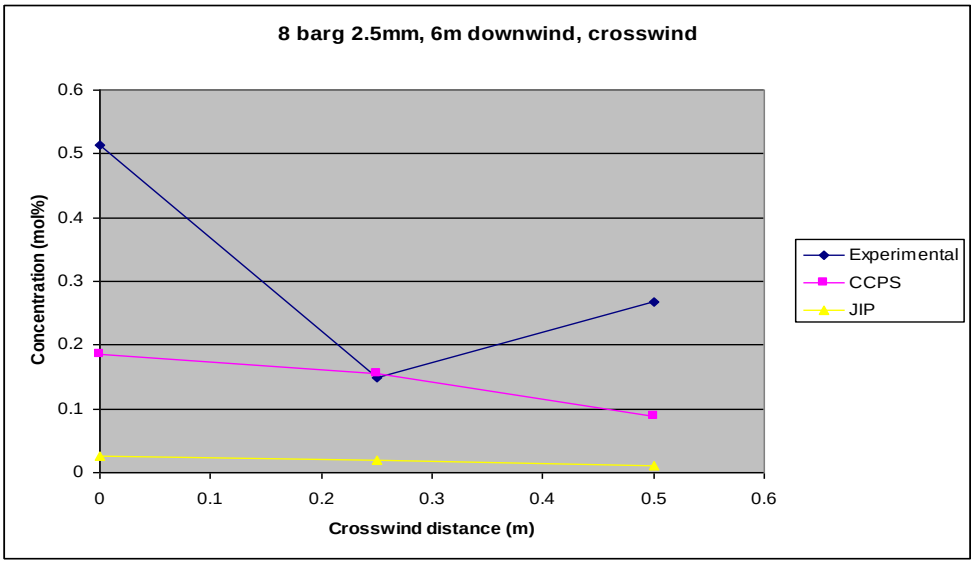

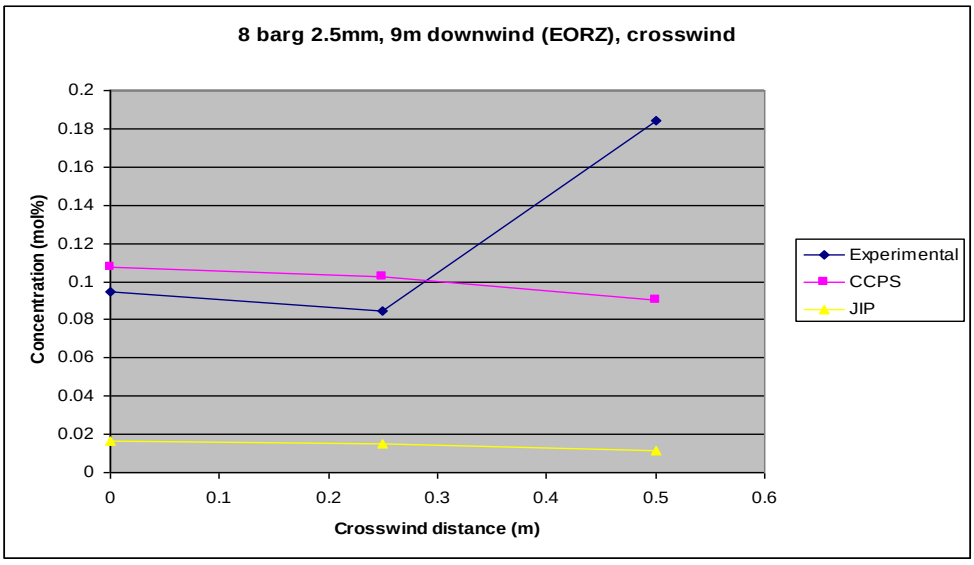

Figure 69. Horizontal concentration profiles for 8 bar 2.5 mm case

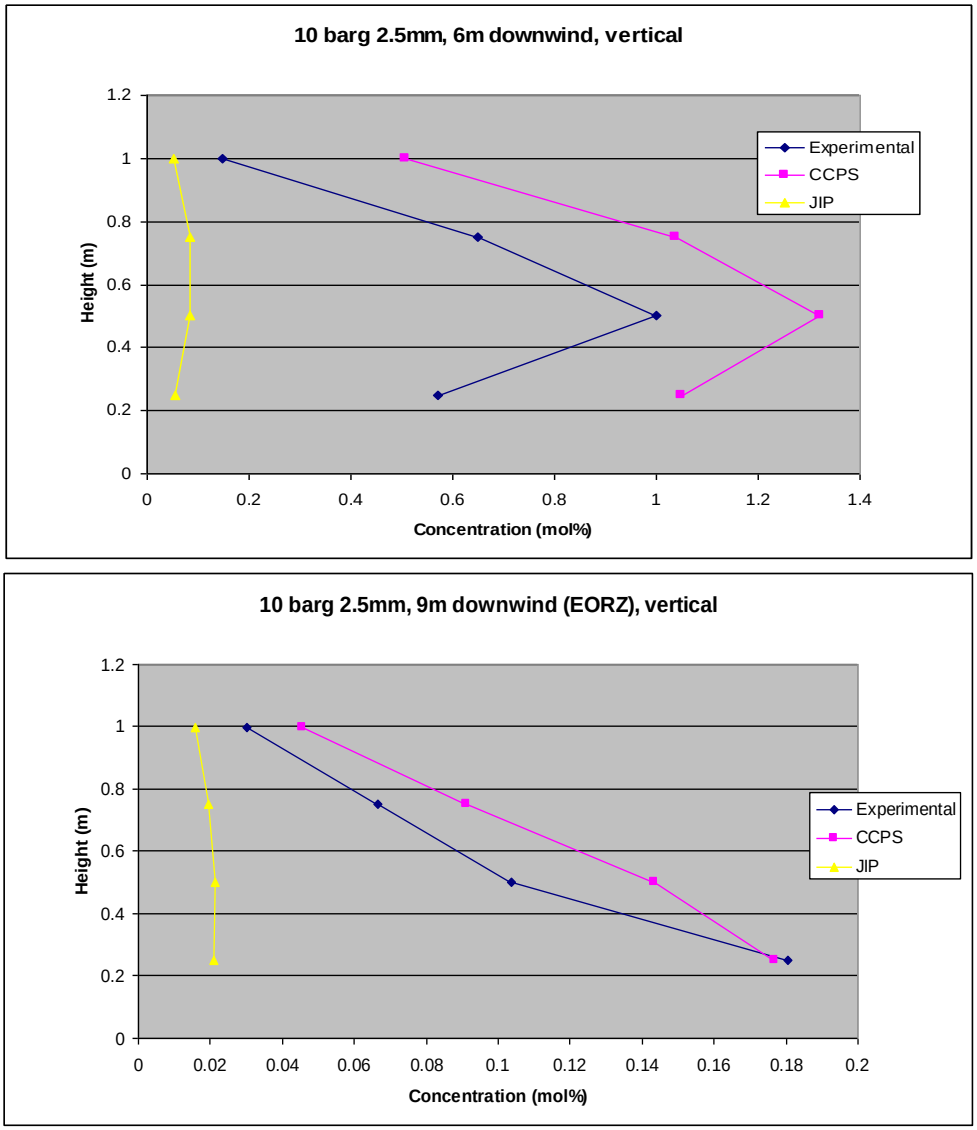

Figure 70. Vertical concentration profiles for 10 bar 2.5 mm case

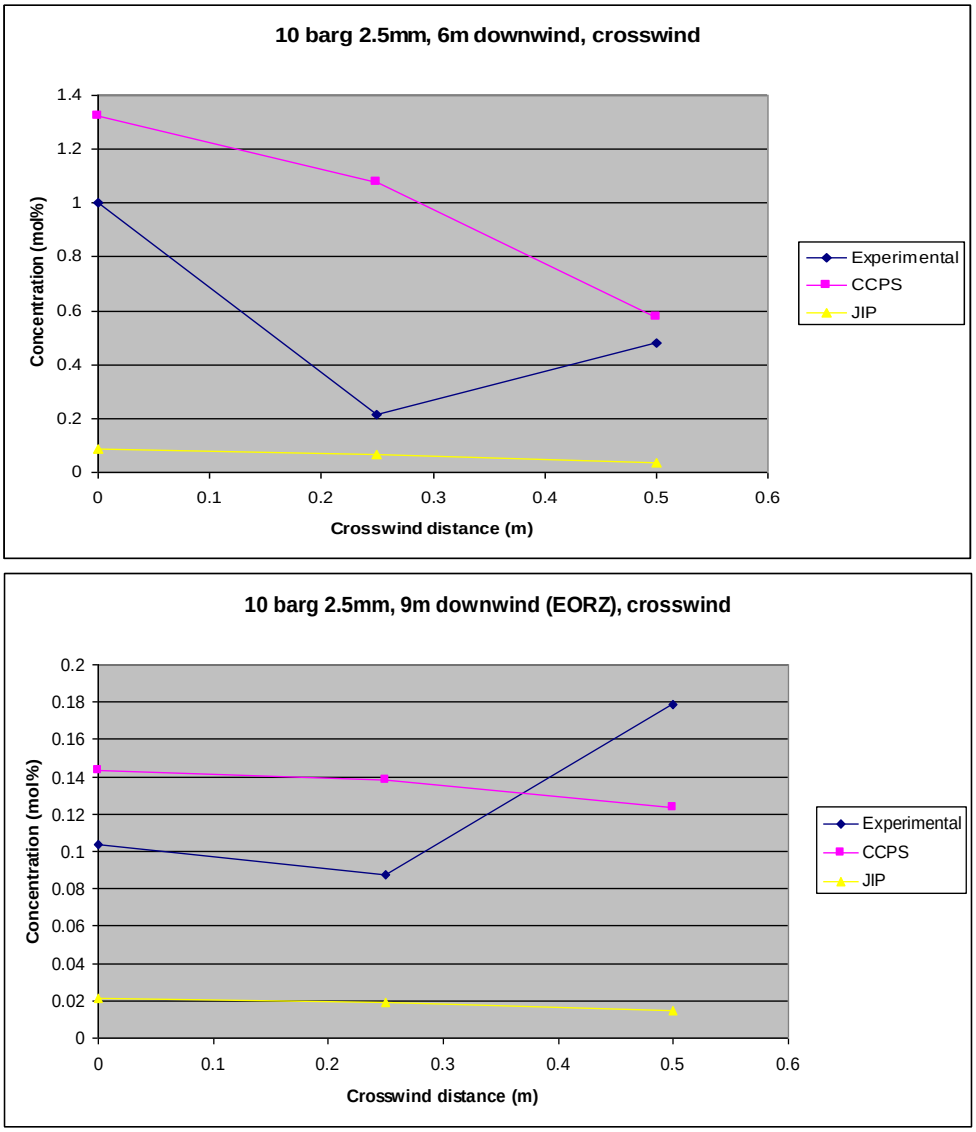

Figure 71. Horizontal concentration profiles for 10 bar 2.5 mm case

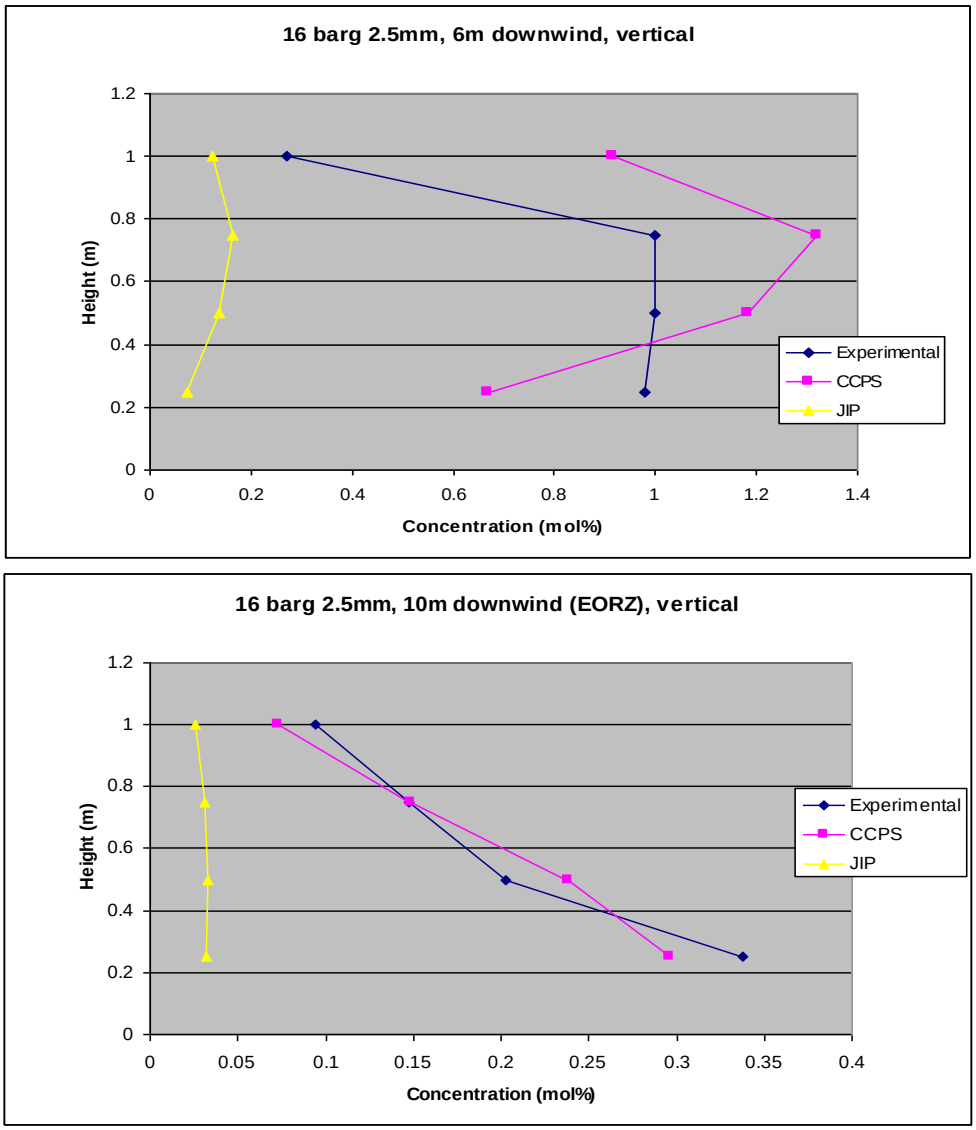

Figure 72. **Vertical concentration profiles for 16 bar 2.5 mm case**

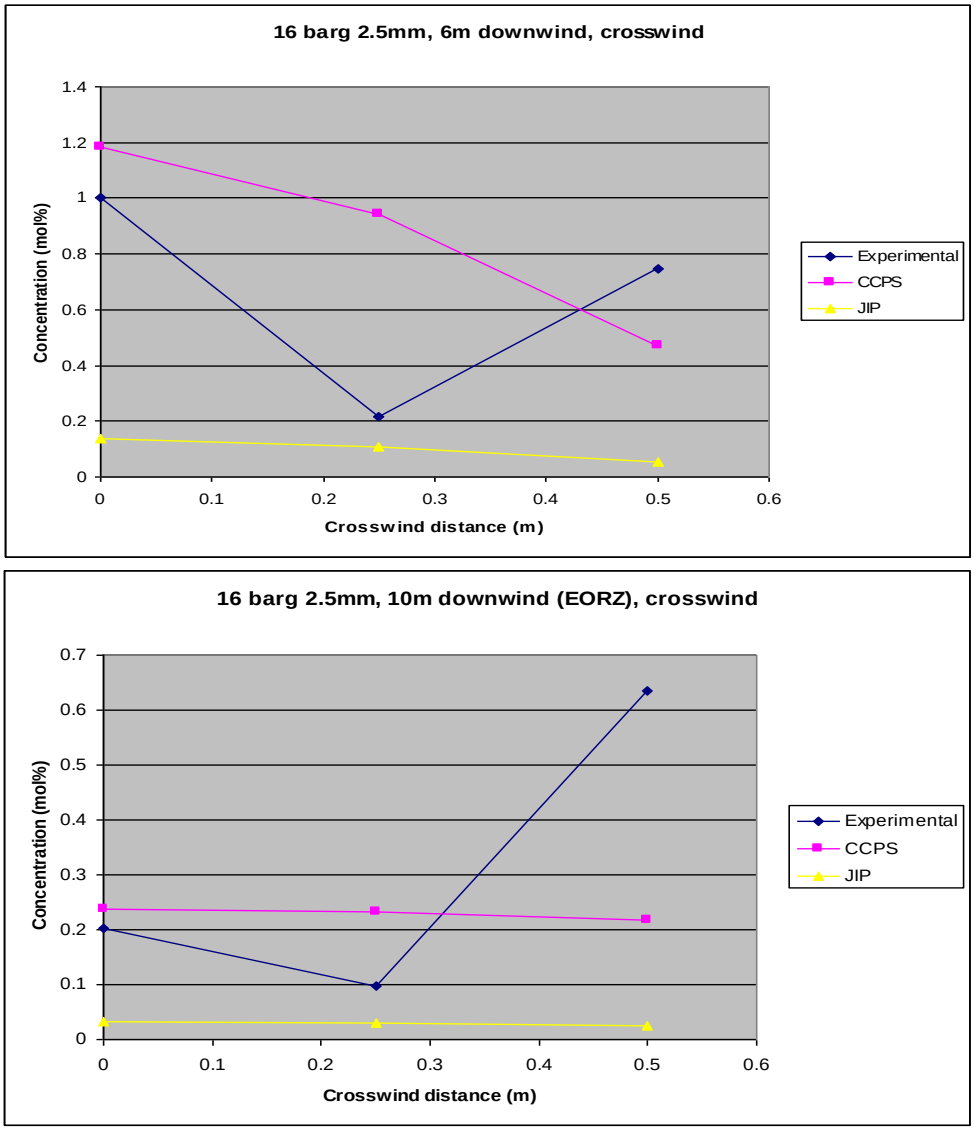

Figure 73. Horizontal concentration profiles for 16 bar 2.5 mm case

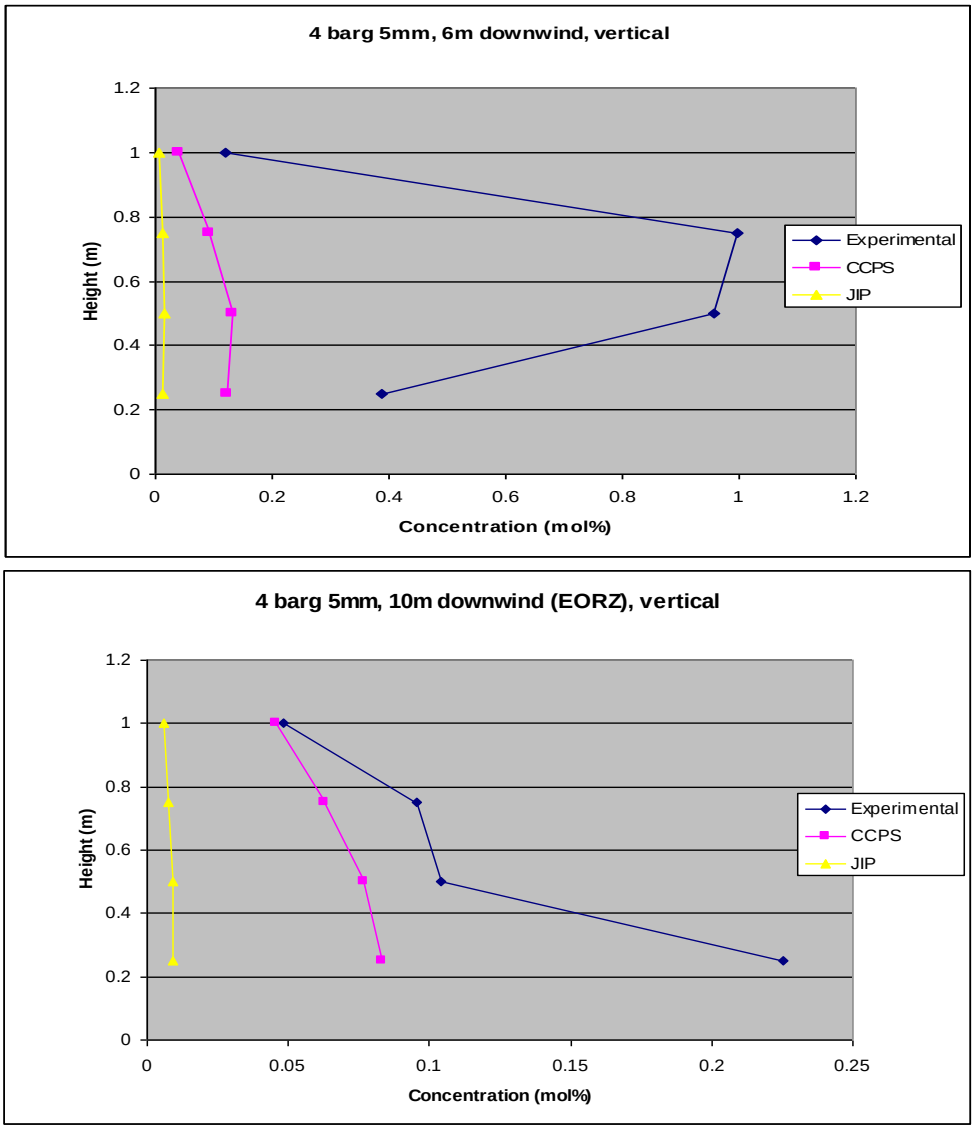

Figure 74. Vertical concentration profiles for 4 bar 5 mm case

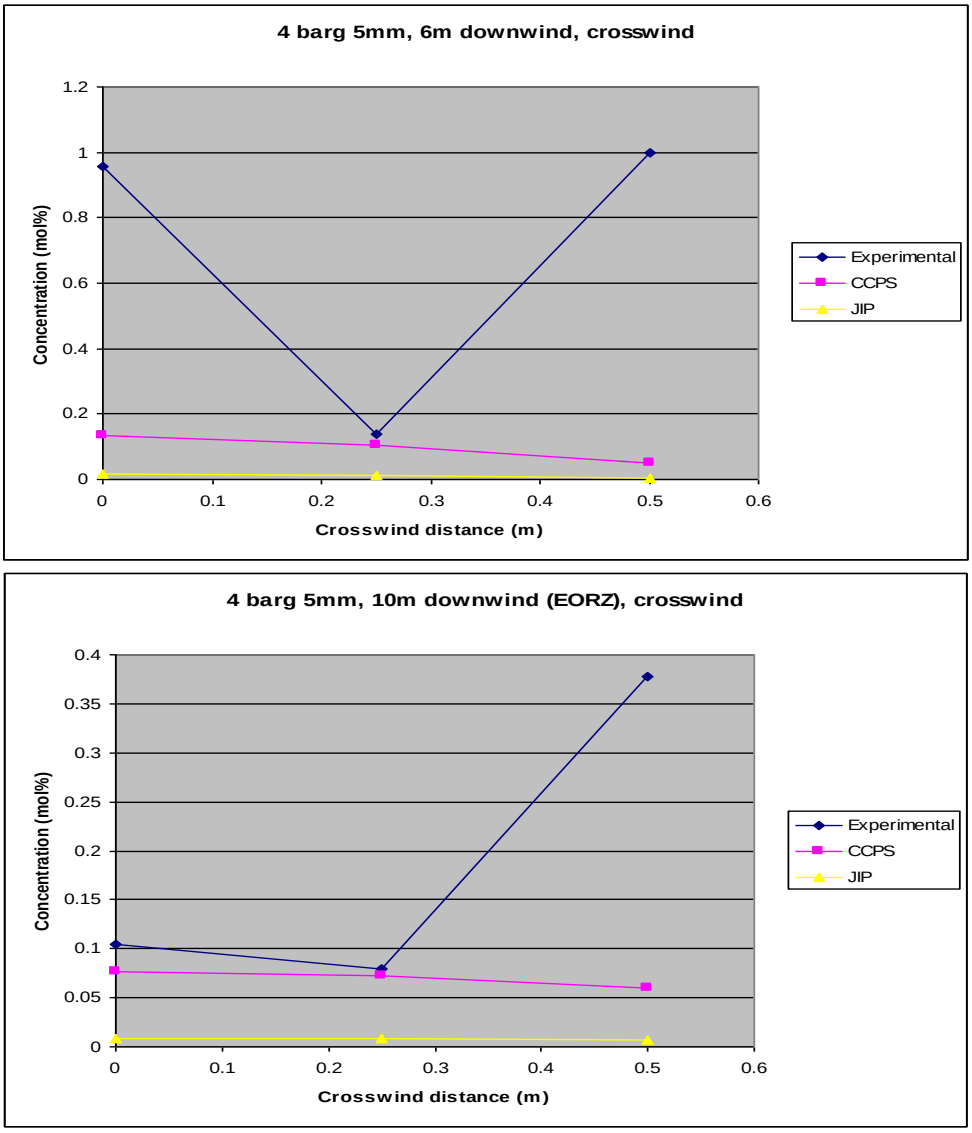

Figure 75. Horizontal concentration profiles for 4 bar 5 mm case

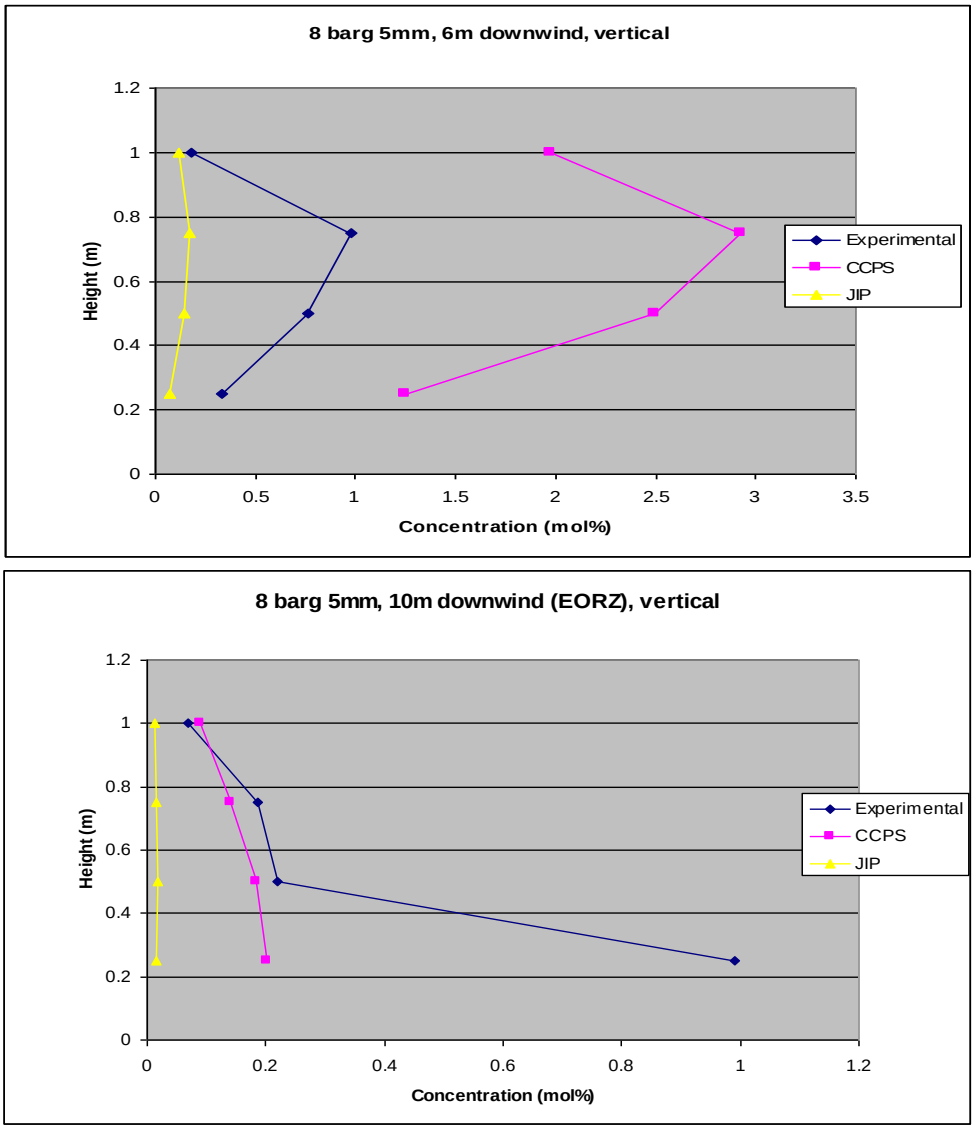

Figure 76. Vertical concentration profiles for 8 bar 5 mm case

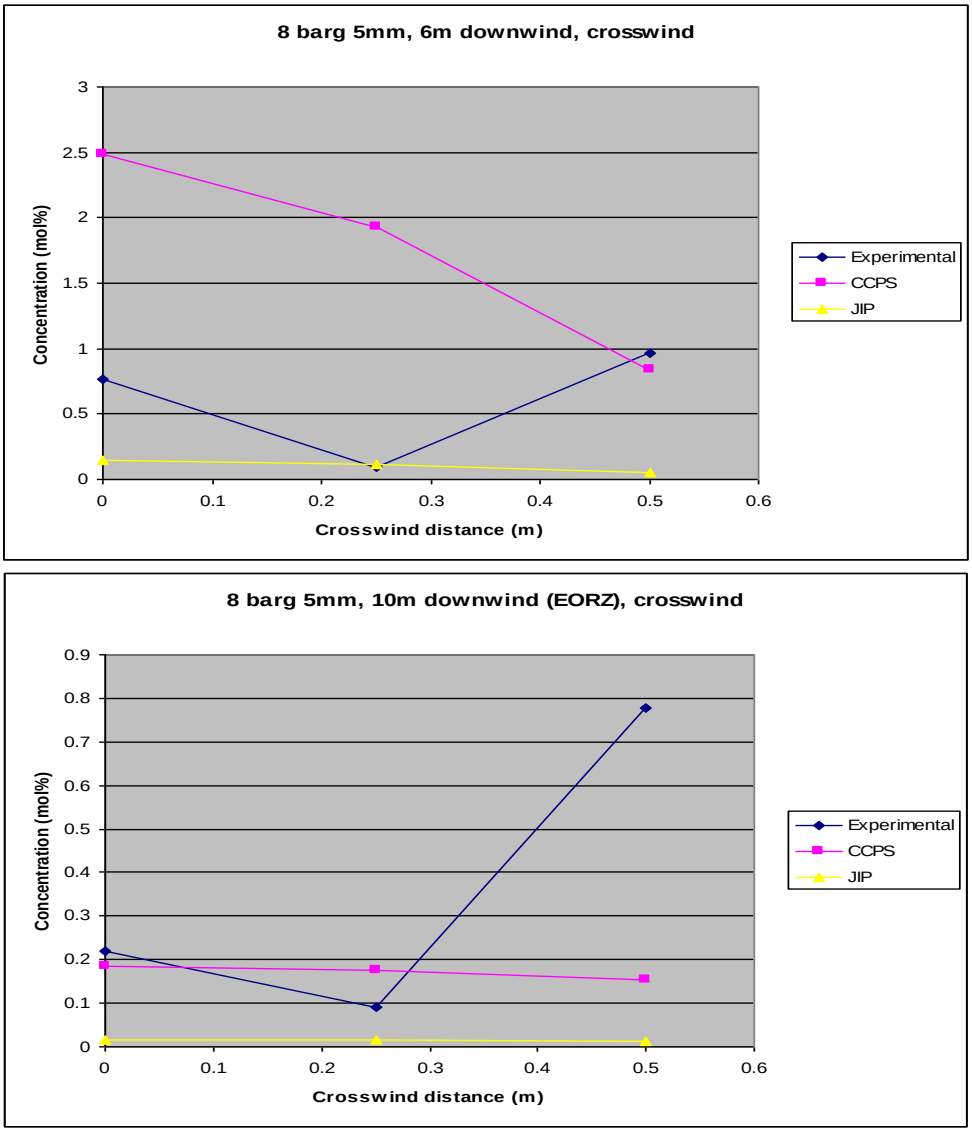

Figure 77. Horizontal concentration profiles for 8 bar 5 mm case

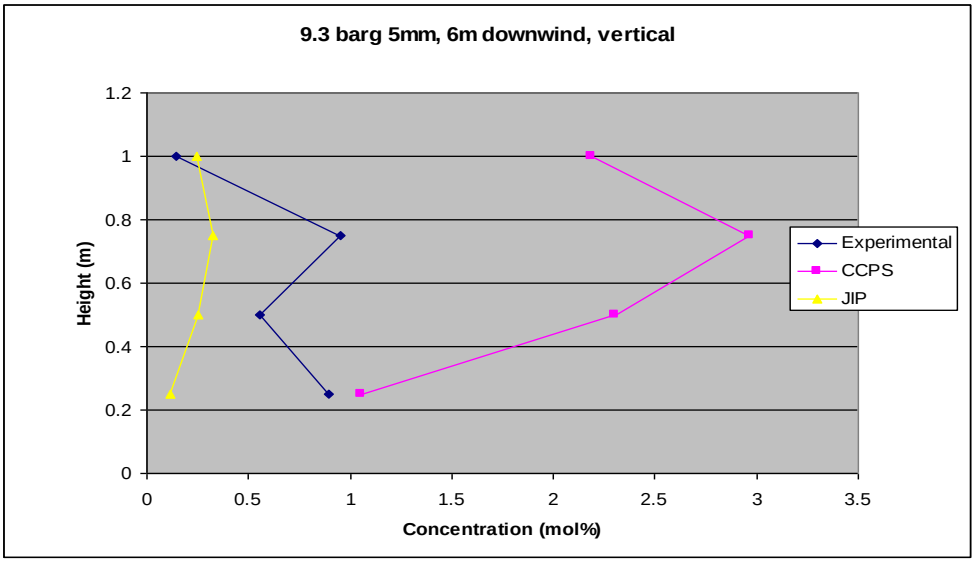

Figure 78. Vertical and horizontal concentration profiles for 9.3 bar 5 mm case

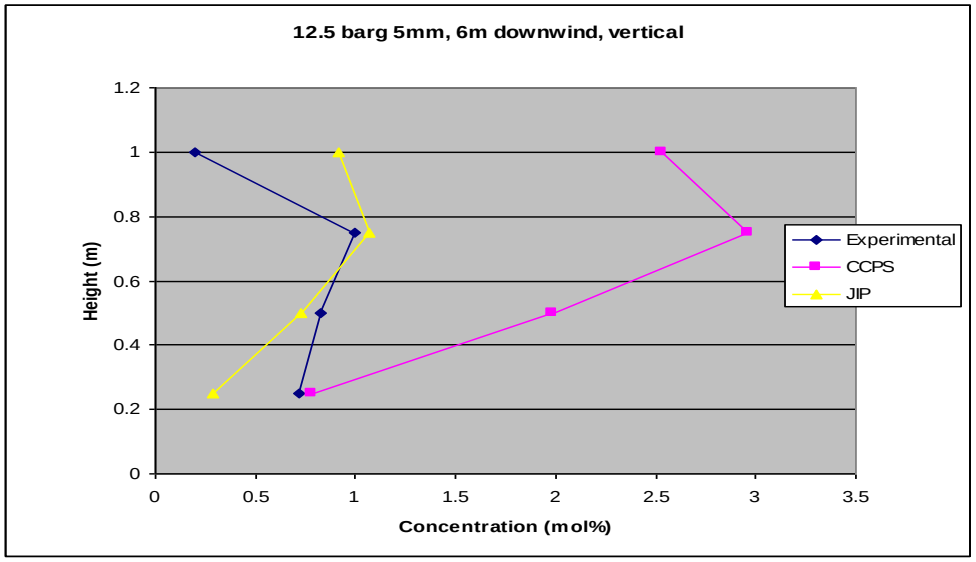

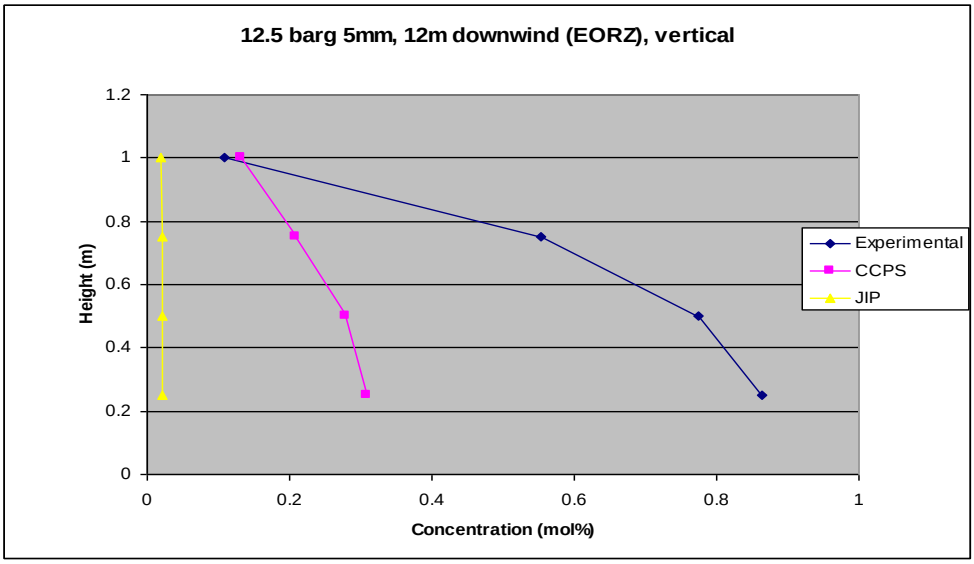

Figure 79. Vertical concentration profiles for 12.5 bar 5 mm case

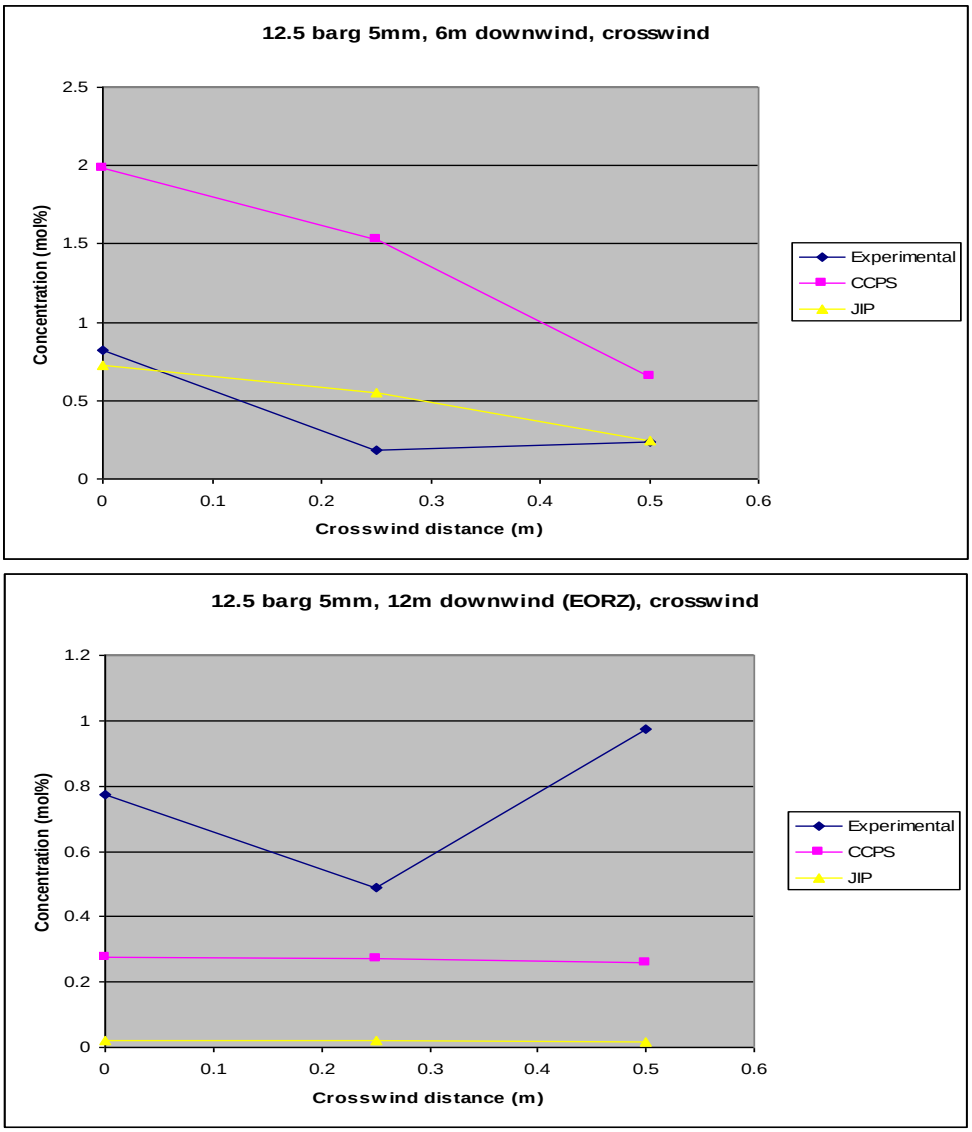

Figure 80. Horizontal concentration profiles for 12.5 bar 5 mm case

There are a number of difficulties in interpreting this data. First and foremost at downstream distance x = 6m the model predicts rainout is complete, whereas the experimental rainout measurements (Figure 50) indicate only about 25% of mass rainout. Predicted concentrations are likely to be too low for this reason. Secondly, large high momentum droplets may not be sampled by the rear-facing funnels. Thirdly high concentrations (> 1%) close to the nozzle cannot be measured. For these reasons the only meaningful comparison may be at the end of the rainout zone (EORZ).

Here agreement is relatively good for the CCPS correlation, because CCPS predicts well the total rainout (and therefore the amount of residual vapour). There should therefore be good agreement between experimental and modelled xylene mass.

At least in the vertical direction the shape of the cloud too is generally well predicted. But for the 5mm 12.5 bar case the experimental results show much greater mass in the cloud than the modelled results. In fact the experimental results for all the 5 mm releases show a concentration that is much higher close to the ground than the modelled one. This is despite the good prediction for the CCPS correlation of total rainout. It may be that more evaporation is occurring from the pool than we predict.

EORZ crosswind experimental profiles show a troubling increase in concentrations towards the edge of the jet. The modelled profiles do not (and cannot) reproduce this, and it is hard to think of a plausible explanation for this behaviour.

For the Phase III JIP droplet size correlation the concentrations are too low as virtually all the mass rains out.

4.3.6 Summary

There are many similarities with results for water. The Bernoulli model predicts well measured flowrates. Droplet size distributions are generally predicted well by the Phase III correlation (with the exception of the 2.5mm 4 barg case), though at higher diameters the influence of very small numbers of very large droplets means we cannot be confident that the measured distribution is accurate. The CCPS correlation under-predicts SMD significantly. Overall SMDs are much smaller than for water.

However rainout results differ markedly. A significant proportion of the mass (up to 20%) did not rain out, and either evaporated or remained in suspension. The JIP Phase III correlation, with its much larger droplet sizes, over-predicts rainout (evaporation of < 3%). The same is true to a lesser extent with the Melhem correlation. The predictions of the CCPS (modified and CCPS default give the same results) on the other hand are very accurate.

The use of parcels does predict some longitudinal spread of rainout (at least more than with water), but still does not approach observed results. Moreover, the rainout distance when using JIP Phase III + parcels is still too small, and CCPS is better in this regard too.

The temperature results do not shed much additional light on our understanding of the releases. There is evidence that liquid is evaporating in the jet, but perhaps this is liquid drops that have adhered to thermocouples.

For concentration measurements there are sampling and analytical problems and a meaningful comparison with modelled results may only be possible at the end of rainout zone (EORZ). Here results are in line with rainout observations: CCPS predictions are relatively good for vertical profiles (though there appears to be insufficient mass in the modelled jets at high release rates). JIP Phase III under-predicts concentrations, most likely due to under-prediction of residual vapour mass.

5 SMD VALIDATION FOR RANGE OF DROPLET SIZE CORRELATIONS

Figure 81 includes comparisons for a range of droplet size correlations against the following experimental data:

- Experiments carried out as part of Phase III JIP[5,6]
  - Scaled experiments by Cardiff University:
    - Subcooled cyclo-hexane and water experiments (against which Phase III JIP correlation was fitted)
    - Subcooled gasoline experiments
    - Superheated propane and butane experiments
  - Large-scale butane experiments by INERIS (range of superheats)

- Other experiments available from the literature (see Phase III JIP report for details)
  - STEP propane (Hervieu and Veneau, 1996)[9]
  - VKI R134-A (Yildiz et al., 2004)[27]
  - HSL propane (Allen, 1998)[12,13]
  - Ecole de Mines water and INERIS butane (Touil et al., 2004)[14] experiments

See the Phase III C4 report for full details on modelling for the above experiments. Figure 81 includes SMD predictions for the following SMD correlations:

- Original CCPS correlation (minimum droplet size from mechanical and flashing breakup). This is the default Phast 6.6 option. This was combined with the Phast default atmospheric expansion breakup (minimum thermodynamic change). It was confirmed that for superheated releases this always corresponded with isentropic expansion (and not conservation of momentum), and therefore the appropriate expansion method was used for flashing breakup droplet size calculations. For sub-cooled releases the choice of expansion method does not affect the SMD results.
- Modified CCPS correlation (mechanical breakup droplet size for sub-cooled releases and flashing breakup size for superheated releases). This is the new recommended Phast option. Again this was combined with the Phast isentropic expansion option as above.
- Phase III JIP correlation. This correlation is expressed in terms of orifice data and therefore the SMD does not depend on the choice of the atmospheric expansion option.
- Melhem correlation. This was combined with the conservation of momentum expansion option. Note that the default Phast expansion option (minimum thermodynamic change) in the superheated cases corresponded to the isentropic option, not conservation of momentum.

The following is concluded from Figure 81:

- Figure 81(a) confirms that the default Phast 6.6 option (original CCPS) leads to a significant under-prediction of the SMD. This is because the correlation erroneously advises taking the minimum of its mechanical droplet-size prediction (based on Weber correlation) and its flashing droplet size prediction (based on CCPS correlation). Consequently the mechanical droplet size is used rather than the more appropriate flashing droplet size for the superheated cases, resulting in the significant under-prediction as seen in Figure 81(a).
- Figure 81(b) shows that compared to the original CCPS correlation, the modified correlation leads to a significantly improved prediction for the superheated releases, whereas results are identical for the sub-cooled releases. Thus the SMD for the Cardiff JIPIII subcooled water, cyclohexane and gasoline releases are still under-predicted.
- Figure 81(d) shows that the Melhem correlation performs relatively well against the Cardiff cyclohexane and water experiments. However it performs poorly against the INERIS and Cardiff butane and propane experiments. Overall the correlation compares relatively well for sub-cooled releases but rather poorly for superheated releases. For the sub-cooled releases, Melhem produces larger SMD's compared to the CCPS correlations. This is because Melhem adopts in its Weber criterion (16) the smaller orifice velocity instead of the larger final velocity (= vena-contracta velocity for subcooled release) used by the CCPS correlation.
- Figure 81(c) shows that on average the Phase III JIP correlation leads to the best predictions for initial droplet size, as compared to predictions from the Melhem and the CCPS correlations.

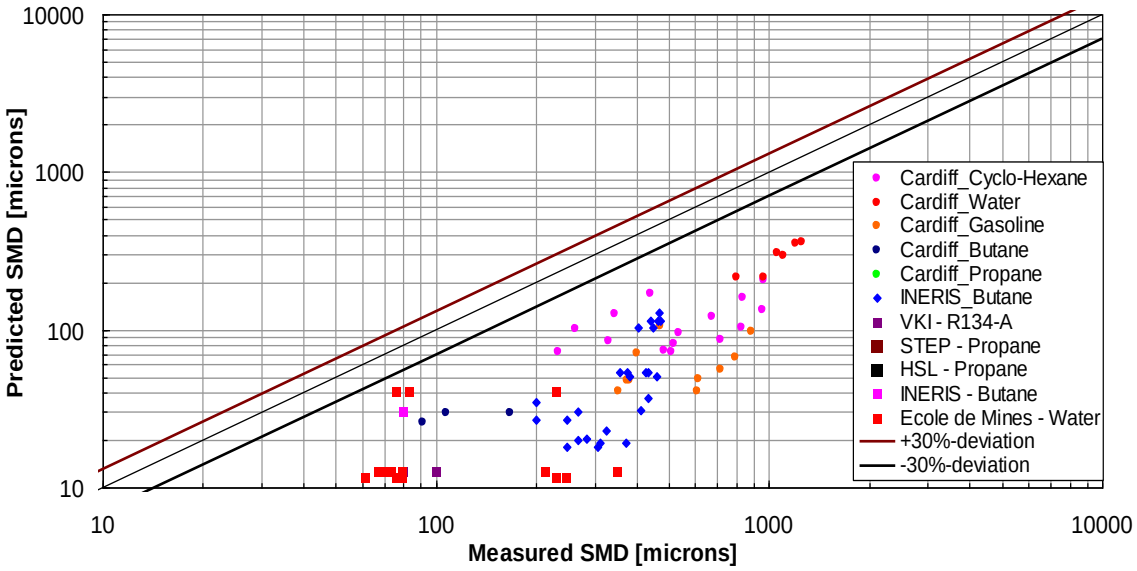

-

(a) Original CCPS correlation - default option in Phast 6.6

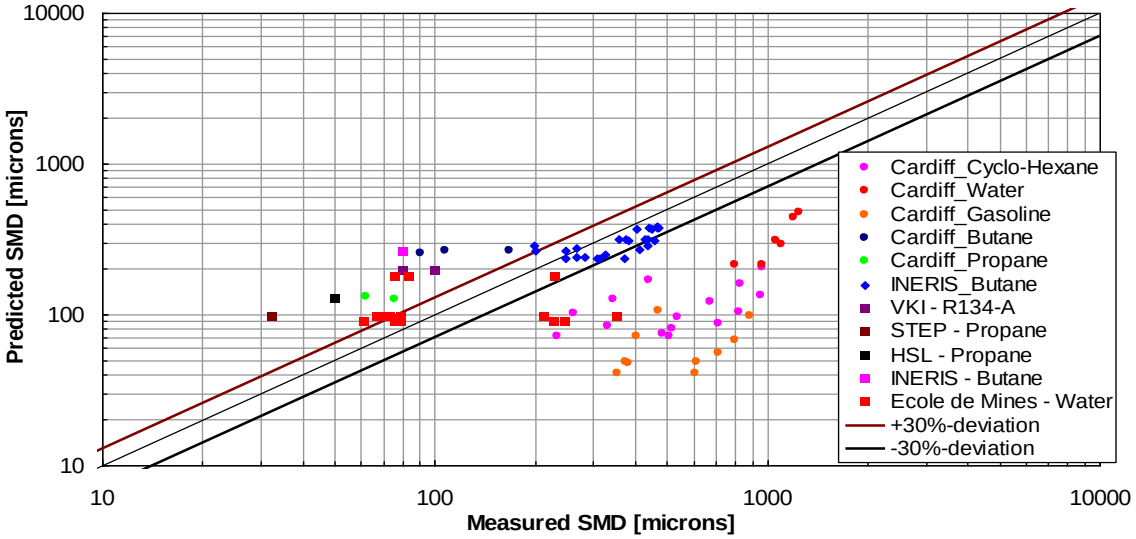

(b) New recommended modified CCPS correlation – default option in Phast 6.7

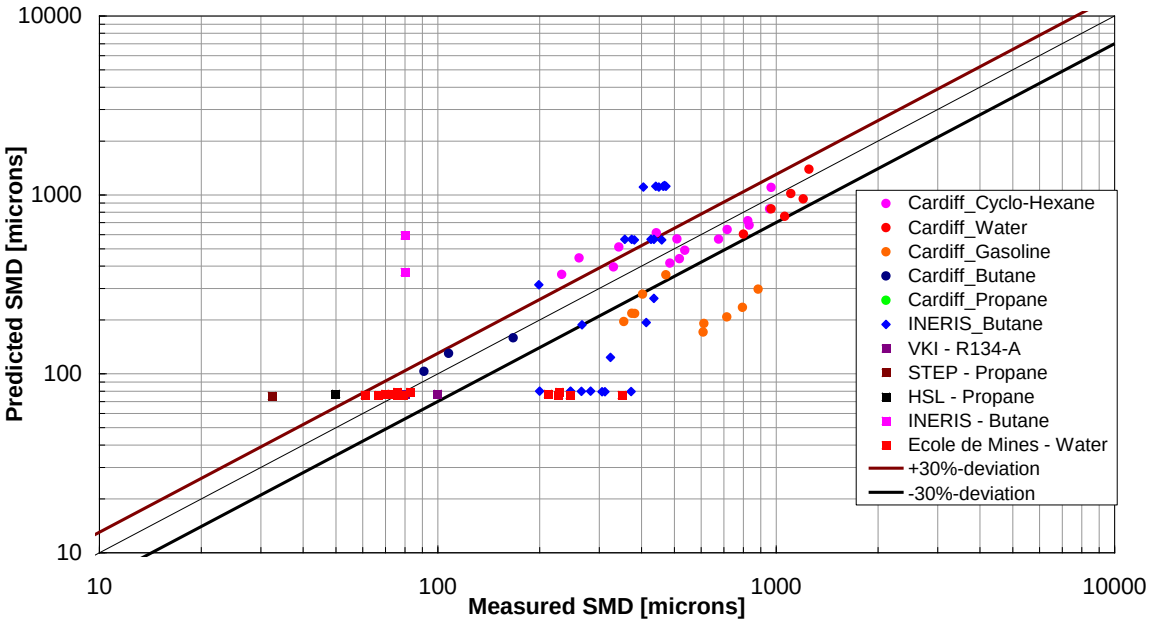

(c) New Phase III JIP SMD correlation

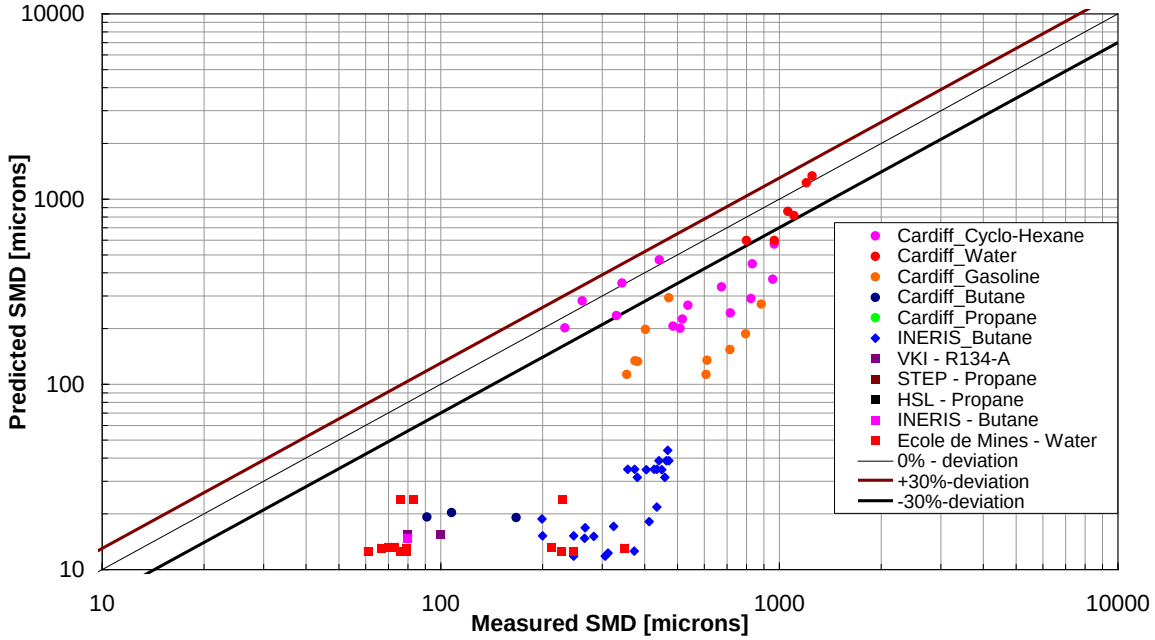

(d) Melhem SMD correlation
(as implemented in Phast combined with the conservation of momentum expansion option)

Figure 81. **Validation of SMD droplet size correlations against experiments**
Phase III experiments (Cardiff: cyclohexane, water, gasoline, butane and propane, INERIS:_butane) are indicated on the upper part of the legend, while the remaining experiments are on the lower part.

6 VALIDATION AND EVALUATION OF RAINOUT METHODS

Chapter 4 included validation of distributed rainout against the HSL experiments using the CCPS correlation and the Phase III JIP correlation. The current chapter includes validation for predicting total amount of rainout following a two-phase release for a wider range of methods and a wider set of experiments. The methods include both UDM methods including explicit modelling of the droplets (range of CCPS and Phase III JIP correlations), as well as more simple methods based on rainout correlations without droplet modelling. The experiments include the Phase IV JIP HSL rainout experiments, the CCPS rainout experiments, as well as all 2-phase elevated releases from the UDM validation dataset (Desert Tortoise, EEC, FLADIS, Goldfish).

Section 6.1 lists and describes the different methods. Section 6.2 lists the experiments for which each of the methods have been validated. Section 6.3 summarises the results of the validation, and provides recommendations for most accurate rainout predictions in Phast.

6.1 List of rainout methods

This section lists the range of methods for calculating the amount of rainout following a two-phase release which have been applied for model validation. For previous reviews of rainout from two-phase releases, the reader is referred to Section 4.3.4 in the Phase I JIP report (Witlox and Bowen[1]), Section 3.6 in the AEA review by Ramsdale and Tickle[xxix], and Appendix E in the RELEASE book by Johnson and Woodward[xxx].

6.1.1 Rainout methods based on UDM simulation including droplet modelling

As discussed in Section 2.5, one must also be careful to apply the correct model for expansion to atmospheric conditions. The Phase I JIP[1] recommended the use of the conservation of the momentum model (particularly for pipe releases), and we use this expansion model for all Phase III correlation results. However, the CCPS correlation should always be used with the isentropic model, as it was derived on this basis.

6.1.2 Rainout methods based on rainout correlations without droplet modelling

Most rainout correlations are based on the assumption of an isenthalpic flash between the stagnation conditions (denoted by subscript 'st') and the final post-expansion conditions (denoted by subscript 'f'). Thus

$$H_{st}\left(P_{st}, T_{st}, \eta_{st}=1\right) = H_f\left(P_a, T_f, \eta_f\right) \qquad (53)$$

Where H denotes specific enthalpy (J/kg), P is pressure (Pa), T is temperature (K) and η the mass fraction, and P_a is the ambient pressure. The above transition from stagnation enthalpy to final enthalpy can be considered to take place by first cooling the liquid from the stagnation temperature T_{st} to its atmospheric boiling point $T_{sat}(P_a)$, and subsequent evaporation of the liquid at the boiling point. Thus by presuming constant specific heat C_{pL}, the following enthalpy balance is obtained

$$C_{pL}\left[T_{st} - T_{sat}(P_a)\right] = (1-\eta_f)\,\Delta H_{vap}(T_{sat}(P_a)) \qquad (54)$$

where ΔH_{vap} is the latent heat of evaporation. Thus the isenthalpic flash fraction x_H is given for superheated jets by[47]

$$x_H = 1 - \eta_f = \frac{C_{pL}\left[T_{st} - T_{sat}(P_a)\right]}{\Delta H_{vap}\left(T_{sat}(P_a)\right)} \qquad (55)$$

Where the constant specific heat is taken as part of the current work at temperature $T = (T_{st} + T_{sat}(P_a))/2$.

Rainout correlation by Kletz

The correlation for the rainout mass fraction η_R proposed by Kletz[xxxi] simplistically assumes that the additional evaporation prior to rainout is the same as the evaporation during the isenthalpic flash, i.e.

[47] Johnson et al.[xxx] incorrectly state that Devaull and King[xxxii] use T_{as} in place of T_{sat} to calculate x_H; This error was also observed by Lautkaski[xxxiii]. Certainly the results in the RELEASE book appear to use T_{sat} in the evaluation of x_H.

$$\eta_R = \max\{0,\ 1-2x_H\} \quad \text{, if superheated}$$
$$= 1 \quad \text{, if sub-cooled} \qquad (56)$$

Appendix E in the RELEASE book includes references to similar rules of thumb.

Rainout correlation by De Vaull and King

De Vaull and King[xxxii] suggest a correlation based on the 'adiabatic saturated temperature' T_{as} defined as the minimum temperature reached by an equilibrium droplet-air mixture as the droplets completely evaporate. This temperature can be found from THRM runs (using equilibrium model) while mixing air (at T_a, P_a) with 100% liquid at $T_{sat}(P_a)$; see Figure 82 which includes figure/table from RELEASE book for application to CCPS experiments.

For non-volatile materials (defined by $T_{as}/T_a > 0.86$), the rainout fraction is given by

$$\eta_R = 1 - x_H - \frac{C_{pL}\left[T_{sat}(P_a) - T_{as}\right]}{\Delta H_{vap}\left(T_{sat}(P_a)\right)} = 1 - \frac{C_{pL}\left[T_{st} - T_{as}\right]}{\Delta H_{vap}\left(T_{sat}(P_a)\right)} \qquad (57)$$

While for volatile materials (defined by $T_{as}/T_a \leq 0.86$),

$$\eta_R = \eta_R^* \left\{ \max\left[0,\ 1 - \left(\frac{x_H}{0.145} \right)^{1.8} \right] \right\} \qquad (58)$$

with the scaling factor η_R^* defined by

$$\eta_R^* = 1 - 2.33\left(\frac{T_a - T_{as}}{T_a} \right) \qquad (59)$$

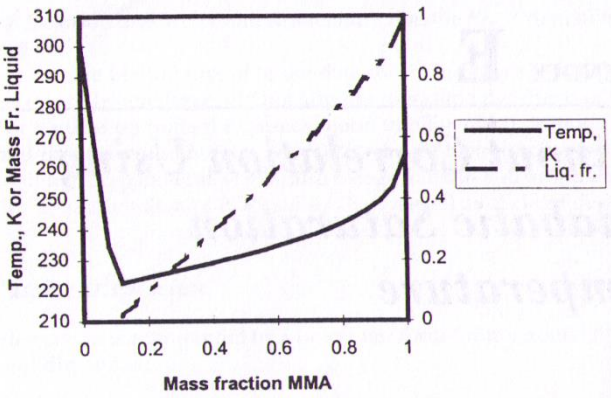

Figure E-1. Adiabatic mixing characteristics of MMA and ambient air.

TABLE E-1 Adiabatic Saturation Temperatures and DeVaull, King Correlators for Rainout

Material	T_s (K)	T_{amb} (K)	T_{as} by Adiabatic Mixing (K)	T_{as} by Quest (K)	$\frac{T_{amb}-T_{as}}{T_{amb}}$	Scaling Factor η_R
Chlorine	239.1	304.4 (303.3±3.1)	199.8	201.3 ± 1.3	0.344	0.200
MMA	266.8	301.3 (290.5±4.2)	221.8	221.45 ± 0.8	0.264	0.385
CFC-11	297.0	288.7 (294.2±9.4)	241.4	245.5 ± 4.8	0.164	0.618
Cyclohex	353.9	308.4 (309.4±1.6)	273.1	270.8 ± 1.9	0.115	0.733
Water	373.2	305.4 (303.0±9.2)	288.1	289.9 ± 3.3	0.057	0.868

Figure 82. Adiabatic saturation temperature for CCPS experiments (from RELEASE book)

Rainout correlation by Lautkaski

Lautkaski[xxxiii] indicated that the above correlation by DeVaull and King was flawed, because they were based on an incorrect value of the liquid specific heat of CFC-11 in the CCPS rainout tests. Lautkaski used the CCPS field test data corrected in 1994 with the UDM model (see RELEASE book by Johnson and Woodward[xxx]) to derive the following new correlation:

$$\eta_R = 0.6\,(1-3x_H), \quad x_H < 1/3 \qquad (60)$$
$$= 0, \quad x_H > 1/3$$

Discussion

Ramsdale and Tickle[xxix] indicate it may be more appropriate to estimate rainout using a simple rainout correlation rather than a more sophisticated method including droplet modelling (like the above UDM rainout methods). However they indicate that the correlations may only be valid for the data they are fitted against, i.e. they are not valid for:

- release heights other than around 1.22 m
- non-horizontal releases
- high wind speeds or humidity's
- substances with unusual properties, such as HF
- orifice diameters outside the range 3.2-12.7 mm
- orifice pressures outside the range 26.7-979 kPa

6.2 List of experiments with observed rainout

The experiments used for the validation are as follows:

- Phase IV JIP HSL water and xylene rainout experiments; see Sections 4.2.3 and 4.3.3 in the current report for the observed rainout for these experiments.
- CCPS rainout experiments (use corrected rainout results from RELEASE book based on old possibly incorrect UDM rainout/evaporation results). The results for these experiments are shown in
- Table 28.
- All 2-phase elevated releases for experiments in the validation dataset for the UDM dispersion model (Desert Tortoise, EEC, Fladis, Goldfish); see Phase III JIP report and the UDM validation manual.

6.2.1 CCPS experiments

The same subset of CCPS experiments is used as in the previous Phase III of the JIP and previous validation exercises conducted by DNV (
Table 28). Two experiments were selected at random for each material.

Experiment	Observed rainout (%)	Corrected rainout (%)
Chlorine 20	21.5	59.0
Chlorine 22	23.4	66.1
MMA34	20.7	23.9
MMA40	39.9	45.5
CFC5	30.6	30.6
CFC8	61.3	61.3
CyclHex41	40.4[48]	45.6
CyclHex56	9.68[48]	13.18
Water5	68.7	68.7
Water10	61.0	61.0

Table 28. List of CCPS experiments used in this report (2 for each chemical, selected at random)

RELEASE included both observed (i.e. measured) rainout, and (for chlorine, MMA and cyclohexane) 'corrected' rainout, the latter based on an estimate of material evaporated from droplets, or from the collecting pans before measurement, obtained by tuning droplet diameters and solubilities. Both these quantities are included in
Table 28.

Ramsdale and Tickle undertook a detailed re-analysis of the methods used to correct measured rainout (numerical simulations using an early version of UDM / PVAP models) and conclude the uncertainties do not warrant use of corrected rather than measured rainout. Where the magnitude of the correction applied is large (e.g. chlorine – see
Table 28) then so is the potential inaccuracy.

We are certainly well aware of errors and numerical instabilities in earlier versions of the UDM (and in fact droplet modelling was significantly improved by Phase II of this JIP). Moreover the correction procedures described in RELEASE seem arcane and open to criticism. It is probably unwise now to take a view on these, but it is hard to argue with Ramsdale and Tickle's conclusion (see also the discussion in the Phase I report by Witlox and Bowen[1]). But we should recognise that uncorrected rainout will in fact be a lower estimate as losses will undoubtedly have occurred.

Lautkaski notes their objection, but then uses corrected data in deriving a correlation, but does not appear to state why the objection of Ramsdale and Tickle is set aside.

6.2.2 Large-scale 2-phase experiments

The validation manual included in the Phast UDM Technical Reference Manual includes details of validation against large-scale field experiments. Here we revisit this validation for the subset of these experiments concerned with 2-phase releases: the FLADIS ammonia, EEC propane, Goldfish HF and Desert Tortoise ammonia experiments.

Rainout was not measured or indeed observed for most of these experiments. The only series of experiments to observe rainout were Desert Tortoise. Recently, Ichard et al. (2010)[xxxiv] have stated that rainout fractions of the four experiments (DT1 – DT4) were as follows:

[48] For cyclohexane, there appears to be an inconsistency in RELEASE. Table 5-4 gives observed rainout for experiments 41 and 56 as 51.7% and 24.7% respectively, but 40.4% and 9.7% in Table 9-6. Given that the corrected values should be higher than the observed ones, the latter data must be correct, and these are in fact the ones plotted by Fig 2-5 in Ramsdale and Tickle.

Test	"Observed rainout" (%)
DT1	20
DT2	36
DT3	39
DT4	40

These percentages are in fact missing mass, rather than 'observed rainout'. Goldwire indeed states that for DT3 there is 30% released mass not accounted for in the integrated concentration results. They also state that "some of this was due to liquid pooling at the source". However they can only be interpreted as upper limits for rainout.

6.3 Rainout validation – simple rainout correlations

6.3.1 CCPS experiments

We start by presenting results for the CCPS rainout experiments. These allow us to verify our calculation method against previous work before applying the correlations to the Phase IV JIP experiments. This is relevant since conflicting confusing statements are published in the literature (RELEASE book, AEA report and Lautkaski paper). This particularly applies for the Devaull and King correlation.

Isenthalpic flash fraction

All the correlations use isenthalpic flash fraction (x_H). Selected data are given in Table 29. In this table, T_{st} and P_a are taken from the RELEASE book, while the other properties are calculated from the DIPPR property database included in Phast 6.6. The calculated flash fractions (2nd last column) agree well with the RELEASE book (the last column).

Experiment	T_{sat} (K)	T_{st} (K)	T_{st}-T_{sat} (K)	C_{pL} (J/Kg.K)	ΔH_{vap} (kJ/kg)	P_a (kPa)	x_H (%)	x_H (REL) (%)
CFC-8	297.9	295.7	2.3	882	182	97.2	1.1	1.1
Cyclohexane-41	359.9	350.2	9.7	2105	361	90.3	5.7	5.7
Chlorine-22	247.4	236.6	10.8	926	291	90.3	3.4	3.5
MMA-40	283.3	264.3	19.0	3309	851	90.3	7.4	7.3
Chlorine-20	256.4	236.6	19.8	924	291	90.3	6.3	6.4
MMA-34	293.8	264.3	29.5	3315	851	90.3	11.5	11.3
CFC-5	330.7	295.7	35.1	898	182	97.2	17.3	17.1
Cyclohexane-56	392.5	350.2	42.3	2203	361	90.3	25.8	26.1
Water-5	443.4	371.9	71.5	4277	2274	96.8	13.4	13.6
Water-10	453.4	371.9	81.5	4287	2274	96.8	15.4	15.7

Table 29. Evaluation of isenthalpic flash fraction (CCPS experiments)

Rainout

The predicted rainout is given in Table 30. The simple Kletz and Lautkaski correlations (56), (60) only require as input the isenthalpic flash fraction x_H. Devaull and King have separate correlations (57), (58)for volatile and non-volatile materials, and require as additional input the adiabatic saturation temperature T_{as} and the ambient temperature T_a. Again to ensure consistency with RELEASE we use T_a and Tas from Table E-1 in the RELEASE book. We have also included in Table 30 the values of Tas calculated49 using the UDM thermodynamic model THRM, which are close to those from the RELEASE book. These scaling factors in Table 30 agree with those given in the RELEASE book (see Figure 82).

Experiment	Kletz	Lautkaski	Devaull and King					
	η_R (%)	η_R (%)	T_{as} (K)	T_{as} (THRM) (K)	T_a (K)	Volatile?	η_R^*	η_R (%)
CFC-8	97.8	58.0	241.4	238.1	288.7	TRUE	0.62	61.2
Cyclohexane-41	88.6	49.8	273.1	274.4	308.4	FALSE	0.73	49.4
Chlorine-22	93.1	53.8	199.8	200.3	304.4	TRUE	0.20	18.4
MMA-40	85.2	46.7	221.8	222.6	301.3	TRUE	0.39	27.0
Chlorine-20	87.4	48.7	199.8	200.2	304.4	TRUE	0.20	15.5
MMA-34	77.0	39.3	221.8	222.4	301.3	TRUE	0.39	13.1
CFC-5	65.4	28.9	241.4	238.3	288.7	TRUE	0.62	0.0
Cyclohexane-56	48.4	13.5	273.1	274.6	308.4	FALSE	0.73	27.2
Water-5	73.1	35.8	288.1	287.7	305.4	FALSE	0.87	70.8
Water-10	69.3	32.3	288.1	287.9	305.4	FALSE	0.87	68.8

Table 30. Evaluation of rainout fraction using rainout correlations (CCPS experiments)

The rainout fractions from Table 30 as a function of superheat are plotted in Figure 83:

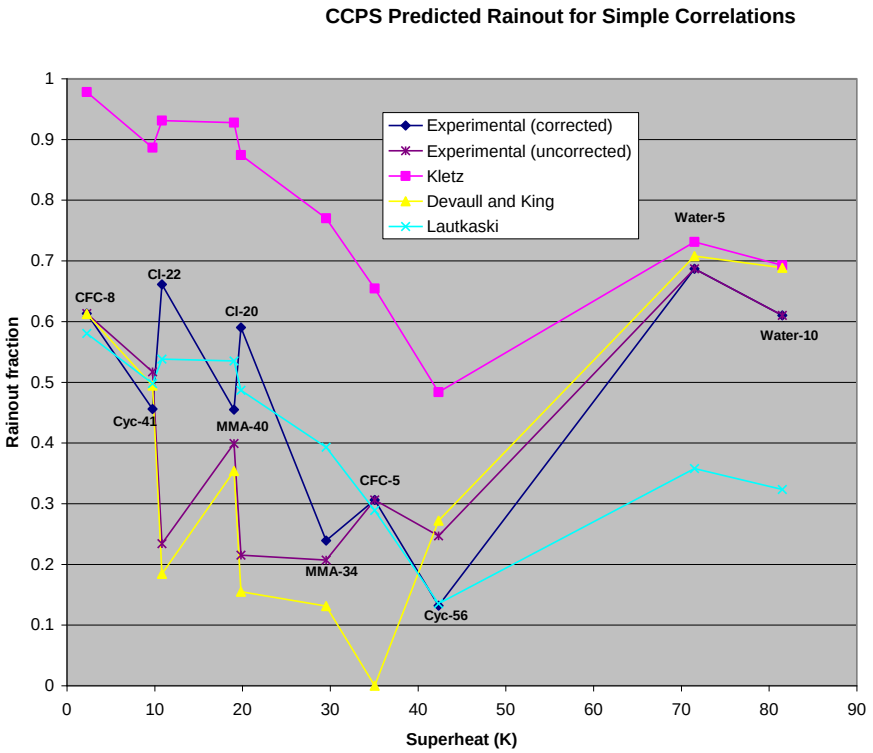

Figure 83. Predicted versus measured and corrected CCPS rainout using simple correlations

[49] In the THRM mixing of the air with the material, the air is assumed to be dry air at the experimental values of ambient pressure P_a and ambient temperature T_a. The differences from using dry or humid air are not significant (≤ 1K), except for water where the dry air T_{as} is ~ 2.5K lower than the humid air one.

The above figure has some discrepancies with plots in RELEASE using Devaull and King. For CFC-5 the prediction in Figure E-4 is ~25% rainout, but this is an error as RELEASE itself gives x_H = 17.1% and therefore rainout fraction from Equation (58) must be zero. For Cyclohexane-56 the prediction from Figure E-5 is in the range 15-17% rainout, but it can be verified using the data in
Table 30 that 27% is the correct figure.

Ramsdale and Tickle re-analysed the CCPS and RELEASE results, and their results for both CFC-5 and Cyclohexane-56 agree with ours. Lautkaski states the disagreement over CFC-11 results stems from an incorrect value of the specific heat C_{pL} by Johnson and Woodward, most likely originating from Yaws (2003)[xxxv]. For the CFC-5 experiment at least this is hard to verify. Our DIPPR-calculated value of C_{pL} yields the same isenthalpic flash fraction x_H as the RELEASE book, but Figure E-4 in the RELEASE book may be based on a different calculation of x_H using the wrong value of C_{pL}.

The choice of measured or corrected rainout changes the interpretation of this figure. If uncorrected rainout is preferred, then Devaull and King performs best, whereas the Lautkaski correlation is evidently the best for corrected rainout. Regardless, Lautkaski significantly under-predicts rainout for water (though Lautkaski does not plot data points for high superheat water releases for us to verify this).

It should be borne in mind that the Devaull and King correlation was based on the uncorrected CCPS results[xxx], and therefore good agreement is expected. Actual rainout is likely to have exceeded uncorrected (regardless of whether one accepts the 'corrected' rainout), and the correlation will may therefore have a tendency to underpredict.

6.3.2 Large scale 2-phase experiments

Calculations for flash fraction are given in Table 31. These results show good agreement with flash fractions calculated as part of the SMEDIS[xxxvi] project, except for Fladis experiment FL24 and EEC experiment EEC560[50].

Experiment	T_{sat} (K)	T_{st} (K)	T_{st}-T_{sat} (K)	C_{pL} (J/Kg.K)	ΔH_{vap} (kJ/kg)	P_a (kPa)	x_H (%)	x_H (%) SMEDIS
FL9	239.9	286.9	47.0	4500	1381	102.0	15.3	16.0
FL16	239.9	290.3	50.4	4504	1381	102.0	16.4	17.0
FL24	239.7	282.6	42.9	4495	1381	101.3	13.9	17.0
EEC360	230.8	286.7	55.9	2406	429	100.0	31.3	29.0
EEC550	230.8	286.2	55.4	2404	429	100.0	31.0	30.0
EEC560	230.8	273.2	42.4	2365	429	100.0	23.3	30.0
DT1	237.6	294.7	57.1	4507	1387	90.9	18.6	17.0
DT2	237.6	293.3	55.7	4505	1387	91.0	18.1	18.0
DT3	237.5	295.3	57.8	4508	1387	90.6	18.8	
DT4	237.5	297.3	59.8	4511	1387	90.3	19.5	
GF1	292.8	313.2	20.4	2637	371	101.3	14.5	
GF2	292.8	311.2	18.4	2629	371	101.3	13.0	
GF3	292.8	312.2	19.4	2633	371	101.3	13.8	

Table 31. Evaluation of isenthalpic flash fraction (large scale 2-phase experiments)

The rainout results are given in
Table 32. Both Kletz and Lautkaski show significant rainout for all experiments, as a consequence of the low flash fractions.

[50] CHECK Possibly to do with the significantly different superheat to other experiments in the same series.

Experiment	Kletz	Lautkaski	Devaull and King				
	η_R (%)	η_R (%)	T_{as} (K)	T_a (K)	Volatile?	Scaling	η_R (%)
FL9	69.4	32.4	202.0	288.7	TRUE	0.30	0.0
FL16	67.1	30.4	202.2	290.0	TRUE	0.29	0.0
FL24	72.1	34.9	202.2	291.0	TRUE	0.29	2.0
EEC360	37.4	3.6	194.3	289.0	TRUE	0.24	0.0
EEC550	38.0	4.2	193.6	282.9	TRUE	0.26	0.0
EEC560	53.3	18.0	193.9	285.0	TRUE	0.26	0.0
DT1	62.9	26.6	202.1	302.0	TRUE	0.23	0.0
DT2	63.8	27.4	202.3	304.0	TRUE	0.22	0.0
DT3	62.4	26.2	202.6	307.1	TRUE	0.21	0.0
DT4	61.1	25.0	202.5	306.9	TRUE	0.21	0.0
GF1	71.0	33.9	247.8	310.4	TRUE	0.53	0.0
GF2	73.9	36.5	247.6	309.4	TRUE	0.53	9.3
GF3	72.4	35.2	247.7	310.0	TRUE	0.53	4.7

Table 32. Evaluation of rainout fraction using rainout correlations (large-scale 2-phase experiments)[51]

These data are plotted in Figure 84. As noted above, actual rainout for the experiments was not measured but thought to be close to zero, with the exception of Desert Tortoise (as discussed above). Again, Kletz over-predicts for all experiments. For experiments other than Desert Tortoise Lautkaski wrongly predicts significant rainout, while Devaull and King performs better (but does predict up to 10% rainout for the Goldfish experiments). For Desert Tortoise Devaull and King most likely under-predicts but Lautkaski is in the right area.

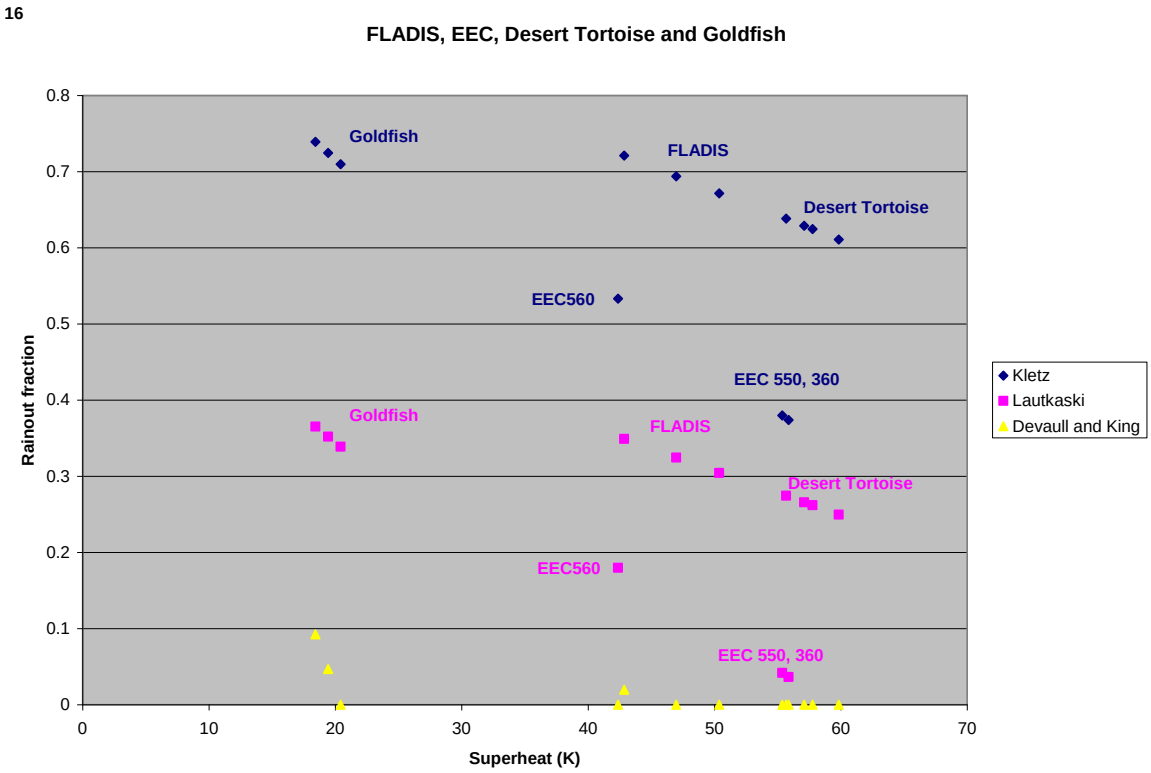

Figure 84. Predicted rainout using simple correlations.

6.3.3 JIP Phase IV experiments

[51] Release heights were 1.5m for FLADIS, 0.5m for EEC, 0.79m for Desert Tortoise and 1.263m for Goldfish

For the purposes of calculating the simple rainout correlations, there are only 4 cases. For xylene, the 'normal' ones where T_a = 284.15K and the 'cold' (2.33ºC) 8.5 barg 5mm release, and the 5C 13.1 barg 5 mm release[52]. The final case is for the water experiments, where we have assumed 280K.

Experiment	T_{sat} (K)	T_{st} (K)	T_{st}-T_{sat} (K)	C_{pL} (J/Kg.K)	ΔH_{vap} (kJ/kg)	P_a (kPa)	x_H (%)
Xylene (normal)	410.9	284.2	-126.8	1883	344	96.8	0
Xylene (cold)	410.9	275.5	-135.4	1869	344	96.8	0
Xylene (13.1bar)	410.9	278.2	-132.8	1873	344	96.8	0
Water	371.9	280.0	-91.9	4177	2274	96.8	0

Table 33. Evaluation of isenthalpic flash fraction (Phase IV JIP experiments)

[52] P_{st} is not used in these correlations

Experiment	Kletz	Lautkaski	Devaull and King				Measured
	η_R (%)	η_R (%)	T_{as} (K)	T_a (K)	Volatile?	η_R (%)	η_R (%)
Xylene (normal)	100	60	281.7	284.2	FALSE	29.2	82.1-96.8
Xylene (cold)	100	60	274.1	275.5	FALSE	25.6	95.3
Xylene (13.1bar)	100	60	276.5	278.2	FALSE	26.7	85.2
Water	100	60	272.0	280.0	FALSE	81.7	98.0-99.0

Table 34. Evaluation of rainout fraction using rainout correlations (Phase IV JIP experiments)

The isenthalpic flash fraction is, as expected, zero. For the Kletz and Lautkaski correlations the rainout fraction is therefore 100% and 60% respectively, and one would expect this to always be the case for sub-cooled liquids (this is consistent with Figure 83). These numbers compare to measured rainout fractions of 85% and above.

Devaull and King predict very low rainout fractions (25 - 29%), and it seems that for materials with very large boiling points, this results from a large $T_{sat} – T_{as}$ term in Equation (57).

On these experiments it seems none of the correlations gives satisfactory results for sub-cooled liquids, though Kletz performs best. It is however interesting to note that these experiments in general satisfy the guidelines of Ramsdale and Tickle (given in Section 6.1) for the correlations to be applicable.

6.4 Rainout validation – UDM droplet modelling

Section 4.2.3 describes the rainout validation against the HSL water experiments, using CCPS, modified CCPS, and JIP Phase III (+parcels) correlations. Section 4.3.3 describes the rainout validation against the HSL xylene experiments using both the CCPS and JIP Phase III droplet size correlations; Table 23 summarises the results of this validation.

In the current section we include additional datasets only using the UDM droplet rainout methods as listed in Section 6.1.1 (CCPS, Modified CCPS, Phase III JIP – single SMD parcel, Phase III JIP – droplet parcels).

6.4.1 CCPS experiments

This revisits the work done in Phase III on validation of CCPS rainout using the CCPS and JIP droplet correlations. The method described in the Phase III C4 report is adopted here, with the following changes:

- Inclusion of a modified CCPS correlation as described in Section 6.1.1, where the mechanical (Weber) correlation is used for sub-cooled releases, and the CCPS flashing correlation for superheated ones. This will therefore use the flashing correlation for all the included experiments, as superheat is always > 0.
- Inclusion of uncorrected CCPS rainout measurements, due to the doubts expressed on the corrections by Ramsdale and Tickle (see Section 6.2.1).
- Removal of JIP Phase II correlation, as this has been superseded by the Phase III one.
- Removal of Phase III ‘Phast 6.5’ results. These imposed conservation of momentum with the CCPS correlation. Note that these in fact would not be the ‘default’ Phast results – the ‘minimum thermodynamic change’ setting here uses the isentropic model. Thus the CCPS results here represent the default Phast 6.6 modelling.
- Correction of an error in the Phast III report, where the L/d ratio used for JIP simulations was 1 instead of zero as stated[53].

Droplet SMD

Additional input data for ATEX calculations (beyond that already given in Table 29 and Table 30) are as follows:

[53] This affects only JIP Phase III results.

Material	Superheat (K)	P_{st} (kPa)	Q (kg/s)	r_h (-)	d_o (mm)	ρ_L (kg/s)	u_{vc} (m/s)
CFC-8	2.3	161.8	0.27	0.08	6.35	1478	5.8
Cyc-41	9.7	209.1	0.283	0.174	6.4	714	12.3
Cl-22	10.8	178.9	0.382	0.086	6.35	1537	7.8
MMA-40	19.0	248.9	1.246	0.109	6.35	674	58.3
Cl-20	19.8	277.0	0.487	0.089	6.35	1513	10.2
MMA-34	29.5	356.1	0.4	0.063	6.35	661	19.1
CFC-5	35.1	302.0	0.46	0.08	6.35	1396	10.4
Cyc-56	42.3	247.0	0.346	0.082	6.4	680	15.8
Water-5	71.5	807.0	0.658	0.8	6.4	899	22.7
Water-10	81.5	1047.2	0.184	0.88	3.2	889	25.7

All data are taken from the RELEASE book, except the vena contracta velocity u_{vc} which is calculated from $u_{vc} = Q / [A_{vc}^2 * \rho_L(P_o,T_o)]$. $A_{vc} = C_d A_o$ is the area of the vena contracta, and C_d is taken to be 0.6.

The droplet SMDs predicted by ATEX from the various correlations are included in Table 35.

	CFC11 - 8	Cyclohexane - 41	Chlorine - 22	Methylamine - 40	Chlorine - 20	Methylamine - 34	CFC11 - 5	Cyclohexane - 56	Water - 5	Water - 10
Superheat (K)	2	10	11	19	20	30	35	42	72	82
CCPS (RELEASE book)	386	345	265	208	431	231	465	203	53	33
CCPS (Phast 6.6)	566	232	435	23	184	27	54	20	11	9
CCPS (modified)	566	401	435	270	350	208	293	208	82	63
JIP Phase III	3465	1889	2834	80	1267	79	79	78	75	74

Mechanical
Transition
Flashing

Table 35. Prediction of SMD (µm) by CCPS & JIPIII correlations (CCPS experiments)

Comparing this with the previous Phase III C4 report, a number of differences are apparent. Most obviously JIP Phase III mechanical and transitional droplet sizes have decreased by about 25% due to the corrected value of L/d_o. [54]

Using CCPS corrected rainout as the basis for comparison, the modified CCPS correlation performs best, unsurprisingly as it was developed from this dataset. Comparing Figure 85 against Figure 40 in the Phase III C4 report, the influence of reduced L/d_o on the JIP III + parcels results is small: low superheat cases using the mechanical correlation have slightly (1-2%) decreased rainout, but others are not affected.

[54] The CCPS results also show some differences in the flashing SMDs; why??

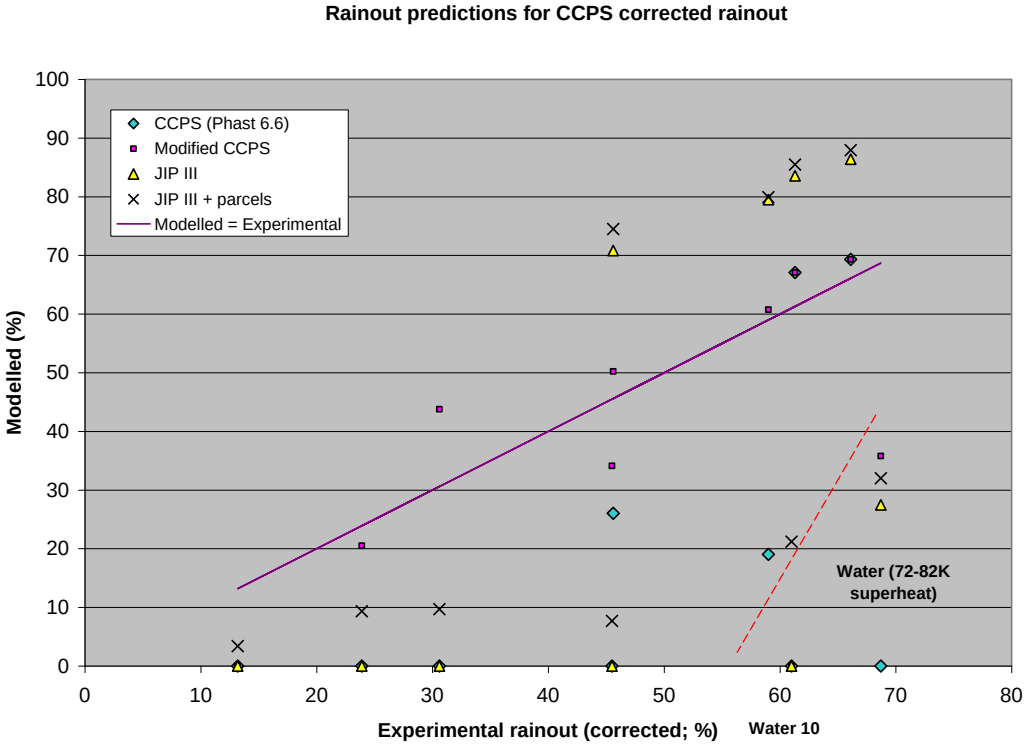

Figure 85. Droplet modelling predictions compared to CCPS corrected rainout[55]

The choice of L/d_o for rainout here seems relatively unimportant but beneficial. Using the corrected L/d_o =0.1 slightly reduces the rainout for the points with the highest modelled values, slightly improving the fit.

For the uncorrected rainout (Figure 86), the principal difference is that the two chlorine experiments (Chlorine-20 and Chlorine-22) with corrected rainouts of 59 and 66.1% have uncorrected rainout of 21.5 and 23.4%. They have therefore a reduced abscissa and have moved leftwards on the plot. This does not improve any of the predictions, though corrected CCPS still performs the best.

[55] Modified CCPS predictions for water are less accurate because of additional rainout because of ambient water condensation. The multi-component version of the UDM correctly models the mixing of water with moist air, but in the standard UDM model erroneously the water from the release and the water in the air are treated as separate components. The latter leads to possibly too low prediction of condensation of the water.

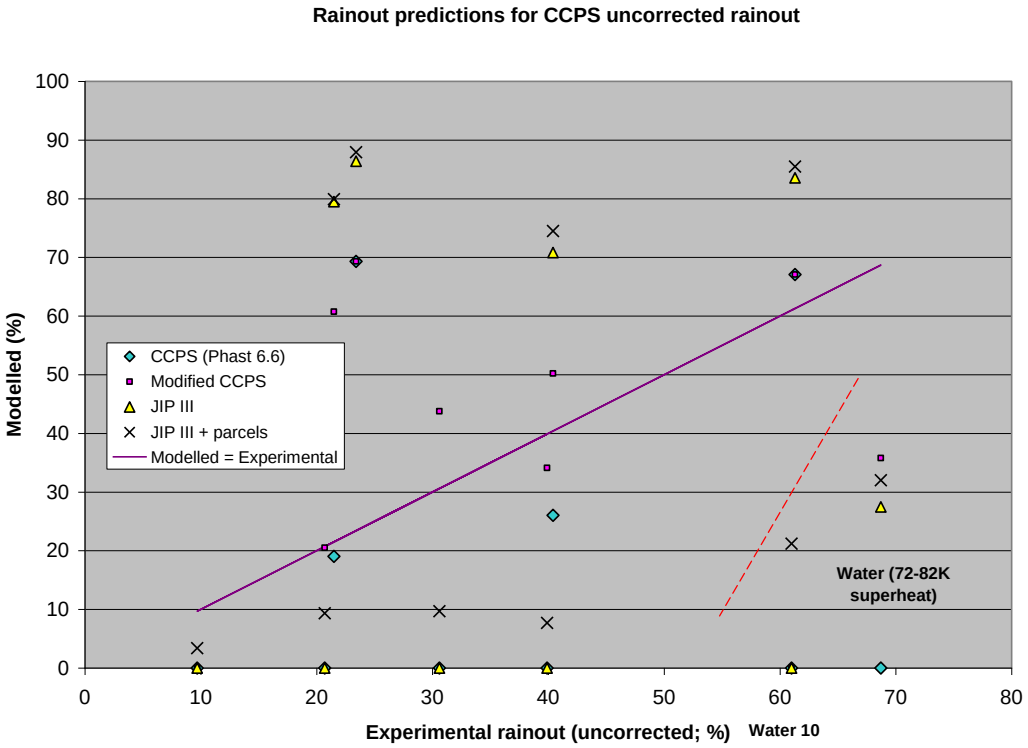

Figure 86. Droplet modelling predictions compared to CCPS uncorrected rainout

An alternative way of looking at this information is plotting rainout against superheat (similar to Figure 83 for the simple correlations):

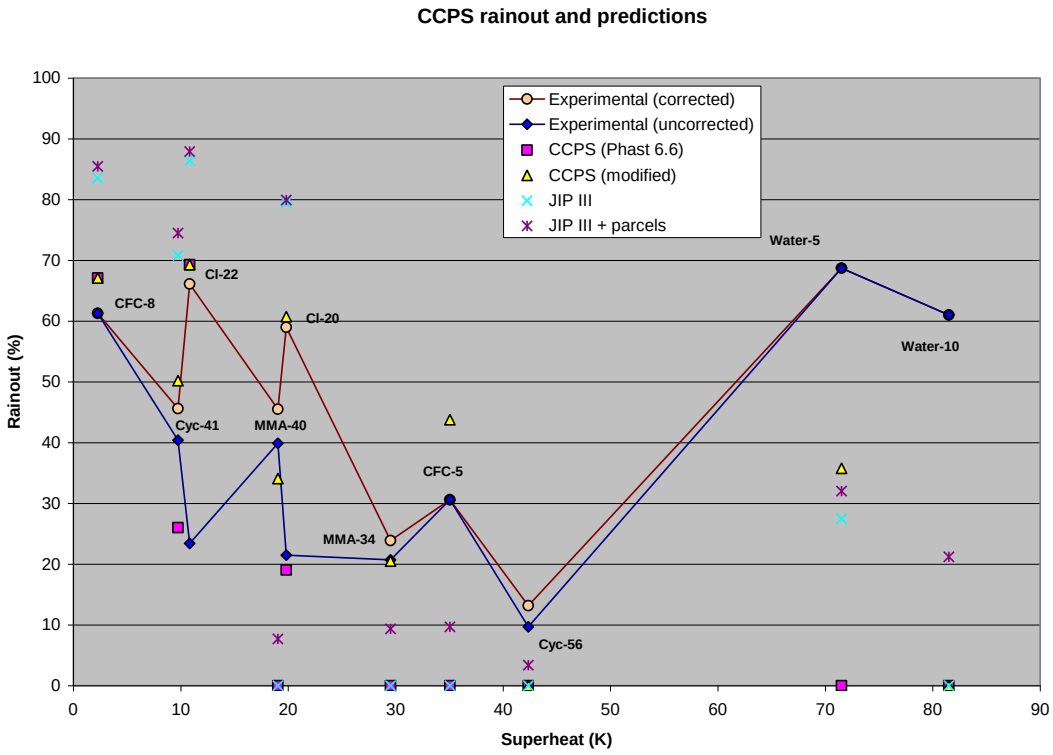

Figure 87. Droplet modelling rainout predictions for CCPS experiments

6.4.2 Large-scale 2-phase experiments

Droplet modelling was carried out for the FLADIS, EEC and Desert Tortoise experiments using the JIP Phase III (with and without parcels), CCPS and corrected CCPS correlations. The method is as described in the Phase III C4 report. Post-expansion inputs to the UDM (with the exception of droplet SMD) are given in the UDM Validation Manual and are taken from SMEDIS.

Droplet SMD is calculated from DISC runs, as only stagnation rather than orifice data were available. We have assumed $L/d_o = 1$ (as in Phase III, though undocumented)[56]. The key input data and results for DISC are given in Table 36.

Case	Inputs			Droplet SMD (µm)		
	Material	Superheat (K)	P_{st} (kPa)	CCPS (Phast 6.6)	Modified CCPS	JIP III
FL9	Ammonia	47.0	693	9	113	77
FL16	Ammonia	50.4	798	7	102	76
FL24	Ammonia	42.9	570	11	131	77
EEC360	Propane	55.9	770	5	137	76
EEC550	Propane	55.4	1013	5	136	76
EEC560	Propane	42.4	1023	5	134	76
DT1	Ammonia	57.1	1012	7	84	75
DT2	Ammonia	55.7	1116	7	87	76
DT3	Ammonia	57.8	1137	7	82	75
DT4	Ammonia	59.8	1179	6	77	75

Table 36. Key DISC input and predicted SMDs for large-scale 2-phase experiments

All the cases have significant degrees of superheat, and therefore are well into the JIP III flashing region, with SMD < 80 µm. The unmodified CCPS correlation picks up the mechanical correlation and predicts very small droplets. The corrected CCPS uses the flashing correlation, and predicts slightly larger droplets than JIP III.

Predicted rainout based on SMEDIS post-expansion results[57], given in Table 37:

Case	CCPS (%)	Modified CCPS (%)	JIP III (%)	JIPIII+ parcels (%)	FLACS[xxxiv] (%)	'Missing' mass (%)
FL9	0	0	0	4		
FL16	0	0	0	4		
FL24	0	0	0	4		
EEC360	0	0	0	3		
EEC550	0	0	0	4		
EEC560	0	0	0	3		
DT1	0	27	26	25	43	20
DT2	0	41	39	28	43	36
DT3	0	42	41	27	45	39
DT4	0	38	38	27	40	40

Table 37. Validation of rainout percentage by UDM droplet methods (large-scale 2-phase experiments)

The experiments divide between Desert Tortoise and the rest. For the former, all except CCPS predict significant rainout. Both JIP III and corrected CCPS predict at the top end of the possible range of rainout (≤ the missing mass). The JIP III + parcels moderates this and predicts less than the maximum. Recent simulations using FLACS predict the highest rainout, and more than the missing mass (especially for DT1).

For the rest of the experiments all methods predict zero rainout, except JIP III + parcels, where a small fraction (< 5%) of the mass is in larger droplets which do rainout.

[56] Both the JIP Cardiff (Phase III) and HSL (Phase IV) experiments used nozzles in the range L/d =0. 5 – 4.5. INERIS Phase III experiments used nozzles with L/d = 0.1 – 0.3. CHECK. It is not known if L/d are available for any of these experiments.

[57] The exceptions are DT3 and DT4, where data are not available from SMEDIS. In these cases post-expansion liquid fraction and velocity are also calculated from DISC using the conservation of momentum model, even where using the CCPS droplet correlation (the isentropic model predicts very large post-expansion velocities compared to SMEDIS or conservation of momentum).

6.5 Summary

Simple correlations without droplet modelling

Overall on the evidence above we can draw the following conclusions about the simple correlations:

- Kletz consistently over-predicts rainout
- Previous published work on Devaull and King has been error prone and exact methodology is open to doubt.
- Based on the CCPS results, Lautkaski gives the best prediction if one accepts the 'corrected' rainout results; whereas Devaull and King is preferred if one uses the measured rainout.
- Lautkaski wrongly predicts significant rainout for large-scale flashing experimental releases, but under-predicts for the sub-cooled JIP phase IV experiments
- Devaull and King performs best for the large-scale releases, but dramatically under-predicts rainout for the sub-cooled JIP phase IV experiments.

No correlation does well across the range of superheats and experiments. Devaull and King is clearly the best for superheated releases if one accepts the uncorrected CCPS results. Lautkaski will always predict 60% rainout and Kletz always 100% for sub-cooled releases, and this is likely to bracket actual results. However if one excludes the CCPS results (which data was used to derive correlations other than Kletz) then none of the correlations appears satisfactory. This is despite the fact that the experiments are largely satisfying the suggested validity range for their application.

UDM methods with droplet modelling

The default CCPS SMD correlation gives poor results in nearly all cases due to the small droplet sizes and the incorrect use of the mechanical droplet-size correlation results for superheated releases. It predicts no rainout for Desert Tortoise, and no rainout for most of the CCPS experiments.

The modified CCPS SMD correlation is derived from the CCPS experiments, and we cannot therefore judge from its performance against corrected rainout for the CCPS experiments. But it performs best against uncorrected results (though 4 out of 10 data points are common between both), and adequately against the large-scale experiments.

The JIP Phase III correlation with or without parcels does not predict very well against the CCPS rainout, corrected or uncorrected. It does perform adequately against EEC, FLADIS and Desert Tortoise.

7 DISCUSSION, CONCLUSIONS AND RECOMMENDATIONS

7.1 Initial SMD and rainout

In Chapter 5 results are summarised of SMD validation for a large range of experiments (Phase III JIP and other experiments from the literature). From this it was confirmed that overall the JIP Phase III SMD correlation provides the most accurate predictions. It was also shown for subcooled releases that the Weber number based on the orifice velocity u_o (as used in the Melhem SMD correlation) provides more accurate results for initial SMD (larger value) than the Weber number based on final velocity (=vena-contracta velocity). These same conclusions also apply for the subcooled Phase IV JIP water and xylene experiments (see Table 19 in Section 4.2.2 and Table 22 in Section 4.3.2).

In Chapter 6 results are summarised of rainout validation using the Phase IV JIP experiments, the CCPS experiments as well as all 2-phase experiments from the UDM validation dataset. It was concluded that overall the modified CCPS correlation provides the most accurate predictions, i.e. more accurate than the Phase III JIP correlation (with or without parcels) and the current default Phast 6.6 CCPS correlation.

Thus there is a contradiction in the results presented above. Measured droplet sizes overall show reasonable agreement with the JIP Phase III correlation simulations, certainly much better than the CCPS correlation. But this does not translate into better rainout results: the CCPS correlation proves highly accurate. Why should this be so?

The critical Weber number adopted by Melhem (based on orifice velocity and not vena contracta velocity) should theoretically give the largest mechanically stable droplet diameters. Above this size, we would expect the droplet distribution to be unstable and for droplets to be subject to secondary break-up. It is apparent from the water experiments that this is indeed the case. However measured droplet sizes were always well in excess of CCPS predicted values (smaller droplet sizes based on larger vena contracta velocity), and they approximately halved in size between 500 and 1000 orifice diameters downwind (1.25 and 2.5m).

The JIP Phase III correlation predicted droplet size distributions well at 500 diameters for water and 800 diameters for xylene. But the UDM does not include a model for secondary droplet break up and, as these are sub-cooled liquids that experience little evaporation (especially water), modelled and actual droplet sizes diverge rapidly.

We might expect though that overall the initial droplet sizes, rather than reduced sizes at some time and distance downwind, were the primary influence on rainout amount and position. This appears not to be the case. For xylene the CCPS correlation is a much better predictor of rainout mass than JIP Phase III, despite that all measurements taken regardless of position downwind showing CCPS under-estimating droplet size.

In the UDM, liquid evaporation rates are correlated inversely with droplet diameter: evaporation rate from a given droplet is proportional to area, but its mass is proportional to volume. Smaller droplets imply faster evaporation of the liquid and less rainout. This effect accounts for the differences in rainout between the two correlations.

The fact that we start with a theoretical lower bound on droplet size yet still predict rainout mass suggests either the UDM underestimates evaporation rates or time to rainout (in which case the small droplet sizes of the CCPS correlation is compensating for these effects), or droplets do not evaporate but become so small they remain in suspension.

Practically it is not important to differentiate between droplets that evaporate or stay in suspension, as the latter will probably behave in a similar manner to vapour and eventually evaporate. But in any case Phase II of the JIP suggested a lower cut-off of 30 µm below which droplets would remain in suspension, and measurements indicate an insignificant proportion of the mass is in droplets of this size. Neither is there any plausible mechanism for droplets that are stable to reduce much in size further. In all likelihood therefore the UDM is underestimating liquid evaporation rates or time to rainout.

7.2 Modelling of droplet dispersion

Currently the UDM applies conservation of momentum to the jet and entrained air, but it enforces a uniform horizontal velocity throughout the jet. All components of the jet (large and small droplets or vapour) travel downwind at the same speed. Consequently the larger droplets rain out sooner than smaller ones due to reduced vertical drag effects (i.e. larger droplets accelerate downwards more rapidly); see Figure 88a.

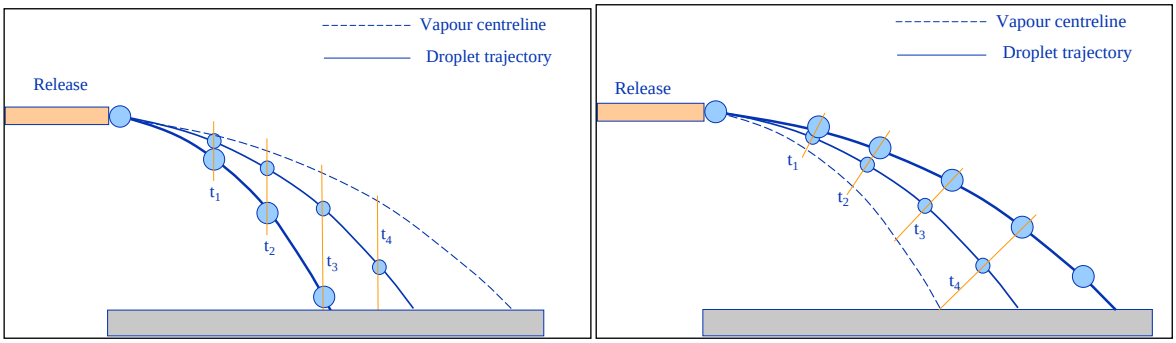

(a) Vertical drag effects (current Phast 6.6 UDM) (b) Horizontal drag effects (potential future model)

Figure 88. Modelling of drag effects for droplet parcels

These momentum effects explain the inability of the parcels logic within the UDM to model accurately the longitudinal spread of rainout. As parcel rainout distances are differentiated only by drag effects, for the large droplets predicted by JIP Phase III rainout distances are very clustered as vertical drag effects are negligible.

Consider now a model where horizontal drag on individual parcels droplets is considered. Large droplets will decelerate slower than smaller ones. As the overall momentum of the plume must be conserved, these must be balanced by reduced velocity of smaller droplets and vapour; see Figure 88b. In other words, the drag effect of entrained air is felt more by small droplets than by large ones. So such a model would predict slower moving small droplets than the current UDM, and faster moving large ones. As it is small droplets that result in most evaporation, this greater time to rainout would lead to significantly increased evaporation.

Such a model would also project larger droplets further downwind and increase the spread of rainout. A high-velocity jet will experience much greater drag in the downwind direction than vertically, as it is proportional to u^2. The effect of droplet diameter therefore will become much more significant.

We can observe in videos the central core of the jet with large droplets moving faster than the periphery. We also observe smaller droplets being detrained from the jet: turbulent mixing along the edge will achieve this as well as entraining air within the plume[58]. The detrained droplets enter the surrounding air. The lower velocity and lower vapour concentrations around the droplets result in increased evaporation (though drops detrained from the lower edge of the plume may intercept the ground and account for the small degree of rainout very close to the release point).

7.3 Recommendations for Phast modelling and future work

The primary purpose of droplet modelling within a package such as Phast or Phast Risk must be accurate estimation of rainout rather than droplet size.

The default CCPS correlation as recommended in RELEASE and currently included in Phast 6.6 is clearly in error, as illustrated by comparison against the CCPS experiments themselves (and the HSL water experiments). Using the minimum of mechanical and flashing droplet sizes means that often the mechanical correlation is used for flashing releases and the flashing correlation for sub-cooled ones. We have therefore suggested (and described earlier) a 'modified' CCPS, where the transition is based on superheat. This will, however, mean that results are discontinuous across the boundary between sub-cooled and superheated liquids.

The modified CCPS correlation produces significant improved predictions for initial droplet size. However it underpredicts droplet sizes for the subcooled Phase IV JIP experiments (water, xylene) and the subcooled Phase III JIP experiments (water and cyclohexane). However the modified CCPS predictions result in the best predictions for rainout of the HSL and CCPS rainout experiments. The too small initial droplets appear to compensate for mechanisms that are not modelled in the UDM, both in terms of rainout amount and distance. One might imagine this is fortuitous in the case of the HSL experiments. One could also argue that as the modified CCPS correlation results are derived from the CCPS experiments good agreement is unsurprising.

Another strategy for improving model performance would be to adopt the JIP Phase III correlation as the best 'source' term, and then extend the UDM in two ways: (a) include a secondary break-up model in the UDM, and (b) modify the droplet horizontal momentum modelling as described above. This would constitute a fundamental modification and increased complexity of the UDM droplet equations, and it is far from certain that the end result would perform any better in terms of rainout than the current UDM using modified CCPS. It may however have the advantage of better predicting the spread of rainout.

[58] Larger droplets will have greater inertia and be less likely to deflected from their trajectory

A brief discussion of droplet break-up length formulations and validation against the xylene HSL experiments in included in 0. However further work is required (literature survey and additional validation) before more precise recommendations can be given for Phast implementation. At this point of time it is recommended to apply the conservative assumption of ignoring the jet break-up length, i.e. air entrainment starts immediately at the release point.

The simple rainout correlations do not perform well beyond the data set from which they have been derived. The best of them would appear to be Devaull and King (though its prediction of rainout for the HSL experiments is very poor). We do not propose therefore to add any of these correlations to Phast.

As predicting rainout is the primary focus for Phast, and given the excellent performance of the modified CCPS correlation, we have set that as the default in Phast 6.7. However, the flashing part of the correlation is validated only against the set of experiments from which it was derived, and this must be a focus for future work. Another issue is that the CCPS flashing correlation is only valid in conjunction with the isentropic expansion assumption, while for some scenario types (e.g. pipe releases) the conservation of momentum option may lead to more accurate results. Thus it is highly recommended to further validate and improve the method of expansion.

7.4 Other future developments

The following potential further work is proposed:

1. General validation of ATEX model and inclusion into models of break-up length. Further validation is required for the ATEX atmospheric expansion model to establish the accuracy of its post-expansion predictions for velocity and liquid fraction. The current Phase II and Phase III projects primarily focussed on validation for flow rate and initial droplet size, and did not carry out an extensive evaluation of the accurate of the post-expansion data. An associated model improvement is the inclusion of an appropriate break-up distance, following which the UDM dispersion calculations can be initiated; see part A of the current report for an initial recommendation.

2. Added release scenarios. Currently the initial-rate DISC model has been applied with the orifice scenario only. Additional scenarios which would need further investigation with respect to droplet modelling are as follows;

    2.1. Initial-rate release from short pipe (DISC with 'line rupture' scenario)
    2.2. Instantaneous releases (DISC with 'catastrophic rupture' scenario)
    2.3. Time-varying releases from vessels or short pipes (Phast model TVDI)
    2.4. Time-varying 2-phase releases from long pipelines (Phast model PIPEBREAK), involving two-phase to two-phase ATEX expansion

3. Multi-compound modelling

    3.1. Following experimental work, SMD droplet correlations could be developed for multi-compound releases which could be implemented into ATEX.
    3.2. Also multi-compound droplet logic would need to be developed for the UDM, which would be a considerable effort (possibly in line with the Mobil model as discussed in the Phase I literature review report[1]).
    3.3. A multi-compound version of the pool model needs to be developed (either based on an extension of PVAP, or based on logic of the HGSYSTEM model LPOOL).
    3.4. Upon multi-compound evaporation, the composition in the cloud would be time-varying and the UDM needs to be extended in order to cope with this.
    3.5. Further improvements of UDM thermodynamics modelling could be considered, e.g. inclusion of reactions and allowing for mixtures with HF

4. Further address footnotes in this report (JUSTIFY, IMPROVE, DOC, ERROR).

APPENDICES

Appendix A. Jet break-up length

The evaluation of break-up length was briefly discussed as Part A of the Phase III JIP report. As part of the current work a further briefly literature survey was carried out with the aid of Cardiff University and Prof. Phil Bowen. The text below thus constitutes first an extended description form Part A of the Phase III JIP report. Subsequently the correlations are compared with estimates of the break-up length from the xylene HSL experiments.

A.1 Break-up length formulations

The break-up length of a spray (L_b) is very important when deciding which downstream distance measurements should be taken to represent the spray as an initial droplet size. For example, if the measurements are recorded too close to the nozzle, maybe within the break-up length, then the data recorded will not be representative as the spray may not have fully atomised and ligaments which are unable to be detected by spherical particle counter techniques such as PDA and are likely to unrealistically distort the data. Conversely if the measurement are recorded too far from the nozzle then the data maybe skewed by processes such as droplet coalescence, droplet rain out, droplet evaporation, etc..

Therefore the downstream distance chosen to record the data is a compromise between getting as close to the nozzle as possible to record the 'initial' droplet diameters, before they affected by secondary modes (rain out, evaporation, etc), whilst ensuring that good quality fully atomised data is measured.

For the Phase III JIP Cardiff experiments 500 mm downstream was found to be a good compromise for recording data in the mechanical break-up regime (with the exception of 0.75 mm for cyclohexane where the downstream distance was found to be of the order of 1000 mm). The downstream distance adopted for the flashing experiments is 250 mm was considered a good compromise between the mechanical break-up, it is possible that data were recorded within the break-up length during this regime, and the fully flashing which has a very short break-up length.

The authors are not aware of specific literature studies concerning break-up length of large-scale atmospheric releases. However one can resort to the considerable literature concerning fuel injection systems for the mechanical break-up length L_{bm} , e.g. for automotive engines.

Beal and Ritz break-up length correlation

One of the most recent correlations for break-up lengths associated with primary atomisation (via the Kelvin-Helmholtz instability) for diesel fuel injectors is proposed by Beale and Reitz[xxxvii]:

$$L_{bm} = \frac{1}{2} B_L \, d_0 \sqrt{\frac{\rho_L}{\rho_a}} \qquad (61)$$

Here B_L is the break-up constant of the Kelvin-Helmholtz model (estimated here to be 40), d_0 the orifice diameter, ρ_L the liquid density (at orifice conditions) and ρ_a the density of the surrounding air (at ambient conditions).

Several issues should be noted at this stage. First, the correlation was developed under conditions of considerably smaller release orifices (typical of diesel injectors, circa 0.3mm) and much higher pressures (1-2 orders of magnitude higher) than those being developed within the scope of this study. Furthermore, influence of L/d is unlikely to have been studied in any depth, and the correlation shows no dependence upon release pressure. However, for the benchmark case in this report (1mm exit orifice), the break-up length predicted corresponds well with that observed (circa 0.5m). By contrast, the predicted linear dependence of break-up length upon orifice size is not corroborated by the qualitative evidence of this study, indicating some potential inconsistencies in extrapolating the correlation for larger scale hazardous releases of interest here.

If a break-up length correlation such as equation (61) is employed in an atmospheric dispersion model, then in the spirit of the approach adopted throughout this report, a simplified method is proposed to accommodate the influence of superheat. A linear reduction in break-up length from that predicted for mechanical break-up [e.g. equation (61)] to break-up length of zero at the critical superheat predicted for the transition to fully flashing conditions is proposed:

$$
\begin{aligned}
L_b &= L_{bm} \quad , && \Delta T_{sh} \le \Delta T_{sh}{}^{A} \\
&= L_{bm}\left[\frac{\Delta T_{sh}{}^{B} - \Delta T_{sh}}{\Delta T_{sh}{}^{B} - \Delta T_{sh}{}^{A}}\right], && \Delta T_{sh}{}^{A} \le \Delta T_{sh} \le \Delta T_{sh}{}^{B} \\
&= 0 \quad , && \Delta T_{sh} \ge \Delta T_{sh}{}^{B}
\end{aligned}
\qquad \text{(62)}
$$

The above correlation is recommended in conjunction with the Phase III JIP correlation. For the modified CCPS correlation, $L_b=L_{bm}$ is recommended for subcooled releases and $L_b=0$ for flashing releases.

The source of the release point leading to atmospheric dispersion predictions should then be displaced by the distance of the above predicted break-up length, beyond which the dispersed phase calculations would prevail.

Grant and Middleman correlation

A brief literature survey was carried out at Cardiff University. Whilst there does some to be some variation/differences of opinion in the literature, the correlation below from Grant and Middleman (1966)[xxxviii] seems to perform best in terms of getting the right sort of numbers at:

- small scale (diesel injector): breakup length L_b about 10-40 mm
- Cardiff lab scale experiments – orifice size around 1mm: L_b up to about 0.5m)
- larger scale experiments such as HSL – orifice size several mm: L_b up to about 2.5m)

L_b does appear to show non-linear trends depending on flow state (laminar, transition, turbulent, high-turbulent). The L/d_o ratio also seems to have an effect. As most of the types of releases pertinent to hazardous releases would be turbulent, then correlation below has been developed for turbulent releases. The proposed correlation for jet break-up length by Grant and Middleman for turbulent flow is as follows for subcooled releases:

$$
L_{bm} = 8.51\ d_0\ We_{Lo}{}^{0.32} \qquad \text{(63)}
$$

Here We_{Lo} is the jet orifice liquid Weber number defined by Equation (35). The above correlation can again be extended to superheated releases as indicated above for the Beal and Ritz correlation.

A.2 Validation against HSL xylene experiments

The Part A report discusses the estimation of the jet break-up length L_b from photographs for the HSL xylene experiments. The experimental results are given by
Table 22; see Section 5.3 of the part A report for further details on the experimental results.

Nozzle Diameter / ***Release Pressure (barg)***	***2.5 (mm)***	***5.0 (mm)***
4	623	479
8	461	348
12	266	357
16	229	277

Table 38: Jet break-up length observed from photographs

Figure 89 summarises the results of the validation of the above correlations against the above HSL experimental data. It is seen that the experimental observed jet break-up length reduces with increasing pressure (increasing velocity). The Beale and Ritz correlation is independent of pressure and orifice velocity and produces a constant too large value. The Grant and Middleman produces the opposite trend (increasing with increasing pressure) than the experimental data, and produces smaller break-up lengths and the Beale and Ritz correlation. A more extensive investigation of jet break-up length forms part of further work.

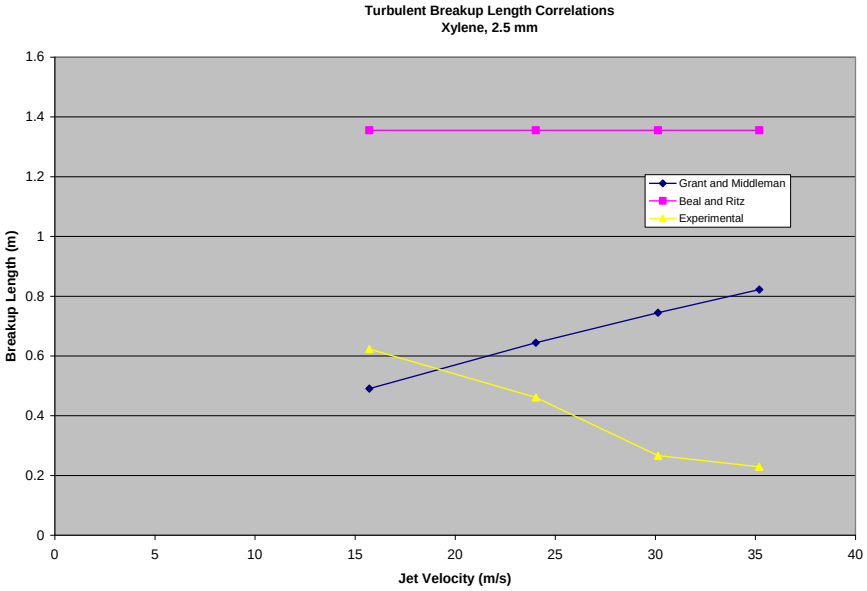

(a) nozzle diameter 2.5 mm

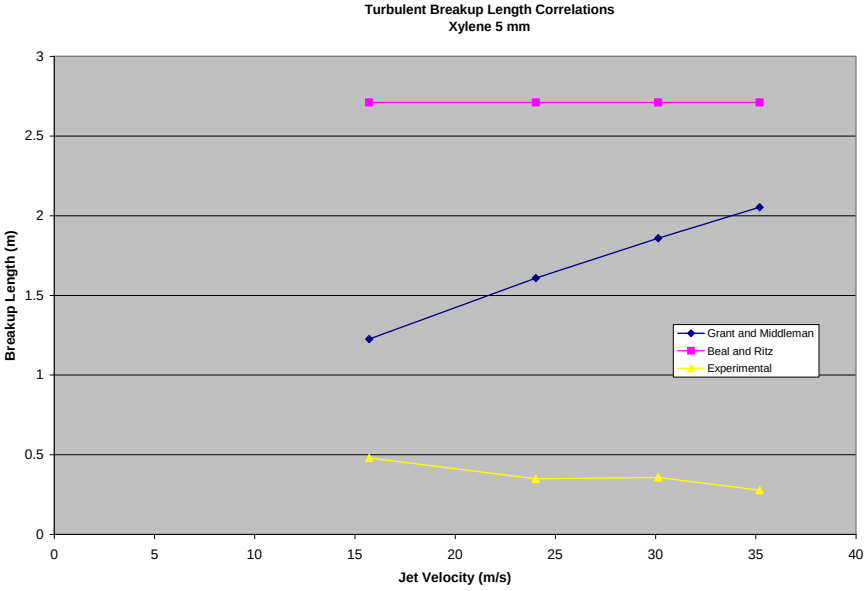

(b) nozzle diameter 5 mm

Figure 89. Validation of break-up lengths for HSL xylene experiments

Appendix B. Experiments including SMD measurements

B.1 STEP experiments

As part of the EEC project STEP for understanding chemical hazards, Herviau and Veneau carried[9, 10] out experiments to measure the liquid droplet size and velocity within a jet at the exit of a discharge pipe of a liquefied propane storage vessel during a sudden blow-down. The nozzle diameter (2, 5 and 8 mm) and the initial vessel pressure (5, 11 and 17 bar) were varied. The propane is stored under saturated conditions, so superheat is varied as a function of storage pressure. The release conditions were representative of a fully flashing jet. See also Section 4.3.4 of the Phase I report[1] for a description of the STEP experiments.

Measurements were undertaken at 3 downstream axial locations, utilising a PDA system as discussed earlier. It was found that whilst a decrease in droplet size was noted along the axis of the jet – due to evaporation – even closest to the nozzle, no droplets greater than 80μm were recorded. Clearly this is markedly different from mechanical break-up conditions, and any modelling approach advocating mechanical break-up for these conditions must be in error. The effects of evaporation were also clearly noticeable in one set of radial droplet size measurements, as mean sizes decreased towards the edge of the jet. For 5 bar releases at 60mm downstream, the measured SMD varied between 39-49 μm for the 2mm and 5mm cases respectively. At 11 bar at 60mm downstream, the droplet sizes reduced to 30-31 μm for the two orifice sizes. These measurements indicate the very small influence of orifice size at the higher pressure, and the more significant dependence of droplet sizes on release pressure and superheat (these two effects cannot be decoupled from this series). At 17bar, SMD droplet size was below 30μm at all locations for the 2mm and 5mm orifices.[59]

Modelling carried out as part of the STEP programme

Vandroux-Koenig and Berthoud[10] developed a mathematical model to link the conditions at the breach to a heavy gas dispersion model. It includes a simple turbulence model to include air entrainment, and takes into account the air humidity. The mathematical model includes 5 mass conservation equations (air, propane vapour/liquid, water vapour/liquid), 2 momentum equations (gas mixture + liquid water, propane droplets), 1 energy equation (gas mixture + liquid water). The model was solved by the MC3D Eulerian finite-volume calculation code. For the runs done the droplets remained in the centre of the jet because of high momentum, and homogeneous equilibrium was shown to be obtained very quickly. They quote that this would be generally expected for propane flashing releases. For releases with a lower superheat (so with bigger droplets), smaller velocities and smaller evaporation this would not be the case anymore. They suggest therefore for these cases to introduce an additional energy equation for the liquid droplets.

An earlier atomisation correlation is quoted for the maximum droplet size within the spray, which under the conditions of the release, predicts 10μm. Whilst this is an order of magnitude less than that observed in the experiments, the authors continue to use this prediction in their future calculations[60], claiming this to be near the measured maximum droplet size, whereas the difference is likely to have a very significant effect. Hence, the claimed agreement must be subject to question given the inherent errors adopted in the initial input data, and consequently it proves difficult to comment on the appropriateness of the proposed strategy for modelling two-phase jets.

B.2 HSL experiments by Allen

The series of papers published by Allen[11,12,13] represent several years experimental study undertaken by the UK Health and Safety Laboratories as part of a CEC joint-industry project on a rig specifically developed for characterisation of two-phase flashing releases. Again LPG is considered as the test fluid, and the work represents progress towards providing a reliable benchmark data-set against which source term models can be verified, and the appropriateness of different characterisation methodologies for flashing release characterisation. The release conditions are reported to have mean release temperature of 16 °C and mean mass release rate of 0.0951 kg/s at saturated conditions. The nozzles utilised in the published work were of 4mm exit orifice size with L/d =10. The researchers commendably persevere to avoid intrusive measurements in the harsh operating conditions provided by flashing releases, and hence attempt to improve upon one potential error source in the STEP[9] programme. This invariably means that non-standard hardware and operating procedures have to be adopted and the data post-processed considerably.

Consistent with the recommendations of this report, LDA measurements provide sufficient particle velocity component quantification after data post-processing, and LIF is developed towards quantification of jet temperature – this could be developed towards providing relative phase information also. However, the choice of particle size diagnostic technique is not considered the most appropriate due to the problems of laser obscuration and vignetting discussed in section 3, although the authors endeavour to process the data towards quantitative size information. The data before manipulation shows 3 characteristic particle size peaks. After data manipulation, useful size information is provided subject to the appropriateness of the manipulation process, and the data is reduced to a bimodal distribution, where the majority of data is noted to be less than 32 μm. Data is subsequently presented in relative size bands – normalised against the total spray volume - where repeatability of the analysis technique is demonstrated. The authors recommend that the data at any point should not be considered in absolute terms, but rather in terms of identifying general trends and overall size distribution behaviour. In this sense, for trend analysis compared with other data-sets and models, the indication that the majority of

[59] (cu) Again at which downstream location can be best apply the post-expansion droplet diameter.

[60] It is not clear from the STEP paper why this simplifying assumption was adopted.

the data is 30 μm or less means, as a broad estimate accounting for the disproportionate influence of larger droplets, SMD values of the order of 30 μm would be appropriate.

The approach adopted by the HSL group to post-process the diffraction-based data is considered plausible ; it is very doubtful that any better could be achieved using the diffraction technology. Hence, this programme serves the purpose of providing qualitative benchmarks, whilst emphasising the inherent unsuitability of diffraction technology for the environment of flashing sprays.

Appendix C. Expansion from orifice to ambient: isentropic versus conservation of energy

C.1 Introduction

The various thermofluid processes which have been considered for this part of the problem are reviewed and analysed in a systematic manner in two EU-funded reports, published by Britter[xxxix, xl]. A more out-of-date review of expansion formulations is given by Van den Akker[xli].

One-dimensional expansion models appear to adopt plausible assumptions from the onset, and apply conservation laws subject to the inherent 1-dimensional approximation. The flashing or depressurisation zone for under-expanded single-phase jets is defined to occur over a short downstream distance. During this phase of the jet, no entrainment is assumed. The transition plane between the entraining and non-entraining region is defined to be plane at which the final jet pressure equates to the ambient pressure (atmospheric for the types of problems specified here). This may be represented schematically as a control volume problem as shown in Figure 90a.

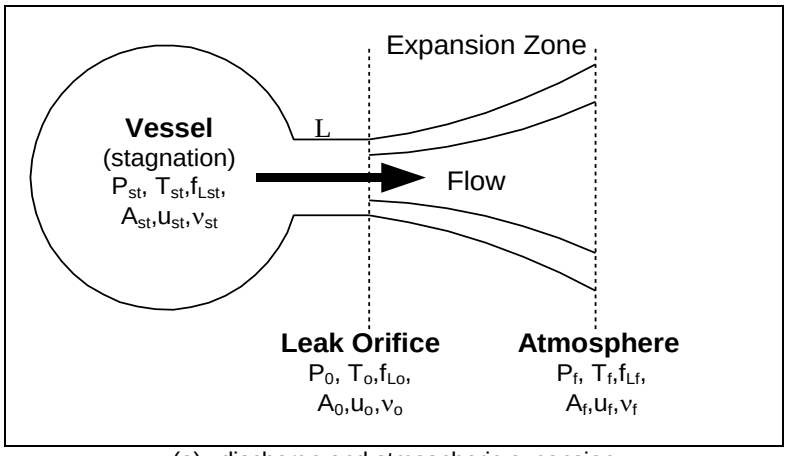

(a) discharge and atmospheric expansion

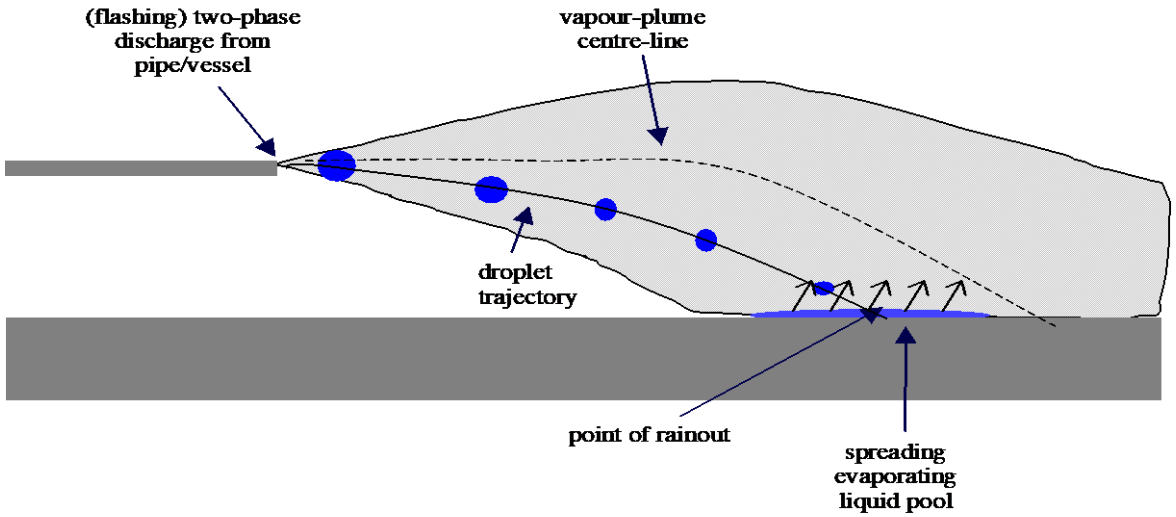

(b) two-phase dispersion (droplet movement/evaporation), rainout and re-evaporation

(c)

Figure 90. Phases in modelling: discharge to atmosphere, atmospheric expansion to ambient pressure, two-phase dispersion, rainout and re-evaporation

Figure 1(a) illustrates the atmospheric expansion to ambient following the release to the atmosphere. Release scenarios to be considered are:

(a) release directly from vessel or from pipe attached to vessel

(b) steady-state release (for small leak), time-dependent release (for larger leak) or instantaneous release (for catastrophic rupture)
(c) choked flow (exit pressure P_o larger than ambient) or unchoked flow (no expansion calculations needed)
(d) release of pure vapour, two-phase or pure liquid

Figure 1(b) illustrates the movement of the droplets in the downwind direction. If the cloud moves in the downwind direction cloud entrainment occurs and the droplets are evaporating. Since the droplets are more heavy than the surrounding vapour, the droplets typically move away from the cloud centre-line. Rainout of the droplets may result in the formation of a spreading evaporation liquid pool.

C.2 Governing conservation equations

The expansion model calculates the final conditions at the end of the expansion from the initial conditions. The final conditions are given by the unknown post-expansion data: area A_f, velocity u_f, temperature T_f or liquid fraction f_{Lf}, specific volume ν_f (= 1 / density = $1/\rho_f$), and specific enthalpy h_f

Within the control volume associated with the depressurisation zone for the one-dimensional, homogeneous flow (though not necessarily single-phase) in thermal equilibrium, the conservation of mass, momentum and energy lead to an unambiguous system of equations:

$$m_f = m_0 \qquad (64)$$

$$m_f u_f = m_o u_o + (P_0 - P_f) A_o \qquad (65)$$

$$m_f \left[h_f + \frac{1}{2} u_f{}^2 \right] = m_o \left[h_o + \frac{1}{2} u_o{}^2 \right] \qquad (66)$$

where m_o, u_o, h_o, P_o, A_o and m_f, u_f, h_f, P_f, A_f are the flow rate (kg/s), specific enthalpy (J/kg), speed (m/s), pressure (Pa), area (m^2) prior and after the expansion respectively.

P_f is the pressure at the end of the flash region, and is therefore, equal to the ambient pressure P_a. P_o is the pressure at the exit plane of the orifice, which for flashing two-phase releases, is usually considered to be the saturated vapour pressure at the reservoir temperature.

The post-expansion data can subsequently be determined as follows:

a) Set post-expansion mass rate m_f from Equation (64)
b) Set post-expansion speed u_f from Equation (65)
c) Set post-expansion specific enthalpy h_f from Equation (66)
d) The post-expansion liquid fraction f_{Lf} can subsequently be set from the enthalpy equation $h_f = f_{Lf}\, h_L(P_a,T_b) + (1-f_{Lf})h_v(P_a,T_b)$, where h_L is the specific liquid vapour enthalpy and $h_v(P_a,T_b)$ the specific vapour enthalpy.
e) Set post-expansion density $\rho_f = \rho_f(P_a,T_b,f_{Lf})$
f) Set post-expansion jet area: $A_f = m_f/(u_f\rho_f)$.

The above formulation corresponds to that included in HGSYSTEM and Phast[xlii], and also corresponds to the formulation recommended by Britter[xxxix,xl] and the TNO Yellow Book[19]. In Phast the above vapour enthalpy, liquid enthalpy and density calculations are carried out rather 'exact' using a DIPPR material property database.

Thus far, subject to the initial reduction of the problem (1-dimensional, homogeneous flow and thermal equilibrium), no further approximations have been introduced, and the system (64), (65), (66) may be referred to as the *exact* equations.

It is noted that application of the above equations (conservation of mass, momentum, energy) may lead to excessive post-expansion velocities for cases where turbulence becomes important (possible occurrence of supersonic speeds and shock waves). To avoid these excessive velocities, Phast adopts a rather arbitrary cut-off velocity of the velocity. Ideally the formulation should be extended to include the effects of turbulence. Moreover the thermodynamic path may need to include non-equilibrium effects and/or slip. The authors are however not aware of a published and validated formulation, which takes these effects into account. As a result the above formulation is recommended (with a possible cut-off for post-expansion velocity), until an improved formulation becomes available.

C.3 Alternative expansion calculations

Further approximations to the above 'exact' system have been proposed within various models proposed for the atmospheric expansion problem:

A. The isenthalpic formulation relies on the change in the kinetic energy being small (hence ignored) compared with the change in enthalpy, in which case the energy equation (66) reduces to conservation of enthalpy across the flashing zone (e.g. Fauske and Epstein[xliii]). Clearly a weakness exists if the change in kinetic energy across the flashing zone – which is known unambiguously from equation (65) - is significant.

B. The 'isentropic' formulation as referred to by Britter, replaces the energy equation (66) with an isentropic assumption, allowing use of the well-known isentropic thermofluid relationships. Thus it applies conservation of mass/momentum/entropy. This approach is adopted in the old TNO Yellow Book (1979)[xliv], for example.

C. The 'isentropic' formulation as referred to as an additional option in Phast, replaces the momentum equation (65) with the isentropic assumption. Thus it applies conservation of mass/entropy/energy. Note that the latter type of assumption is also recommended by Woodward in Perry's Handbook[xlv]. It is also noted that the CCPS droplet size correlation is based on this 'isentropic' assumption and that therefore that therefore this correlation must always be used in conjunction with the CCPS droplet size correlation.

D. The current Phast default is the minimum "thermodynamic change" which can result in either isentropic or conservation of energy.

Influence of simplifying the energy equation

It is straightforward to propose simple scenarios to exemplify the potential and extent of errors introduced by simplifying the exact system.

Britter[xl] shows that for a single-phase gaseous release of 10 bar down to atmospheric pressure, the isenthalpic assumption leads to an error in the final temperature difference of 104K, compared to an error for the isentropic assumption of 42 K. Whilst simple calculations of this nature could be used to argue the case of using the isentropic assumption in favour of the isenthalpic, the point to be emphasised is that both will introduce errors, exacerbated at larger release pressures, and which will become more exaggerated in the case of a two-phase system.

For the more relevant case of a two-phase release, Britter chooses a relevant example from the so-called 'Canvey Island' test data, involving a release of pressurised LPG stored at 288 K. In this example, the isenthalpic assumption gave a post-flash vapour mass fraction of 0.33, whereas the isentropic assumption predicted a value of 0.29. The exact solution would vary depending upon release pressure of course, and taking typical release velocities of 50 m/s and 100 m/s respectively, predictions of 0.33 and 0.32 respectively are deduced. Clearly the isenthalpic assumption performs better in this particular example, but no generality can be inferred from this.

C.4 Summary of recommendations

For flashing jets which can be considered single-phase (liquid) at the orifice exit, the non-entraining control-volume approach resulting in equations (64), (65), and (66) are considered consistent with the spirit of the modelling approach adopted by programs such as Phast and HGSYSTEM, and as recommended in the literature by the new Yellow Book and Britter.

The advantage of using the so-called isenthalpic or isentropic assumptions is not clearly apparent, as there is little additional computational effort required to provide the exact solution for the control-volume approach. Hence, it is recommended that for present, in the case of flashing releases, the assumption of a pure liquid release at the exit orifice, together with the exact system [equations (64), (65), and (66)] be continued.

The main current weakness of the approach is considered to be the assumption of a single-phase liquid jet at the exit orifice, which was adopted in Phast6.4.2 in conjunction with the CCPS droplet size correlation. As discussed in other sections of this report, this is clearly not the case for many flashing releases, where nucleation and bubble-growth has already taken place upstream of the exit orifice. Hence, an additional methodology to determine the two-phase characteristics at the exit orifice as outlined earlier, would provide the additional benefit of an improved model for the post-flash vapour mass fraction. An initial simple methodology has been recommended for this as part of the development of the newly proposed droplet-size correlation in this report.

The other assumptions adopted in the overall 1-dimensional, homogenous, non-entraining approach could be appraised either experimentally by developing and utilising an appropriate LIF system, or numerically by comparing with CFD models. However, it is not immediately obvious how errors in the modelling philosophy identified through these studies could be used to improve the model. They would simply provide input to error analysis.

The authors are not aware of a published and validation formulation, which include the effects of turbulence and/or non-equilibrium (slip). The latter effects may need to be taken into account in the case of large post-expansion velocities (supersonic speeds).

Appendix D. Report on previous Phase III ATEX/UDM validation of CCPS experiments

D.1 Introduction

The CCPS experimental programmes are fully reported in the RELEASE book[8] and accompanying CD.

The first part of the RELEASE report describes the CCPS rainout experiments carried out in Oklahoma (1989) for water (39x) and CFC-11 (15x), and in Nevada (1990) for chlorine (22x), cyclohexane (20x), and monomethylamine (MMA; 18x). Additional MMA experiments (10x) were carried out by Rohm and Haas. Chapters 4 and 5 include details on the test conditions and the experimental results. Chapter 6 in the RELEASE book describes corrections to the experimental Nevada rainout data to account for the effects of droplet evaporation before reaction with the capture solutions (chlorine and MMA) and evaporation from the capture pans (cyclohexane). No correction was carried out for the CFC and the water experiments.

The second part of the RELEASE report describes the modelling of the aerosol release. Chapter 9 describes the correction of the CCPS rainout experiments for re-evaporation using the original UDM model. Chapter 10 describes the RELEASE model for predicting rainout and compares RELEASE predictions against experimental data. Chapter 11 describes the aerosol drop size correlation.

Mass balance
The mass balance for the released material in the CCPS experiments is

$$m_c = m_{de} + m_{pe} + m_{cap}$$

with: m_c = released mass, kg/s (observed)
m_{cap}= captured liquid, kg/s (observed; dissolved or collected)
m_{de} = flashed/droplet evaporation = remaining component mass after rainout, kg/s (predicted by dispersion model)
m_{pe} = pool evaporation from capture pan (predicted by pool evaporation model)

As described in Chapter 9 of the RELEASE report, observed capture data was matched by adjusting the initial droplet size d_d to change m_{de}, and to use the solubility w_s to change the mass dissolved m_{cap}. Note that the dissolution is not 'real dissolution', but it provides an artificial method to correct for the reaction of the Chlorine and MMA with the capture solution.

An increase in w_s results in more dissolution in water, and therefore an increase of m_{cap} and a decrease of m_{pe}. To keep matching with the observed m_{cap}, therefore rainout fraction must decrease, m_{de} increase and therefore d_d decrease. Thus increasing w_s is associated with decreasing d_d and vice versa. Tables 9.1, 9.2 and 9.6 in the RELEASE report included UDM predicted data for chlorine, MMA and cyclohexane. The assumed 'artificial' solubility's for the Chlorine and MMA were 0.20 kg Cl/kg of solution and 0.32 kg MMA/kg[61].

ATEX/UDM simulations.
A representative choice of 10 experiments was selected, whereby 2 experiments were chosen for each chemical: chlorine 20,22; MMA34,40; CFC5,8; Cyclohexane 41,56; Water 5,10.

The previous Phast 6.0 validation of the UDM was described in Section 4.1 of the UDM Thermodynamics Verification Manual, and the latter section has been copied as Appendix E of the current report. Note that this involved the approach of using a dispersion model to predict rainout and adjusting the drop sizes to match observed rainout. Also problems were reporting in doing Phast expansion calculations prior to the UDM calculations, and as a result RELEASE post-flash velocities and post-flash fractions were used in these previous simulations. Therefore as part of Phase II, this approach was re-assessed.

D.2 Method for modelling of discharge and dispersion

The following is deduced from the RELEASE book and accompanying CD.

- The data reported by CCPS as 'orifice' conditions are assumed to correspond in Phast model terms to stagnation data (including liquid head). This is suggested by the small size of the orifices (~ mm - cm) in relation to the pipe diameter, and that temperature and pressure transducers capturing this 'orifice' data are sited some distance along the pipe behind the actual orifice[62]. At this point, therefore, there is likely to be a very slight pressure gradient and negligible velocity.

[61] Thus for a PHAST simulation PHAST should not be run assuming DIPPR properties for the solubility w_s.
[62] Actual distances seem not be given in the RELEASE book/CD.

- The orifice itself is relatively sharp-edged (L/D ≤ 1), and the pipe preceding the orifice short and wide-bore to help suppress flashing. This CCPS experimental design is consistent with modelling in the Phast 'Leak' or 'orifice' scenario.

- The pipe is wide-bore to help suppress flashing. On this point the RELEASE book (p. 27) comments that "all liquid flow represents conditions found during the CCPS experimental program". This may seem to imply that the assumption of metastable liquid can be applied for expansion from stagnation to orifice conditions. As discussed in the preceding section, this would enable us to model the releases using only ATEX. [63]

The following approach will therefore be followed:

1. ATEX (instead of Phast) will be applied to carry out expansion calculations prior to the UDM (to generate UDM input data).
2. The thus calculated droplet size will be directly input to the UDM for dispersion and rainout calculations.
3. The predicted amount of rainout will be compared against the 'corrected' experimentally observed rainout as mentioned in the RELEASE book

D.3 Selection of ATEX and UDM input data

The ATEX input data for simulation of the CCPS and MMA Rohm and Haas experiments have been determined as follows:

1. The ambient data are taken from the experimental conditions given in Appendix A of the RELEASE report: temperature, pressure (Pa), humidity (fraction).

2. The orifice diameter d_o, stagnation temperature T_{st}, stagnation pressure P_{st} and the measured release rate Q (kg/s) and duration (s) are taken from the 'orifice data' reported in Appendix A of the RELEASE. The orifice data: $P_o = P_a$, $T_o = T_{st}$, $\eta_{Lo} = 1$ are applied corresponding to the meta-stable liquid assumption for expansion from stagnation to orifice conditions. The orifice pre-expansion velocity u_o (input to ATEX) is set from $u_o = Q / [0.25\pi\, d_o^2 * \rho_L(P_o,T_o)$.

3. According to the original QUEST report, the pipe length was minimised such to avoid heat loss between the tank and the orifice. As a result the ratio L/d is taken to be L/d=0 (note that values of L/d < 0.1 will all give identical results).

The RELEASE discharge data are indicated in the first five columns of the Table below. The last columns in the table corresponds to the calculation of the partial expansion energy from these data (see Equation (12)]

Experiment	*Exit Temp (K)*	*Exit Pressure (N/m^2)*	*Post- flash Velocity (m/s)*	*Flash Fraction*	*Expansion Energy (J/kg)*	*Expansion Energy (J/kg)*
	Appendix A	*Appendix A*	*Chapter 10*	*Appendix A*	*Chapter 11*	*ATEX*
Chlorine 20	256.4	2.57E+05	21.1	0.9365	775.7	771.4
Chlorine 22	247.4	1.789E+05	15.25	0.9646	237.8	261.7
MMA34	293.8	3.561E+05	40.3	0.883	5371	5170
MMA40	283.3	2.489E+05	30.9	0.9244	2283	2256
CFC5	330.71	3.02E+05	24.5	0.8271	3666	1617
CFC8	297.91	1.618E+05	13.5	0.98773	150.8	60.8
CyclHex41	359.9	2.091E+05	26.2	0.9436	443.6	442.3
CyclHex56	392.5	2.74E+05	33.6	0.7591	4994	5049
Water5	443.4	8.07E+05	56.1	0.8775	41250	28119
Water10	453.4	1.047E+06	65.8	0.8601	53820	36522

The UDM input data for simulation of the CCPS and MMA Rohm and Haas experiments have been determined as follows (see RELEASE report for further details):

1. The ambient data are taken from the experimental conditions given in Appendix A of the RELEASE report: speed (m/s), temperature (= ground = bund temperature), pressure (Pa), humidity (fraction). Stability class D is presumed throughout.

2. For the CCPS (Oklahoma, Nevada) experiments, the release height was 1.22 m above the rectangular capture pan with length of 15.24 m and width 6.096 m. The capture is modelled by a circular bund with the same area. This results

[63] Using DISC is also appropriate with storage conditions equal to CCPS 'orifice' conditions. The flow rate observed in the experiments can be imposed by specifying the appropriate value of the discharge coefficient C_d.

in an equivalent bund diameter of 10.88 m. For the Rohm and Haas MMA experiments, the release height was 1.73 m with the same adopted bund diameter of 10.88 m.

3. Discharge data are based on post-expansion calculations by ATEX as indicated above.

4. The surface roughness is taken to be 0.1 m[64], the dispersing surface water and the pool/bund surface deep open water.

The Table below includes further input data, the corrected percentage of rainout (corrected capture) and the needed droplet diameter.

Exp.	*Ambient Temp* (K) App A	*Ambient Pressure* (N/m2) App A	*Relative Humidity* (-) App A	*Wind Speed* (m/s) App A	*Flow Rate* (kg/s) App A	*Liquid Capture* (%) App A	*Corrected Capture* (%) Chapter 9
Chlorine20	303.6	90300	0.089	7.7	0.487	21.5	59 (370 μm)
Chlorine22	304.35	90300	0.086	6.8	0.382	23.4	66.10 (407 μm)
MMA34	304.9	90300	0.063	4.3	0.4	20.7	23.9 (217 μm)
MMA40	306.4	90300	0.109	4.6	1.246	39.9	45.5 (243 μm)
CFC5	294	97200	0.08	3.3	0.46	30.6	30.6 (220μm)
CFC8	293.2	97200	0.08	7.7	0.27	61.2	61.3 (450μm)
Cyclhex41	309.2	90300	0.174	3.2	0.283	40.4	45.6 (355 μm)
Cyclhex56	309.9	90300	0.082	5.4	0.346	9.68	13.18 (234 μm)
Water5	296.5	96800	0.80	5.7	0.658	68.7	68.7 (59μm)
Water10	297.3	96800	0.88	6.2	0.184	61	61 (38μm)

D.4 Results and discussion

Using the inputs as discussed above, the ATEX model was run using the Phast 6.5 correlation based on the CCPS correlation, and the JIP Phase II and Phase III correlations. The droplet size results are presented in Figure 91 in order of increasing superheat, and also include CCPS droplet sizes from the RELEASE book. The assumptions used in the different rows are described in the Phase II B report. Figure 91 shows the following:

- For Phast6.5 the mechanical break-up correlation is erroneously chosen for higher superheat releases as previously indicated (and conversely the flashing correlation is chosen for low superheats).

- The JIP correlations (see Sections 2.3.4 and 2.3.5) show the expected relationship with superheat – from mechanical through transition to fully flashing – with the three cases to the right being beyond point 'D' in
- Figure 2.

- The JIP Phase III correlation shows significantly increased mechanical break up diameters compared to Phase II as discussed previously, and fully flashing cases are all around 80 μm rather than 30 μm.

[64] CHECK. This is a presumed value of the surface roughness which may affect the results.

	CFC11 - 8	Cyclohexane - 41	Chlorine - 22	Methylamine - 40	Chlorine - 20	Methylamine - 34	CFC11 - 5	Cyclohexane - 56	Water - 5	Water - 10
Superheat (K)	2	10	11	19	20	30	35	42	72	82
CCPS flash correlation	465	386	431	265	345	203	231	208	53	33
Phast 6.5	577	511	1927	33	1147	309	632	328	451	354
CCPS flashing	532	386	424	266	345	205	291	207	81	62
CCPS mechanical	1933	232	508	23	184	27	53	20	11	9
CCPS	532	232	424	23	184	27	53	20	11	9
JIP 2	1192	770	1008	84	677	184	272	30	27	26
JIP 3	4506	2457	3684	80	1639	79	79	78	75	74

Figure 91. Comparison between old and proposed SMD correlations

The droplet sizes and other post-expansion data are then used as inputs to UDM. The rainout is then modelled using Phase II and Phase III correlations, with and without parcels and presuming partial rainout (with droplets < 10µm[65] retained in the cloud upon droplet rainout). The results are compared to the corrected rainout fraction of the CCPS experiments. The results are plotted in
Figure 5 and Figure 6, the latter just showing the Phase III correlation but identifying the different materials. The figures show the following:

The original Phast 6.5 droplet correlation results generally in too large droplet sizes and therefore too much rainout.

For the JIP Phase II correlation the most severe discrepancies are where no rainout is predicted. These are mainly fully flashing cases with droplet diameters ≤ 30 µm. In this region, the UDM predicts complete droplet evaporation before any rainout occurs. Other systematic differences include over-predicting rainout for points in the top right of the graph (though less erratically than the Phast 6.4 correlation). Using parcels moderates the amount of rainout for the Phase II correlation for cases where corrected mass rainout fraction is in the range 0.2 – 0.6 and improves the fit.

The Phase III correlation (with parcels) differs from phase II results in 3 areas.

- Firstly the fully flashed cases where previously rainout was measured but none modelled (i.e. points along the x-axis in the figure). All these now produce rainout (in the case of the water experiments a large amount) [66]. This in itself substantially improves the overall agreement of the phase III correlation compared its predecessors, despite the following two bullet points.

- Secondly, cases CFC5 and MMA34 (corrected rainout 0.31 and 0.24 respectively) show less good agreement with the experimental data. This is because they are now fully flashing with smaller droplet diameters (and therefore less rainout) whereas before they were in the transitional region of the correlation[67].

- Finally low superheat (i.e. mechanical) cases now produce much greater droplet sizes. These are the points clustered in the top-right of the figure. Rainout here was overestimated by other correlations, and increased droplet sizes have exacerbated the problem.

[65] IMPROVE. In the Phase III UDM version one input parameter defines both the cut-off size for partial rainout, d_{pr} and the droplet size until which the droplet equations are solved (i.e. non-equilibrium model is adopted), d_{eq}; thus $d_{pr}=d_{eq}$. If the droplet size of a droplet parcel drops below d_{eq}, all liquid for that parcel is assumed to evaporate resulting in a discontinuity in liquid fraction. As a result the cut-off is currently chosen to be small by default, $d_{eq}= d_{pr} =10µm$. For Phase IV two separate values for d_{eq} and d_{pr} are considered, with $d_{pr} >> d_{eq}$, e.g. $d_{eq}=10µm$ and $d_{pr}=30$ µm.

[66] Interestingly, the MMA experiment with 0.46 corrected rainout shows improved modelled rainout over Phase II, but the droplet size is very similar. This seems to be an effect of the changed parameterisation of the droplet distribution resulting in larger parcels and more rainout

[67] It is possible that the correlation predicts too rapid a transition to fully flashing.

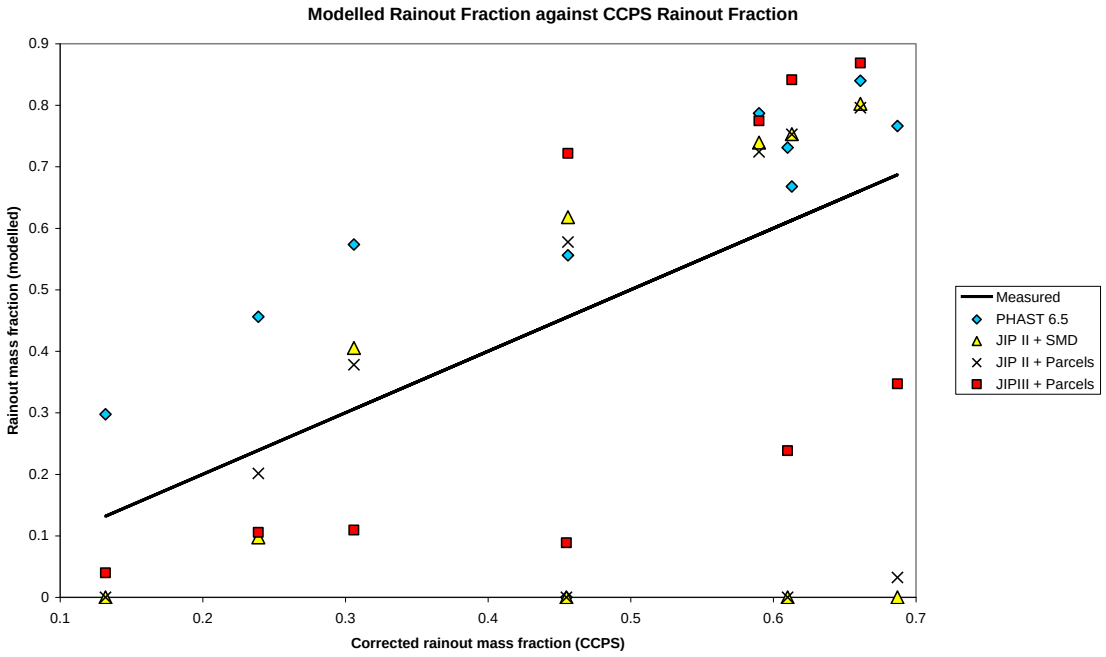

Figure 92. Modelled versus CCPS corrected rainout for the old Phast and the new JIP correlations

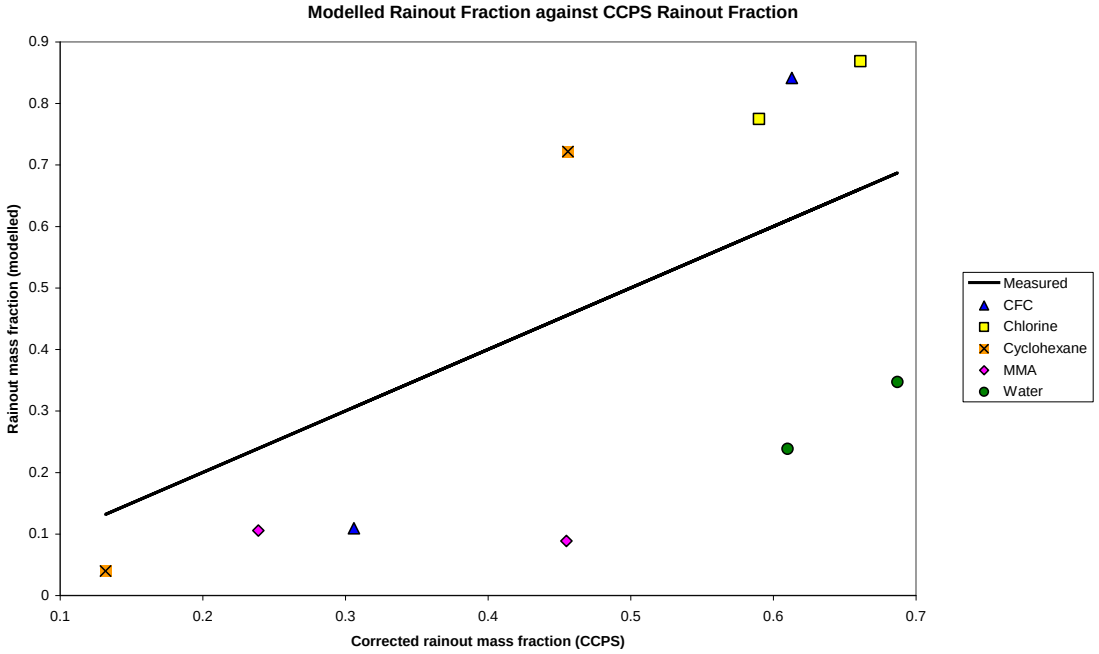

Figure 93. Modelled versus CCPS corrected rainout for the proposed JIP Phase III correlation

Appendix E. Report on previous Phast6.0 UDM simulation of CCPS experiments

The CCPS correlation correlates the droplet diameter to the partial expansion energy E_p(J/kg). The fit is determined such to best match observed rainout data for the CCPS rainout experiments (using the original UDM model).

The RELEASE report contains full details on the CCPS experiments and the derivation of the above droplet correlation from the CCPS experiments. In Section E.1 the CCPS rainout experiments are described. The method for derivation of the initial droplet size (input to the UDM model) from the CCPS rainout experiments is given. The basic premise involves adjusting the droplet size such that the rainout predicted by the UDM matches the experimental rainout data. Using a 'best' fit, subsequently a correlation is derived for the droplet diameter as function of the partial expansion energy.

To verify the above method for determining the needed diameter, this method has been repeated for a limited selection of the CCPS experiments:

- In Section E.2 the Phast discharge calculations are repeated, to check for consistency for the post-flash data (velocity, liquid fraction, expansion energy) reported in the RELEASE book.
- In Section E.3 the UDM dispersion calculations are repeated, to determine the droplet diameter needed to match the 'corrected' experimental rainout.

E.1 UDM method for derivation of correlation from CCPS rainout experiments

UDM input data for NEVADA CCPS experiments

The UDM input data for simulation of the CCPS and MMA Rohm and Haas experiments have been determined as follows (see RELEASE report for further details):

5. The ambient data are taken from the experimental conditions given in Appendix A of the RELEASE report: speed (m/s), temperature (= ground = bund temperature), pressure (Pa), humidity (fraction). Stability class D is presumed throughout.

6. For the CCPS (Oklahoma, Nevada) experiments, the release height was 1.22 m above the rectangular capture pan with length of 15.24 m and width 6.096 m. The capture is modelled by a circular bund with the same area. This results in an equivalent bund diameter of 10.88 m. For the Rohm and Haas MMA experiments, the release height was 1.73 m with the same adopted bund diameter of 10.88 m.

7. The orifice diameter, discharge temperature, discharge pressure and the measured release rate (kg/s) and duration (s) are given in Appendix A of the RELEASE report.

8. Phast discharge calculations are carried out to calculate the post-flash data (droplet diameter, liquid fraction, expansion velocity). Input data are[68]:

   - padded liquid
   - absolute discharge pressure and discharge temperature (corresponding to data at top of liquid)
   - liquid head[69]

9. The surface roughness is taken to be 0.1 m[70], the dispersing surface water and the pool/bund surface deep open water.

Derivation of correlation from CCPS experiments

The correlation is derivated from the above rainout experiments as follows:

1. Select sample cases for testing. These should correspond to a sufficient range of (needed drop diameter to match corrected rainout, partial expansion energy); see table 9-2 and Figure 11-6 in RELEASE book.
2. For each case:

[68] CHECK - JW recommends to adjust the drag coefficient such that observed release rate is obtained. This was cumbersome for PHAST. In Appendices A and C.1, a DIPPR program is therefore used adopting Fauske expansion zone model with a correlation for choke pressure; the drag coefficient C_D was set to C_D = 0.61*[observed discharge rate]/[predicted discharge rate], to match the observed discharge rate. The DIPPR and PHAST approach lead thus to similar discharge rate and flash fraction. However the PHAST expansion velocities is often significantly larger (factor 2-3 is common), and therefore the PHAST flash equations (momentum, energy,….) need to be further screened.
In redoing correlation, RELEASE post-flash velocity (see Chapter 10) and post-flash fraction as reported in Appendix A are used. The values for the partial expansion energy are taken from Chapter 11. This seems to be compatible with the .INT files supplied by JW.

[69] CHECK - to find value from original Johnson's reports; how sensitive are results to this; JW suggest to vary until best fit! Note that tank length is 2.73 m, so typical liquid head may be 2 m!

[70] CHECK - Is this realistic and does it affect the results?

- run Phast to establish post-flash data[68]
- repeatedly run UDM to establish drop diameter needed to match corrected rainout for chlorine, MMA and cyclohexane (see Tables 9.1, 9.2, 9.6) and to match observed rainout for CFC/water (see Tables A.9 and A.11)[71]
- plot data point in (needed drop diameter to match corrected rainout, partial expansion energy) graph (compare with data points in Tables 11.1-5 in RELEASE report).

3. Produce least/square lin/log fit to line $d_d = A_d - B_d \ln(E_p)$, in order to set best estimates for A_d and B_d.[72]

E.2 Phast discharge (flash) calculations for CCPS experiments

The method for deriving the correlation for the initial droplet size described in the preceding section is repeated for a limited selection of 10 CCPS experiments. The Phast discharge calculations were repeated, to compare the Phast results for the post-flash data (velocity, liquid fraction, expansion energy) against those reported in the RELEASE book.

The selected experiments and the discharge data from the RELEASE book are indicated in the first five columns of the Table below. The last column in the table corresponds to the calculation of the partial expansion energy from these data (see UDM thermodynamics theory manual). This equation is adopted in the Phast discharge model.

Experiment	*Exit Temp (K)*	*Exit Pressure (N/m^2)*	*Post- flash Velocity (m/s)*	*Flash Fraction*	*Expansion Energy (J/kg)*	*Expansion Energy (J/kg)*
	Appendix A	*Appendix A*	*Chapter 10*	*Appendix A*	*Chapter 11*	*Phast*
Chlorine 20	256.4	2.57E+05	21.1	0.9365	775.7	385
Chlorine 22	247.4	1.789E+05	15.25	0.9646	237.8	-5.71
MMA34	293.8	3.561E+05	40.3	0.883	5371	6638
MMA40	283.3	2.489E+05	30.9	0.9244	2283	3162
CFC5	330.71	3.02E+05	24.5	0.8271	3666	202
CFC8	297.91	1.618E+05	13.5	0.98773	150.8	-170
CyclHex41	359.9	2.091E+05	26.2	0.9436	443.6	713
CyclHex56	392.5	2.74E+05	33.6	0.7591	4994	5268
Water5	443.4	8.07E+05	56.1	0.8775	41250	24352
Water10	453.4	1.047E+06	65.8	0.8601	53820	32214

It was noted that the values for the flash fraction given in the book, the input files for the original UDM runs and from the Phast6.0 discharge model (using a drag coefficient C_D such that observed release rate was calculated) gave close but differing values. This leads to a very wide scatter in the prediction for the partial expansion energy, which is extremely sensitive to the post-flash fraction. The partial expansion energy values reported in the RELEASE book are used further on in this document to compare the results with the correlation.

E.3 UDM dispersion calculations for CCPS experiments

The UDM input data have been applied as described in Section E.1 (stability Class D, release height 1.22m, bund diameter 10.876 m; reference heights for wind-speed, pressure and temperature 10 m). The Table below includes further input data, the corrected percentage of rainout (corrected capture) and the needed droplet diameter.

Exp.	*Ambient Temp (K)*	*Ambient Pressure (N/m2)*	*Relative Humidity (-)*	*Wind Speed (m/s)*	*Flow Rate (kg/s)*	*Liquid Capture (%)*	*Corrected Capture (%)*	*Required Droplet Diameter (μm)*
	App A	App A	App A	App A	App A	App A	Chapter 9	Testbed
Chlorine20	303.6	90300	0.089	7.7	0.487	21.5	59 (370 μm)	370 (59.2%)
Chlorine22	304.35	90300	0.086	6.8	0.382	23.4	66.10 (407 μm)	463 (66.1%)
MMA34	304.9	90300	0.063	4.3	0.4	20.7	23.9 (217 μm)	238 (23.6%)
MMA40	306.4	90300	0.109	4.6	1.246	39.9	45.5 (243 μm)	261 (45.7%)

[71] CHECK - Note that correction of rainout is not reported in the RELEASE report for the Rohm and Haas experiments. JW is unsure that correction of rainout has really been done!

[72] Compare location of data points relative to old data points. Are droplet diameters to be increased or to be reduced (since larger jet dispersion coefficients and added near-field passive dispersion expected lower concentrations; as a result needed droplet diameters expected to be larger!). Possibly attempt to do some cases with old UDM version to double check results. Ideally to have this process automated!!

CFC5	294	97200	0.08	3.3	0.46	30.6	30.6 (220μm)	240 (30.7%)
CFC8	293.2	97200	0.08	7.7	0.27	61.2	61.3 (450μm)	528 (61.3%)
Cyclhex41	309.2	90300	0.174	3.2	0.283	40.4	45.6 (355 μm)	400 (45.6%)
Cyclhex56	309.9	90300	0.082	5.4	0.346	9.68	13.18 (234 μm)	261 (13.2%)
Water5	296.5	96800	0.80	5.7	0.658	68.7	68.7 (59μm)	170 (68.7%)
Water10	297.3	96800	0.88	6.2	0.184	61	61 (38μm)	171 (61%)

E.4 Comparison of original and new results against UDM droplet correlation

Figure 94 plots the required droplet diameter against the partial expansion energy as obtained from the RELEASE book. Figure 94a includes the original UDM results reported in the RELEASE book, while Figure 94b represents the new results for Phast6.0. The following may be noted[73]:

- The required droplet diameters for Phast6.0 are larger than the original values. This is not surprising considering the introduction of the near-field passive dispersion term and the increase in the jet and cross-wind entrainment coefficients α_1 and α_2 . For all materials except water the difference is approximately 10 %. This difference is sufficiently small to justify *not* retuning the droplet diameter equation at this stage.
- The significant difference in the required water droplet diameters between Phast6.0 and the original values may be attributed to the fact that the higher release velocities and lower density ratios give rise to larger rainout distances. This will mean that the effects of the aforementioned changes will be larger for the water spray releases.

[73] These conclusions could be further substantiated if the set of selected experiments would be enlarged.

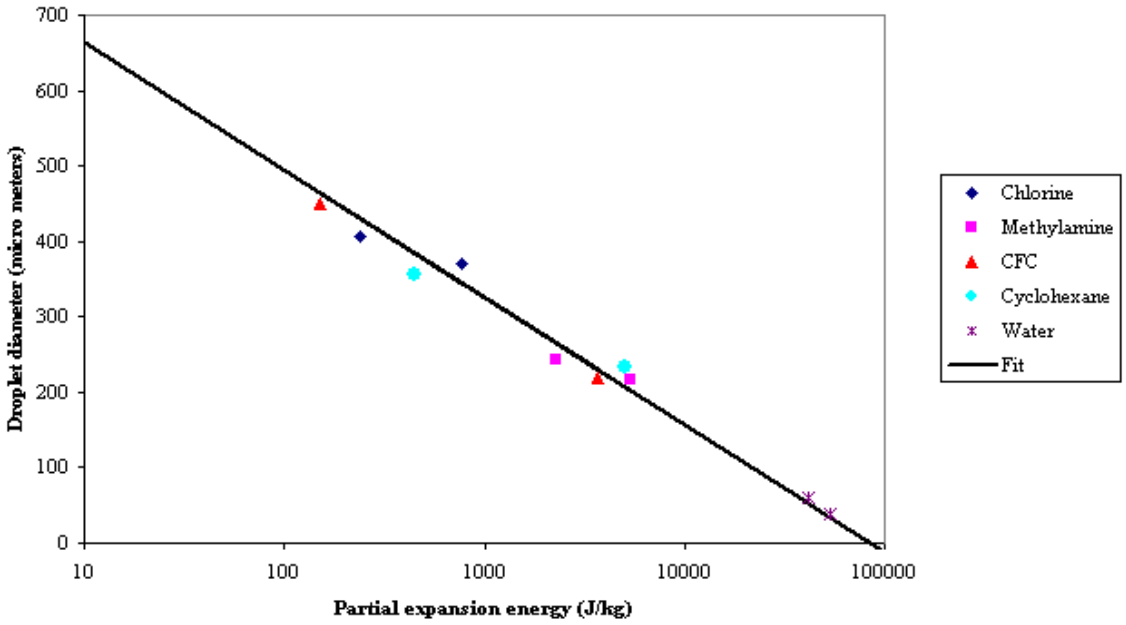

(a) results from RELEASE book

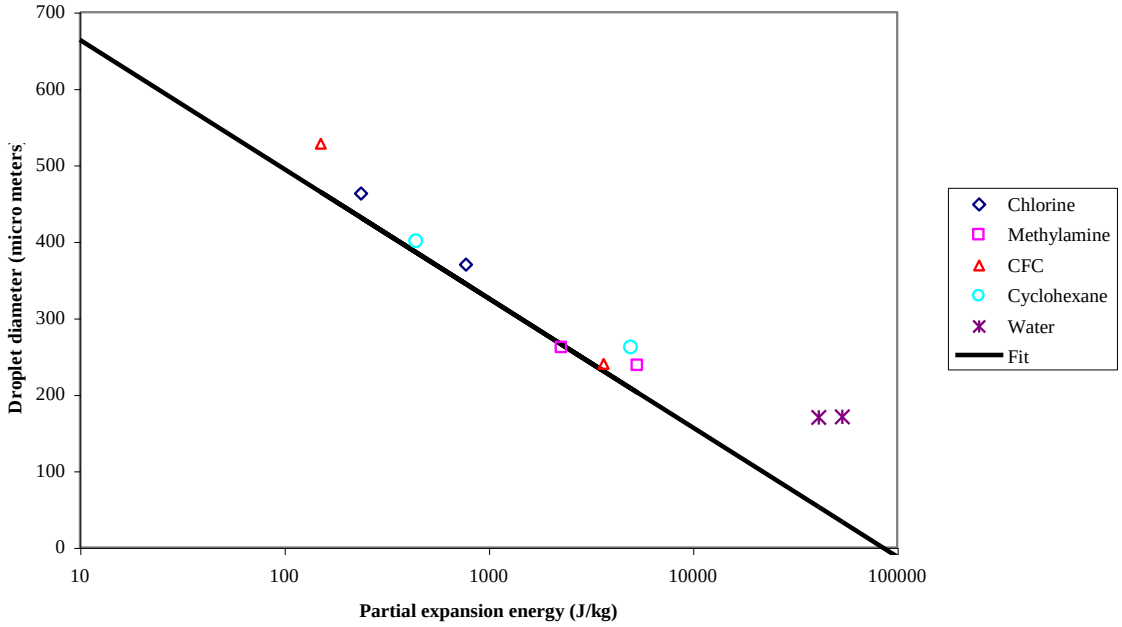

(b) results using new UDM6.0 model

Figure 94. **Needed droplet diameters (to match rainout) as function of partial expansion energy**
Data for selected CCPS experiments are included as well as the fit

NOMENCLATURE

C_p	specific heat, J/kg/K
d_d	Sauter Mean Diameter (SMD) = d_{32} , m
d_{da}	SMD based on aerodynamic (mechanical) break-up criterion, m

d_{df} SMD based on flashing break-up criterion, m
D_p,d_p diameter of droplet particle, m
d_p^{cr} critical value of droplet diameter below which no rainout occurs, m
d_o orifice diameter, m
h specific enthalpy, J/kg
h_{fg} latent heat of evaporation (J/kg)
Ja Jacob number, -
L wall thickness (release from hole in vessel) or pipe length (pipe release), m
P pressure, N/m^2
$P_v^c(T)$ saturated pressure of released component at temperature T, N/m^2
Q discharge flow rate, kg/s
Re Reynolds number, -
t normalised droplet diameter d_p/d_d , -
T temperature, K
$T_v^c(P)$ saturated temperature of released component at pressure P, K
u velocity, m/s
We Weber number, -

Greek letters

ΔT_{sh} superheat, K
η mole fraction
$v_{drop}(D_p)$ mass fraction of droplets with droplet diameter less than D_p, -
ρ density, kg/m^3
φ correction function to Jacob number in criterion for transition to flashing, -

Subscripts

a ambient (atmospheric)
f final (after atmospheric expansion)
L liquid
o orifice (immediately downstream of orifice, prior to atmospheric expansion)
st stagnation (before expansion from storage data to orifice data)
v vapour

Superscripts
A refers to point A (start of transition to flashing, before which mechanical break-up applies)
C refers to point C (end of transition to flashing, after which fully flashing applies)
c component (released material)
D refers to point D (point at which SMD reduces to 30μm)

About DNV

We are the independent expert in risk management and quality assurance. Driven by our purpose, to safeguard life, property and the environment, we empower our customers and their stakeholders with facts and reliable insights so that critical decisions can be made with confidence. As a trusted voice for many of the world's most successful organizations, we use our knowledge to advance safety and performance, set industry benchmarks, and inspire and invent solutions to tackle global transformations.

Digital Solutions

DNV is a world-leading provider of digital solutions and software applications with focus on the energy, maritime and healthcare markets. Our solutions are used worldwide to manage risk and performance for wind turbines, electric grids, pipelines, processing plants, offshore structures, ships, and more. Supported by our domain knowledge and Veracity assurance platform, we enable companies to digitize and manage business critical activities in a sustainable, cost-efficient, safe and secure way.

DNV | digital@dnv.com | dnv.com/digital

REFERENCES

[1] Witlox, H.W.M. and Bowen, P., "Flashing liquid jets and two-phase dispersion - A review", Contract 41003600 for HSE, Exxon-Mobil and ICI Eutech, HSE Books, Contract Research Report 403/2002 (2002)
[2] Witlox, H.W.M., Bowen, P.J., Cleary, V.M., and Harper, M., "Two-phase release and atmospheric dispersion – Phase II", Contract 41008300 for RIVM (Dutch Government), Gaz de France and Atofina, DNV, London (2004)
[3] Cleary, V.M., Bowen, P.J. and Witlox, H.W.M., "Flashing liquid jets and two-phase dispersion – I. Experiments for derivation of atomisation correlations", pp. 786-796, Journal of Hazardous Materials 142 (2007)
[4] Witlox, H.W.M., Harper, M., Bowen, P.J. and Cleary, V.M., "Flashing liquid jets and two-phase dispersion – II. Comparison and validation of droplet size and rainout formulations", pp. 797-809, Journal of Hazardous Materials 142 (2007)
[5] Witlox, H.W.M., Harper, M., Oke, A., Kay, P., and Bowen, P.J., "Sub-cooled and flashing liquid jets and droplet dispersion, I. Overview and model implementation/validation", Journal of Loss Prevention in the Process Industries 23 , pp. 831-842 (2010)
[6] Kay, P., Bowen, P.J., and Witlox, H.W.M., "Sub-cooled and flashing liquid jets and droplet dispersion, II. Scaled Experiments and derivation of droplet atomisation correlations", Journal of Loss Prevention in the Process Industries 23, pp. 849-856 (2010)
[7] Witlox, H.W.M., Harper, M., Bettis, R., Jagger, S., and Bowen, P., "Two-Phase Jet Releases and Droplet Dispersion: Rainout Experiments and Model Validation", 45th Loss Prevention Symposium, 7th Global Congress on Process Safety, Chicago, March 2011
[8] Johnson, D.W., and Woodward, J.L., "RELEASE. A model with data to predict aerosol rainout in accidental releases", Center of Chemical Process Safety (CCPS), New York (1999)
[9] Hervieu, E. and Veneau, T., "Experimental determination of the droplet size and velocity distributions at the exit of the bottom discharge pipe of a liquefied propane storage tank during a sudden blowdown", J. Loss Prev. Ind., Vol. 9, No. 6, pp. 413-455 (1996)
[10] Vandroux-Koenig, S., and Berthoud, G., "Modelling of a two-phase momentum jet close to the breach, in the containment vessel of a liquefied gas", J. Loss Prev. Ind., Vol. 10, No. 1, pp. 17-29 (1997)
[11] Allen J.T. 'Development of a Fluorescent-Based Temperature Measurement Technique for Two-Phase Flashing Propane Jets', HSL Report Number IR/L/FR/96/6 (1996)
[12]Allen J.T. 'Laser-Based Measurements in Two-Phase Flashing Propane Jets. Part two : Droplet Size Distribution', Journal Loss Prevention in Process Ind. V11:299-306 (1998)
[13]Allen J.T. 'Laser-Based Measurements in Two-Phase Flashing Propane Jets. Part One: Velocity Profiles', Journal Loss Prevention in Process Ind. V11:291-297 (1998)
[14] Touil, A., Bigot, J.P., Bonnet, P., Lacome, J.M., and Duplantier, S., "Rainout prediction: initial droplet diameter experimental determination", pp. 3201-3309, Loss Prevention and Safety Promotion in the Process Industries, 11th Int. Symp., Prague, 31 May – 3 June 2004 (2004)
[15] Brown, R. and York, J.L., "Sprays formed by flashing liquid jet", AIChE J., 8, pp149 –153, (1962)
[16] Heinze, J.U., "Fundamental of the hydrodynamics mechanisms of splitting in dispersion processes", AIChE J., 1, pp 289-295, (1955)
[17] Woodward, J.L, and Papadourakis, A., "Reassessment and reevaluation of rainout and drop size correlation for an aerosol jet", J. of Haz. Mat. 44, pp. 209-230 (1995)
[18] Johnson, D.W., and Woodward, J.L., "A model with data to predict aerosol rainout in accidental releases", Center of Chemical Process Safety (CCPS), New York (1999)
[19] van den Bosch, C.J.H., and Duijm, N.J., Sections 2.3.4.6, 2.4.3.5, 2.5.3.7 on 'Finite-duration spray releases' in "Outflow and Spray Release" , Chapter 2 in "Methods for the calculation of physical effects - TNO Yellow Book", CPR14E, Third Edition, Committee for the Prevention of Disasters, SDU, The Hague (1997)
[20] Appleton, P.R., "A study of axi-symmetric two-phase flashing jets", report R303, SRD, Culcheth, Warrington, Cheshire, UK (1984)
[21] Wheatley, C.J., "Discharge of liquid ammonia to moist atmospheres – survey of experimental data and model for estimating initial conditions for dispersion calculations", report R410, SRD, Culcheth, Warrington, Cheshire, UK (1987)
[22] Melhem, G.A., Comey, K.R., and Gustafson, R.M., "The TEXACO/UOP HF Alkylation Additive Technology: aerosolization reduction effects", Proceedings of Int. Conf. and Workshop on Modelling and Mitigating the consequences of accidental releases of hazardous materials, AIChE/CCPS, September 26-29 (1995)
[23] Brodkey, A., "The phenomenon of fluids motions", Addison-Wesley (1967)
[24] Kitamura Y., Morimitsu H. and Takahashi T. "Critical Superheat for Flashing of Superheated Liquid Jets" Ind. Eng. Chem Fundamentals, Vol.25, No.2, pp.207-211 (1986)
[25] Lefebvre A.H. 'Atomisation and Sprays', Hemisphere Publishing (1989)
[26] Eltkobt, M.M., "Fuel atomization for spray modelling", Prog. Energy Comb. Sci 8, pp. 61-91 (1982)
[27] Yildiz D, Rambaud P., van Beeck J. 'Break-up, Droplet Size and Velocity Characterisations of a Two-Phase Flashing R134A Jet', 5th International Conference on Multiphase Flow (ICMF'04), Yokohama, Japan, May 30- June 4, Paper No. 408 (2004)
[28] Oxford University - Physical and Theoretical Chemistry Laboratory. website link http://physchem.ox.ac.uk/MSDS/TE/1,1,1,2-tetrafluoroethane.html, database of MSDS information

[xxix] Ramsdale, S.A., and Tickle, G.A., "Review of RELEASE rainout model and CCPS data", Contract by AEA Technology for HSE, HSE Books, Contract Research Report 277/2000 (2000)
[xxx] Johnson, D.W., and Woodward, J.L., 'RELEASE – A model with Data to Predict Aerosol Rainout in Accidental Releases', CCPS Concept Books, AIChE (1999)
[xxxi] Kletz T. ,'Unconfined Vapour Cloud Explosions', AIChE Loss Prevention (1977)
[xxxii] De Vaull, G.E., and King, J.A., 'Similarity scaling of droplet evaporation and liquid rain-out following the release of superheated liquid to the environment', 85th Annual Meeting, Air and Waste Management Assoc., Kansas (1992)
[xxxiii] Lautkaski, R., 'Experimental correlations for the estimation of the rainout of flashing liquid releases – Revisited', J. Loss Prev. in the Proc. Industries 21, pp. 506-511 (2008)
[xxxiv] Ichard, M., Hansen, O.R., Melheim, J. "Releases of pressurized liquefied gases: simulations of the Desert Tortoise test series with the CFD model FLACS". 16th Conference on Air Pollution Meteorology (2010)
[xxxv] Yaws, C. L. "Yaws' handbook of thermodynamic and physical properties of chemical compounds: Physical, thermodynamic and transport properties for 5000 organic chemical compounds". Norwich, NY: Knovel (2003)
[xxxvi] Daish, N.C., Britter, R.E., Linden, P.F., Jagger. S.F., and Carissimo, B., "SMEDIS: Scientific Model Evaluation techniques applied to dense gas dispersion models in complex situations", International Conference and Workshop on Modelling the Consequences of Accidental Releases of Hazardous Materials, CCPS, San Francisco, California, September 28 – October 1 (1999)
[xxxvii] Beale, J.C. and Reitz, R.D., "Modeling Spray atomization with the Kelvin-Helmholtz/Rayleigh-Taylor Hybrid Model", Atomisation and Sprays 9, pp. 623-650 (1999)
[xxxviii] Grant, R.P. and Middleman, S., "Newtonian Jet Stability", Am. Inst. Chem. Eng. J. 12, pp. 669–678 (1966)
[xxxix] Britter, R.E., "Dispersion of two-phase flashing releases - FLADIS field experiments; a further note on modelling flashing releases", Report FM89/3 by CERC for EEC Commission DGXII (1995)
[xl] Britter, R.E., 'Dispersion of two-phase flashing releases - FLADIS field experiments; the modelling of pseudo-source for complex releases', Report FM89/2 by CERC for EEC Commission DGXII (1994)
[xli] Van den Akker, H.E.A., Snoey, H., and Spoelstra, H., "Discharges of pressurised liquefied gases through apertures and pipes", IchemE Symposium Series 80, pp. E23-E31 (1983)
[xlii] Holt, A., Topalis, P., Witlox, H.W.M., and Clements, F., 'Atmospheric expansion model (ATEX)', DNV, London (2001)
[xliii] Fauske H.K. and Epstein M. 'Source Term considerations in connection with chemical accidents and vapour cloud modelling', J.Loss Prev.Process Ind., V1:75-83 (1988)
[xliv] TNO Yellow Book (1979)
[xlv] Perry, R.H, Green, D.W. and Maloney, J.D., (eds.), "Perry Chemicals Engineering Handbook", 7th Edition, McGrawhill (1999), Section 26 "Process safety"